

Characteristics of Vortices in Equilibrium Scour Holes at Interfering Piers

Thesis Submitted By

HASANUR JAMAN

Doctor of Philosophy (Engineering)

School of Water Resources Engineering

Faculty Council of Engineering & Technology

Jadavpur University

Kolkata, India

2019

*Dedicated to
My
Beloved Parents*

Jadavpur University
Kolkata – 700032, INDIA

INDEX NO. 290/12/E

1. Title of the Thesis:

CHARACTERISTICS OF VORTICES IN EQUILIBRIUM SCOUR
HOLES AT INTERFERING PIERS

2. Name, Designation & Institution of the Supervisors:

- 1. Prof. Dr. Asis Mazumdar**
Professor & Director,
School of Water Resources Engineering
Jadavpur University
- 2. Dr. Subhasish Das**
Assistant Professor
School of Water Resources Engineering
Jadavpur University

3. List of Publications:

- [1] **Jaman, Hasanur;** Das, Subhasish; Kuila, Asim; and Mazumdar, Asis (2017). Hydrodynamic Flow Patterns Around Three Inline Eccentrically Arranged Circular Piers. *Arabian Journal for Science and Engineering*. Springer Berlin Heidelberg, 42(9), 3973–3990. ISSN: 2193-567X (Print) 2191-4281 (Online). DOI: [10.1007/s13369-017-2536-9](https://doi.org/10.1007/s13369-017-2536-9) (UGC, Scopus, SCI/Thompson Reuter, WOS indexed)
- [2] **Jaman, Hasanur;** Das, Subhasish; Das, Rajib; and Mazumdar, Asis (2017). Hydrodynamics of Flow Obstructed by Inline and Eccentrically Arranged Circular Piers on a Horizontal Bed Surface. *Journal of The Institution of Engineers (India): Series A*. Springer Nature, 98(1-2), 77–83. ISSN: 2250-2149 (Print) 2250-2157 (Online). DOI: [10.1007/s40030-017-0187-1](https://doi.org/10.1007/s40030-017-0187-1) (UGC, Scopus indexed)
- [3] Das, Subhasish; **Jaman, Hasanur;** Chatterjee, Anik; Das, Rajib; and Mazumdar, Asis (2017). Hydrodynamic Behaviour of Flow past Three Typically Arranged Circular Piers on Different Horizontal Planes. *International Journal of Fluid Mechanics Research*. American Society of Thermal and Fluids Engineers, 44(5), 457-468 ISSN: 1064-2277 (Print) 2152-5110 (Online). DOI: [10.1615/InterJFluidMechRes.2017019421](https://doi.org/10.1615/InterJFluidMechRes.2017019421) (UGC, Scopus indexed)
- [4] Das, Rajib; Das, Subhasish; **Jaman, Hasanur;** and Mazumdar, Asis (2018). Impact of Upstream Bridge Pier on the Scouring Around Adjacent Downstream Bridge Pier. *Arabian Journal for Science and Engineering*. Springer Berlin Heidelberg, 1-14. ISSN: 2193-567X (Print) 2191-4281 (Online). DOI: [10.1007/s13369-018-3418-5](https://doi.org/10.1007/s13369-018-3418-5) (UGC, Scopus, SCI/Thompson Reuter, WOS indexed)

CERTIFICATE FROM THE SUPERVISORS

This is to certify that the thesis entitled “**Characteristics of Vortices in Equilibrium Scour Holes at Interfering Piers**” submitted by **Mr. Hasanur Jaman**, who got his name registered on **30th March, 2012** for the award of Ph.D. (Engineering) degree of Jadavpur University is absolutely based upon his own work under the supervision of **Prof. Dr. Asis Mazumdar** and **Dr. Subhasish Das** and that neither his thesis nor any part of the thesis has been submitted for any degree/diploma or any other academic award anywhere before.

1. _____

THESIS ADVISOR

Prof. Dr. Asis Mazumdar

Professor & Director,
School of Water Resources Engineering
Jadavpur University

2. _____

THESIS ADVISOR

Dr. Subhasish Das

Assistant Professor
School of Water Resources Engineering
Jadavpur University

Acknowledgements

The author is really grateful to *Prof. Dr. Asis Mazumdar* and *Dr. Subhasish Das* for being guide in the truest sense. It was their initiation, constant encouragement and help rendered in developing the experimental facilities in the Fluvial Hydraulics Laboratory of School of Water Resources Engineering, Jadavpur University which enabled the author to carry out a major part of the present thesis work. It would also be very difficult to inculcate this work in pen and paper without their valuable advises.

He is also indebted to *Prof. Dr. Asis Mazumdar* and *Dr. Subhasish Das* for helping financially in the building up experimental facilities and providing moral support during tenure of his Ph.D. work.

The author also expresses his sincere gratitude to *Dr. Debasri Roy*, Former Associate Professor, School of Water Resources Engineering, Jadavpur University for her constant encouragement throughout. The author would like to thank *Dr. Rajib Das*, Assistant Professor, School of Water Resources Engineering, Jadavpur University for his direct and indirect help and support.

The author will always remain indebted to Mr. Asim Kuila, research scholar, School of Water Resources Engineering, Jadavpur University for providing help during a part of the ADV data measurement.

Lastly, how can the author forget the tremendous sacrifice and encouragement of his parents, brother and wife during the grueling period of his Ph.D. work, especially during the final stage?

HASANUR JAMAN

Ph.D. Scholar

School of Water Resources Engineering

Jadavpur University

Kolkata – 700 032, West Bengal, India

Abstract

Flow behaviour around multiple piers is a classical problem in recent days. Prediction of magnitudes of scour near multiple piers is an important issue to the hydraulic engineers. Nowadays group of similar piers or complex piers are becoming much more significant in performing bridge drawing and design for several reasons related to achieve geophysical and economic advantages. The critical scour mechanism for pier groups is highly complex in nature and is obviously very difficult to estimate local scour depth, where the direct use of the outcomes acquired from single pier may be problematical. An estimate of maximum possible scour around any bridge pier group is essential for its safe design. Due to the mutual interference between piers at close proximity, the inline-eccentric-inline pier arrangements present a mutual interference on scouring and on hydraulic behaviour. Hence, the interference between the wake vortex of the inline-front pier and horseshoe vortex of the eccentric-middle pier in addition to the horseshoe vortex of the inline-rear pier and wake vortex of the eccentric-middle pier play an important role in the creation and formation of the greater scour depth around multiple identical piers. The combined strength of both vortices enhance scour hole at the eccentric-middle pier thereby increasing the rate of sediment transport, moving the sediment away from the upstream axis of symmetry as the flow approaches towards downward direction.

Over the years, a large number of investigation on single pier, of various shapes, arrangement have been studied by many researchers using laboratory flume based experiments and incorporating the use of non-dimensional equations inferencing in some semi-empirical equations for simulating scour depths. A long-standing concern is the tendency of some of these equations to over predict the maximum scour depth for field or even for laboratory conditions. A lack of understanding of the flow structure around the multiple bridge piers and their interaction with the bed sediment seems to be at least partly responsible for such occurrence.

Many researchers highlighted information on velocity and subsequent turbulent fields around single piers. There are a large number of studies around pier groups and complex piers that focus only on the prediction of the maximum scour depth around the pier. For a pier in a multi-pier arrangement, combined effects are notable, in addition with those parameters which influence scouring around single-pier arrangement. Most of the multi-pier experiments have been restricted to two pier arrangements, positioned either inline-eccentric, inline-inline or side by side that focused on the prediction of flow-field, turbulent field and the scour geometry and the effect of pier spacing on flow characteristics and on scour depth. In spite of the large number of investigations focusing on single pier and two piers experiments, a comprehensive understanding about atleast three pier inline-eccentric-inline arrangement, the effects of flow characteristics on bed sediments and vice versa are necessary.

The wake vortex structures change behind the piers depending on the intermediate spacing between three piers. Previously published literatures reveal that,

to date, there is no experimental progress on scour and flow fields around three circular and square piers arrangement. Hence, no comparison has been made comparing experimental results of turbulent horseshoe vortex flow within equilibrium scour holes at three circular piers and square piers.

Hence, in the present research an attempt has been made to carry out experiments of clear water scour around three circular and square pier groups with inline-eccentric-inline arrangement and to delineate the scour geometry, the flow fields and turbulence fields (hydrodynamic flow formations) around the piers. Also it is essential to compare the above mentioned new findings between the experimental results obtained using circular and square piers.

Throughout the entire research, same bed material, same experimental setup and same experimental conditions like approaching flow depth, depth-averaged velocity, pier width have been used. The first part focuses on the scour geometry, flow fields, turbulence fields and vortex (both horseshoe and wake) strengths around the three circular piers positioning in inline-eccentric-inline arrangement with varying longitudinal spacing between them with a constant eccentricity. Longitudinal spacing between inline front and eccentric middle piers were kept constant at 0.5 times the maximum equilibrium length of sediment transport of a single pier of identical shape and constant eccentricity. The detailed three dimensional velocities were captured instantaneously by using a velocimeter at five different vertical azimuth-planes (0° , $\pm 45^\circ$, $\pm 90^\circ$) positioned around the three piers and also at two horizontal-planes around the three piers at 4% (closest to bed) and 50% (mid of bed and water surface) of approaching flow-depth above bed level. The contour profiles and distribution of velocity-components, turbulence kinetic energy and intensities are computed and analysed at both vertical and horizontal planes around the piers. The velocity-vector plot and time-mean absolute-velocity acquired from velocity-profile shows detailed hydrodynamic flow characteristics. The vorticity and circulation generated at the upstream zone near the piers are determined by applying the techniques of computational hydro dynamics.

In the last part of the research, a comparison has been made comparing the present findings of equilibrium scour geometry and hydrodynamic flow characteristics around circular and around square shaped piers' experiments. The increased rate of sediment transport and strength of vortex are always found more for the square piers than circular piers and of larger scour depth just near the square eccentric pier and more transportation of sand along the left (eccentric pier) side wall. Therefore, the square pier causes to produce more scour than the circular pier and as well as shifts more sand towards the side walls of the flume.

Table of Contents

<i>Acknowledgements</i>	<i>xi</i>
<i>Abstract</i>	<i>xiii</i>
<i>List of Figures</i>	<i>xviii</i>
<i>List of Tables</i>	<i>xxii</i>
1. INTRODUCTION	1-14
1.1 Introduction to Sediment Transport Dynamics on Scour	1
1.2 State of the Art	2
1.3 Relevance in the Real Field	6
1.4 Present Scope of Work	9
1.5 References	11
2. BASIC THEORIES	15-46
2.1 Introduction to Turbulence	15
2.1.1 Preliminaries	15
2.1.2 Definitions of Technical Terms	16
2.2 Turbulent Flow Boundary Layer Equations	17
2.3 The Universal Velocity Profiles	19
2.4 Turbulence Intensities and Turbulent Kinetic Energy	21
2.5 Vorticity	21
2.6 Circulation	22
2.7 Conditions of Sediment Transport	22
2.8 Incipient Motion (Threshold Condition)	24
2.9 Clear Water Scour Mechanism	25
2.10 Scour around Bridge Piers	26
2.11 Horseshoe Vortex and Wake Vortex	27
2.12 Flow Pattern at a Circular Pier	28
2.13 Scour in Uniform Sediment	29
2.14 Factors affecting Scour Depth	31
2.14.1 Effect of Sediment Grading	32
2.14.2 Effect of Sediment Size	34
2.14.3 Effect of Flow Depth	34
2.14.4 Effect of Pier Size	35
2.14.5 Effect of Pier Alignment	36
2.14.6 Effect of Pier Shape	37
2.15 Scour at Pier Groups	38
2.15.1 Scouring Mechanism at Pier Groups	39
2.15.2 Two Piers Scour	39
2.16 Velocity Measurement	41
2.16.1 Introduction	41
2.16.2 Velocity Measurement using VectrinoPlus	42

2.17	Nomenclature	43
2.18	Bibliography	45
3.	FLOW AROUND THREE INLINE ECCENTRIC CIRCULAR PIERS	47-102
3.1	Introduction	47
3.2	Brief Review of Relevant Works	48
3.3	Scope of Present Work	51
3.4	General Experimental Setup and Technique	52
3.5	Analysis of Scour Geometry	56
3.6	Velocity Measurement	63
3.7	Analyses of Flow and Turbulence Fields	64
3.7.1	Flow Fields	
3.7.1.1	<i>Tangential Velocity</i>	65
3.7.1.2	<i>Radial Velocity</i>	69
3.7.1.3	<i>Vertical Velocity</i>	74
3.7.1.4	<i>Velocity Vector</i>	78
3.7.1.5	<i>Absolute Velocity</i>	82
3.7.2	Vorticity and Circulation	83
3.7.3	Turbulence Fields	90
3.8	Conclusions	95
3.9	Nomenclature	98
3.10	References	99
4.	FLOW AROUND THREE INLINE ECCENTRIC SQUARE PIERS	103-150
4.1	Introduction	103
4.2	Brief Review of Relevant Works	104
4.3	Scope of Present Work	106
4.4	General Experimental Setup and Technique	107
4.5	Analysis of Scour Geometry	110
4.6	Velocity Measurement	114
4.7	Analyses of Flow and Turbulence Fields	115
4.7.1	Flow Fields	
4.7.1.1	<i>Tangential Velocity</i>	115
4.7.1.2	<i>Radial Velocity</i>	120
4.7.1.3	<i>Vertical Velocity</i>	124
4.7.1.4	<i>Velocity Vector</i>	129
4.7.1.5	<i>Absolute Velocity</i>	133
4.7.2	Vorticity and Circulation	133
4.7.3	Turbulence Fields	140
4.8	Conclusions	146
4.9	Nomenclature	148
4.10	References	149

5. COMPARISON OF SCOUR GEOMETRY AND HORSESHOE VORTEX CHARACTERISTICS	151-154
6. CONCLUDING REMARKS	155-160
6.1 Synthesis of the Present Research	155
6.2 Further Scope of Similar Research	159
<i>Curriculum Vitae</i>	161
<i>Annexure</i>	163

List of Figures

Fig. 1.1	Pier groups of Nivedita Bridge and Vivekananda Bridge in India.	7
Fig. 1.2	Pier groups of First, Second and Third Mandovi Bridges in India.	7
Fig. 1.3	Pier groups of Memphis-Arkansas Bridge, Frisco Bridge and Harahan Bridge.	8
Fig. 1.4	Pier groups of John F.K. Bridge, Abraham Lincon Bridge and Big Four Bridge.	8
Fig. 2.1	Probe response in laminar and turbulent flow.	15
Fig. 2.2	An Eddy notation in turbulent flow.	15
Fig. 2.3	Time series of u -component of velocity.	17
Fig. 2.4	Stresses on a fluid element surface.	19
Fig. 2.5	Classification of flow region (layer thickness not to scale).	20
Fig. 2.6	Velocity profiles in different layers.	20
Fig. 2.7	Development of scour process.	23
Fig. 2.8	Development of scour process.	24
Fig. 2.9	Scour depth at a pier as a function of time (a) and of shear velocity (b) for a given pier and sediment size at constant flow depth.	26
Fig. 2.10	Flow pattern at circular pier.	28
Fig. 2.11	Scour depth in uniform sediment at a circular pier as a function of relative velocity in a deep flow relative to pier diameter (a) as a trend function, and (b) for a set of laboratory data.	30
Fig. 2.12	Coefficient K_σ variation of scour depth as a function of the geometric standard deviation of particle size distribution.	32
Fig. 2.13	Average local equilibrium scour depth at pier diameter $b = 4.5$ cm in uniform $\sigma_g < 1.3$ and non- sediment ($\sigma_g = 3.5$) with $d_{50} = 0.8$ mm and flow depth $h = 17$ cm.	33
Fig. 2.14	The ratio of local equilibrium scour depth $K(b/d_{50})$ affected by the relative size b/d_{50} to that independent of b/d_{50} for clear-water and live-bed scour conditions.	34
Fig. 2.15	Equilibrium Scour depth as a function of relative flow depth, h/b , with the ratio of b/d_{50} as parameter.	35
Fig. 2.16	Diagrammatic scour shapes at a pier aligned with flow and angled to the flow direction.	36
Fig. 2.17	Multiplying factor for scour depth for piers not aligned with flow.	37
Fig. 2.18	Scour at piers tapered in elevation. Dimensions are at original bed level.	38
Fig. 2.19	Scour depth at two piers in line spacing (scale of ordinate changes for the front pier).	40
Fig. 2.20	Scour-depth at two piers as a function of pier spacing. Thick lines	40

refer to piers transverse to flow and thin lines to angle of attack of 45° .

Fig. 2.21	Effect of angle of attack, α , on scour depth at two piers spaced five pier diameter apart.	41
Fig. 2.22	VectrinoPlus velocimeter operating principle.	42
Fig. 2.23	VectrinoPlus velocimeter.	43
Fig. 3.1	Schematic diagram showing the elevation wise flow patterns around three inline-eccentric-inline arranged circular piers.	52
Fig. 3.2	Top view for three inline-eccentric-inline arranged circular piers.	54
Fig. 3.3	Plan view for gauge and Vectrino measurements for three inline-eccentric-inline arranged circular piers.	55
Fig. 3.4	Scoured zones around three identical circular inline-eccentric-inline arranged piers for test nos. 1, 2 and 3.	57
Fig. 3.5	Scoured zones around three identical circular inline-eccentric-inline arranged piers for test nos. 4, 5 and 6.	58
Fig. 3.6	Scoured zones around three identical circular inline-eccentric-inline arranged piers for test nos. 7, 8 and 9.	59
Fig. 3.7	Contours of equilibrium scour holes around circular piers for test nos. 1, 2 and 3.	60
Fig. 3.8	Contours of equilibrium scour holes around circular piers for test nos. 4, 5 and 6.	61
Fig. 3.9	Contours of equilibrium scour holes around circular piers for test nos. 7, 8 and 9.	62
Fig. 3.10	Contours of u in cm/s for inline-front, eccentric-middle and inline-rear circular piers at r - z planes for $\theta = 0^\circ$ and 45° .	66
Fig. 3.11	Contours of u in cm/s for inline-front, eccentric-middle and inline-rear circular piers at r - z planes for $\theta = -45^\circ$ and 90° .	67
Fig. 3.12	Contours of u in cm/s for inline-front, eccentric-middle and inline-rear circular piers at r - z plane for $\theta = -90^\circ$ and at x - y planes for $z=0.04h$ and $z=0.5h$.	68
Fig. 3.13	Contours of v in cm/s for inline-front, eccentric-middle and inline-rear circular piers at r - z planes for $\theta = 0^\circ$ and 45° .	70
Fig. 3.14	Contours of v in cm/s for inline-front, eccentric-middle and inline-rear circular piers at r - z planes for $\theta = -45^\circ$ and 90° .	72
Fig. 3.15	Contours of v in cm/s for inline-front, eccentric-middle and inline-rear circular piers at r - z planes for $\theta = -90^\circ$ and at x - y planes for $z=0.04h$ and $z=0.5h$.	73
Fig. 3.16	Contours of w in cm/s for inline-front, eccentric-middle and inline-rear circular piers at r - z planes for $\theta = 0^\circ$ and 45° .	75
Fig. 3.17	Contours of w in cm/s for inline-front, eccentric-middle and inline-	76

	rear circular piers at r - z planes for $\theta = -45^\circ$ and 90° .	
Fig. 3.18	Contours of w in cm/s for inline-front, eccentric-middle and inline-rear circular piers at r - z planes for $\theta = -90^\circ$ and at x - y planes for $z=0.04h$ and $z=0.5h$.	77
Fig. 3.19	Velocity vector plots for inline-front, eccentric-middle and inline-rear circular piers at r - z planes for $\theta = 0^\circ$ and 45° .	79
Fig. 3.20	Velocity vector plots for inline-front, eccentric-middle and inline-rear circular piers at r - z planes for $\theta = -45^\circ$ and 90° .	80
Fig. 3.21	Velocity vector plots for inline-front, eccentric-middle and inline-rear circular piers at r - z planes for $\theta = -90^\circ$ and at x - y planes for $z=0.04h$ and $z=0.5h$.	81
Fig. 3.22	Contours of V in cm/s for inline-front, eccentric-middle and inline-rear circular piers at r - z planes for $\theta = 0^\circ$ and 45° .	83
Fig. 3.23	Contours of V in cm/s for inline-front, eccentric-middle and inline-rear circular piers at r - z planes for $\theta = -45^\circ$ and 90° .	84
Fig. 3.24	Contours of V in cm/s for inline-front, eccentric-middle and inline-rear circular piers at r - z planes for $\theta = -90^\circ$ and at x - y planes for $z=0.04h$ and $z=0.5h$.	85
Fig. 3.25	Contours of ζ (in s^{-1}) for inline-front, eccentric-middle and inline-rear circular piers at r - z planes for $\theta = 0^\circ$ and 45° .	87
Fig. 3.26	Contours of vorticity ζ (in s^{-1}) for inline-front, eccentric-middle and inline-rear circular piers at r - z planes for $\theta = -45^\circ$ and 90° .	88
Fig. 3.27	Contours of ζ (in s^{-1}) for inline-front, eccentric-middle and inline-rear circular piers at r - z planes for $\theta = -90^\circ$.	89
Fig. 3.28	Contours of (a) u^+ (b) v^+ in cm/s for inline-front, eccentric-middle and inline-rear circular piers at r - z plane for $\theta = 0^\circ$.	91
Fig. 3.29	Contours of w^+ in cm/s for inline-front, eccentric-middle and inline-rear circular piers at r - z plane for $\theta = 0^\circ$.	92
Fig. 3.30	Contours of (a) u^+ , (b) v^+ , and (c) w^+ in cm/s for inline-front-rear and eccentric-middle piers at x - y plane for $z=0.04h$ and $z=0.5h$.	93
Fig. 3.31	Contours of k in cm^2/s^2 for inline-front, eccentric-middle and inline-rear circular piers at r - z plane for $\theta = 0^\circ$ and at x - y plane for $z=0.04h$ and $z=0.5h$.	94
Fig. 4.1	Schematic diagram of flow pattern at three inline eccentrically arranged square piers.	107
Fig. 4.2	Top view for three inline eccentrically arranged square piers.	108
Fig. 4.3	Plan view for gauge and Vectrino measurements for three inline-eccentrically arranged square piers.	109
Fig. 4.4	Scoured zones around three square piers for test nos. 1, 2 and 3.	111
Fig. 4.5	Scoured zones around three identical square piers for test nos. 4 and 5.	112

Fig. 4.6	Contours of equilibrium scour hole around three square piers for test nos. 1, 2 and 3.	113
Fig. 4.7.	Contours of equilibrium scour hole around three square piers for test nos. 4 and 5.	114
Fig. 4.8.	Contours of u/U for square front, square eccentric and square rear piers at r - z planes for $\theta = 0^\circ$ and 45° .	116
Fig. 4.9.	Contours of u/U for square front, square eccentric and square rear piers at r - z planes for $\theta = -45^\circ$ and 90° .	117
Fig. 4.10.	Contours of u/U for square front, square eccentric and square rear piers at r - z plane for $\theta = -90^\circ$ and at r - y planes for $z=0.04h$ and $z=0.5h$.	118
Fig. 4.11.	Contours of v/U for square front, square eccentric and square rear piers at r - z planes for $\theta = 0^\circ$ and 45° .	121
Fig. 4.12.	Contours of v/U for square front, square eccentric and square rear piers at r - z planes for $\theta = -45^\circ$ and 90° .	122
Fig. 4.13.	Contours of v/U for square front, square eccentric and square rear piers at r - z planes for $\theta = -90^\circ$ and at r - y planes for $z=0.04h$ and $z=0.5h$.	123
Fig. 4.14.	Contours of w/U for square front, square eccentric and square rear piers at r - z planes for $\theta = 0^\circ$ and 45° .	126
Fig. 4.15.	Contours of w/U for square front, square eccentric and square rear piers at r - z planes for $\theta = -45^\circ$ and 90° .	127
Fig. 4.16.	Contours of w/U for square front, square eccentric and square rear piers at r - z planes for $\theta = -90^\circ$ and at r - y planes for $z=0.04h$ and $z=0.5h$.	128
Fig. 4.17.	Velocity vector plots for square front, square eccentric and square rear piers at r - z planes for $\theta = 0^\circ$ and 45° .	130
Fig. 4.18.	Velocity vector plots for square front, square eccentric and square rear piers at r - z planes for $\theta = -45^\circ$ and 90° .	131
Fig. 4.19.	Velocity vector plots for square front, square eccentric and square rear piers at r - z planes for $\theta = -90^\circ$ and at r - y planes for $z=0.04h$ and $z=0.5h$.	132
Fig. 4.20.	Contours of V/U for square front, square eccentric and square rear piers at r - z planes for $\theta = 0^\circ$ and 45° .	134
Fig. 4.21.	Contours of V/U for square front, square eccentric and square rear piers at r - z planes for $\theta = -45^\circ$ and 90° .	135
Fig. 4.22.	Contours of V/U for square front, square eccentric and square rear piers at r - z planes for $\theta = -90^\circ$ and at r - y planes for $z=0.04h$ and $z=0.5h$.	136
Fig. 4.23.	Contours of ζ (in s^{-1}) for square front, square eccentric and square rear piers at r - z planes for $\theta = 0^\circ$ and 45° .	137

Fig. 4.24.	Contours of ζ (in s^{-1}) for square front, square eccentric and square rear piers at r - z planes for $\theta = -45^\circ$ and 90° .	138
Fig. 4.25.	Contours of ζ (in s^{-1}) for square front, square eccentric and square rear piers at r - z planes for $\theta = -90^\circ$.	139
Fig. 4.26.	Contours of (a) u^+/U (b) v^+/U for square front, square eccentric and square rear piers at r - z plane for $\theta = 0^\circ$.	142
Fig. 4.27.	Contours of w^+/U for square front, square eccentric and square rear piers at r - z plane for $\theta = 0^\circ$.	143
Fig. 4.28.	Contours of (a) u^+/U , (b) v^+/U , and (c) w^+/U for square front, square eccentric and square rear piers at r - y plane for $z=0.04h$ and $z=0.5h$.	144
Fig. 4.29.	Contours of k/U^2 for square front, square eccentric and square rear piers at r - z plane for $\theta = 0^\circ$ and at r - y plane for $z=0.04h$ and $z=0.5h$.	145

List of Tables

Table 2.1.	Pier shape coefficients.	37
Table 2.2.	Shape factors for tapered piers.	38
Table 3.1.	Experimental conditions for all conducted tests.	54
Table 3.2.	Magnitudes of geometric parameters at equilibrium scour for nine tests conducted.	56
Table 3.3.	Circulation Ω for five azimuth angles in r - z plane (units in $10^{-2} \times m^2/s$).	86
Table 4.1.	Experimental conditions for all conducted tests.	108
Table 4.2.	Run duration for all conducted tests.	110
Table 4.3.	Magnitudes of geometric parameters at equilibrium scour for five tests conducted.	112
Table 4.4.	Circulation Ω for five azimuth angles in r - z plane (units in $10^{-2} \times m^2/s$).	140

1. INTRODUCTION

1.1 Introduction to Sediment Transport Dynamics on Scour

The formation of clear water scour around a pier is due to the interaction within the pier, the approach flow and the erodible bed particles. The obstruction of a pier results in a stagnation pressure build up in the frontal region of the pier and a three dimensional turbulent flow, which is characterized by a down flow ahead of the pier within the horseshoe vortex, which forms along the base of the pier itself. The flow reshapes the erodible sand bed around the region of the pier, where, local scour takes place. The downward flow initiates the scouring process, further up, influenced by the vortices. The process of scouring takes place either in clear water or in live bed condition along the channel the phenomenon of local scouring occurs for the interaction among various parameters, like the fluid, the fluid flow, the time, the bed material and the pier.

Nowadays, multi pier arrangements are becoming much more popular in design of bridges due to its geotechnical and economical usefulness. In past-recent years, there is a need and subsequent trend to construct new road bridges and new rail bridges beside the old existing bridges because of the heavy cross-river traffic, increase of vehicles and heavy vehicles day by day.

In multi pier arrangement, the wake vortex of the upstream pier may influence the horseshoe vortex of the downstream positioned pier. When the piers are arranged inline-eccentrically, the sediment may move towards the bank of the waterways or towards the downstream. Here, in case of inline-eccentric-inline pier arrangement, the interference between the wake vortex of the inline-front pier and horseshoe vortex of the eccentric-middle pier in addition to the horseshoe vortex of the inline-rear pier and wake vortex of the eccentric-middle pier may play important role in the creation and formation of the greater scour depth around all the three piers. From each pier bases the sediment particles may get removed and deposited towards downstream region, mostly on one side of hydraulic flume. Therefore the shifting of sediment particles may deposited onto the eccentric-middle pier region and on that side, diversion angle may also be more. This may occur due to the separation of curvilinear streamlines from the inline-front pier and thereafter if it proceeds along downstream.

On the upstream right side of the inline-front pier these streamlines are expected to move straight towards downstream. Whereas on the upstream left side of the inline-front pier streamlines may get obstructed by eccentric-middle pier. Further up, these curvilinear streamlines may stretch and move downstream towards the left side of the eccentric-middle pier.

Therefore, one needs a set of measured scour geometry analysis and a basic knowledge of sediment transport dynamics (both horseshoe and wake vortex) and structure information like flow fields, vorticity, circulation, turbulent intensities, kinetic energy, bed shear stress etc to describe the sediment transport dynamics around the multi pier arrangements for future research.

1.2 State of the Art

Flow behaviour around multiple piers is a classical problem. Prediction of local scour holes at hydraulic structures plays an important role in their design and especially in designing bridge structure. Excessive local scour can progressively make the foundation of the structure weaker and lead to failure of the hole structure. Sediment transport for local scour around piers is the main reason for destruction of many piers that causes bridges to become unsafe and further up to collapse inside the river. For safe bridge design, an estimation of maximum possible scour around the pier is necessary. Over the year there are various laboratory-flume experiments to predict the scour depth around the base of the piers by Laursen and Toch (1956), Liu *et al.* (1961), Shen *et al.* (1969), Breusers *et al.* (1977), Jain and Fischer (1979), Raudkivi and Ettema (1983), Froehlich (1989), Breusers and Raudkivi (1991), Melville (1992), Sumer and Fredsoe (1992), Dey (1997), Hoffmans and Verheij (1997), Melville and Chiew (1999); Melville and Coleman (2000), Richardson and Davis (2001), Barbhuiya and Dey (2004), Ashtiani and Beheshti (2006) Khwairakpam *et al.* (2012) and Das *et al.* (2014a-c). Most of these studies are confined to single pier. These studies have been performed primarily by means of laboratory-flume experiments, including the use of dimensionless equations finally resulting in some semi-empirical equations for computing the maximum scour depth.

From these equations, there is a tendency to over predict the maximum scour depth for field or even for laboratory conditions [Melville (1975) and Dargahi (1990)]. A lack of understanding of the flow structure around the bridge piers and their interaction with the bed sediment seems to be at least partly responsible for this problem. Therefore, many laboratory flume based experiments were investigated by numerous researchers to for accumulating more information on flow behaviour and sediment transport dynamics and to compute scour depth with more precession. Many of the researchers stressed on velocity and subsequent pattern of the turbulent flow-field at differently shaped pier [Melville (1975), Melville and Raudkivi (1977), Dargahi (1989), Dargahi (1990), Dey *et al.* (1995), Ahmed and Rajaratnam (1998), Graf and Yulistiyanto (1998), Istiarto and Graf (2001), Graf and Istiarto (2002), Muzzammil and Gangadhariah (2003), Roulund *et al.* (2005), Ettema *et al.* (2006), Unger and Hager (2007), Kirkil *et al.* (2008, 2009)].

For better understanding of the sediment transport dynamics based on flow field and turbulent flow field at clear water equilibrium condition around piers and cylinders, there are a few experiments which were conducted on single-pier for determining more accurate scour depth based on vortex velocity flow fields [Dey and Raikar (2007), Raikar and Dey (2008), Das *et al.* (2013a-c), Das and Mazumdar (2015a)]. These studies have been confined to only single pier and provide detailed information around single pier. Some of the studies are discussed below.

Melville (1975) [also see, Melville and Raudkivi (1977)] was the pioneer who measured mean flow directions, mean flow magnitude, turbulent flow fluctuations and shear stresses around a circular pier (5.08 cm in diameter) for flat bed, intermediate an equilibrium scour holes in a 45.6 cm wide laboratory flume. He found that a strong vertically downward flow developed ahead of the circular pier as the scour hole enlarged. The size and the circulation of the horseshoe vortex increased rapidly, and the velocity near the bottom of the hole

decreased as the scour hole was enlarged. The magnitude of the downflow appeared to be directly associated with scour. The rate of increase of circulation fell off as the scour hole developed and reached a constant value at the equilibrium stage. The combination of temporal mean bed shear and turbulent agitation at the bed tended to decrease as the scour hole enlarged until equilibrium was reached.

Dargahi (1990) experimentally investigated the flow field around a circular pier mounted vertically on a flat bottom. Hydrogen bubble flow visualisation was carried out for Reynolds numbers ranging from 6600-65000. It was observed that the main flow characteristics upstream of the circular piers in a system of horseshoe vortices which are shed quasi-periodically. The vortex system was found to be independent of the vortices that are shed in the wake of the circular pier. The dimensions of vortex system were found to be independent of the Reynolds number and were primarily determined by the width of the pier.

Dey *et al.* (1995) investigated the quasi-steady vortex flow field around circular pier in clear-water quasi-equilibrium scour hole. Velocity vectors were measured by a five hole pitot sphere at different azimuthal planes; 0, 15, 30, 45, 60 and 75 degrees. Variation of circulation was presented with respect to pier Reynolds number ($R_p = Ub/\nu$ where U is the depth averaged approaching flow velocity, ν is the kinematic viscosity) at 0° for all eighteen tests. The study showed satisfactory agreement with the observation of Melville (1975).

Ahmed and Rajaratnam (1998) explained the velocity distributions in the upstream axis of symmetry within a scour hole at a circular pier by using a Clauser-type defect method.

Graf and Yulistiyanto (1998) investigated experimentally the flow fields around the circular pier position normal to the flow in an open channel for two types of flow. An acoustic-Doppler velocity profiler (ADVP) was used to obtain instantaneously the three directions of the velocity in the flow. Subsequently, the vorticity of the flow field was calculated. Results of the experiments showed that a horseshoe vortex system had been established, consisting of a measurable vortex with an underneath return flow of negative vorticity. The system develops itself in the upstream corner at the nose of the pier and stretches around the pier towards the downstream flow. They observed that the strength and location of this horseshoe vortex system depend on the approach flow velocity. It could be parameterised by the flow Reynolds number. The system is stronger and closer to the base of the pier, which causes a higher flow velocity. Flow separation and reversal occurred downstream from the pier and turbulence intensity increased. The horseshoe vortex system, where the turbulence becomes very strong, produced a high bed shear stress beneath it.

Graf and Istiarto (2002) [see also, Istiarto and Graf (2001)] experimentally investigated the three dimensional flow fields in an established (equilibrium) scour hole. An ADVP was used to measure instantaneously the three components of the velocities in the vertical symmetry (stagnation) plane of the flow before and after the pier. The velocities, turbulence intensities, Reynolds stresses, bed shear stresses and vorticity of the flow field were calculated in different azimuthal planes within the equilibrium scour hole around the circular pier. Outcomes showed that a vortex system was established near the front and a trailing wake vortex system of strong turbulence was formed at the rear of the pier.

Muzzammil and Gagadhariah (2003) demonstrated how that the primary horseshoe vortex forms in front of a circular pier which is the prime agent responsible for scour during the entire process of scouring. An expression for the maximum equilibrium scour depth was

also developed from the vortex velocity distribution inside the scour hole. The resulting scour prediction equation was found to give better results compared to the results of well-known predictor models when applied to model scour data.

Dey and Raikar (2007) stated the outcomes of an experimental research on turbulent horseshoe vortex flow within the developing intermediate stages (having depths of 0.25, 0.5 and 0.75 times the equilibrium scour depth) and equilibrium scour holes at azimuth angle 0° , 45° and 90° for cylindrical and square piers captured by an ADV. The flow characteristics of horseshoe vortex were discussed from the point of view of the similarity with the velocity and turbulence characteristics scale. They compared experimental outcomes on the turbulent horseshoe vortex flow within equilibrium scour holes at circular and square piers.

Raikar and Dey (2008) made an experimental investigation on the characteristics of the development of turbulent horseshoe vortex flow in an evolving intermediate stages (having depths of 0.25, 0.5 and 0.75 times the equilibrium scour depth) and equilibrium scour hole around square cylinder gauged by ADV. The flow characteristics of the horseshoe vortex were studied from the point of view of similarity with the velocity and turbulence characteristic scales for better understanding of the hydrodynamic flow fields at clear water equilibrium condition.

Das and Mazumdar (2015a) conducted experiments on single flat plate, circular pier, square pier, and equilateral triangular pier (side facing flow) for determining more accurate scour depth. They also measured velocity components by ADV. They explained the horseshoe vortex flow and turbulence characteristics from the point of similarity with velocity and turbulence intensity characteristic scales.

There are a large number of studies around pier groups and complex piers that provide detailed information on sediment transport dynamics. For a pier in a multi-pier arrangement, combined effects are notable, in addition with those parameters which influence scouring around single-pier arrangement. Sheppard *et al.* (1995) carried out researches on two pier arrangements, where the piers were located along the direction (inline) of flow and found that two additional parameters reinforcement and sheltering effect the flow. Most of the multi-pier experiments have been restricted to two pier arrangements, positioned either inline-eccentric, inline-inline or side by side that focused on the prediction of flow-field, turbulent field and the scour geometry [Zdravkovich (1987), Sumner *et al.* (1999), Akilli *et al.* (2004), Coleman (2005), Ashtiani and Beheshti (2006), Mahjoub *et al.* (2008), Ashtiani *et al.* (2010), Ashtiani and Kordkandi (2012, 2013), Das *et al.* (2014b), Das and Mazumdar (2015b, 2018)] and the effect of pier spacing on flow characteristics and on sediment transport dynamics [Raudkivi (1998), Graf (2003), Das *et al.* (2014, 2016) and Yilmaz *et al.* (2017)].

The information on sediment transport dynamics around two-piers arrangements are discussed below.

A research [Michael *et al.* (1991)] on two-pier with inline-eccentric arrangement can amplify sediment to move towards the river bank flowing downstream was described. The horseshoe vortex at the middle of two piers will take a major role in enhancing the scour hole around the downstream pier and sediments are transported away from the downstream axis of symmetry.

Zdravkovich (1987) found that depending on the pier spacing, the wake vortex structures change behind the piers.

Beheshti and Ashtiani (2010) experimentally investigated the three-dimensional turbulent flow field around a complex bridge pier placed on a rough fixed bed. The complex pier foundation consisted of a column, a pile cap and a 2×4 pile group. All of the elements were exposed to the approaching flow. An ADV was used to measure instantaneously the three components of the velocities at different horizontal and vertical planes. Their study does not provide a better understanding of flow field around piles situated under a pile cap and inside the scour hole.

Ashtiani and Kordkandi (2012) investigated the three-dimensional flow around two side-by-side circular piers. The flow characteristics in the near-wake region around piers were investigated. They addressed how the horseshoe vortex flow and corresponding turbulence characteristics change between the two piers and how the two piers affect the flow structure and its intensity in comparison with a single pier case. The single pier tests were carried out by the authors in order to have a comparative study in the same experimental conditions as for the two side-by-side piers. They observed that the scour is initiated at, or close to the nose of the cylinders as well as around the piers, especially between the two piers and the scour hole of each pier increase and then overlaps each other at the region between the two piers. Due to decrease in the flow area between the two piers, a contracted flow is formed.

Ashtiani and Kordkandi (2013) investigated the three-dimensional flow around two circular piers in tandem and around a single pier. Velocities were measured by an ADV. In addition, they addressed how the horseshoe vortex flow and corresponding turbulence characteristics change between the two piers and how the two piers affect the flow structure and its intensity in comparison with a single pier case. The single pier tests were carried out in the same experimental conditions as for the two circular piers in tandem. The presence of rear pier changes the flow structure to a great extent, particularly in the near-wake region. Within the gap between the two piers, a stronger and substantial upflow was shaped.

Three dimensional flow-fields, turbulence-fields for horseshoe-vortex around two equilateral triangular piers [Das *et al.* (2014c)], two circular piers [Das and Mazumdar (2015b)] and two square piers [Das and Mazumdar (2018)] of equal width b positioned in inline front and eccentric rear arrangement with constant eccentricity $3b$ under similar experimental conditions were investigated. Eccentricity and longitudinal gap were taken as thrice of pier size and half the maximum length transported by sediment particles at equilibrium state for single pier test, respectively.

The three-dimensional flow and turbulence field interactions around two equilateral triangular, two circular and two square piers with inline front and eccentric rear pier arrangement at different vertical planes, were investigated. The contours and distributions of the time-averaged velocity components, turbulence intensities and turbulence kinetic energy at different vertical planes are presented. They addressed how the horseshoe vortex flow formations and consequent turbulence characteristics vary between the two identical piers and how the two piers influence the flow formation and its intensity. The end results of the each lab-flume experiment were compared with the result of a single pier experiment for corresponding pier-shape with same experimental conditions.

And lastly the outcomes of the three experiments were compared. Further lab-flume experiments [Das *et al.* (2016)] were executed for investigating the pattern of scour formation around two circular, square and equilateral-triangular tandem piers at constant eccentricity. It

was observed that pattern of scour varies by changing longitudinal distance (spacing) between the piers. The scour angle of diversion and deposition of the sand was observed more on of eccentric pier side towards the wall. Biggest scour hole was found near square-piers compared to the triangular and circular-piers, respectably.

On basis of the previous studies on scouring, the present study on scouring differs in the context of dealing with three identical circular and square shaped piers and how the scouring differs with it. It is obvious that almost no experimental work was carried out to study the sediment transport dynamics and also the horseshoe vortex flow pattern and characteristics around the three piers with inline-eccentric-inline arrangement placing two of them inline along the flow and the third one eccentrically in mid of them with a constant eccentricity.

The main objective of this research is to observe the interactions between three-dimensional flow fields and turbulence fields around the three piers. In the present study an attempt has also been made to carry out experiments with inline-eccentric-inline arrangement of pier groups varying the longitudinal spacing and to delineate the scour geometry.

1.3 Relevance in the Real Field

In past-recent years, due to heavy cross-river traffic, increase of vehicles and heavy vehicles many new road and rail bridges have been constructed beside the old existing bridges. The shapes of the bridge piers are not always alike but for each case the bridge pier of the new bridge and the bridge pier of the old bridge are placed eccentrically (across the flow) and they have a common gap (longitudinal spacing) along the flow as well. Examples of such new and old bridges having eccentrically arranged piers are addressed below and photographs are shown in Fig. 1.1-1.4.

One such set of bridges are located at Kolkata in West Bengal, India, where the Nivedita Setu (bridge) was constructed just downstream of the old existing Vivekananda Setu (bridge). In this case there is an influence of piers of one bridge on another as the bridges are very near to each other and also new bridge (Nivedita) piers are not positioned in tandem with respect to the piers of old bridge (Vivekananda) (Fig. 1.1).

Another such example is at Goa in India. The Mandovi Bridge is one of the most famous and longest bridges in Goa. Before the bridge was built, the ferry was the main mode of transport across River Mandovi well into the 1970s between Panaji and Betim village. Due to heavy traffic the first bridge was built in the 1970s. The second bridge was constructed in 1998 in order to accommodate heavy transport vehicles. The third bridge was constructed in between the two existing bridges and opened on 5th February 2019 to accommodate heavy traffic especially during the peak year end tourist season. In the case of first, second and third Mandovi bridges, the pier of the third and second bridges were constructed in eccentric arrangement with respect to the first (old) Mandovi Bridge (Fig. 1.2).

There are three bridges over Mississippi river in Tennessee, USA. The upstream structure is Harahan Bridge (1916), the Frisco Bridge (1892) is middle structure and the third structure is Memphis-Arkansas Memorial Bridge (1949). Harahan Bridge and Memphis-Arkansas Memorial Bridge were constructed for heavy load transportation and safer navigation. The three bridges follow approximately the same pier spacing. The piers of the

Harahan Bridge, Frisco Bridge and Memphis and Arkansas Memorial Bridge were constructed in-line (Fig. 1.3).

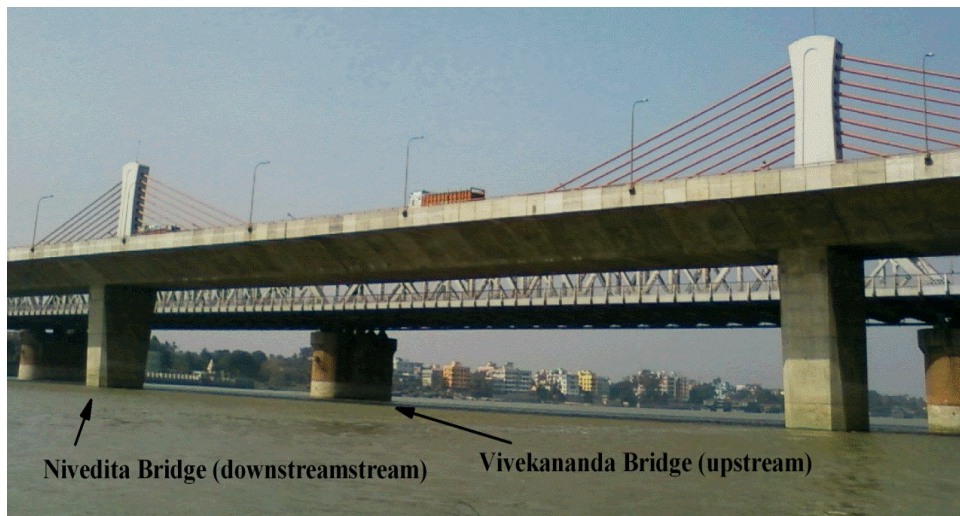


Fig. 1.1. Pier groups of Nivedita Bridge (new) and Vivekananda Bridge (old) in India.



Fig. 1.2. Pier groups of First, Second and Third Mandovi Bridges in India.

Another example of side-by-side arranged multiple bridge piers is shown in Fig. 1.4. Here the names of such bridges are Big four bridge constructed in 1885, John F. Kennery Memorial Bridge constructed in 1963 and the Abraham Lincon Bridge constructed in very recently in 2015. These bridges are positioned side-by-side across the Ohio River, Indiana in USA. The recent one was constructed in between the previous two bridges. But actually it is very close to the oldest bridge. From Fig. 1.4, it is clear that the oldest and newest bridges were positioned inline whereas the other one is located eccentricly with respect to these oldest and newest bridges.

There must be influence of pier of one bridge onto another to cause more scour if the bridges are constructed closely to each other. Therefore in a multi-pier arrangement, for each

pier such combined effects must be observed in addition with those parameters which influence scour around single pier arrangement.



Fig. 1.3. Pier groups of Memphis-Arkansas Bridge, Frisco Bridge and Harahan Bridge.



Fig. 1.4 Pier groups of John F.K. Bridge, Abraham Lincon Bridge and Big Four Bridge.

In relevance with present study, it is clear that very few researches were performed to study the scour geometry and flow hydrodynamics and subsequent turbulence patterns around multiple piers for existing side by side bridges or for such three pier group arrangements where one eccentric and two inline piers are placed. The vortices in between the three piers can enlarge the scour holes around the piers and the scour hole around the eccentric pier may become bigger. As a result of eccentric positioning of new bridge piers with the existing bridge piers and longitudinal spacing (gap) between them, the time span of the new bridges may be reduced and may lead to a manmade collapse in future. In relevance with the real

field, here principal endeavour is to perform laboratory flume tests using three circular/square piers in inline-eccentric-inline arrangement and to determine the flow hydrodynamics including the characteristics of vortices.

1.4 Present Scope of Work

Previous researchers evidently showed the way in which the present work scope should be investigated. Experimental work are needed in the field of sediment transport dynamics with special emphasis on the clear water scour mechanism and turbulence effect around the three (circular / square) piers with inline-eccentric-inline arrangement.

Chapter 2

In chapter 2, a general explanation about a brief introduction to the subjects relevant to clear water scour mechanism, vortex effect and scour at pier groups backed by a literature review can be found. This chapter includes some essential information about transport mechanism of sediments, different types of scour, local scour mechanism due to acceleration of flow and resulting vortices.

Chapter 3

In this chapter an attempt has been made to conduct laboratory flume based experimental studies on the formation and characteristics of local equilibrium scour around a set of three circular piers with inline-eccentric-inline arrangement placed in staggered manner on sand bed. Two inline-front circular pier and inline-rear circular piers were set along the flow and the third one is set eccentrically in mid region of inline-front and inline-rear circular piers.

A set of nine experiments were carried out in clear water scour condition, with the objective to observe the nature of scour evolved and to study the nature and location of scour formed around the piers and the mutual interference of flow between the piers during the formation of scour hole, by varying the longitudinal spacing between the two inline circular piers. The eccentricity was kept constant equal to $3b$ (where b is the diameter of a pier) and the spacing along the flow between the inline front and eccentric-middle circular pier considered were $0.25 l_{ss}$, $0.375 l_{ss}$, $0.50 l_{ss}$, $0.625 l_{ss}$, $0.75 l_{ss}$, $0.875 l_{ss}$, $1.00 l_{ss}$, $1.125 l_{ss}$ and $1.25 l_{ss}$ where, l_{ss} is the maximum equilibrium length of sediment transport (sum of maximum equilibrium scour length and dune length) of a single circular pier. For each experiment, maximum equilibrium scour depth, length, width, surface area and volume of bed material removed were observed.

In order to have a comparative and more accurate study, this chapter provides the experimental results of the hydrodynamic flow and turbulent flow pattern around the three identical circular piers in inline-eccentric-inline arrangement, with constant longitudinal spacing $0.5l_{ss}$ and constant eccentricity $3b$. The detailed 3-D velocities were captured instantaneously by using ADV at five different vertical azimuth-planes (0° , $\pm 45^\circ$, $\pm 90^\circ$) positioned around the three circular piers and also at two horizontal-planes around the three circular piers at 4% and 50% of approaching flow-depth above bed level ($h=0$).

The contour profiles and distribution of velocity-components, turbulence kinetic energy and intensities are computed and analysed at the vertical r - z planes and horizontal x - y planes around the three circular piers. The velocity-vectors plot and time-mean absolute-velocity acquired from velocity-profile shows detailed hydrodynamic flow characteristics. Vorticity and circulation generated at the upstream zone near the three square piers are presented.

Chapter 4

An attempt has been made to conduct a set of laboratory flume based experimental studies on the formation and characteristics of local equilibrium scour around a set of three identical square piers with inline-eccentric-inline arrangement placed in a staggered manner on sand bed. Subsequent hydrodynamic outcomes are explained in this chapter. The two piers – square-front and square-rear ones were positioned along the flow and the third one square eccentric was set eccentrically in mid region of two inline piers with a constant eccentricity $3b$, where b is the base width of each pier.

Square shaped three identical piers were chosen to carry out a set of five experiments in clear water condition with the objective to observe the nature of scour evolved and to study the nature and location of scour formed around the piers and the mutual interference of flow between the piers during the formation of scour hole, by varying the longitudinal spacing between the two inline square piers. The eccentricity was kept constant and set equal to $3b$ throughout all the experiments. The considered spacing along the flow between the square front and square eccentric pier were $0.25 l_{ss}$, $0.375 l_{ss}$, $0.50 l_{ss}$, $0.625 l_{ss}$, $0.75 l_{ss}$ where l_{ss} is the maximum equilibrium length of sediment transport (sum of maximum equilibrium scour length and dune length) for a single square pier experiment.

Outcomes for each experiment, maximum equilibrium scour depth, length, width, surface area and volume were observed and determined. In order to have a comparative study, this chapter also provides the experimental results of the hydrodynamic turbulent flow pattern around the three identical square piers arranged inline-eccentrically with constant longitudinal spacing equal to half of the l_{ss} and constant eccentricity $3b$.

The detailed three dimensional velocities were captured instantaneously by using an ADV at five different vertical azimuthal planes (-90^0 , -45^0 , 0^0 , 45^0 and 90^0) positioning around the three square piers and also at two horizontal planes having 4% and 50% of approaching flow-depth above bed level ($h=0$). The contour profiles and distributions of non-dimensional velocity-components, non-dimensional turbulence intensities and non-dimensional kinetic energy are computed and analysed at the vertical r - z planes and horizontal x - y planes around the three square piers. The velocity-vectors plot and non-dimensional time-mean absolute-velocity acquired from velocity-profile shows detailed hydrodynamic flow characteristics. Vorticity and circulation generated at the upstream zone near the three square piers are also presented.

Chapter 5

In the two previous chapters the nine experiments on circular pier (Chapter 3) and five experiments on square pier (Chapter 4) on similar investigational setup and conditions, the

outcomes obtained for the clear water equilibrium scour holes, geometrical parameters like scour depth, length, width, hole surface area and volume and flow fields and turbulence fields were analysed. It is essential to compare the present findings of scour geometry and horseshoe vortex characteristics around circular shaped pier with the square shaped piers and a comparison has been made between the circular and square pier experiments in this chapter.

1.5 References

- Ahmed, F.; Rajaratnam, N.: Flow around bridge piers. *J. Hydraul. Eng.* 124(3), 288-300 (1998)
- Akilli, H.; Akar, A.; Karakus, C.: Flow characteristics of circular cylinders arranged side-by-side in shallow water. *Flow Meas. Instrum.* 15(4), 187-189 (2004)
- Ashtiani, A.B.; Beheshti, A.A.: Experimental investigation of clear-water local scour at pile groups. *J. Hydraul. Eng.* 132(10), 1100-1104 (2006)
- Ashtiani, A. B.; Ghorghi, B.Z.; Beheshti, A.A.: Experimental Investigation of Clear-Water Local Scour of Compound Piers. *J. Hydraul. Eng.* 136(6), 343–351 (2010)
- Ashtiani, A.B.; Kordkandi, A.A.: Flow field around side-by-side piers with and without a scour hole. *Eur. J. Mech. B/Fluid.* 36, 152-166 (2012)
- Ashtiani, A.B.; Kordkandi, A.A.: Flow field around single and tandem piers. *Flow Turbul. Combust.* 90(3), 471-490 (2013)
- Barbhuiya, A.K.; Dey, S.: Local scour at abutments: A review. *Sadhana, Academy Proc. in Eng. Sci.* 29(5), 449-476 (2004)
- Blanckaert, K.; Lemmin, U.: Means of noise reduction in acoustic turbulence measurements, *J. Hydraul. Res.* 44(1), 3–17 (2006)
- Breusers, H.N.C.; Raudkivi, A.J.: Scouring, IAHR Hydraulic Structures Design Manual, Vol. 2, A. A. Balkema Publ., Rotterdam, The Netherlands. (1991)
- Breusers, H.N.C.; Nicollet, G.; Shen, H.W.: Local Scour Around Cylindrical Piers. *J. Hydraul. Res.* 15(3), 211-252 (1977)
- Coleman, S.E.: Clear water local scour at complex piers. *J. Hydraul. Eng.* 131(4), 330-334 (2005)
- Dargahi, B.: The turbulent flow field around a circular cylinder. *Exp. Fluid.* 8(1–2), 1–12 (1989)
- Dargahi, B.: Controlling Mechanism of Local Scouring, *J. Hydraul. Eng.* 116(10), 1197–1214 (1990)
- Das, R.; Khwairakpam, P.; Das, S.; Mazumdar, A.: Clear-water local scour around eccentric multiple piers to shift the line of sediment deposition. *Asian J. Water Environ. Pollut.* 11(3), 47-54 (2014)
- Das, S.; Das, R.; Mazumdar, A.: Velocity profile measurement technique for scour using ADV. In: Proceedings of the 2015 International Conference on Testing and Measurement: Techniques and Applications, TMTA 2015. Taylor & Francis Group, London, pp. 249-252 (2015)
- Das, S.; Das, R.; Mazumdar, A.: Comparison of local scour characteristics around two eccentric piers of different shapes. *Arab. J. Sci. Eng.* 41(4), 1193-1213 (2016)

- Das, S.; Mazumdar, A.: Comparison of kinematics of horseshoe vortex at a flat plate and different shaped piers. *Int. J. Fluid Mech. Res.* 42(5), 418-448 (2015a)
- Das, S.; Mazumdar, A.: Turbulence flow field around two eccentric circular piers in scour hole. *Int. J. River Basin Manag.* 13(3), 343-361 (2015b)
- Das, S., Mazumdar, A.: Evaluation of Hydrodynamic Consequences for Horseshoe Vortex System developing around two eccentrically arranged Identical Piers of Diverse Shapes. *KSCE J. Civil Eng.* 22(7), 2300-2314 (2018)
- Das, S.; Das, R.; Mazumdar, A.: Circulation characteristics of horseshoe vortex in the scour region around circular piers. *Water Sci. Eng.* 6(1), 59-77 (2013a)
- Das, S.; Das, R.; Mazumdar, A.: Comparison of Characteristics of Horseshoe Vortex at Circular and Square Piers. *Research J. Appl. Sci. Eng. Tech.* 5(17), 4373-4387 (2013b)
- Das, S.; Midya, R.; Das R.; Mazumdar, A.: A Study of Wake Vortex in the Scour Region around a Circular Pier. *Int. J. Fluid Mech. Res.* 40(1), 42-59 (2013c)
- Das, S.; Das, R.; Mazumdar, A.: Variations of clear water scour geometry at piers of different effective widths. *Turkish J. Eng. Environ. Sci.* 38(1), 97-111 (2014a)
- Das, S.; Ghosh, S.; Mazumdar, A.: Kinematics of horseshoe vortex in a scour hole around two eccentric triangular piers. *Int. J. Fluid Mech. Res.* 41(4), 296-317 (2014b)
- Das, S.; Ghosh, R.; Das, R.; Mazumdar, A.: Clear Water Scour Geometry around Circular Piers. *Ecol. Environ. Conserv.* 20(2), 479-492 (2014c).
- Dey, S.: Local Scour at Piers, Part 1: A Review of Development of Research, *Int. J. Sediment Res.* 12(2), 23–44 (1997).
- Dey, S.; Bose, S.K.; Sastry, G.L.N.: Clear water scour at circular piers: a model. *J. Hydraul. Eng.* 121(12), 869-876 (1995)
- Dey, S.; Raikar, R.V.: Characteristics of horseshoe vortex in developing scour holes at piers. *J. Hydraul. Eng.* 133(4), 399-413(2007)
- Ettema, R.; Kirkil, G.; Muste, M.: Similitude of large scale turbulence in experiments on local scour at cylinders. *J. Hydraul. Eng.* 132(1), 33–40 (2006)
- Elliott, K.R.: Effect of pier spacing on scour around bridge piers. *J. Hydraul. Res.* 1105-1109 (1985)
- Froehlich, D.C.: Local scour at bridge abutments. *Proc. Nat. Conf. on Hydraul. Eng.*, New York. 13-18 (1989)
- Graf, W.H.: Fluvial Hydraulics, Flow and transport processes in channels of simple geometry. *John Wiley and Sons*, Great Britain. (2003)
- Graf, W.H.; Istiarto, I.: Flow pattern in the scour hole around a cylinder. *J. Hydraul. Res.* 40(1), 13-20 (2002)
- Graf, W.H.; Yulistiyanto, B.: Experiments on flow around a cylinder: the velocity and vorticity fields. *J. Hydraul. Res.* 36(4), 637-653 (1998)
- Hoffmas, G.J.C.M.; Verheij, H.J.: Scour Manual. *A. A. Balkema Publ.*, Rotterdam, The Netherlands. (1998)
- Istiarto, I.; Graf, W. H.: Experiments on flow around a cylinder in a scoured channel bed. *Int. J. Sediment Res.* 16(4), 431-444 (2001)
- Jain, S.C.; Fischer, E.E.: Scour around bridge piers at high Froude numbers. Report no. FHWA-RD-79-104, *Federal Highway Administration*. Washington D. C.

- Khwairakpam, P.; Ray, S.S.; Das, S.; Das, R.; Mazumdar, A.: Scour hole characteristics around a vertical pier under clear water scour conditions. *ARPN J. Eng. Appl. Sci.* 7(6), 649-654 (2012)
- Kirkil, G.; Constantinescu, S.G.; and Ettema, R.: Coherent structures in the flow field around a circular cylinder with scour hole. *J. Hydraul. Eng.* 134(5), 572–587 (2008)
- Kirkil, G.; Constantineous, S.G.; Ettema, R.: Detached eddy simulation investigation of turbulence at a circular pier with scour hole. *J. Hydraul. Eng.* 135(11), 888-901 (2009)
- Laursen, E.M.; Toch, A.: Scour around bridge piers and abutments. *Iowa Highway Res. Board.* Ames, Iowa. (4) (1956)
- Lui, H.K.; Chag, F.M.; Skinner, M.M.: Effect of bridge construction on scour and backwater. Report No. CER60HKL22, *Civil Eng. Section, Colorado State Univ.* Fort Collins, Colo. (1961)
- Mahjoub, S.N.; Mhiri, H.; Bournot, P.H.; LePalec, G.: Experimental and numerical modeling of the three-dimensional incompressible flow behavior in the near wake of circular cylinders. *J. Wind Eng. Ind. Aerodyn.* 96(5), 471-502 (2008)
- Melville, B.W.: Local scour at bridge sites. *Ph.D. Thesis.* School of Eng., Univ. Auckland, New Zealand. (1975)
- Melville, B.W.: Local Scour at Bridge Abutments, *J. Hydraul. Eng.* 118(4), 615–631 (1992)
- Melville, B.W.; Chiew, Y.M.: Time scale for local scour at bridge piers, *J. Hydraul. Eng.* 125(1), 59-65 (1999)
- Melville, B.W.; Coleman, S.E.: Bridge scour, *Water Res. Pub.* Fort Collins, Colorado, USA. (2000)
- Melville, B.W.; Raudkivi, A.J.: Flow characteristics in local scour at bridge piers. *J. Hydraul. Res.* 15(4), 373-380 (1977)
- Michael, S.A.; Mohamed, G.M.; Mohamed, S.B.A.M.: Wake Vortex Scour at Bridge Piers, *J. Hydraul. Eng.* 117 (7), 891-904 (1991).
- Muzzammil, M.; Gangadhariah, T.: The mean characteristics of horseshoe vortex at a cylindrical pier. *J. Hydraul. Res.* 41(3), 285–297 (2003)
- Michael, S.A.; Mohamed, G.M.; Mohamed, S.B.A.M.: Wake vortex scour at bridge piers. *J. Hydraul. Eng.* 117(7), 891–904 (1991)
- Raikar, R.V.; Dey, S.: Kinematics of horseshoe vortex development in an evolving scour hole at a square cylinder. *J. Hydraul. Res.* 46(2), 247-264 (2008)
- Raudkivi, A.J.: *Loose Boundary Hydraulics.* A. A. Balkama, Rotterdam (1998)
- Raudkivi, A.J.; Ettema, R.: Clear-Water scour at cylindrical piers. *J. Hydraul. Eng.* 109(3), 338-350 (1983)
- Richardson, E.V.; Davis, S.R.: Evaluating scour at bridges. HEC18 FHWA NHI-001. *Federal Highway Administration, US department of transportation,* Washington, USA (2001)
- Roulund, A.; Sumer, B.M.; Fredsøe, J.; Michelsen, J.: Numerical and experimental investigation of flow and scour around a circular pile. *J. Fluid Mech.* 534, 351–401 (2005)
- Shen, H.W.; Scheider, V.R.; Karaki, S.: Local scour around bridge piers. *J. Hydraul. Div.* 95(6), 1919-1940 (1969)

- Sheppard, D.M.; Zhao, G.; Copps, T.H.: Local scour near multiple pile piers in steady currents. In: Proceedings of ASCE, International Conference on Water Resources Engineering, San Antonio, USA (1995)
- Song, T.; Chiew, Y.M.: Turbulence measurement in nonuniform open-channel flow using Acoustic Doppler Velocimeter (ADV). *J. Eng. Mech.* 127(3), 219-232 (2001)
- Sumer, B.M.; Fredsoe, J. The mechanics of scour in the marine environment. *World Scientific*, Singapore. (1992)
- Sumner, D.; Wong, S.S.T.; Price, S.J.; Paidoussis, M.P.: Fluid behavior of side-by-side circular cylinders in steady cross-flow. *J. Fluid. Struct.* 13(3), 309-338 (1999)
- Unger, J.; Hager, W.H.: Down-flow and horseshoe vortex characteristics of sediment embedded bridge piers. *Exp. in Fluids*, 42(1),1-19 (2007)
- Yilmaz, M.; Yanmaz, A.M.; Koken, M.: Clear-water scour evolution at dual bridge piers. *Canadian J. Civil Eng.* 44(4), 298-307 (2017)
- Zdravkovich, M.M.: The effects of interference between circular cylinders in cross flow. *J. Fluid Struct.* 1(2), 239-261 (1987)

2. BASIC THEORIES

2.1 Introduction to Turbulence

2.1.1 Preliminaries

In fluid dynamics, turbulence in a fluid refers to three dimensional, unsteady motions of particles characterized by chaotic changes in pressure and flow velocity. It appears in the flow field as a random process that is completely unpredictable. This is quite constant with the laminar state where flow is apparently uniform and well behaved. Laminar flow could be unsteady and three dimensional but can always be represented mathematically as a continuous function. The laminar and turbulent flows are schematically shown in Fig. 2.1, measured by a velocity measuring probe (FAMATF, 1995).

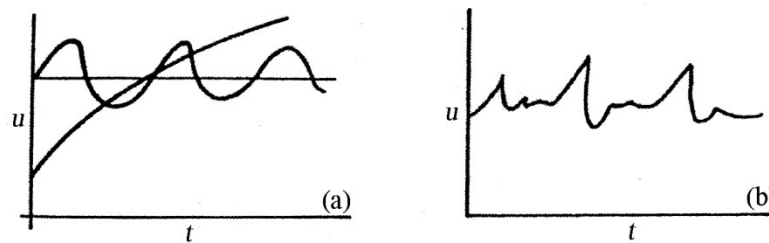


Fig. 2.1. Probe response in laminar and turbulent flow.

Turbulent fluctuations occur at a macroscopic scale. They are governed by the appropriate forms of continuity and Navier Stokes equations. The loss of randomness can be seen in the dependence of flow property (say, velocity u) at point x , at an instant t , with its value at $u(x, t - \Delta t)$ in the past or its value $u(x - \Delta x, t)$ in the intermediate neighbourhood. Here, Δx and Δt are called the length and time scales of turbulence. Over a distance corresponding to the length scale, an increase in a velocity at a point will include an increase in velocity in the neighbourhood or a consistent change in any other property. This can be visualized conveniently in terms of local circulation that is responsible for the fluctuation in the flow properties (Fig. 2.2)

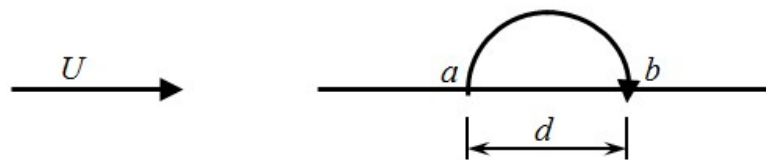


Fig. 2.2. An eddy notation in turbulent flow.

This is the concept of an eddy, since vorticity fluctuations are complex functions of time, it is clear that the turbulence must be viewed as being composed of a superposition of eddies of varying sizes. If U is the local velocity at a point, the time scale Δt is approximately $\Delta x/U$. Since a collection of length scales are present, it follows that a collection of time scales are also present in the flow.

Similarly, the distributions of length and time scales are presented in terms of frequencies ($\sim U/\Delta x$ Hz). For example a particular turbulence field can be described in terms of distribution of kinetic energy of fluctuations as a function of frequency. The notion of eddies, length scales, time scales and frequencies are however, fully equivalent.

2.1.2 Definition of Technical Terms

Discussions on turbulence are possible only when the meaning of certain technical terms is agreed upon. Commonly used words and their interpretation are reviewed in this section. Turbulence is said to be *stationery* in the associated base flow (obtained generally by averaging over a specified period of time) is itself independent of time. The assumption of stationery fluctuations (in velocity, temperature and pressure) is central to the development of analytical techniques and models. Unless otherwise stated, it is to be taken as valid in all subsequent analysis. A turbulence field is said to be *statically stationery* if its statistics is independent of time t .

Turbulence is said to be *isotropic* if the individual velocity fluctuations are equal in all the three (x , y and z) directions. Otherwise it is stated to be *anisotropic*.

A flow field where turbulence labels do not change from one point to another are called *homogeneous*. A purely homogeneous turbulence field is not physically realisable since velocity fluctuations in uniform flow must decay in the flow direction owing to the action of viscosity. Of greater interest is the problem where turbulence is uniform in a plane normal to the mean flow direction. This is called as *cross flow homogeneity*. If the velocities are high, decay rates will be smaller in comparison.

The characteristics of turbulence depend quite crucially on whether or not the region being studied lies adjacent to a solid wall (channel bed). Accordingly one distinguishes between *wall turbulence* (for example, boundary layers) and *free turbulence* (for example, free stream turbulence generated by devices, mixing layers and far wakes of bluff objects). In these two cases flow is neither homogeneous nor isotropic. However, experiments show that it is possible for the flow as a whole to attain a certain invariant state in terms of appropriate variables. Turbulence is then said to be *fully developed*. Examples are boundary layers that have evolved over a sufficiently long distance and far wakes of bluff objects. In the respective cases, the boundary layer thickness dimensionless velocity profile and the dimensionless power spectrum would have become invariant, at large distances in downstream directions. In a majority of problems, a fully developed state is attained owing to a balance between energy input to the turbulent eddies and the rate of energy dissipation by viscosity. This is called as an *equilibrium state*. Terms such as fully developed boundary layers and equilibrium boundary layers (wakes) are often interchangeably used.

The kinetic energy of turbulence refers to the portion of the total kinetic energy present in the velocity fluctuations. One can associate this quantity with the stream wise velocity (giving rise to stream wise kinetic energy) or with the transverse components. Further, it can be associated with each eddy or the related time scale (and hence frequency) and this results in the concept of an energy spectrum. The fraction of the kinetic energy present in the largest eddies is usually much larger than that in the smallest eddies. The latter correspond to the site

of viscous dissipation. It is worth noting that the slope of the certain portion of the spectrum of kinetic energy with respect to frequency on a log log scale approaches to $-5/3$, as the flow attains a fully developed state. This result is called Kolmogorov's hypothesis, after the Russian mathematician who derived it based on dimensional analysis.

The dissipation rate of turbulence is that rate at which turbulent kinetic energy is converted to internal energy of the fluid by molecular viscosity. In a fully developed flow, dissipation equals the rate of kinetic energy and hence the rate at which the mean flow supplies energy to sustain the turbulent fluctuations.

In turbulent flow viscous dissipation equals the square of the velocity gradient plus a value that depends on fluid viscosity and gradients in the velocity fluctuations. The second factor can be thought of as arising from an *eddy viscosity*, a property not of the fluid but the flow itself. Other interpretations of eddy viscosity are possible. In laminar flow, one views kinematic viscosity as responsible for momentum transport across streamlines. In turbulent flow, this transport is substantially amplified by transverse components of velocity fluctuations.

Eddy viscosity can be thought of as the associated momentum transport coefficient in turbulent flows. At a more fundamental level, the increase in momentum transport rates manifest as an increase in the magnitudes of the components of the stress tensor, over and above the laminar value. The turbulent contribution to the stress tensor is called as *Reynolds Stress*, after the O. Reynolds who visualized a turbulence field as having a base flow with superimposed fluctuations. The relationship between eddy viscosity and Reynolds stress tensor can be treated as analogous to that between molecular viscosity and stress tensor in laminar flow. This is called as *Boussinesq's hypothesis* (FAMATF, 1995).

2.2 Turbulent Flow Boundary Layer Equations

In turbulent flow, it is convenient to describe the hydrodynamic quantities by separating the time-averaged values from their fluctuations. Such decomposition of an instantaneous value of a hydrodynamic quantity is called the *Reynolds decomposition*. Fig. 2.3 illustrates the decomposition of u -component of velocity.

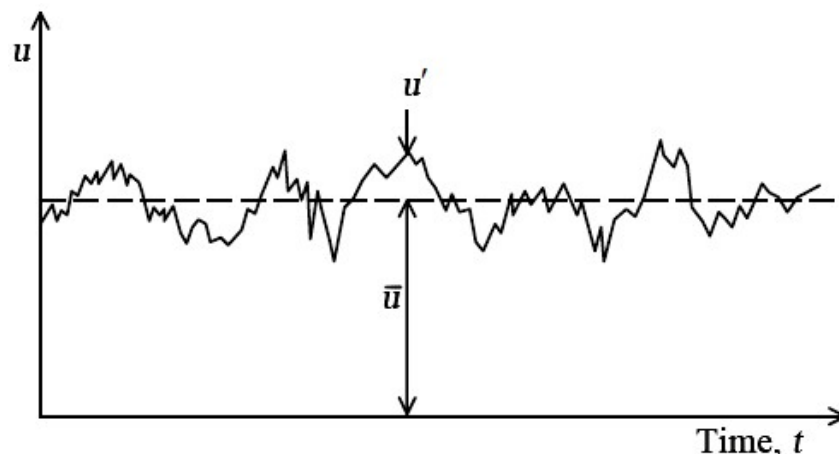


Fig. 2.3. Time series of u -component of velocity.

The instantaneous velocity components (u, v, w) at any point in turbulent flow in the Cartesian coordinate system (x, y, z) and the pressure intensity p are given by

$$u = \bar{u} + u' \quad (2.1)$$

$$v = \bar{v} + v' \quad (2.2)$$

$$w = \bar{w} + w' \quad (2.3)$$

$$p = \bar{p} + p' \quad (2.4)$$

where $\bar{u}, \bar{v}, \bar{w}$ are the time-averaged or temporal mean velocities in x, y, z directions; u', v', w' are the fluctuations of u, v, w ; \bar{p} is the time-averaged pressure intensity; and p' is the fluctuations of p .

The time-averaged value of a hydrodynamic quantity, say \bar{u} , is given by

$$\bar{u} = \frac{1}{t_1} \int_{t_0}^{t_0+t_1} u dt \quad (\text{By definition}) \quad (2.5)$$

where t_0 is any arbitrary time and t_1 is the time over which the mean is taken.

$$\text{Similarly, } \bar{v} = \frac{1}{t_1} \int_{t_0}^{t_0+t_1} v dt, \quad \bar{w} = \frac{1}{t_1} \int_{t_0}^{t_0+t_1} w dt \quad \text{and} \quad \bar{p} = \frac{1}{t_1} \int_{t_0}^{t_0+t_1} p dt \quad (2.6)$$

The time t_1 is taken as a sufficiently long interval of time in order to obtain the time independent quantities. Thus, the time-averaged values of all the fluctuations are equal to zero. Similarly, the time-averaged values of the derivatives of velocity fluctuations also vanish.

$$\overline{u'} = \overline{v'} = \overline{w'} = \overline{p'} = 0 \quad (2.7)$$

$$\frac{\overline{\partial u'}}{\partial x} = \frac{\overline{\partial^2 u'}}{\partial x^2} = \frac{\overline{\partial^3 u'}}{\partial x^3} = \dots = 0 \quad (2.8)$$

However, the quadratic terms resulting from the products of cross-velocity fluctuations such as $\overline{u'u'}$, $\overline{u'v'}$ and $\overline{\partial u'v'}/\partial x$ do not reduce to zero.

It is pertinent to mention that, in turbulent flow, the velocity fluctuations u', v', w' influence the time-averaged velocity components $\bar{u}, \bar{v}, \bar{w}$, so that $\bar{u}, \bar{v}, \bar{w}$ exhibit an apparent increase in the resistance to deformation, which is called as *turbulent stresses* or *Reynolds stresses*.

The Reynolds averaged Navier Stokes (RANS) and the continuity equations for an incompressible fluid flow in the Cartesian coordinate system are given by

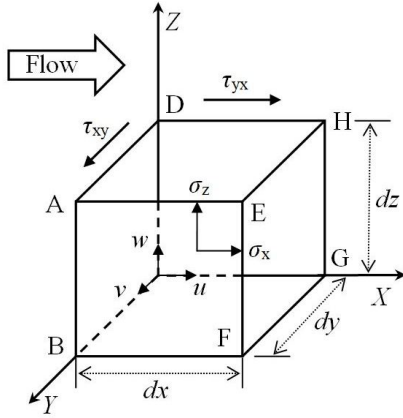
$$\frac{\partial \bar{u}}{\partial t} + \bar{u} \frac{\partial \bar{u}}{\partial x} + \bar{v} \frac{\partial \bar{u}}{\partial y} + \bar{w} \frac{\partial \bar{u}}{\partial z} = g_x - \frac{1}{\rho} \frac{\partial \bar{p}}{\partial x} + \nu \nabla^2 \bar{u} - \frac{\partial}{\partial x} \overline{u'u'} - \frac{\partial}{\partial y} \overline{u'v'} - \frac{\partial}{\partial z} \overline{u'w'} \quad (2.9)$$

$$\frac{\partial \bar{v}}{\partial t} + \bar{u} \frac{\partial \bar{v}}{\partial x} + \bar{v} \frac{\partial \bar{v}}{\partial y} + \bar{w} \frac{\partial \bar{v}}{\partial z} = g_y - \frac{1}{\rho} \frac{\partial \bar{p}}{\partial y} + \nu \nabla^2 \bar{v} - \frac{\partial}{\partial x} \overline{v'u'} - \frac{\partial}{\partial y} \overline{v'v'} - \frac{\partial}{\partial z} \overline{v'w'} \quad (2.10)$$

$$\frac{\partial \bar{w}}{\partial t} + \bar{u} \frac{\partial \bar{w}}{\partial x} + \bar{v} \frac{\partial \bar{w}}{\partial y} + \bar{w} \frac{\partial \bar{w}}{\partial z} = g_z - \frac{1}{\rho} \frac{\partial \bar{p}}{\partial z} + \nu \nabla^2 \bar{w} - \frac{\partial}{\partial x} \overline{w'u'} - \frac{\partial}{\partial y} \overline{w'v'} - \frac{\partial}{\partial z} \overline{w'w'} \quad (2.11)$$

$$\frac{\partial \bar{u}}{\partial x} + \frac{\partial \bar{v}}{\partial y} + \frac{\partial \bar{w}}{\partial z} = 0 \quad (2.12)$$

These are also known as *Reynolds Averaged Basic Differential Equation for Turbulent Mean Continuity*. The last three terms in Eqs. (2.9) - (2.11) are obtained from three cross products of velocity fluctuations and provide additional stresses developed due to turbulence. Hence, they are called as *turbulent shear stresses* or *Reynolds stresses* and can be expressed as a stress tensor called *Reynolds stress tensor* given as



$$\begin{pmatrix} \sigma_x & \tau_{xy} & \tau_{xz} \\ \tau_{yx} & \sigma_y & \tau_{yz} \\ \tau_{zx} & \tau_{zy} & \sigma_z \end{pmatrix} = -\rho \begin{pmatrix} \overline{u'u'} & \overline{u'v'} & \overline{u'w'} \\ \overline{v'u'} & \overline{v'v'} & \overline{v'w'} \\ \overline{w'u'} & \overline{w'v'} & \overline{w'w'} \end{pmatrix} \quad (2.13)$$

where $\sigma_x, \sigma_y, \sigma_z$ are the normal stresses in x, y, z directions; and $\tau_{xy} (= -\rho \overline{u'v'})$, τ_{yx} , τ_{yz} , τ_{zy} , τ_{zx} , τ_{xz} are the turbulent shear stresses in x, z, y, y, z and x directions.

Fig. 2.4. Stresses on a fluid element surface.

These Reynolds stresses are developed due to turbulent fluctuations and are given by the time-averaged values of the quadratic terms in the turbulent fluctuations. As these terms are added to the ordinary viscous stresses in the laminar flow and have a similar influence on the flow, it is often called *eddy viscosity*. In general, these Reynolds stresses far outweigh the viscous stresses in turbulent flow.

2.3 The Universal Velocity Profiles

Any turbulent flow along a solid wall like a channel bed, may be considered to have two regions - a region very close to the bed, where the flow is governed directly by the conditions at the bed or the molecular viscosity and second region far away from the bed, where the molecular viscosity does not play any significant role. The former is known as the *inner layer* or the *wall region* and the latter is called the *outer region*. Even in channel, two regions are distinguishable. There are region away from the bed, which includes the central part of the channel is called the *core region*.

Within the inner layer, a very thin region close to the bed can be identified where the flow is predominantly viscous. This is called the viscous sub-layer. On the other hand, the flow in the turbulent outer layer is fully turbulent where the inertial effects are predominant. Here velocities are almost constant because of the presence of large eddies, which produce strong mixing of flow. Thus in the region between the viscous sub-layer and the turbulent outer layer, both viscous and inertial effects are important.

The intermediate layer is called the *buffer layer* or *transition layer* or *inertial sub-layer*. Between the transition layer and turbulent outer-layer there is another region which is known as the *turbulent logarithmic-layer* in which viscous shear stress is negligible and the shear stress is due to the turbulence only. Both the viscous sub-layer and the buffer layer constitute the bed region, which constitute about 15% of the whole boundary layer (Fig. 2.5).

In Fig. 2.5, τ_v is the shear stress due to viscosity and is equal to $\mu(d\bar{u}/dz)$; τ_t is the shear stress due to turbulence or Reynolds stress and is equal to $-\rho\overline{u'w'}$; τ is the total shear stress and is equal to $(\tau_v + \tau_t)$; and τ_0 is the bed shear stress and is equal to $\rho g R \sin \lambda$, where ρ is the mass density of water, g is the gravitational acceleration, R is the hydraulic radius, and λ is the angle made by the longitudinal sloping bed with horizontal.

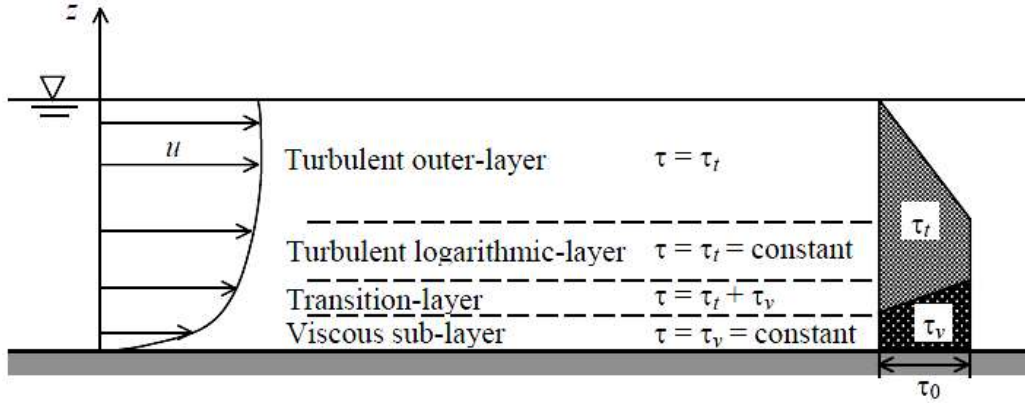


Fig. 2.5. Classification of flow region (layer thickness not to scale) (after Dey, 2006).

The flow zone over a boundary is characterized by the two-layer: an *inner-layer* where the flow is directly affected by the bed roughness and an *outer-layer* where the bed roughness indirectly influences the flow. The inner-layer consists of viscous sub-layer and transition-layer or buffer-layer. On the other hand, the outer-layer is divided into turbulent logarithmic-layer and turbulent outer-layers.

Fig. 2.6 depicts the velocity profiles in different layers over a smooth boundary. The velocity distributions in different layers are given in the succeeding sub-sections. Following the above, the relations for the mean velocity for the inner and the outer layers can be expected to be quite different for the two regions. While the wall or bed region is governed by what is called the *law of the wall* (*linear-law* in viscous sub-layer and *logarithmic-law* in turbulent-layer), the outer region follows the *velocity defect law*.

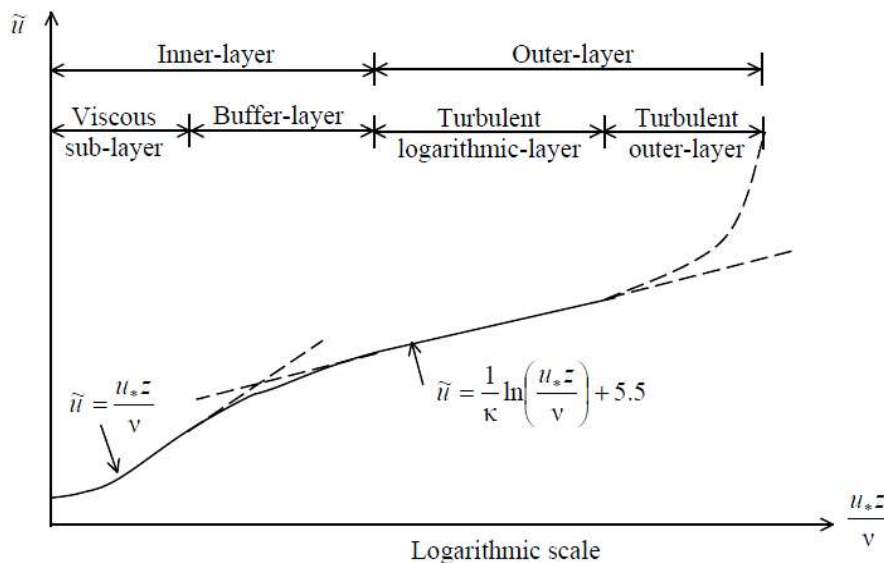


Fig. 2.6. Velocity profiles in different layers (after Dey, 2006).

Since the flow in the bed region is affected directly by the condition at the bed, viz., the bed shear stress τ_0 and its roughness, the mean velocity in this region can be expected to be a function of essentially the following quantities: the bed shear stress, the bed roughness, the distance from the bed and the water properties ρ and μ . Dimensional analysis shows that a *characteristic velocity* u_* can be defined as equal to $\sqrt{\tau_0 / \rho}$. This is called the *bed friction velocity*.

2.4 Turbulence Intensities and Turbulent Kinetic Energy

The *tangential* turbulent intensity $u^+ (= \sqrt{\overline{u'u'}})$, *radial* turbulent intensity $v^+ (= \sqrt{\overline{v'v'}})$ and *vertical* turbulent intensity $w^+ (= \sqrt{\overline{w'w'}})$ are the Root Mean Square (RMS) values of u' , v' and w' velocity fluctuations of flow u , v and w , correspondingly.

Many attempts were made to add “turbulence conservation” relations to the time-averaged continuity, momentum, and energy equations. The most obvious single relation would be a relation for the *turbulence kinetic energy* of the fluctuations, defined by

$$k = \frac{1}{2}(\overline{u'u'} + \overline{v'v'} + \overline{w'w'}) = \frac{1}{2}(\overline{u_i u_i}) \quad (2.14)$$

Here for convenience the Einstein summation notation is introduced, where $u_i = (u_1 + u_2 + u_3) = (u, v, w)$ and a repeated subscript implies summation. For example $u_i u_i = (u_1^2 + u_2^2 + u_3^2)$. If turbulence is to be described by only one velocity scale, it should be \sqrt{k} (White, 1991).

The turbulent kinetic energy (TKE) is also defined as

$$k = \frac{1}{2}(u^{+2} + v^{+2} + w^{+2}) \quad (2.15)$$

The rate of change of turbulence kinetic energy is equal to its convective diffusion, plus its production, plus the work done by turbulent viscous stresses, plus the turbulent viscous dissipation. The terms in this relation are so complex that they cannot be computed from first principles. Therefore modeling ideas are needed.

2.5 Vorticity

Vorticity is a concept used in fluid dynamics. In the simplest sense, vorticity is the tendency for elements of the fluid to “spin”. More formally, vorticity can be related to the amount of “circulation” or “rotation” (or the local angular rate of rotation) in a fluid. The average vorticity ζ_y , in a small region of fluid flow is equal to the circulation Ω around the boundary of the small region, divided by the area A of the small region.

$$\zeta_y = \left(\frac{\partial v}{\partial z} - \frac{\partial w}{\partial x} \right) = \frac{\Omega}{A} \quad (2.16)$$

Notionally, the vorticity at a point in a fluid is the limit as the area of the small region of fluid approaches zero at the point:

$$\zeta = \frac{d\Omega}{dA} \quad (2.17)$$

Mathematically, vorticity is a vector field and is defined as the curl of the velocity field:

$$\vec{\zeta} = \vec{\nabla} \times \vec{u} \quad (2.18)$$

In fluid dynamics, vorticity is the curl of the fluid velocity. It can also be considered as the circulation per unit area at a point in a fluid flow field. It is a vector quantity, whose direction is along the axis of the fluid's rotation. For a two-dimensional flow, the vorticity vector is perpendicular to the plane.

For a fluid having locally a "rigid rotation" around an axis (that is, moving like a rotating cylinder), vorticity is twice the angular velocity of a fluid element. An irrotational fluid has no vorticity. Somewhat counter-intuitively, an irrotational fluid can have a non-zero angular velocity (for example, a fluid rotating around an axis with its tangential velocity inversely proportional to the distance to the axis has a zero vorticity).

2.6 Circulation

The *Circulation* (Ω) is defined as the integral of the velocity vector around a closed path, that is

$$\Omega = \oint_c \vec{V} \cdot d\vec{s} = \iint_A \zeta \, dA \quad (2.19)$$

The existence of closed streamlines in a flow pattern implies that there are loops for which $\Omega \neq 0$ and thus that the flow is not irrotational everywhere.

The circulation Ω of the vortex can be estimated as at different azimuthal planes from the vorticity contours by using Stokes theorem, where \vec{V} is the velocity vector, $d\vec{s}$ is the differential displacement vector over a closed curve and A is the area enclosed.

2.7 Conditions of Sediment Transport

Clear-water scour occurs when no upstream sediment is present, that is when the bed material in the natural flow upstream of the scour hole is at rest or when the bed upstream of the scour hole is fixed.

If the scour is caused by flow that is not transporting sediment (bed load and suspended load), the depth of scour should approach a limit asymptotically. When the approach velocity is greater than the critical mean flow velocity, the upstream bed is usually covered to prevent the approaching flow from moving the bed particles. Live-bed scour is scour with sediment transport over the upstream undisturbed bed. Sediment particles which are continuously transported by the flow enter the scour hole. In such cases, the equilibrium scour depth is smaller than that in clear-water scour conditions. In general, for the live-bed case, the scour increases rapidly with time (Fig. 2.7) and then fluctuates about a mean value in response to the bed features which are being passed. The maximum scour depends on the variations in the

depth of flow and is approximately maximum scour depth (d_{sm}) plus half the height of bed features.

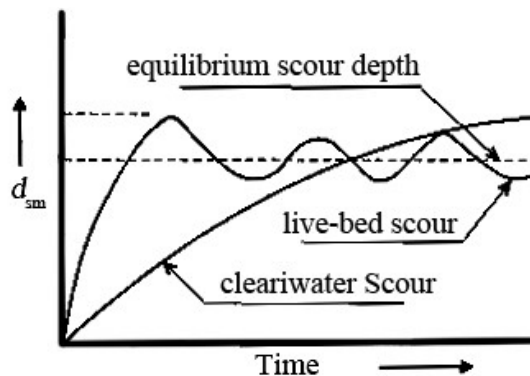
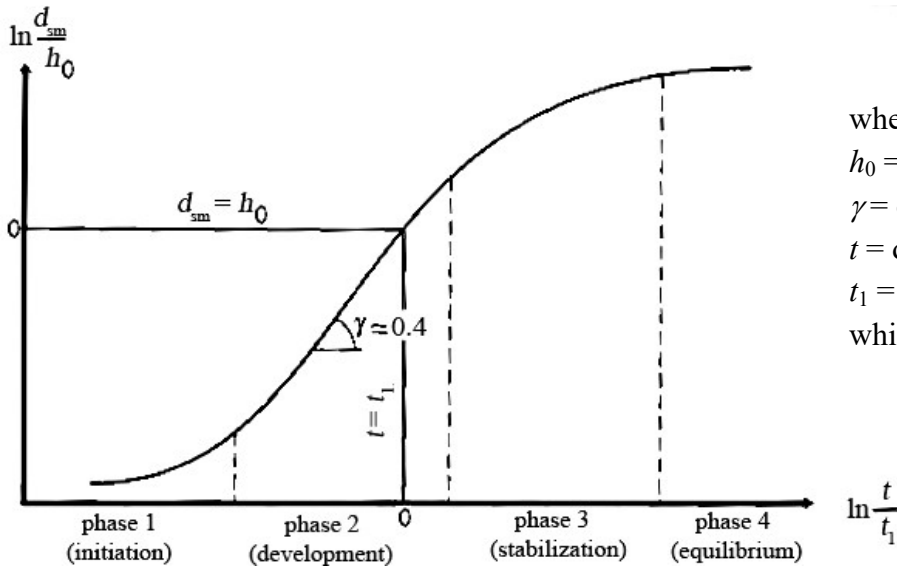


Fig. 2.7. Development of scour process (after Hoffmans, 1997).

Based on clear-water scour experiments using scale models with small Froude numbers (Breusers, 1966; Dietz, 1969; Zanke, 1978) distinguished four phases in the evolution of a scour hole (Fig. 2.8): an initial phase, a development phase, a stabilisation phase and an equilibrium phase. In the initial phase, the flow in the scour hole is nearly uniform in the longitudinal direction. This phase of the scour process can be characterised as the phase in which the erosion capacity is most severe. Observations with fine sediments (e.g. Breusers, 1966) showed that at the beginning of the scour hole development some bed material near the upstream scour slope goes into suspension. Most of the suspended particles follow convectional paths within the main flow and remain in suspension due to the internal balance between the upward diffusive flux and the downward flux due to gravity. Some of the particles will settle and will be re-suspended owing to the large bursts of the turbulent flow near the bed, while some particles with a jump height smaller than a defined saltation or reference height are transported as bed load.

During the development phase the scour depth increases considerably, but the shape of the scour hole does not change. In this phase the ratio between the maximum scour depth (d_{sm}) and the distance from the end of the bed protection to the point where the scour hole is at its maximum is more or less constant. Measurements by Hoffmans (1990) showed that the upper part of the upstream scour slope is in equilibrium, whereas the lower part is still developing. The suspended load close to the bed has decreased significantly compared to the condition in the initial phase. This can mainly be ascribed to the decrease in the flow velocities near the bed over time, despite the increase of the turbulence energy. Though bed particles are picked up and carried by the flow, the time-averaged value of the sediment transport in the upper part of the upstream scour slope is negligibly, since the contribution of the sediment transport due to the instantaneous velocities in the downstream direction is approximately equal to the transport resulting from the instantaneous velocities in the upstream direction.



where,
 h_0 = initial flow depth
 γ = coefficient (or angle)
 t = duration of scour
 t_1 = characteristic time at which $d_{sm} = h_0$

Fig. 2.8. Development of scour process (after Hoffmans, 1997).

In the stabilisation phase the rate of development of the maximum scour depth decreases. The erosion capacity in the deepest part of the scour hole is very small compared to the erosion capacity downstream of the point of reattachment, so that the dimensions of the scour hole increase more in the longitudinal direction than in the vertical direction. The more the scour process continues, the more the flow velocities above the lower part of the upstream scour slope decreases. In the stabilisation phase, the equilibrium situation for both the upstream scour slope and the maximum scour depth is almost achieved. The equilibrium phase can be defined as the phase in which the dimensions of the scour hole do no longer change significantly.

2.8 Incipient Motion (Threshold Condition)

When a stream-flow takes place over a loose sedimentary bed, hydrodynamic forces are exerted on the sediment particles at the bed surface. An increase in flow velocity causes an increase in the magnitude of hydrodynamic forces. Hence, sediment particles start to move if a situation is eventually reached when the hydrodynamic forces induced by the flow exceed a certain limiting value. The initial movement of sediment particles is frequently called incipient motion. The condition being just sufficient to initiate sediment motion is termed threshold or critical condition or the condition of incipient motion of the sedimentary particles. The threshold of sediment motion in open channels having erodible bed is an important component of the management of river systems and occupies the central position of the sediment transport theory. If the stream flow is further increased, then sediment transport takes place.

The first type of definition is based on sediment flux. Shields (1936) put forward a concept of sediment threshold that the bed shear stress has a value for which the extrapolated sediment flux becomes zero. On the other hand, USWES (1936) set a concept of sediment threshold that the tractive force brings about general motion of bed particles. For sediment particles less than 0.6 mm, this concept was found to be inadequate and general motion was

redefined that sediment in motion should reasonably be represented by all sizes of bed particles and that sediment flux should exceed $4.1 \times 10^{-4} \text{ kg/m}^2$. The second type of definition is based on bed particle motion. Kramer (1935) indicated four different bed shear stress conditions for sedimentary bed for which:

1. No particles are in motion, termed no transport.
2. A few of the smallest particles are in motion at isolated zones, termed weak transport.
3. Many particles of mean size are in motion, termed medium transport.
4. Particles of all sizes are in motion at all points and at all times, termed general transport.

However, Kramer (1935) pointed out the difficulty of setting up clear limits between these regimes but defined threshold bed shear stress to be that stress initiating general, transport. Vanoni (1964) proposed that the sediment threshold is the condition of particle motion in every two seconds at any location of a bed.

2.9 Clear Water Scour Mechanism

Scour is a natural phenomenon of lowering the level of riverbeds by the erosive action of the flowing stream. The amount of reduction in the level of riverbeds below an assumed natural level is termed *scour depth*. Scour is classified as *general scour* and *local scour*.

General scour in the river occurs as a result of the change in the characteristics of the river. Based on the time taken for scour development, general scour can be categorized as *short-term scour* and *long-term scour*. Short-term general scour develops during a single or several closely spaced floods, while long-term general scour takes considerably long time, normally of the order of several years, and includes progressive degradation and lateral bank erosion. Short-term general scour may occur due to convergence of flow, a shift in the channel thalweg or braids within the channel, and bed-form migration. On the other hand, the long-term general scour may be caused by the natural changes in the catchments (for example, channel straightening, volcanic activities, climate change etc.) or by the human activities (for example, channel alterations, streambed mining, dam / reservoir construction, and land-use changes).

In contrast, *local scour* (also termed *localized scour*) develops near the structures, due to modification of the flow field as a result of obstruction to the flow by the structures. Scour within the contracted portion of the channel, scour downstream of an apron due to submerged jets, scour below horizontal pipes, scour at bridge piers and abutments, scour at spur dikes and other river training works are the examples of local scour.

Local scour is classified as *clear-water scour* and *live-bed scour*. Clear-water scour occurs when the sediment is removed from the scour hole but not supplied by the approaching stream. The equilibrium scour depth is attained when the fluid induced force can no longer dislodge the sediment particles from the scour hole. On the other hand, live-bed scour, occurs when the scour hole is continuously fed with the sediment by the approaching stream. The equilibrium scour depth is attained over a period of time, when the rate of removal of sediment out of the scour hole equals the rate of supply of sediment into the scour hole.

2.10 Scour around Bridge Piers

Failure of bridges due to scour at their supports is a common occurrence. It may be due to scour at a pier or at an abutment. Major scouring usually occurs during floods, that is, when the flow is unsteady and may even have a changed angle relative to low flow direction. Additional problems are caused by floating debris or ice packs.

Chabert and Engeldinger (1956) described first the behavioural pattern of scour at a circular pier, Fig. 2.9(a-b), in terms of development with time and flow velocity. They showed that the clear water scour approaches equilibrium asymptotically, over a period of days, whereas the live-bed scour develops rapidly and its depth fluctuates in response to the passage of bed features. A second peak was forecasted by Raudkivi (1982) as shown by the dashed line in Fig. 2.9(b).

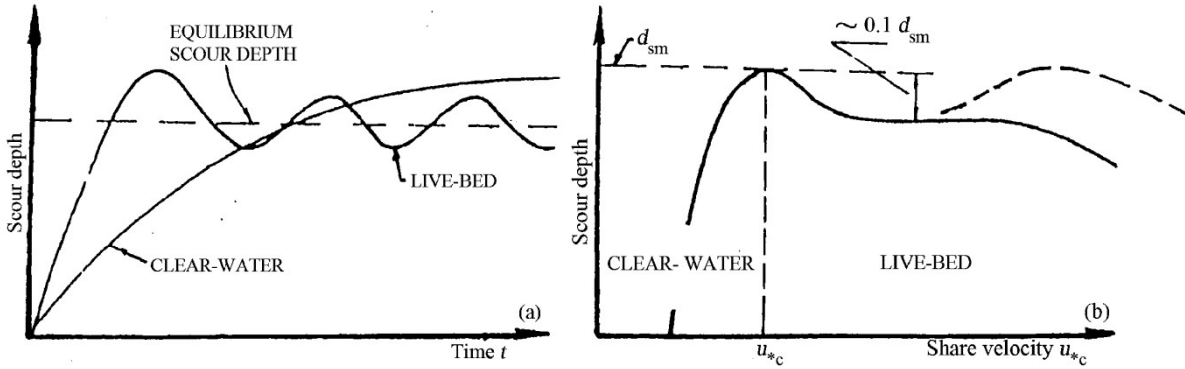


Fig. 2.9. Scour depth at a pier as a function of time (a) and of shear velocity (b) for a given pier and sediment size at constant flow depth (after Raudkivi, 1998).

The treatments of the scour problem usually start with the statement that the depth of scour depends on variables which characterize the fluid, bed material in the stream and at bridge crossings (grading, layering, particle size and shape, alluvial or cohesive), the flow, the geometry of the bridge pier and stream, e.g. as

$$d_s = f_1(\rho, \nu, g, d_{50}, \rho_s, h, U, b) \quad (2.20)$$

or

$$\frac{d_s}{b} = f_2\left(\frac{Ub}{\nu}, \frac{U^2}{gb}, \frac{h}{b}, \frac{d_{50}}{b}, \Delta\right) = f_3\left(\frac{u_*b}{\nu}, \frac{u_*^2}{\Delta gb}, \frac{h}{b}, \frac{d_{50}}{b}, \Delta\right) \quad (2.21)$$

where b is the width or diameter of the pier. The usual result is an empirical formula incorporating some of the parameters.

A literature survey of the various formulae for estimating scour depth was published by Breusers *et al.* (1977) and Raudkivi and Sutherland (1981). Some of the formulae are for clear water scour, some for live-bed and others are supposed to serve both regimes. The functional trends of scour at bridge piers were discussed by Raudkivi (1986). The formulae give widely differing estimates. These disparities have been discussed by Anderson (1974), Melville (1974) and Hopkins *et al.* (1983).

2.11 Horseshoe Vortex and Wake Vortex

The flow deflected by sediment embedded bridge piers causes scour at its foundations. Scour may endanger the stability of the complete bridge structure. In bridge hydraulics circular-shaped pier foundations are commonly used. Due to the similar flow structures of fluid flow around circular bodies in open channels, the basic researches concern flow visualization in fluid flow dynamics. The main flow features involve a vertically deflected flow along the pier front, a *horseshoe vortex* system upstream of the circular pier, a flow separation beside the pier and a wake zone downstream of it.

Wake vortices form at the downstream side of piers and are the result of flow separation at the sides of the pier Fig. 2.10. Called *cast-off vortices* by Raudkivi (1986), these have vertical axes. One vortex develops on one side, sheds away, and is convected downstream. Immediately, other forms on the other side, finally shedding also. The wake vortices dissipate as they move downstream. The frequency of vortex shedding is directly proportional to the approach velocity and inversely proportional to the pier diameter.

Information on wake vortex scour at bridge piers is particularly scanty. As wake vortex scour occurs at the downstream of the pier, it has little or no destructive potential. Because the horseshoe vortex scour occurs at the face of the pier and threatens to undermine the pier, this type of scour has been given considerable theoretical thought Bruesers *et al.* (1977) and is well-documented with model studies Raudkivi (1986). Knowledge about wake vortex scour due to bridge piers has come mainly from a few laboratory tests Melville (1975). To describe the scouring action, Melville wrote “each of the concentrated vortices acts with its low pressure center as a vacuum cleaner,” picking up material from the bed, which is then transported downstream.

At most bridges, wake vortex scour is insignificant and confluence scour does not exist. In clear water rivers flowing on fine sand, these two forms of local scour can be very large. The deep scour holes downstream from the large circular piers (10 and 15 m in diameter) at the Tahrir and Imbaba bridges over the Nile River in Cairo, Egypt were produced by the conflicting velocity fields at the intersection of the wake vortex streams from adjacent piers. The depths of scour due to these wake vortices are now 8 to 11 m where the normal depth of flow is approximately 8 m. Confluence scour where the main and side channel join upstream from the Imbaba bridge was 9 m in 1981 and 1987 and was aligned with the bisector of the intersection angle of the two channels. These depths of scour can be considered nearly clear-water scour as the bridges are in the backwater of the Delta Barrages, the velocity is less than 1 m/s and sediment transport was very low. There is concern that the holes may enlarge or move upstream endangering the piers and the bridges.

Michael *et al.* (1991) made observations in the vicinity of the scour holes and have come to the conclusion that, in each case, the scour was caused by two streams of wake vortices from adjacent piers intersecting downstream. The vortices that result from the two conflicting velocity fields create local scour. At one bridge, the scour is enhanced by the vortices that occur at the confluence of the main channel and its side channel. This is known as *confluence scour*.

2.12 Flow Pattern at a Circular Pier

The *flow pattern past a circular pier*, protruding vertically from a horizontal plane boundary, in uniform open channel flow is complex in detail, and the complexity increases with the development of a scour hole at the base of the circular pier. Studies of flow patterns for such a case have been reported by Hjorth (1975), Melville (1975), Melville and Raudkivi (1977) and Ettema (1980). The component features of the flow pattern are the downflow in front of the circular pier, cast-off vortices and wake, boundary layer, horseshoe vortex and bow wave, as shown diagrammatically in Fig. 2.10.

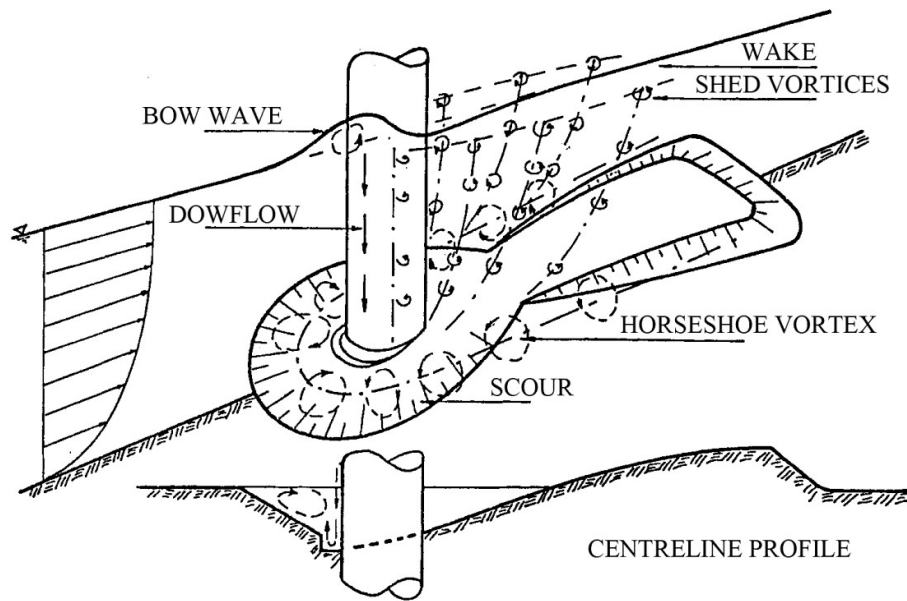


Fig. 2.10. Flow pattern at circular pier (after Raudkivi, 1998).

The approach flow velocity goes to zero at the upstream face of the pier, in the vertical plane of symmetry, and since the approach flow velocity decreases from the free surface downward to zero at the bed, the stagnation pressure, $\rho u^2 / 2$, also decreases. This downward pressure gradient drives the downflow. The downflow, in the vertical plane of symmetry, has at any elevation a velocity distribution, with zero in contact with the pier and again some distance upstream of it. The v_{mas} value according to the experimental data by Ettema (1980), Raudkivi (1986) at any elevation is 0.05 to 0.02 circular pier diameters upstream of it, being closer to the circular pier lower down and increases towards the bed. Just above the bed, if no scour hole is present, v_{mas} is approximately $0.4U$. The maximum of v_{mas} / U occurs when the depth of scour is about 2 times the pier diameter or more. This maximum is located at about one pier diameter below the approach flow bed and is about 80% of the mean approach flow velocity U .

The so-called horseshoe vortex develops as the result of flow separation at the upstream rim of the scour hole; it is a *lee eddy* similar to the eddy or ground roller downstream of a dune crest. The horseshoe vortex extends downstream, a few pier diameters past the sides of the pier, before losing its identity and becoming part of general turbulence. The horseshoe vortex also pushes the maximum downflow velocity within the scour hole closer to the pier.

A comment on the horseshoe vortex is inserted here because of the frequent reference in literature to it as the scouring agent. Uniform flow at velocity U has a vorticity $-U$ per unit streamwise length which is advected at approximately $\frac{1}{2}U$. The rate of advection is $-\frac{1}{2}U^2$ and if the vorticity filaments were caught on the pier the vorticity $-\frac{1}{2}U^2t$ would increase their monotonically.

Generation of vorticity occurs at the boundaries but only where there is a pressure gradient. In approaching the pier the flow meets an adverse pressure gradient. This leads to generation of vorticity of opposite sense to that in the boundary layer. The circulation decreases and goes to zero over the depth on the centre line of a circular pier protruding from a plane bed (as does the velocity). The vortex filament divides along this line, as vorticity is generated on the cylinder and base plate by the pressure gradients, and passes the pier. The parts on the circular pier separate and form the *Karman vortex street* (cast-off vortices). There is no accumulation of vorticity upstream of the circular pier. The observed vortices are weak and of both senses as illustrated in the Frontispiece of *Incompressible Aerodynamics* by Thwaites, Oxford UP, 1960. The concentration of vorticity develops with the scour hole as a lee or separation eddy.

The stagnation pressure, apart from downflow, also causes a sideways acceleration of flow past the circular pier. The flow separates at the sides of the circular pier and the surfaces of separation enclose a wake downstream of the pier. The discontinuity in the velocity profile from flow to wake leads to the development of concentrated vortices in the interface, the cast-off vortices, which translate with the flow. Near the bed these vortices interact with the horseshoe vortex causing the trailing parts of it to oscillate at the vortex shedding frequency n of approximately $nb/U \approx 0.2$. The cast-off vortices with their vertical low pressure centres lift sediment from the bed like miniature tornados.

A *bow wave* develops at the surface with rotation in the opposite sense to that in the horseshoe vortex. The bow wave becomes important in relatively shallow flows where it interferes with the approach flow and causes a reduction in the strength of the downflow.

2.13 Scour in Uniform Sediment

The scour hole development at the sides of the circular pier commences when the shear velocity reaches about 50% of the threshold value u_{*c} for the bed material. The scour rapidly propagates upstream leading to a groove around the perimeter over about $\pm 120^\circ$ after which the downflow, acting like a vertical jet, takes over. It cuts a groove and in the process is turned 180° upward. The upward flow is deflected by the developing horseshoe vortex upstream, up the slope of the scour hole. At the turning point the lip of the groove is sharp and the face of the groove is almost vertical. The groove gradually disappears as the scour approaches equilibrium depth. In the developing stages the rim of the groove collapses at irregular intervals leading to little local avalanches of bed material. The deflected downflow ejects this material up into the flow and the horseshoe vortex. The upstream part of the scour develops into a frustum of an inverted cone with slope equal to the angle of repose. A bar develops downstream in the wake region.

Clear water scour conditions prevail with non-ripple-forming bed material up to the threshold shear velocity value ($u_* \approx 0.95u_{*c}$). With fine sands it is difficult to avoid the development of ripples, well before the u_{*c} value for d_{50} -size is reached. This leads to some sediment transport and reduced maximum equilibrium scour depth. The development of maximum equilibrium clear water scour depth takes several days.

After the onset of live-bed conditions the equilibrium scour depth initially decreases and then increases again, reaching a second peak at transition flat bed conditions, and its magnitude fluctuates with time in response to the passage of bed features past the pier. Consequently, *the equilibrium depth must be defined as a time-average scour depth*, not a maximum. The range of the fluctuations in scour depth is a function of the size of bed features, which is a function of flow depth and not of pier size. The range of fluctuations from laboratory data is 0.75η (dune height) or approximately $\pm 0.5\eta$. The fluctuations of scour depth do not vanish at transition flat bed conditions because of the avalanching of sediment into the scour hole. The minimum scour depth occurs approximately when the dunes have maximum steepness, and in that region also the functions of scour for ripple and non-ripple forming sediments merge. The initial drop in the local scour depth reflects the very rapid increase in sediment transport rate with bed shear stress when the latter is only slightly in excess of τ_c , whereas the stagnation pressure and local scouring power increase only gradually. The subsequent increase in scour depth with bed shear stress indicates that the scouring power increases faster than the sediment transport rate. However, this increase is at least partly due to the longer troughs of the bed features at higher shear stress excesses, giving more time for the scour hole to deepen before the next crest arrives. Only a small number of data points are available for scour depth beyond the transition flat bed condition, and these show a decrease from the transition flat bed peak value. Live bed scour develops rapidly.

The trends of development of equilibrium scour depth in uniform sediment at sub-critical flow conditions according to laboratory data are displayed in Fig. 2.11(a) and in Fig. 2.11(b) for a set of laboratory experiments.

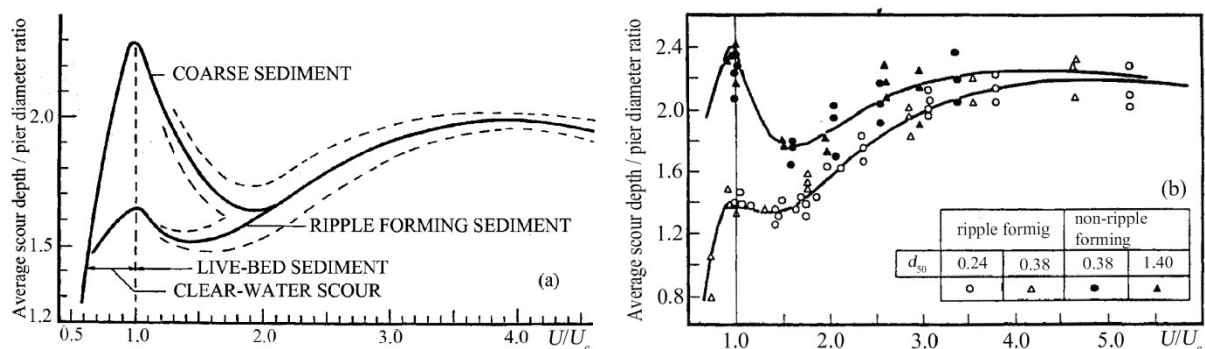


Fig. 2.11. Scour depth in uniform sediment at a circular pier as a function of relative velocity in a deep flow relative to pier diameter (a) as a trend function, and (b) for a set of laboratory data (after Raudkivi, 1998).

The peak clear water scour depth is of the order of 2.3 to 2.4 times of pier diameters (widths) if the flow is deeper and the grain size is smaller relative to the pier diameter. The effects of shallow flow depth, grain size, etc will be discussed separately. The use of velocity ratio U/U_c or u_*/u_{*c} instead of a Froude number collapses data from experiments with different sediment sizes. The scour depths are relative to local bed level which itself may be subjected to general and/or constriction scour.

Local variations in bed level may also arise from three-dimensional features of flow, associated bed features and localized channels in cross section. The localized channels in some gravel-bed rivers may have an appreciable depth, as was shown by Thompson and Davoren (1983) from field measurements in Ohau River, New Zealand. The local channel had a depth of about 3 m in a broad gravel river with an average depth of the order of 0.75 m and a mean velocity of 2.38 ms^{-1} (bed material $d_{50} = 20 \text{ mm}$, $d_{65} = 35 \text{ mm}$, $d_{84}/d_{50} = 3.5$). The local scour depth at a 1.5 m diameter circular pier was an extra 1.28 m.

2.14 Factors affecting Scour Depth

The large range of predicted and measured values of local scour depths at bridge piers, for what appear to be identical conditions, can be explained by the effects of a variety of specific parameters. These include the characteristics of bed material, flow, pier and channel geometry.

Scour at piers is influenced by various parameters (Breusers *et al.*, 1977), which are grouped as follows:

- Parameters relating to the pier: Size, shape, spacing, number and orientation with respect to the approaching flow direction.
- Parameters relating to the bed sediment: Median size, particle size distribution, mass density, angle of repose and cohesiveness.
- Parameters relating to the approaching flow condition: Approaching flow velocity, approaching flow depth, shear velocity and roughness.
- Parameters relating to the fluid: Mass density, viscosity, gravitational acceleration and temperature (may not be important in scour problems).
- Parameters relating to the time: Time of scouring for an evolving scour hole.
- Parameters relating to the unsteadiness: Passage of flood wave in rivers and waves in marine environment.

The relationship showing the influence of various parameters on the equilibrium scour depth d_s at piers can be given in functional form as follows:

$$d_s = f_1(\rho, \nu, g, d_{50}, \rho_s, h, U, b) \quad (2.22)$$

where h = pier width; and t = duration of scour. The dependency of scour depth on various parameters is given in the following subsections.

2.14.1 Effect of Sediment Grading

A systematic study of the effect of grain-size distribution on the depth of local scour was carried out by Raudkivi and Ettema (1977a,b), using a 102 mm diameter pier in a 1.5 m wide flume at maximum clear water scour conditions, Fig. 2.12, summarizes the results of maximum equilibrium scour depth d_{se} in terms of σ_g

$$\frac{d_{se}(\sigma_g)}{b} = \frac{K_\sigma d_{se}}{b} \quad (2.23)$$

where K_σ is the coefficient due to sediment gradation. With graded sediments the d_{50} -size is only an order of magnitude indicator for threshold shear stress. On graded sand beds the finer fractions start to move at lower shear velocities than u_{*c} for d_{50} and small ripples form. This leads to some sediment transport and reduced maximum equilibrium scour depth but if the surface armours full clear water scour depth may occur. With coarse-grained sediments the fines that are not sheltered or trapped are usually winnowed out and a clear water scour develops. Its' depth decreases rapidly with increasing width of the grain-size distribution. However, the clear water scour depth with graded sediment is governed by the armouring process and this scour depth reaches a maximum at the limiting armour conditions that occurs at u_{*c} larger than that for the d_{50} -size. Consequently, the first peak of scour depth is reached at $u_{*c} > u_{*c50}$ as shown in Fig. 2.13. The scour depth function in graded sediments was fitted to data by Chiew (1984) omitting experimental data points. The spread of data was generally less than $0.2ds/b$ and less in individual test series. If the critical armour flow conditions are maintained for long time the scour depth increases but does not quite reach the uniform sediment value. The armoured bed scour peak is physically similar to the clear water peak.

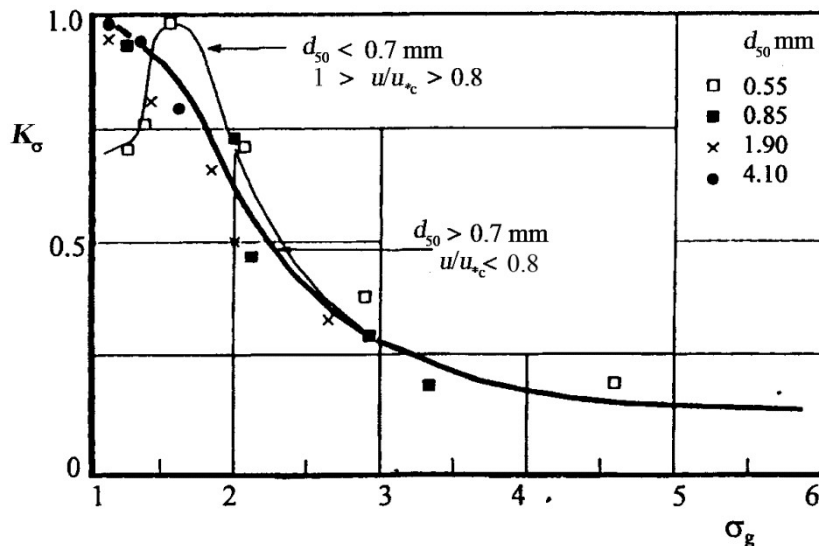


Fig. 2.12. Coefficient K_σ variation of scour depth as a function of the geometric standard deviation of particle size distribution (after Raudkivi, 1998).

On exceeding the shear stress for the limiting armour layer, the armour layer fails and sediment transport increases rapidly. The scour depth decreases, like with live-bed scour in

uniform sediments, but the fluctuations are smaller because gravel beds do not have high dunes.

After the initial decrease, the scour depth starts to increase again with increasing applied shear stress, up to the transition flat bed condition. First, the coarser fractions of sediment are still effective in armouring the bed of the local scour hole but their effectiveness decreases with increasing bed shear stress and vanishes at the transition flat bed conditions, that is, if the largest stones in the sediment are not large relative to the width of the groove excavated by the downflow (not larger than about one-tenth of the pier diameter).

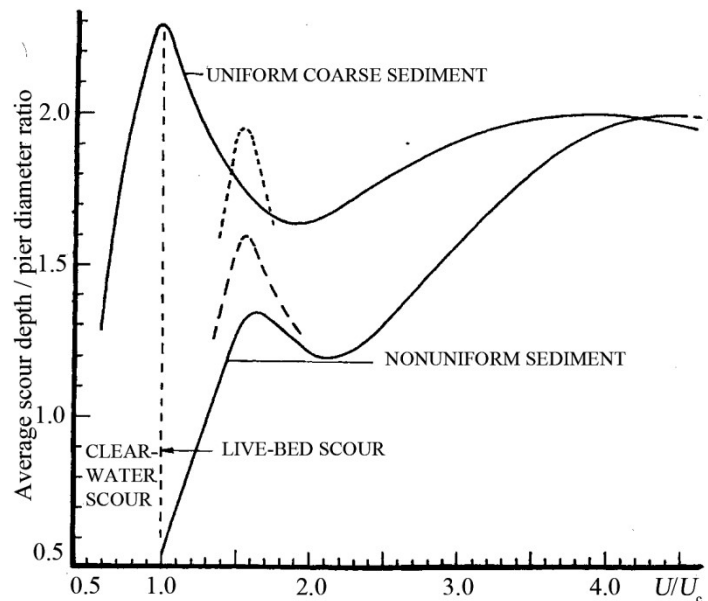


Fig. 2.13. Average local equilibrium scour depth at pier diameter $b = 4.5$ cm in uniform $\sigma_g < 1.3$ and non- sediment ($\sigma_g = 3.5$) with $d_{50} = 0.8$ mm and flow depth $h = 17$ cm. Full lines in both cases are for recirculating sediment transport. Dotted lines show the peak by as the bed armours and sediment transport diminishes (after Raudkivi, 1998).

Limited laboratory data indicate that the effect of sediment grading is too small to be separated from the usual scatter present when $\sigma_g < 2$ and the data follow the uniform sediment function. On the other hand, field data indicate that during floods the fluid shear stresses in gravel-bed rivers seldom exceed about double that of the critical armour layer shear stress τ_{ca} . Thus, if prolonged periods of flow at just below τ_{ca} are not likely, the actual scour depths observed may be appreciably less than the peak values, according to Fig. 2.13.

Under live-bed conditions the major effects of sediment grading are:

- The grain size and grain-size distribution affect the type and size of bed features. These in turn will control the range of fluctuations of scour depth from the mean value at given conditions.
- The grain-size distribution affects the armouring process and mean scour depth at given flow conditions.
- The grains that are near the threshold for movement accumulate in the scour hole.

This increases the porosity of the bed, more of the downflow disperses in the porous bed and scour depth is reduced.

- Grains large relative to pier size lead to a decrease in local scour depth.

2.14.2 Effect of Sediment Size

The data by Ettema (1980), Chee (1982) and Chiew (1984) for clear-water and live-bed scour using six pier sizes and sediment sizes from $d_{50} = 0.24$ mm to 7.80 mm are plotted in Fig. 2.14. It shows that the maximum scour depth is unaffected by the grain size as long as the ratio b/d_{50} is larger than about 50. For smaller values the grains are large relative to the width of the groove excavated by the downflow and the erosion process is impeded. If b/d_{50} becomes smaller than ten, the stones are so large that the scour is mainly by entrainment at the flanks of the pier. The relative grain size effect in nature is rare, but some laboratory data are affected by it.

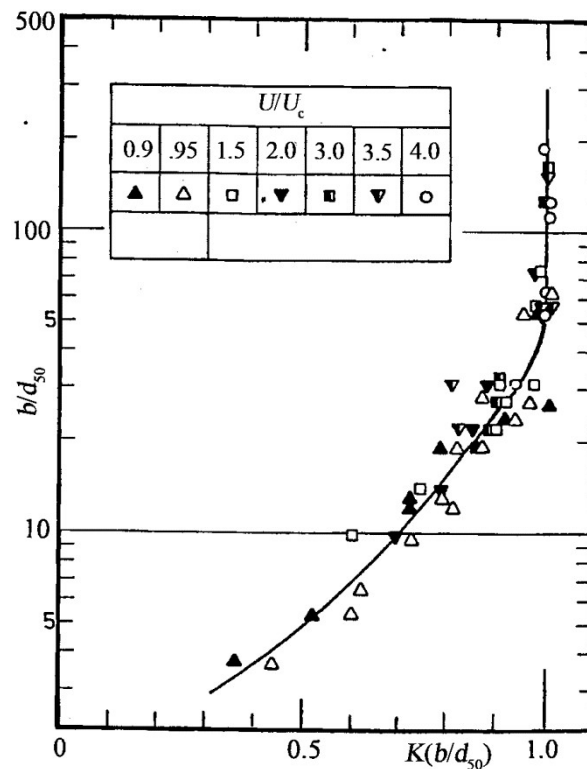


Fig. 2.14. The ratio of local equilibrium scour depth $K(b/d_{50})$ affected by the relative size b/d_{50} to that independent of b/d_{50} for clear water and live-bed scour conditions (after Raudkivi, 1998).

2.14.3 Effect of Flow Depth

There are several references in the literature stating that the scour depth is affected by the flow depth relative to the pier size; for example, the scour depth becomes independent of flow depth greater than three pier diameters. A decreasing depth of flow leads to increasing prominence of the surface roller (bow wave), which interferes with the downflow and reduces its strength. No exact dependence has been obtained for the relative flow depth effect but data

collected at clear-water, live-bed and at transition flat bed conditions, are shown in Fig. 2.15 as relative flow depth h/b versus K_h . The scour depth at the given pier in relatively deep water (unaffected by flow depth) is to be multiplied by K_h , to obtain the scour depth in shallow flow. For $b/d_{50} > 75$ and $h/b < 3$ the K_h factor is approximately given by

$$K_h = 0.77(h/b)^{0.21} \quad (2.24)$$

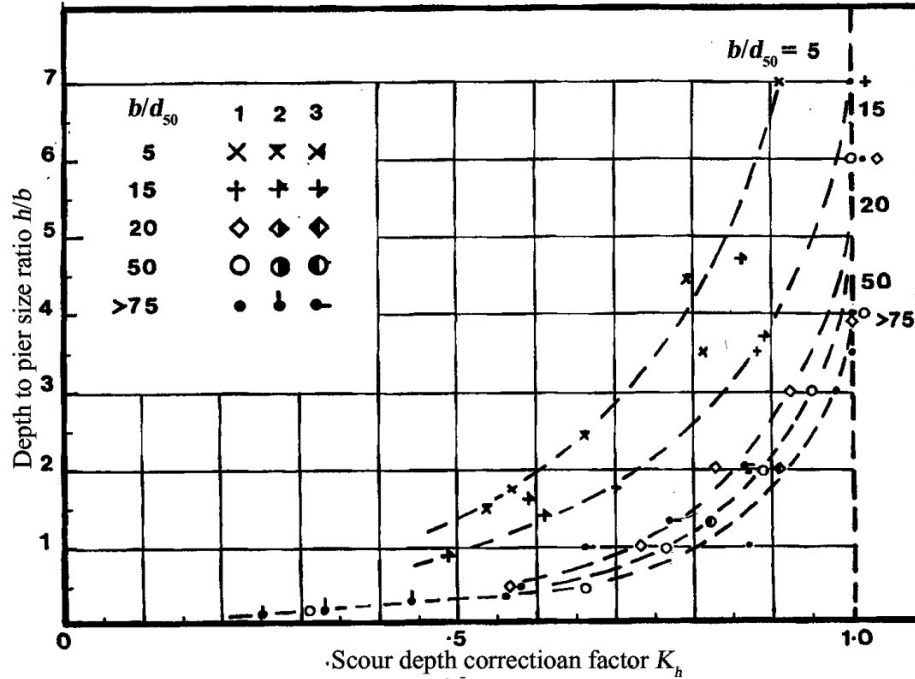


Fig. 2.15. Equilibrium Scour depth as a function of relative flow depth, h/b , with the ratio of b/d_{50} as parameter. Data: 1 - Ettema (1980), 2 - Chew (1984), 3 - Chee (1982) (after Raudkivi, 1998).

2.14.4 Effect of Pier Size

The effect of pier size on depth of local scour is of major interest for interpretation of laboratory data for field use. Pier size affects the time required for the local clear water scour to develop to its maximum depth, but not the ultimate scour depth d_s/b if the effects of relative grain size b/d_{50} on the scour depth are excluded. The actual value of d_{sc}/b also depends on the grading of bed material. The development of live-bed scour is much more rapid and dependent on u_* / u_{*c} .

The volume of the local scour hole formed around the upstream half of the perimeter of the pier is proportional to the cube of pier diameter (or the projected width). The larger the pier the longer is the time required for it to develop at a given flow conditions. Laboratory data show that the rate of scour depth increase is a logarithmic function of $(d_{50}v/b^3)t$ with σ_g as parameter that affects the final value of d_s/b , according to Fig. 2.12. Laboratory sized piers in sand beds require about three to four days for the development of the maximum clear water equilibrium scour depth. It is unlikely that the flow in the field stays constant long enough for this condition to be reached at full sized piers. However, it could be established starting from a residual scour created by a preceding live-bed condition.

A special case arises if the bed material is readily suspendible, like fine sand in strong flow or light weight particles in a laboratory flume. The depth of scour is a function of turbulence intensity which is high in the interface and wake region where the cast-off vortices can lift significant amounts of sand into the flow. The bed is lowered at the rear of the pier which in turn eases the removal of material from the front part. The result is a deeper scour.

2.14.5. Effect of Pier Alignment

The depth of local scour at all shapes of piers, except cylindrical, depends strongly on the alignment of flow. The depth of scour is a function of the projected width of the pier, normal to the flow which, with long piers in streamwise direction, increases rapidly with increasing angle of attack. As the angle of attack increases the point of maximum scour depth moves along the exposed side towards the rear of the pier, Fig. 2.16, and the maximum scour depth may move to the rear. The angle of attack for the maximum scour to be located at the rear depends on the ratio of the streamwise length of the pier to its thickness.

The classic studies of the effect of pier shape, alignment and velocity profiles by Tison (1940) form the foundation of subsequent studies. Laursen and Toch (1956) published a graph of multiplying factors for the scour depth, K_α , as a function of the angle of attack, α , and the pier length to width ratio L/b , as in Fig. 2.17. In general, angles of attack greater than $5-10^\circ$ should be avoided. If this is not possible the use of a row of circular piers would be preferable to a long solid one (Section 2.15.2).

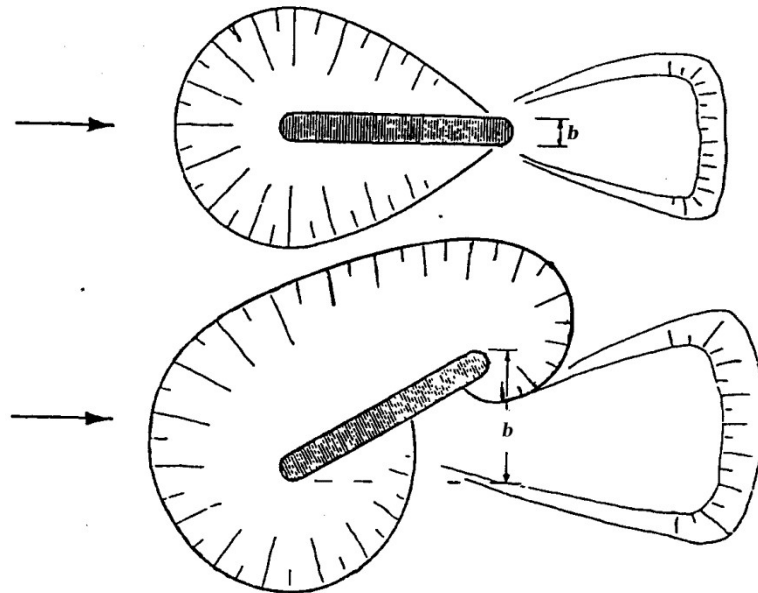


Fig. 2.16. Diagrammatic scour shapes at a pier aligned with flow and angled to the flow direction (after Raudkivi, 1998).

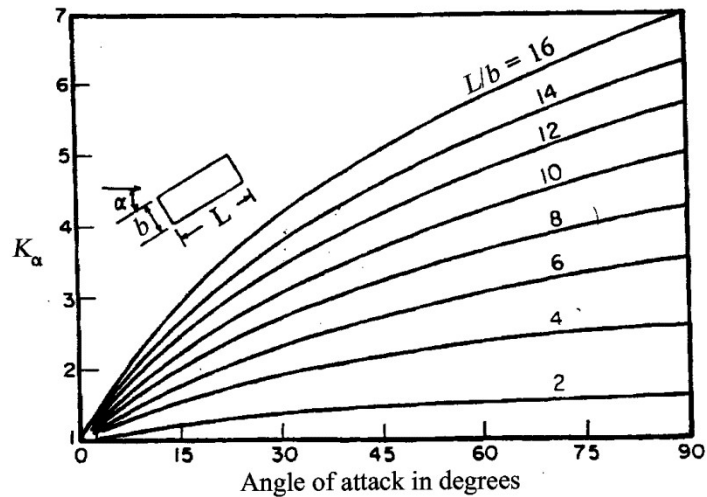


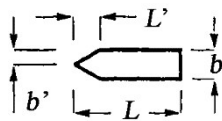
Fig. 2.17. Multiplying factor for scour depth for piers not aligned with flow (after Laursen and Toch 1995).

2.14.6. Effect of Pier Shape

Piers are often streamlined to reduce the drag exerted by flow and the size of the wake. Streamlining, however, is effective only within quite narrow limits of alignment with the flow.

Table 2.1. Pier shape coefficients (after Raudkivi, 1998).

Pier shape	b/L	b'/L'	K_s
Circular			1.0
Rectangular	1:1		1.22
	1:3		1.08
	1:5		0.99
Rectangular with semi-circular nose	1:3		0.90
semi-circular nose with wedge-shaped tail	1:5		0.86
Rectangular with chamfered corners	1:4		1.01
Rectangular with wedge-shaped nose	1:3	1:2	0.76
		1:4	0.65
Elliptical		1:2	0.83
		1:3	0.80
		1:5	0.61
		1:2	0.80
Lenticular			
		1:3	0.70
Aerofoil		1:3.5	0.80



The effect of pier shape can also be accounted for by a shape factor, K_s . However, in the field the effective shape can change substantially due to debris trapped during floods or ice jams. For piers aligned with flow, values of the shape factor K_s are listed for some types of pier cross sections in Table 2.1 in terms of width to overall length ratio, b/L , and pier shape (Dietz, 1972). The reported K_s values show an appreciable range of variation. The circular shape is used for comparative purposes. In practice, shape factors are important only if axial flow and freedom from debris can be assured. A small angle of attack can eliminate any benefit from pier shape.

The scour depth is also dependent on the slope of the leading edge of the pier to vertical. Laboratory results of scour depth at piers tapered, as illustrated in Fig. 2.18, are listed together with scour depth at a cylindrical/circular pier of the same diameter as the thickness of the tapered piers in the same sand bed ($d_{50} = 0.60$ mm, $\sigma_g = 2.0$) and same flow conditions in Table 2.2. The results show that a pier sloping downstream has a reduced scour. Frequently piers have footings (caissons) that are broader or have a larger diameter than the pier. Such caissons can reduce the scour depth by intercepting the downflow.

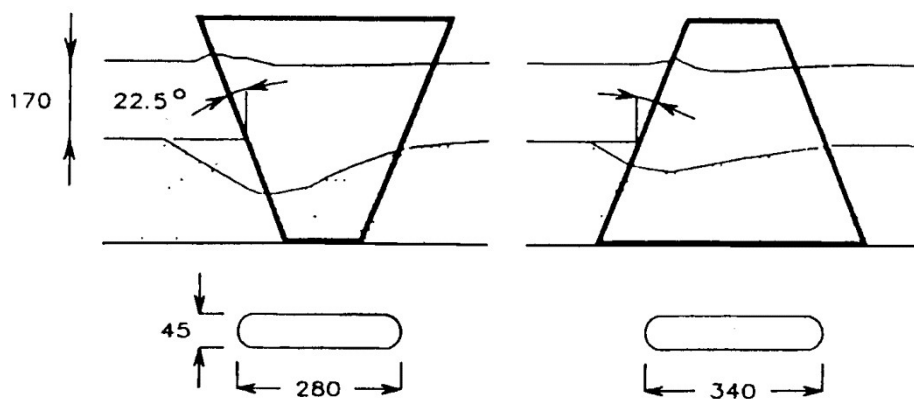




Fig. 2.18. Scour at piers tapered in elevation. Dimensions are at original bed level (after Raudkivi, 1998).

Table 2.2. Shape factors for tapered piers (after Raudkivi, 1998).

Shape	Velocity(m/s)	d_{se}/b (-)	K_s
Circular	0.67	1.69	1.00
	0.81	1.71	
 	0.67	2.03	1.20
	0.81	2.06	
	0.67	1.31	0.78
	0.81	1.26	0.74

2.15 Scour at Pier Groups

The designer has the control over the geometry of bridge foundations and can minimize the local scour depth by an appropriate choice. For example, a row of piers instead of a streamwise long pier that may lead to large scour depth due to an angle of attack. Scouring at

piers has been more extensively investigated than at pier groups. Useful insight into the local scour processes at pier groups was provided by the study by Hannah (1978). The study used circular piers in a steady flow at clear water scour conditions and uniform sand of 0.75 mm. Tests were first made with a single circular pier and with a pier of same thickness as the diameter of the pier, but six times the streamwise length. These provided the basis for comparison with pier groups. The tests showed that 80% of the equilibrium scour depth was reached after 7 hours. All subsequent tests were run for 7 hours. This scour depth at the 33 mm diameter pier was 62 mm ($h = 140$ mm, $u_* = 0.72u_{*c}$, $U = 0.285$ m/s).

2.15.1 Scouring Mechanism at Pier Groups

Four of the scouring mechanisms affecting scour at pier groups that are not present with a single pier are:

1. *Reinforcing* that leads to increased scour depth at the front pier if the scour at the downstream pier overlaps with that at the front pier. The lowering of the bed level at the rear eases the escape of material from the scour hole and leads to deeper scour.
2. *Sheltering* by the upstream pier can reduce the effective approach velocity for the downstream pier and reduce the scour depth. This can be augmented by the bar deposited downstream of the first pier. The bar deflects flow upwards and the effectiveness of downflow is reduced and horseshoe vortex weakened.
3. Vortices are shed from the upstream pier and advected downstream. If the downstream pier is close to the path of vortices these will assist scouring by lifting material from the scour hole.
4. If the transverse distance between the piers is decreased to the extent that the horseshoe vortices start to interact the inner arms of these vortices will be compressed. This causes the velocities within the arms to increase with a consequent increase in the scour depth.

2.15.2 Two Piers Scour

The scour depth at two piers in-line (zero angle of attack) is shown in Fig. 2.19 at each of the piers and for the bed level between the piers as a function of the relative spacing l/b . If the piers touch ($l/b = 1$), the scour depth at the front pier is the same as at a single pier but with increasing separation the front pier experiences the reinforcing effect which reaches a maximum at $l/b = 2.5$ and is evident until $l/b = 11$. For larger spacing, the scour depths are the same as for a single pier. With three piers in line at equal spacing up to $l/b = 6$, the scour at the middle pier was deeper and at the third pier, shallower than at the downstream pier of the two-pier arrangement (Raudkivi, 1998).

The results for *two-piers transverse to flow* (angle of attack 90°) are shown in Fig. 2.20. Both piers scoured to the same depth (± 2 mm) and the results have been averaged to define a single curve. The mid-distance scour is also shown. For the twin pier arrangement, $l/b = 1$, the scour depth is $1.93d_s$. This is in accordance with the concept of scour depth being proportional to the frontal width of the pier. The scour depth reduces rapidly with separation

to $1.3d_s$, at $l/b = 1.5$ and with l/b greater than 8, the scour depth is essentially that of a single pier. The scour holes become separate entities at $l/b = 11$ when the bed midway between them regains its original level.

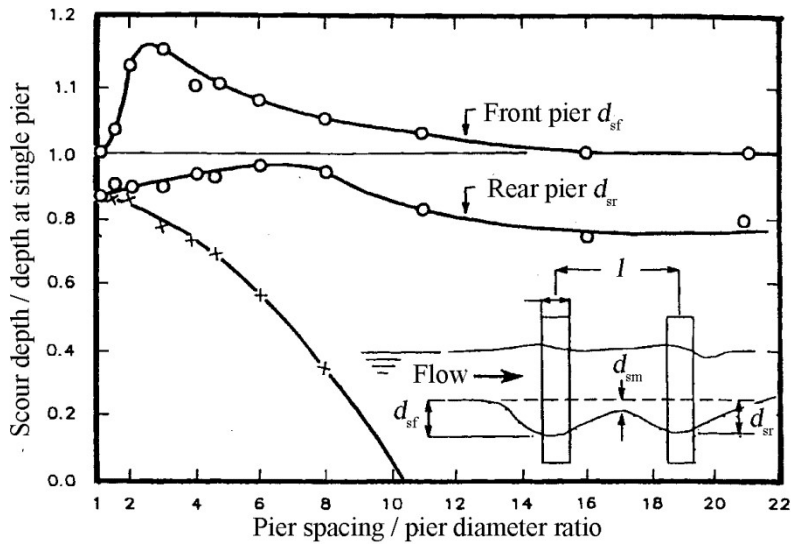


Fig. 2.19. Scour depth at two piers in line spacing (scale of ordinate changes for the front pier) (after Raudkivi, 1998).

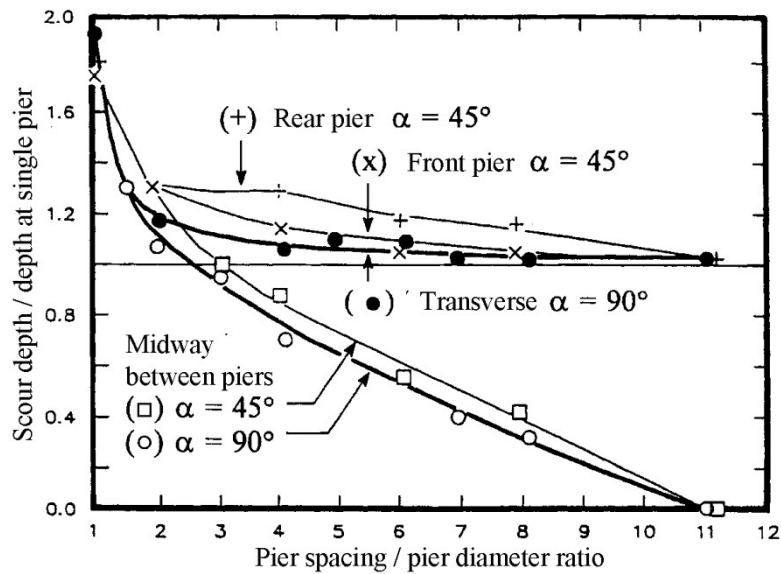


Fig. 2.20. Scour-depth at two piers as a function of pier spacing. Thick lines refer to piers transverse to flow and thin lines to angle of attack of 45° (Raudkivi, 1998).

At close spacing, $l/b < 2$, the increased scouring results from the increase in effective pier diameter. At $l/b > 2$, separate ‘horseshoe vortices’ form. These are compressed between the piers, and create higher velocities and greater scouring potential which decreases as l/b increases, reaching zero at $l/b = 8$. Figure 2.20 also shows the results of tests with two piers having their line of centres at 45° to the approach flow. The twin pier scour depth was 1.77 times of d_s . This is of the same order as the scour depth based on frontal width, namely $1.71 d_s$. Scour depth at the rear pier exceeded that at a front pier for all l/b -ratios between 1 and 11. At greater separations, the piers will act independently having scour depths equal to that of a

single pier and the bed-level midway between the piers will remain unaffected. Increased depths at the rear pier are caused by a combination of the action of the shed vortices from the front pier and compression of the ‘horseshoe vortices’ between the two piers. Evidently, these two processes overcome any sheltering effects and have their maximum influence at $l/b = 4$ where the difference between front and rear scour depths was a maximum.

Effect of angle of attack (α) Tests were carried out with a $l/b = 5$ for $0^\circ < \alpha < 90^\circ$ at 15° intervals and the results are shown in Fig. 2.21. Scour at the front pier was not sensitive to angle of attack, varying by less than 5% of its value at $\alpha = 0^\circ$. Because the scour at the rear pier is affected by the various scouring mechanisms (described above) its depth at the rear pier is more sensitive to the angle of attack. At small angles, ($\alpha < 15^\circ$), the dominant effect at the rear pier is the sheltering by the front pier. As the angle increases, sheltering is reduced and the pier is affected by shed vortices. Consequently, scour depths increase, reaching a maximum (for $l/b = 5$) at approximately 45° . Scour depths reduce when the pier moves clear of the shed vortices and approach that of a single pier as angle of attack approaches 90° .

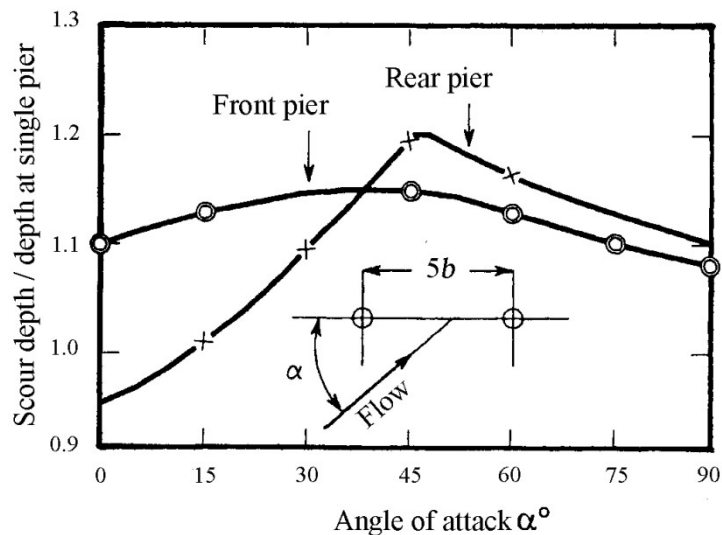


Fig. 2.21. Effect of angle of attack, α , on scour depth at two piers spaced five pier diameter apart (after Raudkivi, 1998).

2.16 Velocity Measurement

2.16.1 Introduction

Pilot tubes are very commonly used for velocity measurement in a wide variety of flow situations due to their simple construction and low cost. Although their application is primarily meant for laminar incompressible flows at high velocities, measurements can be made in turbulent or compressible flows with some modifications.

A *hot film anemometer* measures local instantaneous velocity based on principles of heat transfer. It can be used to measure three components of velocity and velocity fluctuations arising in turbulent flow.

2.16.2 Velocity Measurement using VectrinoPlus

The VectrinoPlus is a high-resolution acoustic velocimeter (make: Nortek AS, Norway made) used to measure turbulence and 3D water velocity in a wide variety of applications from the laboratory to the ocean.

The VectrinoPlus probe is made of titanium and consists of four receiver transducers and a transmit transducer (Fig. 2.22). It is mounted on a fixed stem connected to the main housing through the probe end bell. Each of the four receive transducers is mounted inside a *receiver arm*. The transmit transducer is in the centre of the probe. The transducers are covered with hard epoxy. The electronics module is located inside the pressure case and consists of a single board with the power transmitter, analogue and digital signal processing, power conditioning, and interface circuits. And also the temperature sensor (thermistor) is located inside the probe head.

The basic measurement technology is coherent Doppler processing, which is characterized by accurate data and no appreciable zero offset. The VectrinoPlus uses the Doppler effect to measure current velocity by transmitting a short pulse of sound, listening to its echo and measuring the change in pitch or frequency of the echo (Vectrino Manual, 2004) i.e. a pulse is transmitted from the centre transducer, and the Doppler shift introduced by the reflections from particles suspended in the water, is picked up by the four receivers of the vectrinoPlus probe.

The signal-to-noise ratio (SNR) is defined as

$$\text{SNR} = 20\log_{10}(\text{Amplitude}_{\text{Signal}}/\text{Amplitude}_{\text{Noise}}) \quad (2.25)$$

Some noise will always be present, so amplitude depends upon amplitude signal plus amplitude noise. However, for SNR values in the magnitude applicable to typical VectrinoPlus situations, the difference is negligible.

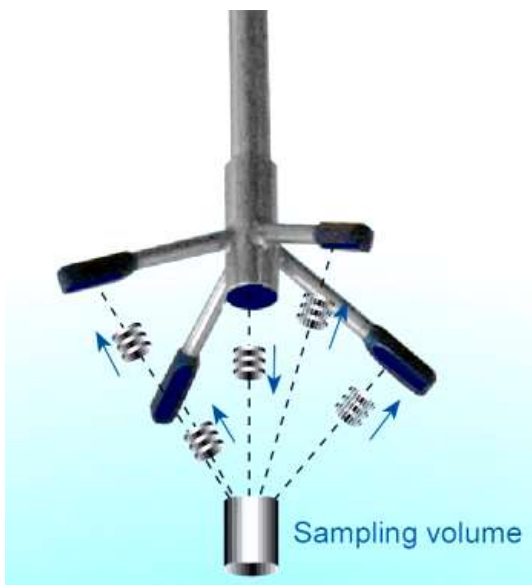


Fig. 2.22. VectrinoPlus velocimeter operating principle.

Sampling rate sets the output rate for the velocity, amplitude, correlation and pressure data. The VectrinoPlus allows data collection rates up to a *sampling rate* of 200 Hz. *Sampling volume height* is cylindrical with a user selectable height of 3-15 mm. *Sampling diameter* is 6 mm. Distance from the probe is 5 cm. If the *transmit length* is increased then SNR ratio will be increased. Speed of sound depends upon *salinity* of water. The salinity is 0 for fresh water and typically 35 ppt for the ocean water.

The VectrinoPlus software saves data as binary files, which are easily converted to ASCII format files, using the conversion module in the software.

- The *.hdr file is a self-documented table. Please note that this file contains a detailed data format description of all files that are generated.
- The *.dat file contains velocity data at the full sample rate.

ASCII files are easily imported into most spreadsheets and data analysis programs.



- 1) Transportation and storage case
- 2) VectrinoPlus velocimeter
- 3) External power/signal cable
- 4) Tool kit, Nortek
- 5) USB to serial converter
- 6) Seeding material (bottle of 250 ml)
- 7) AC/DC voltage transformer, 24V DC.
- 8) International kit with AC plugs
- 9) USB memory stick with Vectrino software.

Fig.2.23. VectrinoPlus velocimeter.

2.17 Nomenclature

A	area enclosed between successive vorticity contours [L ²]
b	pier width (L)
d_s	scour depth [L]
d_{se}	equilibrium scour depth [L]
d_{sm}	maximum scour depth [L]
$d\vec{s}$	differential displacement vector over a closed curve
d_{16}	16% finer sand diameter [L]
d_{50}	median diameter of sand [L]
d_{84}	84% finer sand diameter [L]
d_{90}	90% finer sand diameter [L]
F	Froude number of flow, U/\sqrt{gh}
g	acceleration due to gravity [LT ⁻²]
h	approaching flow depth [L]
h_0	initial flow depth [L]
i,j,k	direction indices along the x , y and z axes, respectively
k	turbulent kinetic energy, $k = \frac{1}{2}(u'^2 + v'^2 + w'^2)$ [L ² T ⁻²]
l	Longitudinal spacing between two consecutive piers [L]

L	Length of pier [L]
n	vortex shedding frequency [T^{-1}]
p	instantaneous pressure [$ML^{-1}T^{-2}$]
p'	fluctuation of p [$ML^{-1}T^{-2}$]
R	hydraulic radius [L]
s	relative density of sand, ρ_s/ρ [--]
t	time [T]
t_0	initial start time [T]
t_1	the time over which the time-averaged mean is taken [T]
u, v, w	time-averaged velocity in the x, y and z directions, respectively [LT^{-1}]
u', v', w'	fluctuations of u, v, w , respectively [LT^{-1}]
u^+, v^+, w^+	$\sqrt{u'u'}, \sqrt{v'v'}$ and $\sqrt{w'w'}$ respectively [LT^{-1}]
u_*	$(\sqrt{\tau_0/\rho})$ shear or characteristic velocity [LT^{-1}]
\bar{u}	u/u_* [--]
u_{*c}	critical shear or characteristic velocity [LT^{-1}]
U	local or depth-averaged approaching flow velocity [LT^{-1}]
U_c	critical local or depth-averaged approaching flow velocity [LT^{-1}]
\vec{V}	velocity vector over a closed curve
x, y, z	coordinate axes [L]
Δ	(s-1) Apparent roughness [--]
ρ	mass density of water [ML^{-3}]
ρ_s	mass density of sand [ML^{-3}]
Δt	change of time [T];
Δx	spacing between the grid points along x direction [L]
h/b	flow shallowness or relative inflow depth [--]
ζ	vorticity, $\partial v/\partial z - \partial w/\partial r$ [T^{-1}]
ζ_y	y -component of vorticity [T^{-1}]
μ	dynamic viscosity [$ML^{-1}T^{-1}$];
ν	(μ/ρ) kinematic viscosity [L^2T^{-1}]
γ	coefficient (or angle) [--]
λ	angle made by the longitudinal sloping bed with horizontal [degree]
α	angle of attack [degree]
η	height of bed features [--]
κ	von Karman's constant [--]
τ	$(\tau_v + \tau_i)$ total shear stress [$ML^{-1}T^{-2}$]
τ_c	critical shear stress [$ML^{-1}T^{-2}$]
τ_{ca}	critical armour layer shear stress [$ML^{-1}T^{-2}$]
τ_0	$(\rho g R \sin \lambda)$ average bed shear stress [$ML^{-1}T^{-2}$]

τ_t	shear stress due to turbulence [ML ⁻¹ T ⁻²]
τ_v	shear stress due to viscosity [ML ⁻¹ T ⁻²]
τ_u, τ_v, τ_w	turbulent shear stresses in x, y and z directions respectively [ML ⁻¹ T ⁻²]
σ_g	$(\sqrt{d_{84} / d_{16}})$ geometric standard deviation [--]
$\sigma_u, \sigma_v, \sigma_w$	normal stresses in x, y and z directions respectively [ML ⁻¹ T ⁻²] and
Ω	circulation [L ² T ⁻¹]

2.18 Bibliography

- Anderson, A.G.: Scour at bridge waterways - A review. *U. S. Dept. Transportation. Office Res. and Dev., Environmental Design and Control Div.* (1974).
- Breusers, H.N.C.; Raudkivi, A.J.: Scouring, IAHR Hydraulic Structures Design Manual, Vol. 2, *A. A. Balkema Publ., Rotterdam, The Netherlands.* (1991)
- Breusers, H.N.C.; Nicollet, G.; Shen, H.W.: Local Scour Around Cylindrical Piers. *J. Hydraul. Res.* 15(3), 211-252 (1977)
- Chee, R.K.W.: Live-bed scour at bridge piers. *Report No. 290. M.E. Thesis.* Dept. Civil Engg., Univ. Auckland, New Zealand. (1982).
- Chiew, Y.M.: Local scour at bridge piers. *Report No. 403. Ph.D. Thesis.* Dept. Civil Engg., Univ. Auckland, New Zealand. (1984).
- Chabert, J.; Engeldinger, P.: Etude des Affouil-Lements autour des Piles des Ponts. *Laboratoire National d'Hydraulique, Chanton, France.* (1956).
- Das, S: Study of the impact of sediment transport dynamics on clear water scour. *Ph.D. Thesis.* School of Water Resources Eng., Jadavpur Univ., India. (2013)
- Dey, S.: Lecture Note on Sediment Transport and Scour. Dept. Civil Engg., Indian Institute of Technology Kharagpur, India. (2006)
- Dey, S.: Fluvial Hydraulics-Hydrodynamic and Sediment Transport Phenomena. Springer-Verlag, Berlin, Heidelberg. (2014)
- Dietz, J.W.: Systematische Modellversuche iiber die Pfeilerkolkbildung. *Mitteilungsblatt der Bundesanstalt für Wasserbau, Karlsruhe, Germany, Nr. 31, 95-109* (1972)
- Enema, R.: Scour at bridge piers. *Report No. 216.* School of Engg., Univ. Auckland. Auckland, New Zealand. (1980).
- FAMATF F.: Fundamentals and modeling aspects of turbulent flow. *Report on Short Term Course.* ITT Kanpur, Dept. of Mech. Engg. (1995)
- Hannah, C.R.: Scour at pile groups. *Report No. 78-3, 92.* Univ. Canterbury, New Zealand, Civil Engg. Res. (1978)
- Hjorth, P.: Studies on the nature of local scour, No. 46. *Dept. Water Res. Engg., Lund Inst. Tech., Bulletin Series A.* (1975)
- Hoffmas, G.J.C.M.; Verheij, H.J.: Scour Manual. *A. A. Balkema Publ., Rotterdam, The Netherlands.* (1998)

- Hopkins, G.R.; Vance, R.W.; Kasraie, B.: Scour around bridge piers. *Final reports FHWA-RD-78-163, FHWA-RD-75-56 (1975) and FHWA-RD-78-103 (1980)*. Federal Highway Administration. Washington, D. C. (1983)
- Horizon ADV. Sontek ADV User Guide. SonTek/YSI, Inc., CA, USA. (2005).
- Kramer, H.: Sand mixtures and sand movement in fluvial levels. *Transactions of the American Society of Civil Engineers*. 100(1), 798-838 (1935)
- Laursen, E.M.; Toch, A.: Scour around bridge piers and abutments, 4. *Iowa Highway Res. Board*. Ames, Iowa. (1956)
- Melville, B.W.: Scour at Bridge sites. *Report No. 104*. School Eng., Univ. Auckland, New Zealand. (1974)
- Melville, B.W.: Local scour at bridge sites. *Report no. 117*. School Engg., Univ. Auckland. Auckland, New Zealand. (1975)
- Melville, B.W.; Raudkivi, A.J.: Flow characteristics in local scour at bridge piers. *J. Hydraul. Res.* 15(4), 373-380 (1977)
- Michael, S.A.; Mohamed, G.M.; Mohamed, S.B.A.M.: Wake vortex scour at bridge piers. *J. Hydraul. Eng.* 117(7), 891–904 (1991).
- Raudkivi, A.J.: *Grundlagen des Sedimenttransports*. Springer-Verlag (1982).
- Raudkivi, A.J.: Functional trends of scour at bridge piers. *J. Hydraul. Eng.*, 112(1), 1-13 (1986)
- Raudkivi, A.J.: *Loose Boundary Hydraulics*. A. A. Balkema, Rotterdam. (1998)
- Raudkivi, A.J.; Enema, R.: Effect of sediment gradation on clear-water scour. *Proc. ASCE*, 103(HY 10), 1209-1213 (1977a)
- Raudkivi, A.J.; and Enema, R.: Effect of sediment gradation on clear-water scour and measurements of scour depth. *Proc. 171th International Congress JAHR*, 4, 521-527. Baden-Baden. (1977b)
- Raudkivi, A. J.; Sutherland, A. J.: Scour at bridge crossings. *National Roads Board Res. Unit, Bulletin No. 54*, Wellington, N.Z., 100. (1981)
- Shields, A.: Application of similarity principles and turbulence research to bed-load movement. *Mitteilungen der Preussischen Versuchsanstalt für Wasserbau und Schiffbau*. 26, 5-24. Berlin, Germany. (1936).
- Thompson, S.M.; Davoren, A.: Local scour at a pier. *Report No. WS 756*. Ohau River, Otago, New Zealand. Ministry of Works and Developments, Christchurch, New Zealand. (1983)
- Tison, L.J.: Erosion autour de piles de pont en riviere. *Ann. Des Travaux Publics de Belgique*, 41, 813-871 (1940)
- USWES: Flume tests made to develop a synthetic sand which will not form ripples when used in movable bed models. *Tech. Memo. 99-1*, United States Waterways Experiment Station, Vicksburg, Mississippi, USA. (1936)
- Vanoni, V.A.: Measurements of critical shear stress. *Rep. No. KH-R-7*, California Inst. Tech., USA. (1964)
- Vectrino Manual. Nortek Vectrino Velocimeter User Guide. Nortek AS, Norway. (2004)
- White, F.M.: *Viscous Fluid Flow*, 2nd Edition. McGraw-Hill, Inc., Singapore. (1991)

3. FLOW AROUND THREE INLINE ECCENTRIC CIRCULAR PIERS

3.1 Introduction

Local scour at single pier and multiple piers has been extensively studied by several investigators, but scanty work is available on scour around piers placed in close proximity. The work explained in this chapter is concerned with laboratory flume experimental studies of the formation and characteristics of local equilibrium scour around a set of three identical circular shaped piers in inline-eccentric-inline arrangement placed in a staggered manner on scoured sand bed. The inline-front circular pier and inline-rear circular pier were set along the flow and the third one is set eccentrically in mid region of inline-front and inline-rear circular piers. The experimental research was carried out at equilibrium scour state and at clear-water condition. Throughout the experiments, depth mean approach flow-velocity and approaching flow depth was fixed to 24.7 cm/sec and 12.5 cm respectively on a uniform sand bed, having median diameter 0.825 mm. A set of nine experiments were carried out in clear water scour condition, with the objective to observe the nature of scour evolved and to study the nature and location of scour formed around the piers and the mutual interference of flow between the piers during the formation of scour hole, by varying the longitudinal spacing between the two inline piers.

The eccentricity was kept constant equal to $3b$ (where b =base of a pier) and the spacing along the flow between the inline-front and eccentric-middle and between the eccentric-middle and inline-rear circular piers considered were $(2/8)$, $(3/8)$, $(4/8)$, $(5/8)$, $(6/8)$, $(7/8)$, $(8/8)$, $(9/8)$ and $(10/8)$ of l_{ss} where, l_{ss} is the maximum equilibrium length of sediment transport (sum of maximum equilibrium scour length and maximum dune length) for a single circular pier experiment. For each experiment maximum equilibrium scour depth, length, width, surface area and volume of removed bed material have been observed.

In order to have a comparative and more accurate study, this chapter provides the experimental results of the flow patterns and hydrodynamic turbulence patterns around the three identical circular piers arranged in inline-eccentric-inline arrangement, with constant longitudinal spacing equal to $(4/8)l_{ss}$ that is half of the maximum equilibrium length of sediment transport of a single circular pier and constant eccentricity $3b$. The detailed 3-D velocities were captured instantaneously at five different vertical azimuth-planes (0° , $\pm 45^\circ$, $\pm 90^\circ$) by using an ADV, Nortek-USA made Vectrino+, changing positions around three circular piers and also at two horizontal-planes around the three circular piers at 4% and 50% of approaching flow-depth above bed level ($h=0$). The contour profiles and distribution of velocity-components, turbulence kinetic energy and intensities have been computed and analysed at the vertical r - z planes and horizontal x - y planes around the three circular piers. The velocity-vectors plot and time-mean absolute-velocity acquired from velocity-profile shows detailed hydrodynamic flow characteristics. Vorticity and circulation generated at the upstream zone near the three circular piers are presented.

Three circular-piers combined arrangement and interferences between on another, plays an essential role in formation and enhancement of larger scour-depth near circular

eccentric pier and the sand-particles transport was found more towards flume-wall. During the experimentation pressure drag becomes much higher than skin friction drag, because of the presence of bluff body. The flow characteristics of the horseshoe vortex are discussed. Vortex strength of the eccentric-middle and inline-rear pier is found higher and lower, respectively, than the inline-front pier.

3.2 Brief Review of Relevant Works

Flow behaviour around circular cylinders is a classical problem. Prediction of scour magnitude around multiple piers is a valuable issue to the field engineers. Nowadays, multiple piers group are becoming more popular in bridge design due to geotechnical and economical usefulness. An estimation of the maximum possible scour around bridge pier is necessary for its safe and secure design. The scour mechanism for multiple pier groups is highly complex and it is very difficult to estimate local scour depth, where the direct use of the outcomes acquired from single pier may be problematical.

Over the years there are various laboratory-flume experiments to predict the scour depth around the base of the piers by Breusers *et al.* (1977), Raudkivi and Ettema (1983), Breusers and Raudkivi (1991), Melville (1992), Dey (1997), Hoffmans and Verheij (1997), Melville and Chiew (1999); Melville and Coleman (2000), Richardson and Davis (2001), Ataie-Ashtiani and Beheshti (2006) Khwairakpam *et al.* (2012) and Das *et al.* (2014a, 2014c). Most of these studies were confined to single pier. These studies were performed primarily by means of laboratory-flume experiments, including the use of dimensionless equations finally resulting in some semi-empirical equations for computing the maximum scour depth.

A long-standing concern is the tendency of some of these equations to over predict the maximum scour depth for field or even for laboratory conditions [Melville (1975) and Dargahi (1990)]. A lack of understanding of the flow structure around the bridge piers and their interaction with the bed sediment is also responsible for this problem. Therefore, many laboratory flume based experiments were investigated by numerous researchers for accumulating more information on flow behaviour and scour mechanism and to compute scour depth with more precision. Many of the researchers stressed on velocity and subsequent patterns of the flow fields and turbulence fields around piers of different shapes [Melville (1975), Melville and Raudkivi (1977), Dargahi (1989), Dargahi (1990), Dey *et al.* (1995), Muzzammil and Gangadhariah (1995), Ahmed and Rajaratnam (1998), Graf and Yulistiyanto (1998), Istiarto and Graf (2001), Graf and Istiarto (2002), Muzzammil and Gangadhariah (2003), Roulund *et al.* (2005), Ettema *et al.* (2006), Unger and Hager (2007), Kirkil *et al.* (2008) and Kirkil *et al.* (2009)].

For better understanding of the flow fields and turbulence fields at clear water equilibrium condition around piers and cylinders, there are a few experiments which were conducted on single-pier for determining more accurate scour depth based on vortex velocity flow fields [Dey and Raikar (2007), Das *et al.* (2013a-c), Das and Mazumdar (2015a)]. These studies were confined to only single pier and provided detailed information around single pier.

In the context of geotechnical and economical reasons, bridge designs often lead to complex multi pier arrangement in which case the direct use of the results obtained from single pier may be very problematic. There are a large number of studies around pier groups and complex piers that focused on the prediction of the maximum scour depth. For a pier in a multi-pier arrangement, combined effects are notable, in addition with those parameters which influence scouring around single-pier arrangement. Sheppard *et al.* (1995) carried out researches on two pier arrangements, where the piers were located along the direction (inline) of flow and found that two additional parameters reinforcement and sheltering affect the flow. Most of the multi-pier experiments have been restricted to two circular pier arrangements, positioned either inline-eccentric, inline-inline or side by side that focused on the prediction of flow-fields, turbulence fields and the scour geometry [Zdravkovich (1987), Sumner *et al.* (1999), Akilli *et al.* (2004), Coleman (2005), Ataie-Ashtiani and Beheshti (2006), Mahjoub *et al.* (2008), Ataie-Ashtiani *et al.* (2010), Ataie-Ashtiani and Aslani-Kordkandi (2012, 2013), Das *et al.* (2014*b*) and Das and Mazumdar (2015*b*)] and the effect of pier spacing on flow characteristics and on scour depth [Raudkivi (1998), Graf (2003), Das *et al.* (2014,2016) and Yilmaz *et al.* (2017)]. A research on two-pier with inline-eccentric arrangement can amplify sediment to move towards the river bank flowing downstream was described by Michael *et al.* (1991).

Very few researchers described some detailed analysis of turbulent flow fields around multi-pier (two circular pier) arrangements at clear water scour condition.

Zdravkovich (1987) found that depending on the pier spacing, the wake vortex structures changes behind the piers. The down flow and surface roller formed in front of the pier are similar to those in single pier.

Beheshti and Ataie-Ashtiani (2010) experimentally investigated the three-dimensional turbulent flow field around a complex bridge pier placed on a rough fixed bed. The complex pier foundation consisted of a column, a pile cap and a 2×4 pile group. All of the elements were exposed to the approaching flow. An acoustic Doppler velocimeter (ADV) was used to measure instantaneously the three components of the velocities at different horizontal and vertical planes. Profiles and contours of time-averaged velocity components, turbulent intensity components and turbulent kinetic energy as well as velocity vectors were presented and discussed for different vertical and horizontal planes. Their study does not provide a better understanding of flow fields around piles situated under a pile cap and inside the scour hole.

Ashtiani and Kordkandi (2012) investigated the three-dimensional flow around two side-by-side circular piers. The flow characteristics in the near-wake region around piers were investigated. They addressed how the horseshoe vortex flow and corresponding turbulence characteristics change between the two piers and how the two piers affect the flow structure and its intensity in comparison with a single pier case. The single pier tests were carried out by the authors in order to have a comparative study in the same experimental conditions as for the two side-by-side piers. They observed that the scour is initiated at, or close to the nose of the cylinders as well as around the piers, especially between the two piers and the scour hole of each pier increase and then overlaps each other at the region between the two piers. Due to decrease in flow area between the two piers, a contracted flow is formed. The contours and distributions of the time-averaged velocity components, turbulence

intensities, turbulence kinetic energy and velocity vectors were presented at different horizontal and vertical planes.

Ashtiani and Kordkandi (2013) investigated the 3-D flow around two circular piers in tandem and a single pier. Velocities were measured by an ADV. The contours of the time-averaged velocity components, turbulence intensities and turbulence kinetic energy at different horizontal and vertical planes were presented. They addressed how the horseshoe vortex flow and corresponding turbulence characteristics change between the two piers and how the two piers affect the flow structure and its intensity in comparison with a single pier case. The single pier tests were carried out in the same experimental conditions as for the two circular piers in tandem. The presence of rear pier changes the flow structure to a great extent, particularly in the near-wake region. Within the gap between the two piers, a stronger and substantial upflow was shaped. In tandem piers, the high values of turbulence characteristics were found near the rear pier.

Three-dimensional flow-fields, turbulence-fields for horseshoe-vortex around two equilateral triangular piers [Das *et al.* (2014c)], two circular piers [Das and Mazumdar (2015b)] and two square piers [Das and Mazumdar (2018)] of equal width b positioned in inline front and eccentric rear arrangement with constant eccentricity $3b$ under similar experimental conditions were investigated. Eccentricity and longitudinal gap were taken as thrice of pier size and half the maximum length transported by sediment particles at equilibrium state for single pier test, respectively

Das and Mazumdar (2015b) investigated the three-dimensional flow and turbulence field interactions around two circular piers with inline front and eccentric rear pier arrangement. They observed the three-dimensional flow fields and turbulence fields' interactions. The contours and distributions of the time-averaged velocity components, turbulence intensities and turbulence kinetic energy at different vertical planes are presented. They addressed how the horseshoe vortex flow formations and consequent turbulence characteristics vary between the two identical piers and how the two piers influence the flow formation and its intensity.

Velocity vectors obtained from the time-averaged velocity fields are used to illustrate further flow features. The two identical circular piers influence the structure of flow and its flow intensity. The plots of time mean absolute velocity components presented a good perceptible of vortex characteristics at pier upstream. Vorticity determination and circulation estimation were conducted using dynamics of computational fluid and the theorem of Stokes. For the eccentric rear pier, circulation magnitude was found greater than circulation magnitude for inline front pier. It was detected that the streamlines at the frontal side of eccentric rear pier diverged with a higher tangential velocity than that of the inline pier. A partial sheltering effect occurred in between the piers. For the eccentric rear pier, the magnitude of radial velocity was almost always higher than inline front pier. The co-shedding regime was developed at the downstream of inline pier. The horseshoe vortex core size for eccentric rear pier was found always bigger than the inline front pier. For eccentric rear pier, magnitude of circulation was always higher compared to inline front pier for subsequent azimuth angles in vertical planes. The end results of the experiment were compared with the result of a single pier lab-flume experiment for corresponding pier-shape with same experimental conditions.

Further lab-flume experiments were executed for investigating the pattern of scour formation around two circular, square and equilateral-triangular tandem piers at constant eccentricity [Das *et al.* (2016)]. It is observed that pattern of scour varies by changing longitudinal distance (spacing) between the piers. The scour angle of diversion and deposition of the sand was observed more on the eccentric pier side towards the wall. Biggest scour hole was found in case of square-piers compared to the equilateral triangular-piers and the circular-piers, respectably.

Michael *et al.* (1991) showed how eccentrically arranged piers can cause sediment to move towards the flume wall flowing downstream. The horseshoe vortex in the middle of two piers can enlarge the scour hole of the downstream pier while shifting the sediments away from the downstream plane of symmetry.

Yilmaz *et al.* (2017) established a semi-empirical model for computing scour-depth at clear-water around inline two circular-piers. The investigations were investigated using piers of three different diameters and using three different longitudinal gaps within the piers. As a result, near front-pier, shape and size of the scour-hole stays almost invariable with time. A design-chart was established, made from the measured scour-depth and the time.

The present study though inspired by the aforementioned pioneer works on scouring differs in the context of dealing with three identical piers. It is obvious that almost no experimental work was carried out to study the horseshoe vortex flow pattern and characteristics around the piers in case of (present study) three circular piers with inline-eccentric-inline arrangement. The main objective of this research is to observe the interactions between three-dimensional flow fields and turbulence fields around the piers. This study addresses how the horseshoe vortex flow and corresponding turbulence characteristics change between three circular piers of identical width. In this study, the contours and distributions of the time-averaged velocity components, turbulence intensities and turbulence kinetic energy at different vertical planes and horizontal planes are presented. Velocity vectors obtained from the time-averaged velocity fields are used to illustrate further flow features. Vorticity and circulation of the horseshoe vortex around the three piers are also presented.

3.3 Scope of the Present Work

The present study though inspired by the aforementioned pioneer researches on scouring, velocity fields and subsequent turbulence fields interactions differ in the context of dealing with three identical circular piers. Hardly there were any lab-flume based experimental investigation done to find out the vortex flow pattern and characteristics around the three longitudinally equidistant circular piers having a plan of (inline-front, inline-rear) two inline circular piers and an eccentric-middle circular pier arrangement. In the present study an attempt has been made to carry out experiments with inline-eccentric-inline arrangement of pier groups varying the longitudinal spacing and to delineate the scour geometry. Here, the vital objective is to study the hydrodynamic interactions between three-dimensional turbulent velocity flow fields around the circular piers. This study also addresses the change of flow patterns due to horseshoe vortices and related variations in turbulence characteristics in that

zone around the three-piers. This study represents the contours and the distributions of time-averaged velocity components, turbulence intensities, and turbulence kinetic energy at five vertical planes and at two horizontal planes (4% and 50% of the approaching flow depth) around the three circular piers. The velocity vectors obtained from the time-averaged velocity fields and absolute velocity addresses more hydrodynamic flow characteristics. Besides that, the vorticity and the circulation computed for the horseshoe vortex around the circular piers are also well furnished.

3.4 General Experimental Setup and Technique

In this present study, the outcomes acquired for the equilibrium clear-water scour holes that is the geometrical parameters like scour depth, length, width, hole surface area, volume were analysed. The instantaneous tangential (u), radial (v) and vertical (w) velocities were measured with the help of ADV. The detailed laboratory experimental setup is shown in the schematic diagram as given in Figs. 3.1, 3.2 and 3.3. Table 3.1 lists the experimental conditions for all the tests.

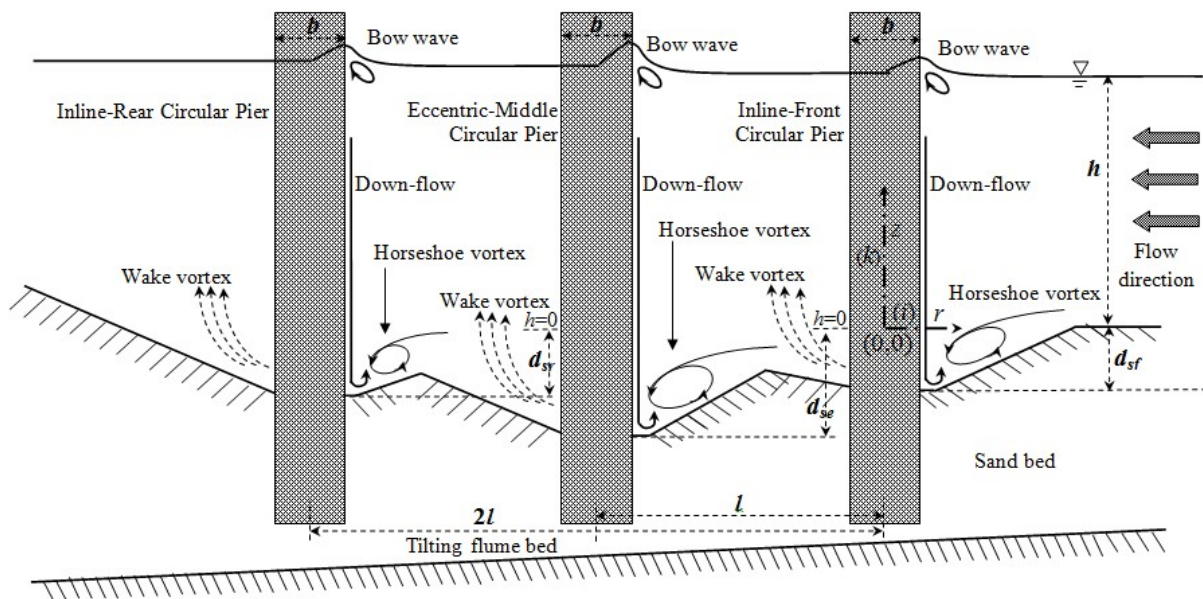


Fig. 3.1. Schematic diagram showing the elevation wise flow patterns around three inline-eccentric-inline arranged circular piers.

Here the experimental runs were conducted in the Fluvial Hydraulics Laboratory of the School of Water Resources Engineering in Jadavpur University, Kolkata, West Bengal, India in a hydraulic rectangular flume of tilting and re-circulating type having transparent Perspex sided walls. Dimensionally, the flume is 1100 cm long, 81 cm wide (internal) and 60 cm deep. The effective working section of the flume where the piers were placed carefully was located 290 cm downstream from inlet of the flume, piled up with experimental sand particles of fixed breath covering the complete base was 20 cm and length of 300 cm. For all the experiments, three identical circular shaped piers were considered with a constant diameter (b) of 7 cm.

The entire study was completed using the same sand particle with size: median diameter $d_{50}=0.825$ mm, $d_{16}=0.5$ mm and $d_{90}=1.78$ mm. Those sand particle sizes were calculated from sieve analysis using a vibrating shaker. The geometric standard deviation $\sigma_g = \sqrt{d_{84}/d_{16}}$ of such bed particles was calculated 1.8. According to Raudkivi (1998), the sediment is uniform if $\sigma_g < 2$. Bed slope of prepared sand bed (S) was retained at 1:2400 for all the experiments.

The re-circulating flow system was maintained continuously through a variable speed 7 hp centrifugal pump capable of delivering a maximum discharge of 25.5 l/s, with rpm of 1450 and power of 7.5 kW. Water was pumped directly into the flume inlet through a 20 cm diameter pipe line from the reservoir, with a discharge of 25 l/s, which was measured and maintained with an analogue type flow meter coupled to inlet flow pipeline just before the flume inlet by adjusting both the delivery outlet and bypass valves.

A point-gauge of Vernier-type was fixed within a movable trolley to slide on the flume having ± 0.1 mm accuracy and was used to measure water depth, initial bed level and scour hole near the piers. Approach flow depth (h) in the flume was retained as 12.5 cm, by operating flume downstream gate, which was required for all the experimentations. The ratio of mean depth (h) to pier width (b) i.e. h/b is 1.786. It is greater than 0.6 which confirms uninterrupted approach depth of flow throughout all the experiments and possibly is considered to be 2-D as $h/b > 1.7$.

For all the tests, Froude number, $F [=U/\sqrt{gh}]$ and densimetric Froude number, $F_{d_{50}} [=U/\sqrt{g'd}]$ were set constant. Here, g' denotes relative gravity $[=g(\rho_s - \rho)/\rho = g\Delta]$, U indicates mean approach flow velocity, g indicates acceleration due to gravity, h indicates approaching water depth, ρ indicates water mass density, ρ_s indicates bed particles mass density and $\Delta = (\rho_s - \rho)/\rho$. For all tests, particles relative density $[(\Delta + 1) = 2.58]$ was also set constant; angle of repose of the bed sediment in still water (ϕ_r) was calculated 36° , average bed shear stress was calculated 0.39 Pa, and shear induced threshold bed stress shear was calculated 0.40 Pa. Here, Pier Reynolds number (R_p), Flow Reynolds number (R_e) and subcritical (F) Froude number were measured and kept constant as 17709, 24165 and 0.223, respectively.

Based on the concept, as published by Das and Mazumdar (2015b), perspex hollow circular piers of 7 cm side were considered for the entire experimentation, for comparing the outcomes between present study (inline-eccentric-inline arrangement) and previous study (inline-eccentric arrangement) [Das and Mazumdar (2015b)]. Here, three identical piers of 7 cm width (b) were placed centrally on the effective working section of hydraulic flume and it was levelled carefully as in Fig. 3.1.

The sidewall of flume has no impact on scouring, because width of the flume and pier ratio is higher than 6.5 [Ashtiani and Kordkandi (2012)] and size of experimental sand particle has no impact on scoured-depth, because $b/d_{50} > 50$ [Melville and Raudkivi (1977)].

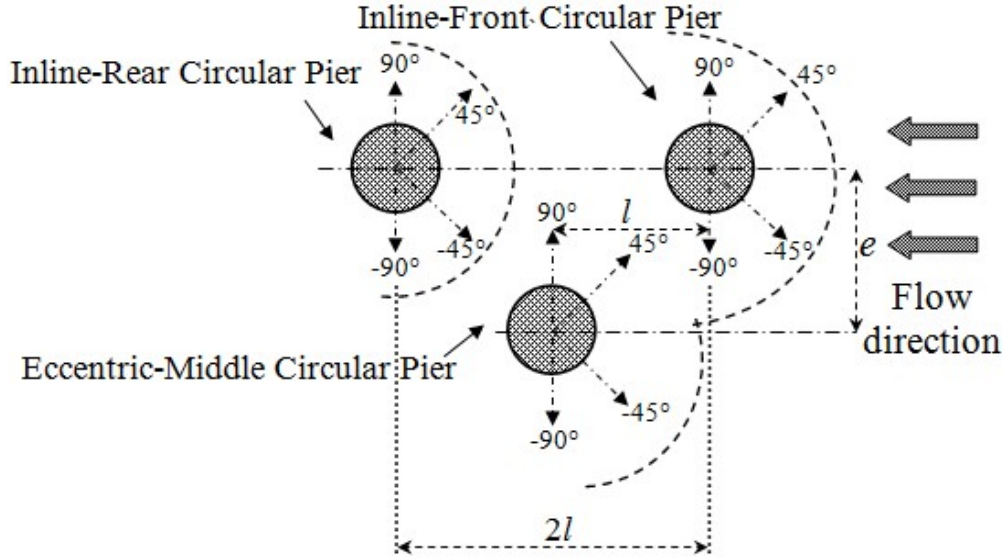


Fig. 3.2. Top view for three inline-eccentric-inline arranged circular piers.

Table 3.1. Experimental conditions for all conducted tests.

Parameter description	Magnitude
Pier width (b)	= 7 cm
Water discharge (Q)	= 25 l/s
Bed slope, S ($=\tan \lambda$)	= 1:2400
Eccentricity between front and eccentric pier, e ($=3b$)	= 21 cm
Median diameter of sand (d_{50})	= 0.825 mm
Geometric standard deviation of sediment size, σ_g ($=\sqrt{d_{84}/d_{16}}$)	= 1.8
Approaching flow depth (h)	= 12.5 cm
Depth averaged approaching flow velocity (U)	= 24.66 cm/s
Critical velocity (u_c)	= 36.2 cm/s

Here, the longitudinal spacing in-between the inline-front and inline-rear circular piers was expressed as $2l$ and in-between inline-front and eccentric-middle piers was denoted by l as shown in Fig. 3.2. The eccentric pier was positioned transversally in-middle of inline-front and inline-rear circular piers with a constant eccentricity, $e=3b$. For all the nine experiments, the longitudinal spacing in-between the inline-front and eccentric-middle circular piers along the flow was $(2/8)$, $(3/8)$, $(4/8)$, $(5/8)$, $(6/8)$, $(7/8)$, $(8/8)$, $(9/8)$ and $(10/8)$ times of the maximum lengths of sediment transportation for single circular pier under equilibrium clear-water scour [equal to the sum of maximum scour and maximum dune lengths at equilibrium scour = $l_{ss} = 48.4$ cm as investigated and adopted by Das and Mazumdar (2015b) and Das *et al.* (2016)].

As suggested by Elliott and Baker (1985), eccentricity (e) and pier width (b) ratio will be seven as a limit for pier independency i.e. the permissible limit for pier width are 7cm, within which the equilibrium scour formed was expected to remain independent of the wall effects of the laboratory flume of 81cm width. After placing the piers properly, lastly, effective working section of sand bed was piled and levelled carefully. Ashtiani and Beheshti

(2006) found that the maximum scour depth rises by 20% in case of two tandem piers with the eccentricity (e) equal to the thrice of the width of the pier.

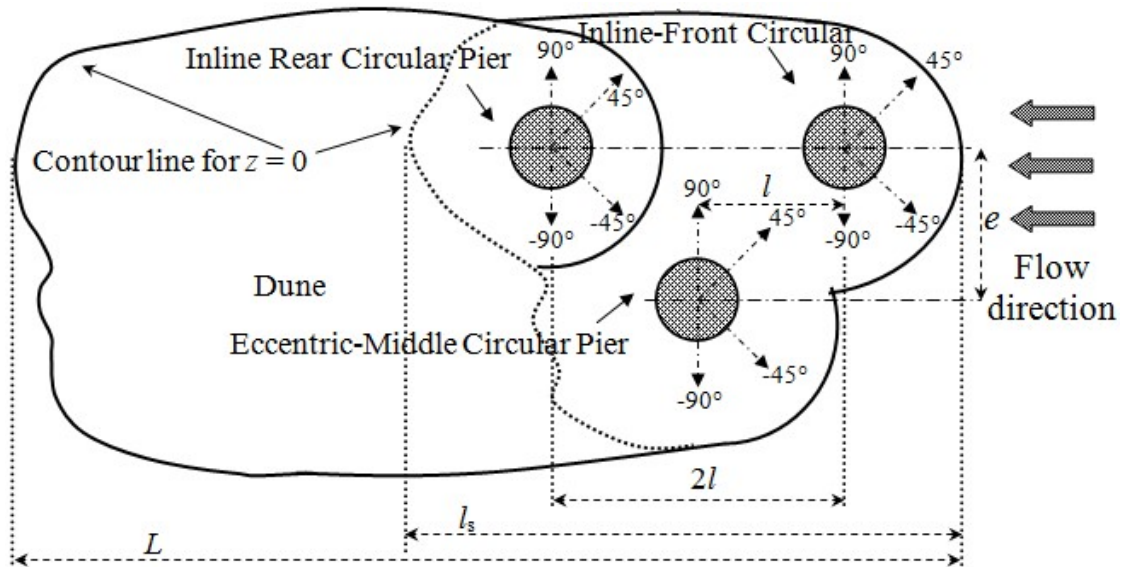


Fig. 3.3. Plan view for gauge and Vectrino measurements for three inline-eccentric-inline arranged circular piers.

The depth mean approach velocity of flow U was kept fixed at 24.69 cm/s for all the nine tests for maintaining equilibrium scouring at clear water criteria, that is 68.18% of threshold velocity U_c , as expressed by a threshold velocity ratio (U/U_c) equal to 0.6818 [Das and Mazumdar (2015a-b)]. The depth mean approach velocity of flow was measured from 2.1 m upstream of inline-front pier, thus, presence of piers does not change U . The flow shallowness (h/b) is normally kept more than 0.60 to obtain controlled flow in the flume during the whole experimentation [Raudkivi and Ettema (1983)]. Thus, in this experimentation the comparative inflow depth was taken 1.786.

For attaining equilibrium scouring, the test run period of each experimental test was kept approximately 65 h. For each test, after 65 h of run, it was clearly observed that the enhancement in scoured depth was smaller than 1 mm for every 2 h interval [Dey and Raikar (2007) and Das and Mazumdar (2015b)]. After every test stopped, water draining out from the flume and reasonably drying the sand bed, the bed profile around inline-front circular pier, eccentric-middle circular pier and inline-rear circular pier was gauged using the sharp point gauge of Vernier type attached on the movable trolley. From the gauged data, contour profiles of scoured zone around three circular piers are plotted. Also the scour affected hole surface planar area along with scouring hole volume were obtained using the Surfer software. A thorough study of the contours of equilibrium scour hole, it is clearly found that the dune forms more along the sidewall of eccentric-middle pier. It shows clearly that the experimental sand particles are transported from surrounding area of the three piers and it is deflected and settled toward eccentric-middle circular pier.

Only for the test no. 3, the sand bed was allowed to dry after carefully releasing water from the flume. Then glue mixed with water, in 1:3 ratio by volume, was sprayed over the sand bed to stabilize it and also to freeze it. The scoured bed was then saturated and soaked

with glue so that it becomes hard rock when left over for a time-period of 72 h. Then, same experiment was repeated again at equilibrium scour condition under same experimental condition i.e. at flow discharge 25 l/s, approach depth 12.5 cm, and mean approach velocity of flow (U) 24.7 cm/s, for facilitating 3-D velocity measurements at different azimuthal planes ($0^\circ, \pm 45^\circ, \pm 90^\circ$) and horizontal planes ($z=0.04 h$ and $z=0.5 h$).

3.5 Analysis of Scour Geometry

Here, the three circular pier arrangements present a mutual interference on scouring and on hydraulic behaviour. In the present study the equilibrium scour affected zones around the three piers are displayed in Figs. 3.4, 3.5 and 3.6. Also, from the gauged data, contour lines of the equilibrium scour holes around the circular piers have been plotted with Golden software Surfer v8.06.39, which are shown in Figs. 3.7, 3.8 and 3.9. After conducting all the nine tests, the outcomes obtained for the equilibrium scour holes, geometrical parameters like scour depth, length, width, whole surface area and volume were analysed and were summarized in the Table. 3.2. The negative contour values indicate scouring area and the positive contour values indicate dune formation.

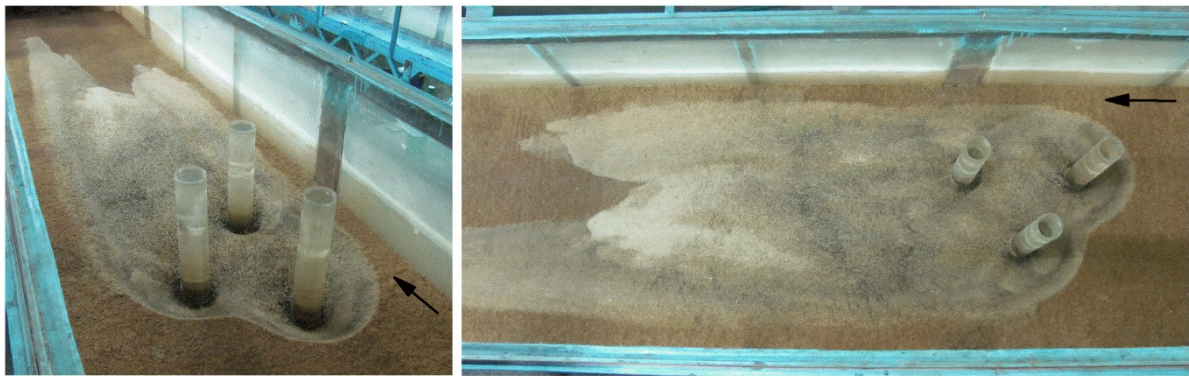
Table 3.2. Magnitudes of geometric parameters at equilibrium scour for nine tests conducted.

Test No.	b (cm)	Spacing of piers (cm) l	d_{sf} (cm)	d_{se} (cm)	d_{sr} (cm)	l_s (cm)	w_s (cm)	L (cm)	a_s (cm ²)	∇_s (cm ³)
1	7	0.25 l_{ss}	5.5	6.5	5.0	45.25	51.6	132.52	5777.34	2996.27
2	7	0.375 l_{ss}	6.2	7.1	5.2	69.45	60.0	195.45	6232.17	9249.48
3	7	0.5 l_{ss}	6.7	7.7	5.5	78.80	59.5	191.90	5585.18	6901.81
4	7	0.625 l_{ss}	6.8	8.4	5.7	95.65	60.0	206.25	7428.08	8547.51
5	7	0.75 l_{ss}	7.2	8.5	6.3	105.41	60.0	220.67	7367.03	9498.95
6	7	0.825 l_{ss}	7.13	7.9	5.9	118.19	58.7	234.03	8091.04	6747.03
7	7	l_{ss}	7.0	8.1	5.7	126.34	60.6	236.96	8156.77	7682.91
8	7	1.125 l_{ss}	6.5	8.0	5.7	142.58	58.6	224.02	7297.45	6922.26
9	7	1.25 l_{ss}	6.2	7.4	5.5	153.17	58.1	246.74	8045.43	6642.28

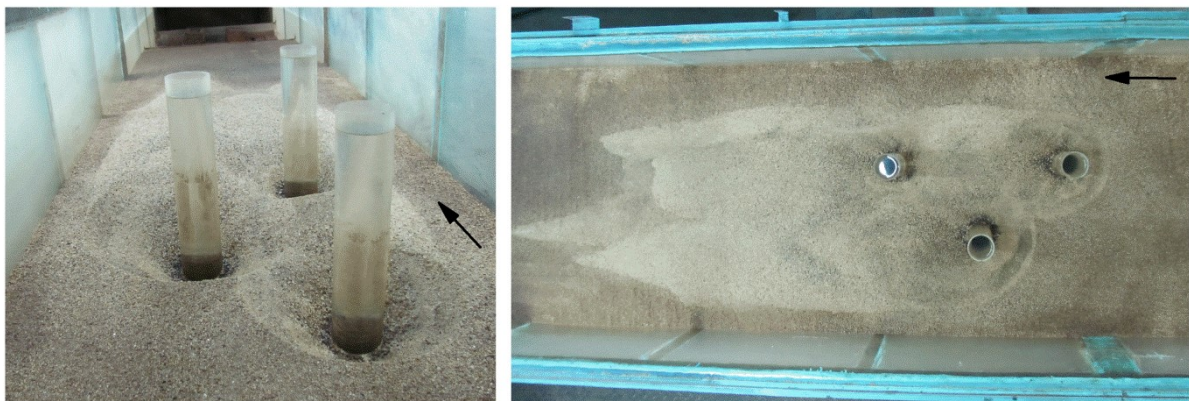
b =Pier diameter (cm), d_{sf} =Maximum equilibrium scour depth for inline-front circular pier (cm), d_{sr} =Maximum equilibrium scour depth for inline-rear circular pier (cm), d_{se} =Maximum equilibrium scour depth for eccentric-middle circular pier (cm), l_s =Maximum equilibrium scour length for three pier arrangement (cm), w_s =Maximum scour width for three pier arrangement (cm), L =Maximum equilibrium length of sediment (cm)



Test No. 1



Test No. 2

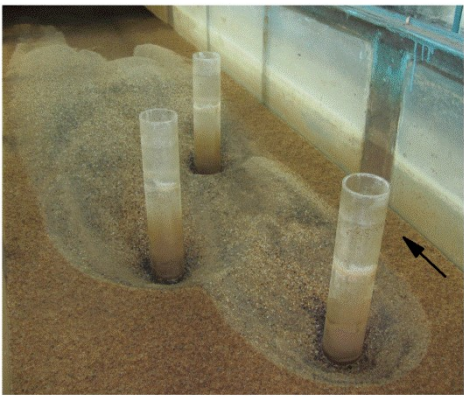


Test No. 3

Fig. 3.4. Scoured zones around three identical circular inline-eccentric-inline arranged piers for test nos. 1, 2 and 3.



Test No. 4



Test No. 5



Test No. 6

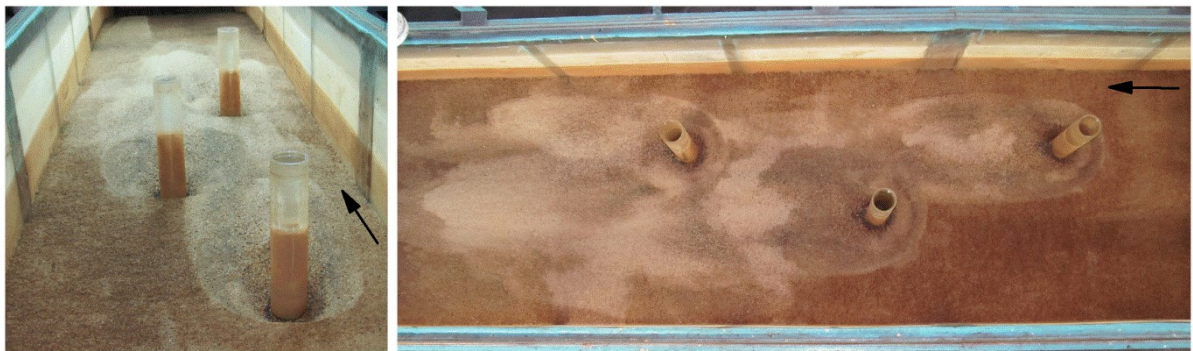
Fig. 3.5. Scoured zones around three identical circular inline-eccentric-inline arranged piers for test nos. 4, 5 and 6.



Test No. 7

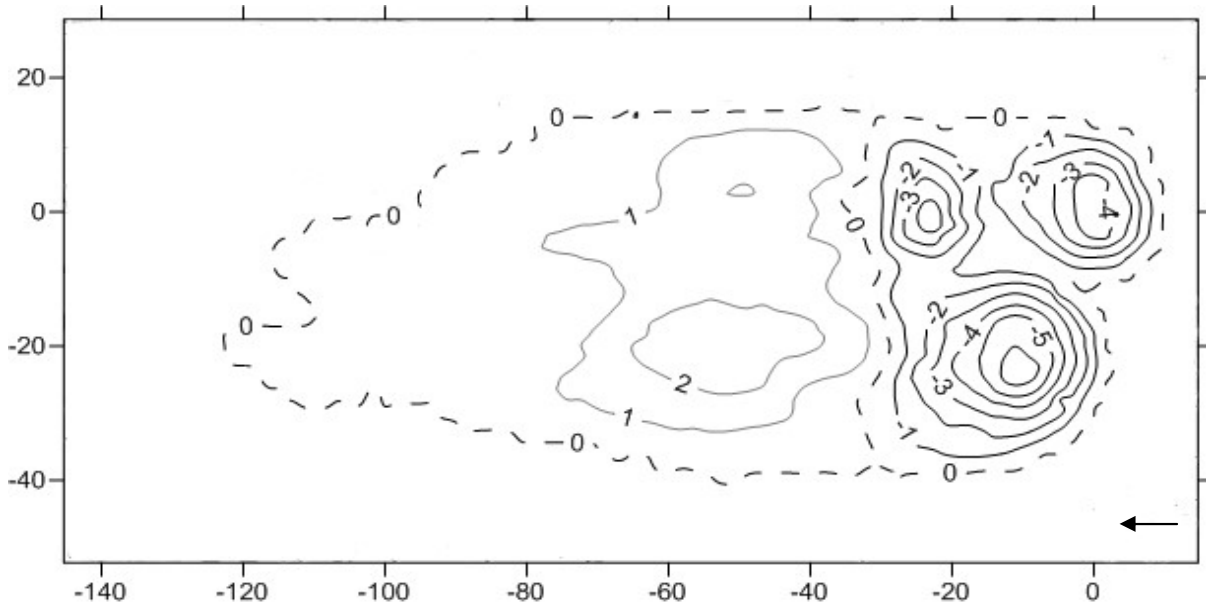


Test No. 8

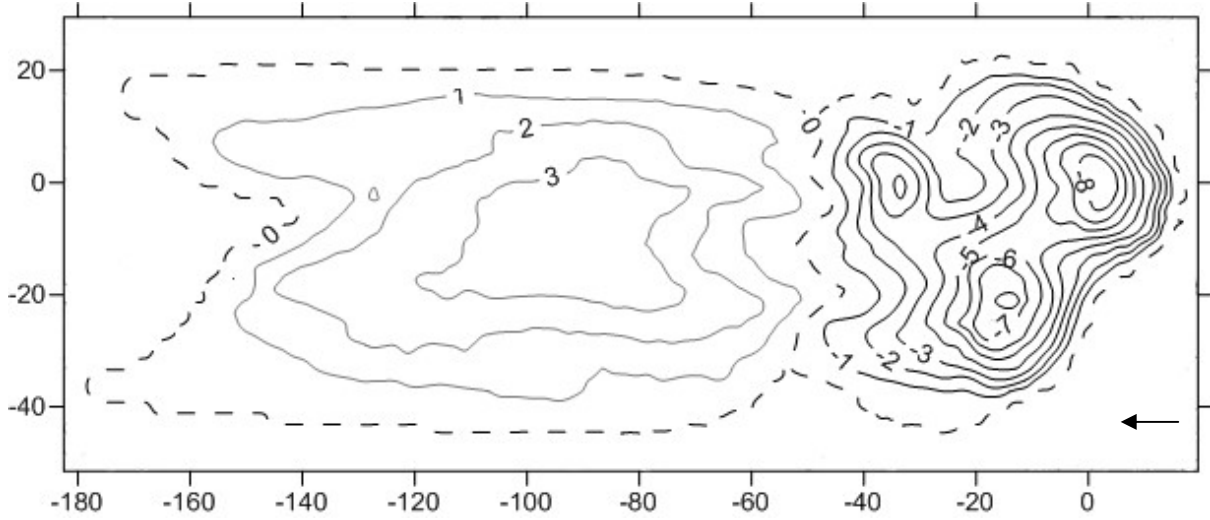


Test No. 9

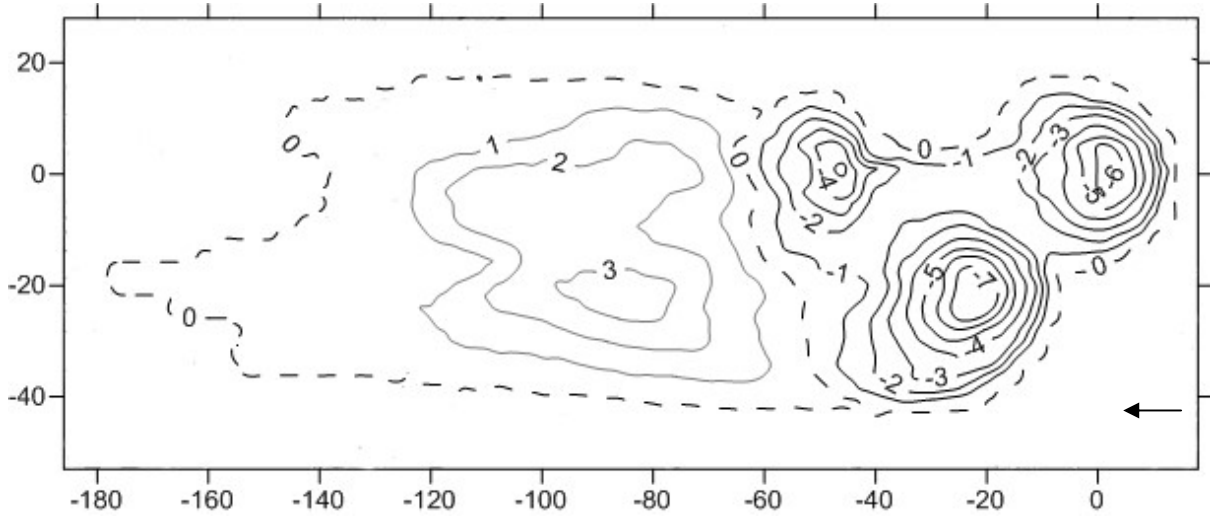
Fig. 3.6. Scoured zones around three identical circular inline-eccentric-inline arranged piers for test nos. 7, 8 and 9.



Test No. 1



Test No. 2



Test No. 3

Fig. 3.7. Contours of equilibrium scour holes around circular piers for test nos. 1, 2 and 3. (all units are in cm)

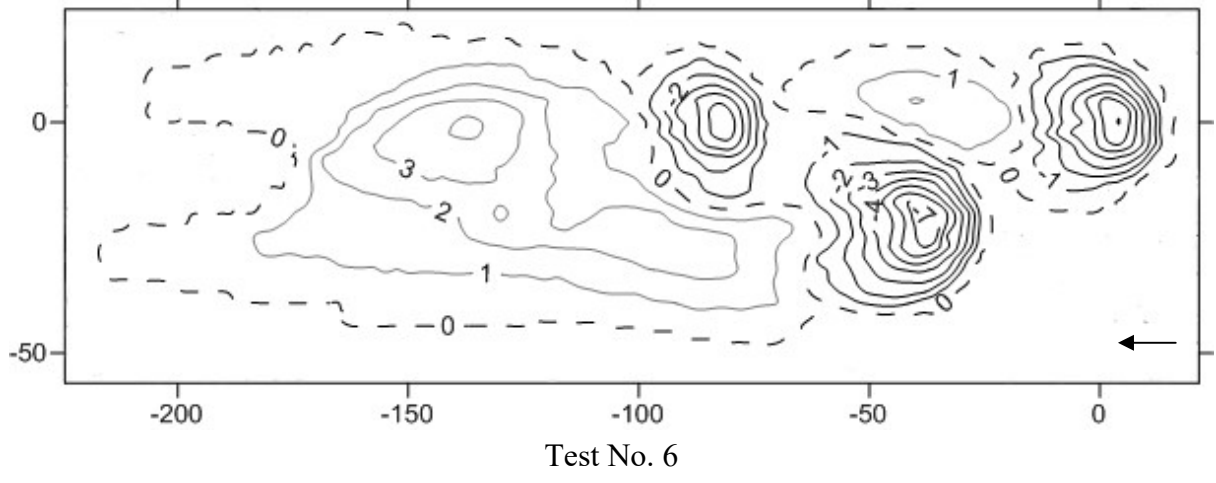
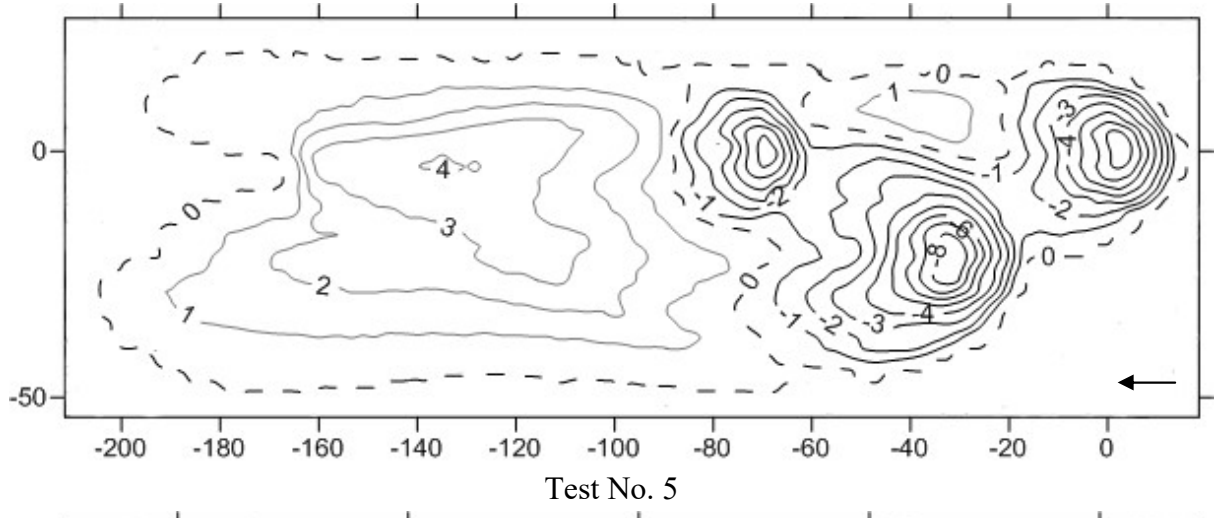
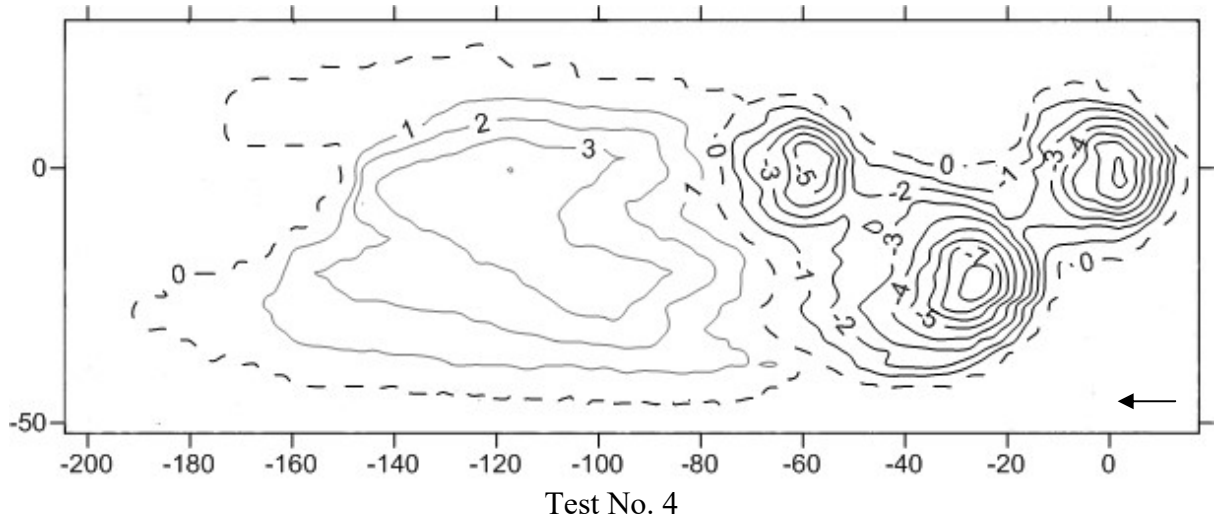


Fig. 3.8. Contours of equilibrium scour holes around circular piers for test nos. 4, 5 and 6. (all units are in cm)

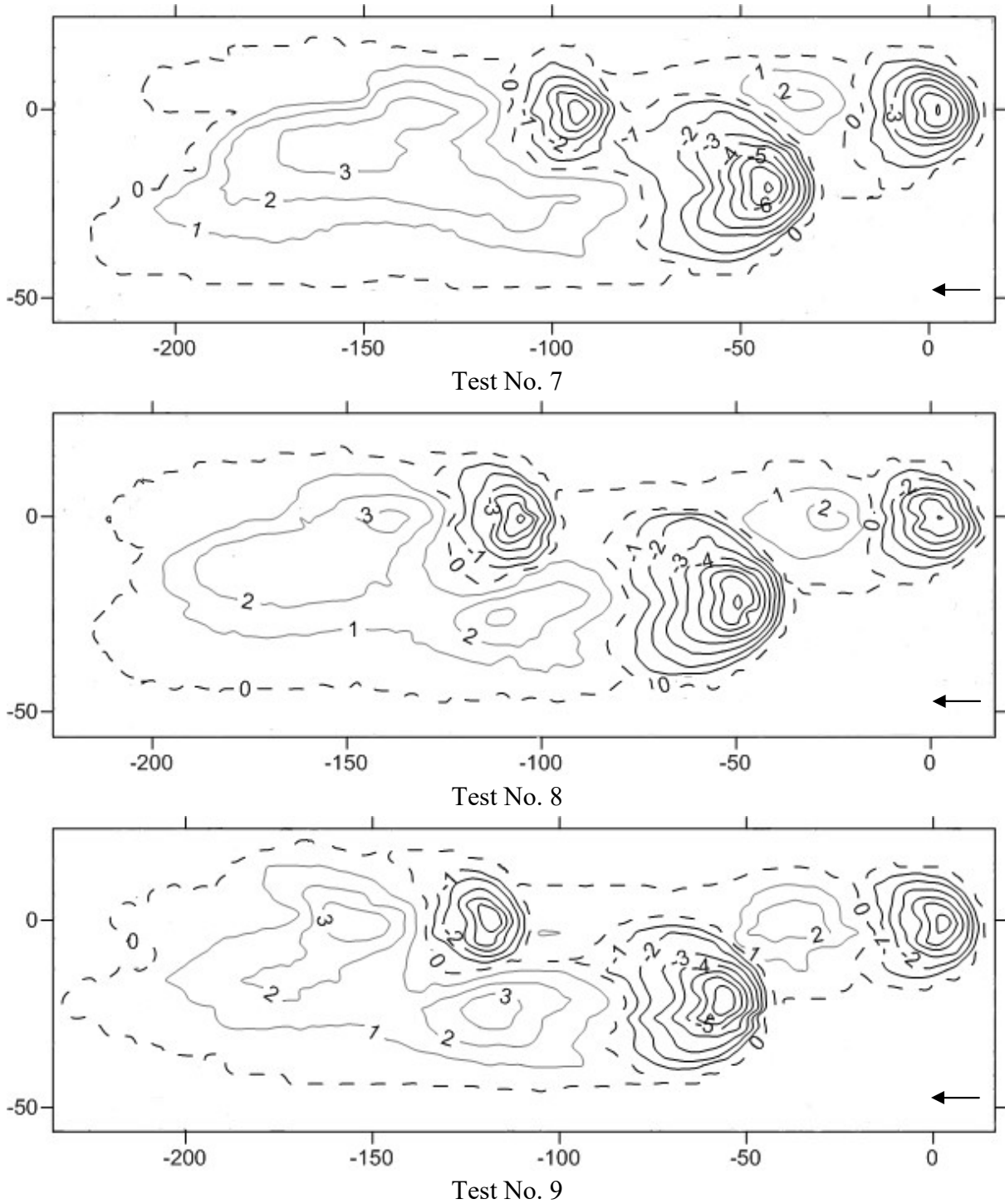


Fig. 3.9. Contours of equilibrium scour holes around circular piers for test nos. 7, 8 and 9. (all units are in cm)

The measured values of equilibrium scour parameters for all 1-9 three pier tests, it is evident that, for similar experimental conditions the scour depth around the eccentric-middle circular pier is maximum and the scour depth around the inline-rear circular pier is minimum. From the measured values it is found that scour depth gradually increases with increasing pier distance until the inline-front and eccentric-middle pier spacing is $(6/8)l_{ss}$. Further increase in pier distance shows that the scour depth around the circular piers decreases. This

phenomenon is similar for all the three piers inline-front pier, inline-rear pier and eccentric-middle pier.

Here, the interference between the wake vortex of the inline-front pier and horseshoe vortex of the eccentric-middle pier in addition to the horseshoe vortex of the inline-rear pier and wake vortex of the eccentric-middle pier plays an important role in the creation and formation of the greater scour depth around all the three circular piers. It was also found that minimum scour occurred around the inline-rear circular pier, since the flow of water is obstructed by the inline-front circular pier and vortices are shed and scattered downstream. So that the flow removes less sediment from the vicinity of the inline-rear pier compared to the inline-front pier. The same phenomenon was found in case of all other parameters such as scour area, scour volume etc.

Figs. 3.7, 3.8 and 3.9 disclose that if an imagery flow centreline through centre of the inline-front and inline-rear circular piers is considered, then towards the side of eccentric-middle circular pier, dune formation will be more. From these figures, it is clear that scour and succeeding dune formation are not symmetric, i.e. for all the experiments dune is more towards the side of eccentric-middle circular pier. From each pier bases the sediment particles are getting removed and deposited towards downstream region, mostly on one side of hydraulic flume. It is clearly noted that shifting of sediment particles are largely deposited onto the eccentric-middle circular pier region and on that side, diversion angle is more. This particular phenomenon for all the nine experiments is found similar.

This phenomenon was occurred because of flow physics that the curvilinear streamlines which are mostly separated from the inline-front circular pier and thereafter proceeds along downstream. On the upstream right side of the inline-front circular pier these streamlines are moving straight towards downstream. Whereas on the upstream left side of the inline-front circular pier streamlines are getting obstructed by eccentric-middle circular pier. Further up, these curvilinear streamlines stretches and moves downstream towards the left side of the eccentric-middle circular pier. This may be for above-discussed flow physics, the diversion angle on the left is found much higher than its right of upstream inline-frontal circular pier.

From the figures, for tests 4–9, the dunes formations are mostly between the inline-front and inline-rear circular piers. That is, no such dune is formed between the inline-front and inline-rear circular piers, until the intermediate inline pier spacing is $(5/8)l_{ss}$. When the intermediate inline pier spacing is $(6/8)l_{ss}$, small dunes are formed between the inline-front and inline-rear circular piers. Further up, as the intermediate inline pier spacing increases, simultaneously, the dune volume also increases.

3.6 Velocity Measurement

The three components of velocity were recorded instantaneously using a down facing four-receiver 5 cm acoustic Doppler-type VectrinoPlus probe, Nortek made [NorTek AS (1996), Das *et al.* (2015), Das and Mazumdar (2015b)]. The vectrino functions on pulse Doppler effect for sampling instant 3D velocity-components at 100 Hz sampling rate. An adjustable cylinder type sampling volume, 6 mm diameter having sampling height (Δz) of 5–2 mm was selected for sampling. Sampling height 5 and 2 mm were used for the measurement of

discharge above and within the interfacial sub-layer when the velocity component decreases rapidly. Minimum horizontal resolution (Δr) during the Vectrino sampling was 1 cm. Sampling by ADV down-facing probe was impossible beneath the region 4.5 mm above sand-bed. Because of the interference due to echoes from the bed, the received signal is disturbed, which results in inaccurate velocity measurement [Song and Chew, (2010)]. Vectrino output readings were converted by VectrinoPlus software, version 1.18. Throughout filtering of converted ADV-data, the minimum signal-to-noise ratio and minimum correlation parameter were maintained at 17 or above and 70% and above, respectively [Das *et al.* (2013b), Das and Mazumdar (2015b)]. A sampling time of 2–3 min was considered verifying a statically time-independent averaged-velocity, comparatively long sampling time of 3 min near scoured bed was taken as taken in previous researches [Das *et al.* (2013a-c) and Das and Mazumdar (2015b)]. According to Be'linger and Roy (2005) for most turbulence statistics, the optimal record length to achieve low standard errors ranges between 1 and 1.5 min. Measured ADV-data near to bed is sometimes found spiked due to the interference between incident and reflected beams. Spikes were removed by filtering the measured data using an algorithm as stated by Blanckaert and Lemmin (2006). The minimum limits for de-spiking were selected in a way, that the power-spectra of velocity fit with $-5/3$ scaling-law of Kolmogorov in inertial sub-range [Das and Mazumdar (2015b)]. The error analysis of Vectrino-gauged data was done by calculating standard deviation and average of maximum errors E_{\max} for u , v and w . the magnitudes of S.D and E_{\max} for u , v and w are found 0.0261, 0.0167, 0.0203 and 0.451, 0.163, 0.279% respectively.

3.7 Analysis of Flow and Turbulence Fields

A cylindrical-polar axis system, given in Figs. 3.1, 3.2 and 3.3, is utilized to represent velocity and subsequent turbulence flow fields at five vertical azimuth-planes 0° , 45° , -45° , 90° and -90° around the piers. The time-mean velocities in (r, θ, z) is symbolized by (u, v, w) , whose resulting fluctuation is (u', v', w') . Positive direction of tangential (u) velocity, radial (v) velocity and vertical (w) velocity are respectively counter clockwise, outward and upward. The velocity and turbulence fields are projected in r - z planes for five azimuth-planes around the three piers. To evade solid section of all three piers in diagrammatic illustrations, abscissa scale has been furnished by r_0 [$= (r - b/2)$], i.e. $r_0 = 0$ shows the circular pier boundary. Also, the abscissa scales are considered larger than scales of ordinate for showing a clear illustration of velocity fields within scour holes that are having smaller dimension and it enlarges such figures along horizontal direction for which a better illustration is likely to describe velocity contour in addition the turbulence contour profiles. It is imperative to address that external radius of vectrino probe was around 2 cm having four receiving transducers mounted on short arms around the transmitting transducer at 90° azimuth intervals. Therefore, velocity measurement was possible close to 2 cm grid from each pier boundary.

Also a Cartesian coordinate axis system is also used to address velocity and resulting turbulent flow fields at two horizontal x - y planes $z = 0.5$ cm and $z = 6.25$ cm from the zero bed level (or $z = 0.04h$ and $z = 0.5h$ of the flow) around the piers. Similarly, components of

time-mean velocity are symbolized by (u , v and w), whose resulting fluctuations are (u' , v' and w'). According to the right thumb rule, positive direction of u is along flow, v is towards left side from the symmetry-line and w is upward. The velocity flow fields and turbulence fields are projected in x - y plane for $z/h = 0.5$ and $z/h = 0.04$.

3.7.1 Flow Fields

3.7.1.1 Tangential Velocity

At five different azimuthal planes 0° , 45° , 90° , -45° and -90° and at two horizontal planes $z=0.04h$ and $z=0.5h$ from zero bed levels around the three circular piers, the contours of time mean tangential velocity ' u ' for the equilibrium clear-water scour state are plotted using OriginLab software, which are shown in the Fig. 3.10, Fig. 3.11 and Fig. 3.12. These figures represent the flow characteristics around the three piers.

The tangential velocity at 0° azimuthal plane is almost zero and is insignificant as was gauged by the ADV. The tangential velocity becomes finite and increases with an increase in the azimuthal angle θ . Just near the upstream of the scour hole, u for the inline-front circular pier is slightly lower than the u near upstream of the scour hole for the eccentric-middle and inline-rear circular piers. As observed by Dey and Raikar (2007), Etema (1980) and Das and Mazumdar (2015b), in the present study, at any elevation the maximum u is $0.058U$ upstream of the inline-front circular pier and as it approaches the value lowers down and increases towards the bed. Just near the upstream of the scour region the maximum u value of the inline-front, eccentric-middle and inline-rear circular piers are found approximately as $0.08U$, $0.12U$ and $0.22U$ respectively. In the absence of scour hole just above the upstream zone near bed of eccentric-middle and inline-front circular piers, u is observed approximately as $0.06U$. It signifies the variation of u in that zone with higher values for inline-front and eccentric-middle circular piers than those for the inline-rear circular pier.

Horseshoe vortices, with downward and subsequent reverse flow, are formed at pier bases just upstream near bed at a small region of all three piers. In similar way, upward and subsequent reverse flows are found downstream region of the three piers extending by flowing away from scoured bed. These horseshoe vortex flow move downstream of three piers and mixes with the corresponding wake region of the three piers. The downward and subsequent reverse flows are found maximum for eccentric-middle circular pier among the three piers and they are also found higher for inline-front circular pier than for inline-rear circular pier. It verifies that at 0° , just upstream near the bed, values of u for eccentric-middle circular pier are lesser than the other two circular piers. The value of u increases with increase in height z and corresponding vertical gradients of u (i.e. $\partial u/\partial z$) inside scour holes (i.e. $z \leq 0$), and are found more than $\partial u/\partial z$ above scour holes (i.e. $z > 0$).

At azimuthal planes 45° and -45° for the three piers, u found higher than u for 0° azimuthal plane. For the inline-eccentric-inline piers the magnitude of u at 45° azimuthal plane is 0.96, 0.68 and 1.48 times greater than the magnitude of u at -45° , respectively. Between the 45° plane of the eccentric-middle and -45° plane of the inline-front pier and between the -45° plane of the eccentric-middle and 45° plane of the inline-rear pier sheltering effects takes place.

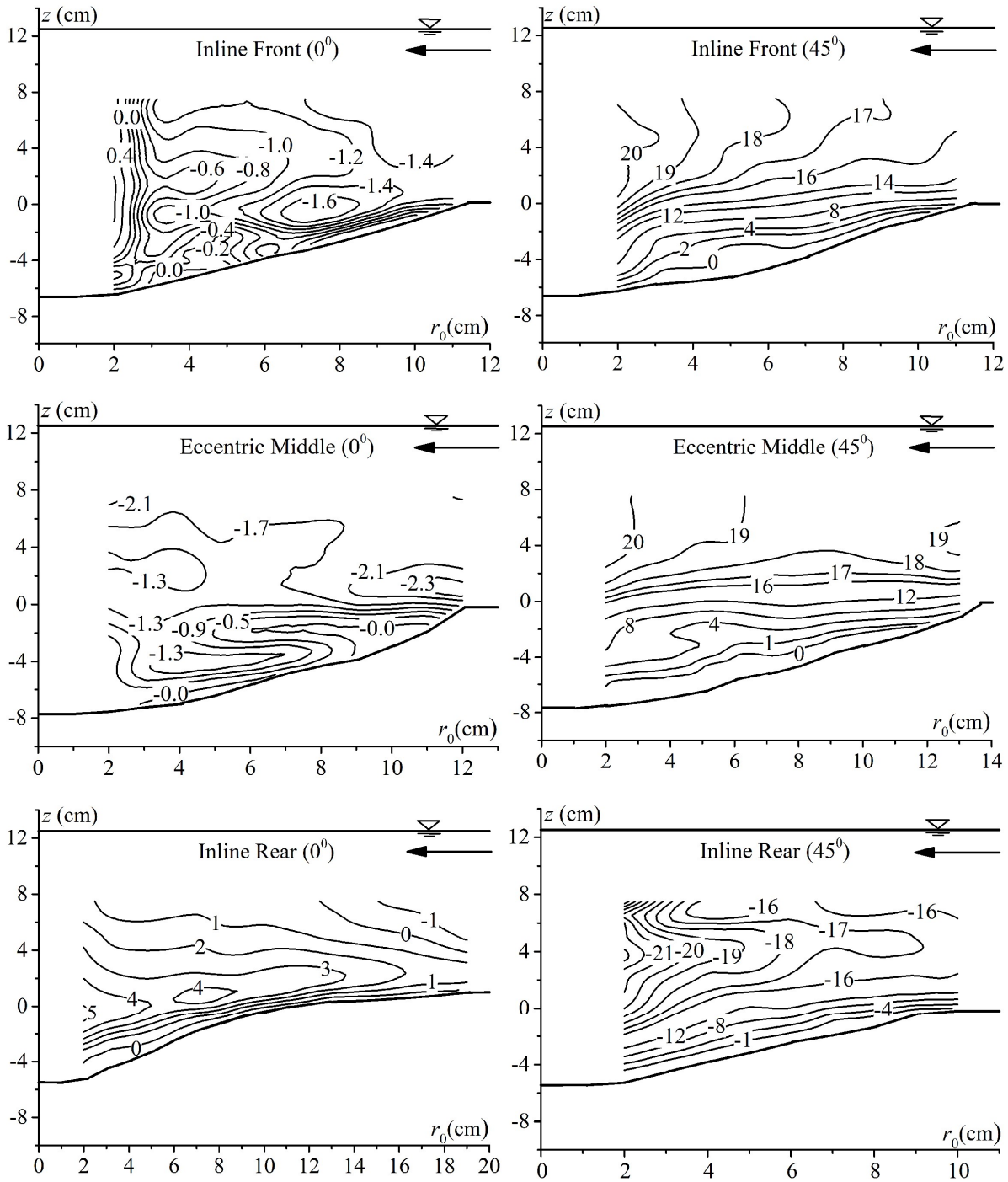


Fig. 3.10. Contours of tangential velocity (u) in cm/s for inline-front, eccentric-middle and inline-rear circular piers at r - z planes for $\theta = 0^\circ$ and 45° .

It is obvious that due to this sheltering effect of inline-front and eccentric-middle piers, the maximum u at 90° azimuthal plane for inline-front, eccentric-middle and inline-rear pier are 1.003, 0.95 and 0.97 times higher than the maximum u at -90° plane. For all three piers with inline-eccentric-inline positioning, at 90° and -90° planes u is always higher than u at 45° and -45° planes, respectively, as the dimension of the scour holes are small, but it decreases progressively. At 45° , 90° , -45° and -90° u is relatively strong as dimensions of scour holes are small, but decreases progressively due to increase in flow area as scour depth increases.

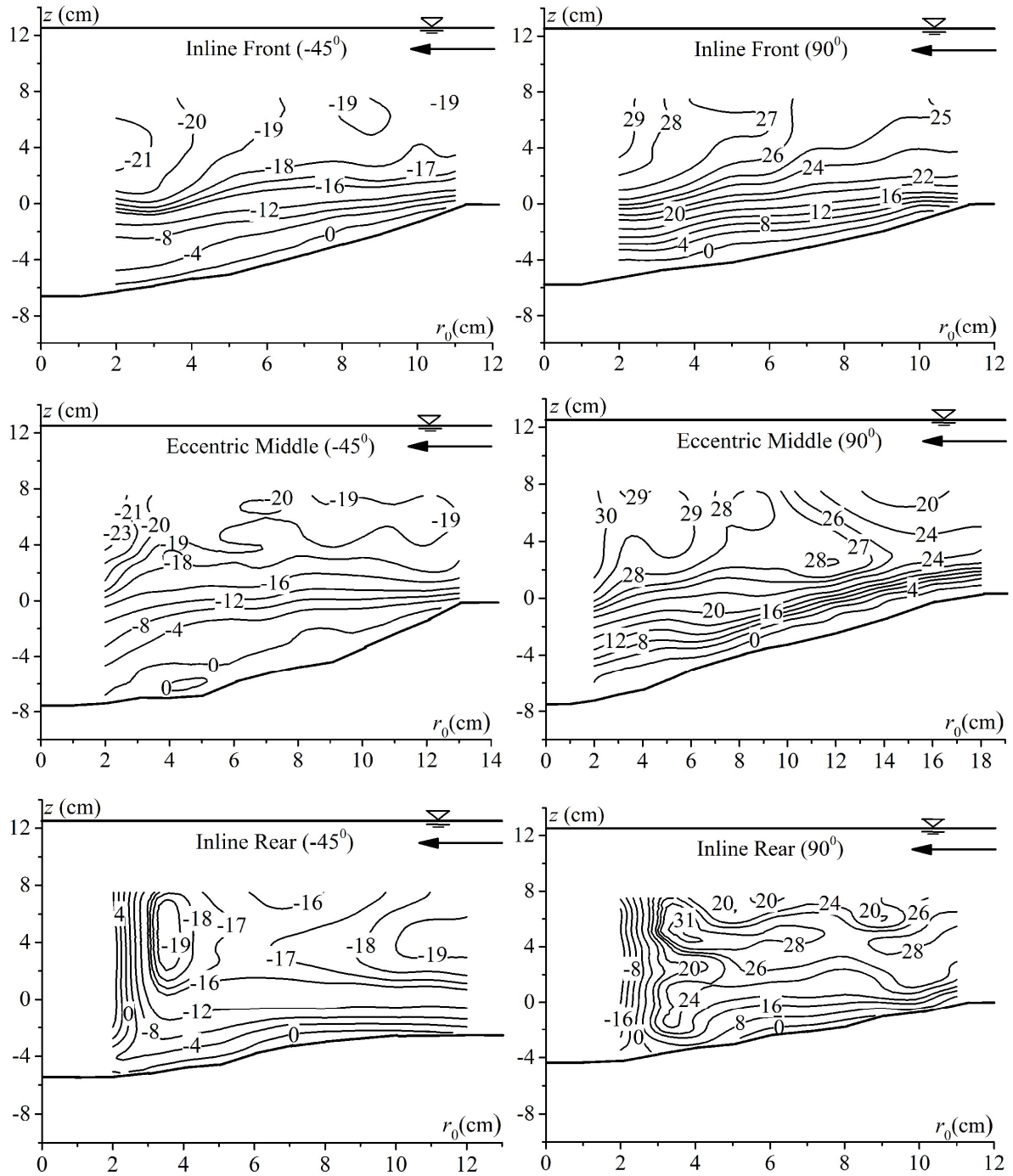


Fig. 3.11. Contours of tangential velocity (u) in cm/s for inline-front, eccentric-middle and inline-rear circular piers at r - z planes for $\theta = -45^\circ$ and 90° .

The passageway of the down flow flux beside the three piers results in a considerable enhancement of u near each pier and thus decreases with increase in radial distance r_0 from each pier and remains almost constant over the flat bed.

Stagnation pressure becomes zero, as u moves near the pier. The velocity U decreases from upper level of water toward the bed and it confirms, stagnation pressure decreases while depth decreases, the reason of formation of weak pressure gradient in the upstream of piers and increase in downflow magnitude.

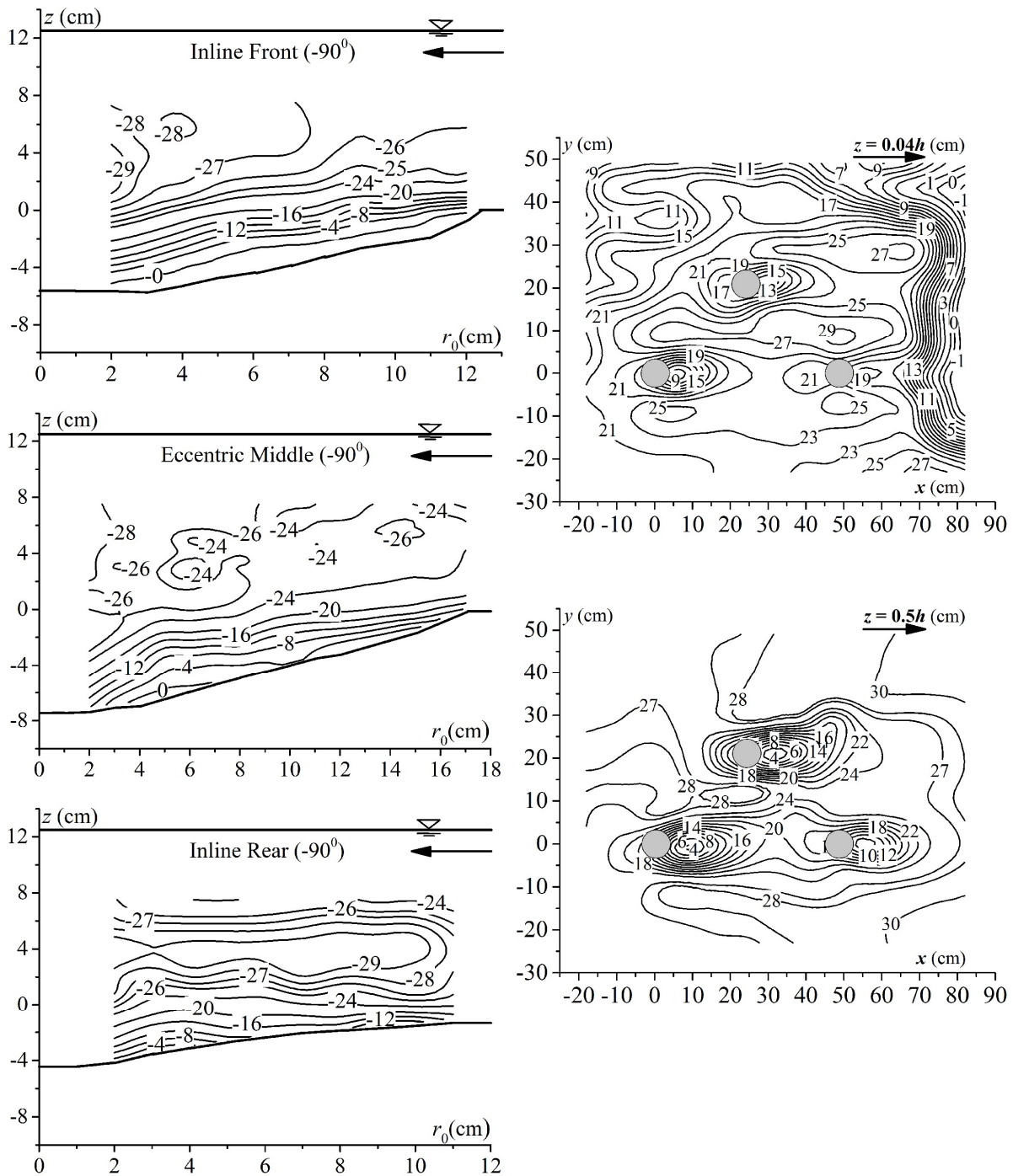


Fig. 3.12. Contours of tangential velocity (u) in cm/s for inline-front, eccentric-middle and inline-rear circular piers at r - z plane for $\theta = -90^\circ$ and at x - y planes for $z=0.04h$ and $z=0.5h$.

In the upstream region at $\pm 90^\circ$ the flow starts decelerating and layer separates and moves further downstream and both reaches on the frontal surface of the eccentric-middle circular pier. Similarly the layers are separated from the inline front and eccentric middle circular piers and move downstream and both reaches on the frontal surface of the inline rear circular pier. In other wards the boundary layer moves at a low velocity than the fluid flow in the free stream. Thus, negative velocities occur at the inner region of the boundary layer. In the contours, the zero velocity lines downstream of the inline-front and eccentric-middle circular pier divides the regions of positive and negative velocity and indicate the occurrence

of flow separation. As the negative velocity developed the pressure within the zone is small compared to these in the free stream, the outward fluid is therefore drowned inward to the low pressure zone. Powerful eddies generated from the inline-front circular pier are then drowned downstream region by the flow velocities and reaches to the -90° plane of eccentric-middle circular pier and 90° of the inline-rear circular pier and simultaneously the eddies generated from the eccentric-middle circular piers reach to the -90° plane of inline-rear circular pier.

The contours of time-mean longitudinal velocity (along the flow) u for the two horizontal planes $z=0.04h$ and $z=0.5h$ above the bed level ($h=0$) are shown in Fig. 3.12. From these figure it is clearly observed that the time-mean longitudinal velocity u is greater around the downstream region of the inline-rear circular pier than u around the downstream region of the inline-front and eccentric-middle circular piers. The velocity u is found more around the inline-rear circular pier for the united effect of the inline-front and eccentric-middle circular piers. These zones in between the three piers have higher-order longitudinal velocity than the average depth velocity. This increase becomes visible in the form of expansion in the high-velocity region plus the magnitude of u . Since the formation of wake occurs in a recirculating zone that does not contribute to net transport of sediment towards downstream direction, flow in that zone next to the wake leads to accelerate and results in transport of the extra quantity of sediment. Behind the inline-front circular pier, vortex formation has an effect over the eccentric-middle circular pier. Similarly, combined action of the inline-front and the eccentric-middle circular piers, has an effect over the inline-rear circular pier. At the three piers downstream region, u at $z = 0.04h$ is almost similar to the corresponding values of u at $z = 0.5h$ but a bit higher in magnitude as compared to the velocities at $z = 0.5h$.

3.7.1.2 Radial Velocity

The contours of the time-mean radial velocity ' v ' at five different azimuthal planes 0° , 45° , 90° , -45° and -90° and at two horizontal planes $z=0.04h$ and $z=0.5h$ from zero bed level for equilibrium clear-water scour state for the inline front, eccentric middle and inline rear circular piers are shown in Fig. 3.13, Fig. 3.14 and Fig. 3.15, respectively.

At 0° plane as v approaches towards the upstream of the three piers, stagnation pressure decreases with establishment of depth itself and produces a weaker pressure gradient $[\partial(\rho v^2/\partial z)]$ along the frontal sides of all the piers and thus induces a downward flow velocities from high to low velocities with decreasing magnitude. This downstream flow laterally diverts as strong pressure gradients exist around all the three piers. According to the previous research [Graf and Yulistiyanto (1998)] vertical component of the flow is responsible for scour. As this stagnation pressure increase becomes sufficiently strong, the three-dimensional boundary layer undergoes a separation. At the base of the pier horseshoe vortex systems are formed itself and are stretches into the downstream direction, diminishing its strength. These are very active in the local scour process. In the downstream of all the three piers, trailing wake vortex systems are formed over entire flow depth. There, turbulence intensities are increased and at the same time erosion and sediments transport are enhanced. It is observed, around the eccentric-middle circular pier scour is more than the inline-front and inline-rear circular piers.

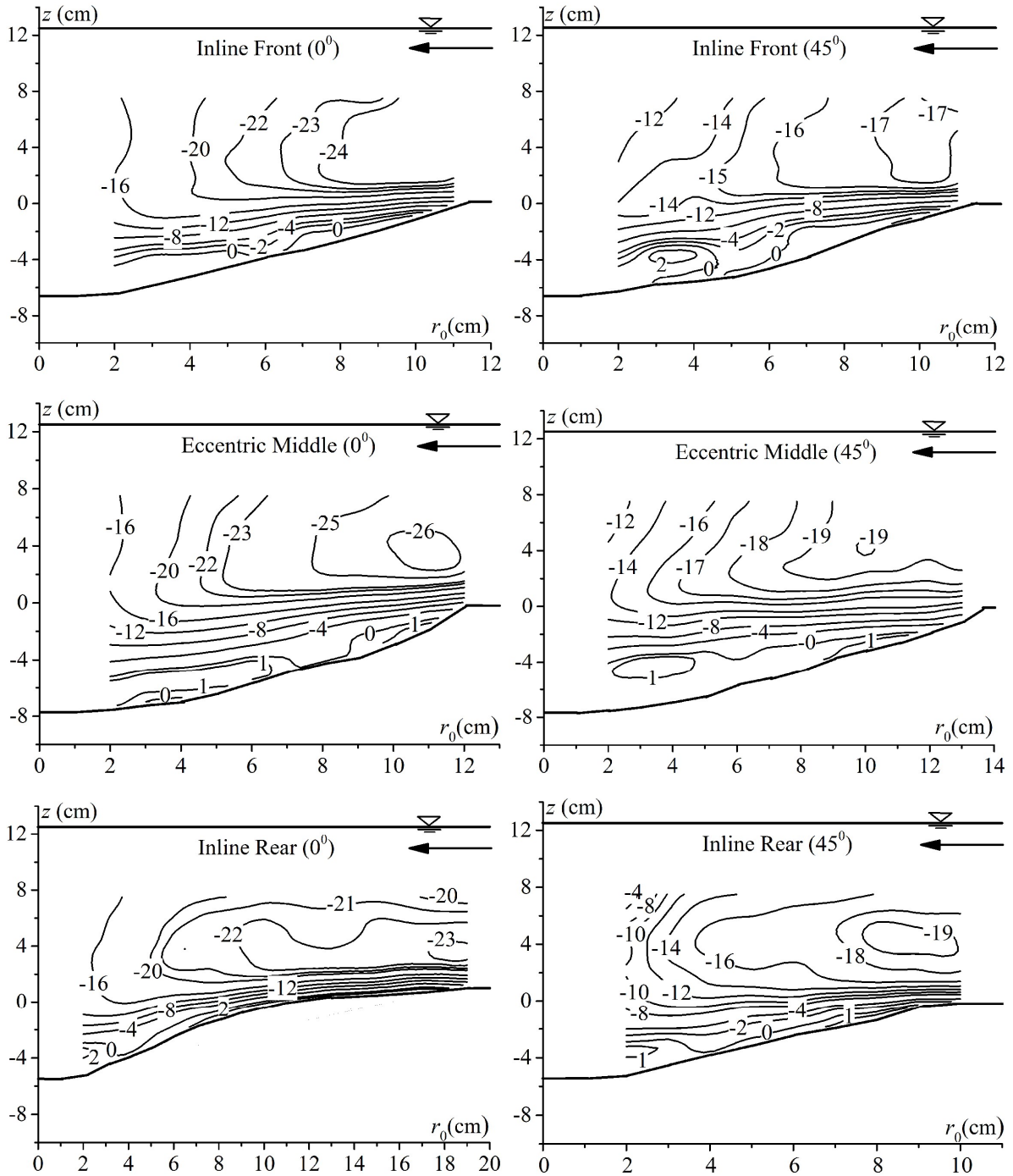


Fig. 3.13. Contours of radial velocity (v) in cm/s for inline-front, eccentric-middle and inline-rear circular piers at x - z planes for $\theta = 0^\circ$ and 45° .

At the 0° plane for the three inline-eccentric-inline circular piers, the resembling flow separation is evident just beneath the edge of all the scour holes forming a reversal flow field inside the scour holes ($z \leq 0$). Thus, radial velocity changes the direction on either side of the contour line of $v = 0$, at the depths for the inline-front, eccentric-middle and inline-rear circular piers are approximately 0.65, 0.57 and 0.55 times the local depth of the scour hole below the pre-experimental bed level, respectively. As stated by Dey and Raikar (2007), and Das and Mazumdar (2015a) for single circular pier experiment under equilibrium clear-water scour state, it is 0.5–0.6 times and 0.40–0.45 times of local scour depth below the pre-

experimental bed level, respectively. It confirms the existence of horseshoe vortices inside the scour hole just upstream of all the three circular piers.

At $z \leq 0$ and $z > 0$, the variations of radial velocity are different. In $z \leq 0$, from $z=0$ towards the bed v reduces rapidly to be comes zero. It becomes positive near the bed outwards from the piers as the flow goes back from the base of the piers resulting in overturned flow down to the sloping beds of the three scour holes. The maximum reversed radial velocity that occurs near the bed of the inline-front, eccentric-middle and inline-rear circular piers are approximately $0.12U$, $0.25U$ and $0.26U$ respectively. In $z \leq 0$, due to the obstruction of the piers and due to the reversed and unidirectional flow just above the scoured bed, v is positive.

Above the scour holes ($z>0$) along z , v varies relatively less and is almost logarithmic due to the influence made by the non-uniform approaching flow, starting from the $z=0$ line and becomes maximum, negative in sign near the free surface. Along the vertical axis, v varies exponentially above the turbulent-logarithmic layer. Along the radial axis, in r - z plane radial velocity distribution reveals a parabolic variant starting with zero line at the pier boundaries and become positive upper limit at bed and negative v on the other sides of the locus of $v=0$ at $z<0$ and maximum, when r is equal to radius of each scour hole at $z>0$. According to previous researches [Dey and Raikar (2007) and Das and Mazumdar (2015b)] on the upstream of flat bed, v remains nearly logarithmic and then decreases upon entering the scour hole for the exposure of the larger flow region. Then, it progressively reduces towards the piers, due to obstruction of vertical circular piers which causes the diversion of flow velocity and an increase in scour depths towards the piers.

As compared to 0° the overall distribution of v is almost similar at 45° and -45° azimuthal plane, the magnitude of v at inline-front, eccentric-middle and inline-rear circular pier is lesser than the value of v at 0° azimuthal plane at corresponding piers. At the edge of the scour hole upstream, flow separation occurs. At the separation point ($\partial v / \partial z = 0$), separation is caused by the reduction of velocity in the boundary layer, combined with a positive pressure gradient which opposes the flow. The line of separation is shallower as compared to that at 0° for inline-front, eccentric-middle and inline-rear circular pier.

The reducing character of radial velocity is observed with an increase in θ from 0° to $\pm 90^\circ$ as a result $\partial v / \partial z$ reduces and thereby horseshoe vortex reduces its strength, whereas the radial velocity distribution is strongest around 0° . At $\pm 90^\circ$ azimuth planes, overall flow features can be reviewed as v acts towards each pier within the scour hole ($z \leq 0$) and a thin zone of reversed flows exist close to the bed. Thereafter, the flow deflects outwards away from the scour holes by the side of the three piers above the scour hole ($z > 0$). At all five azimuthal planes 0° , 45° , 90° , -45° and -90° , radial velocity for the eccentric-middle circular pier is almost always higher than the v for the inline-front and the inline-rear circular piers.

In the reattachment regime, the upflows are found everywhere within the transverse gap (above the scour hole) between two circular tandem piers as stated by Ashtiani and Kordkandi (2013). Here, in the present study in between the inline-front and eccentric-middle circular piers upflows are found indicating the primary wake of the inline-front circular pier (Fig. 3.21 inline front -90° , eccentric middle -90° and inline rear -90°). The interactions in between these upflows and downflows (due to the variation of pressure gradient) decrease the

magnitude of the resultant downward flows (Fig. 3.16 eccentric middle 0°). For inline-rear circular pier, between the inline-front and inline-rear circular piers upflows indicate the presence of wake of the inline-front and eccentric-middle circular piers. Similarly the interactions between these upflows and the downflows (due to the change of pressure gradient) decrease the resultant downflow (Fig. 3.16 inline rear 0°). This behaviour causes to increase dynamic pressure ($\rho v^2/2$), and therefore, at the upstream zone of the eccentric-middle and inline-rear circular piers, v increases and then becomes greater than the v for the inline-front circular pier at corresponding locations.

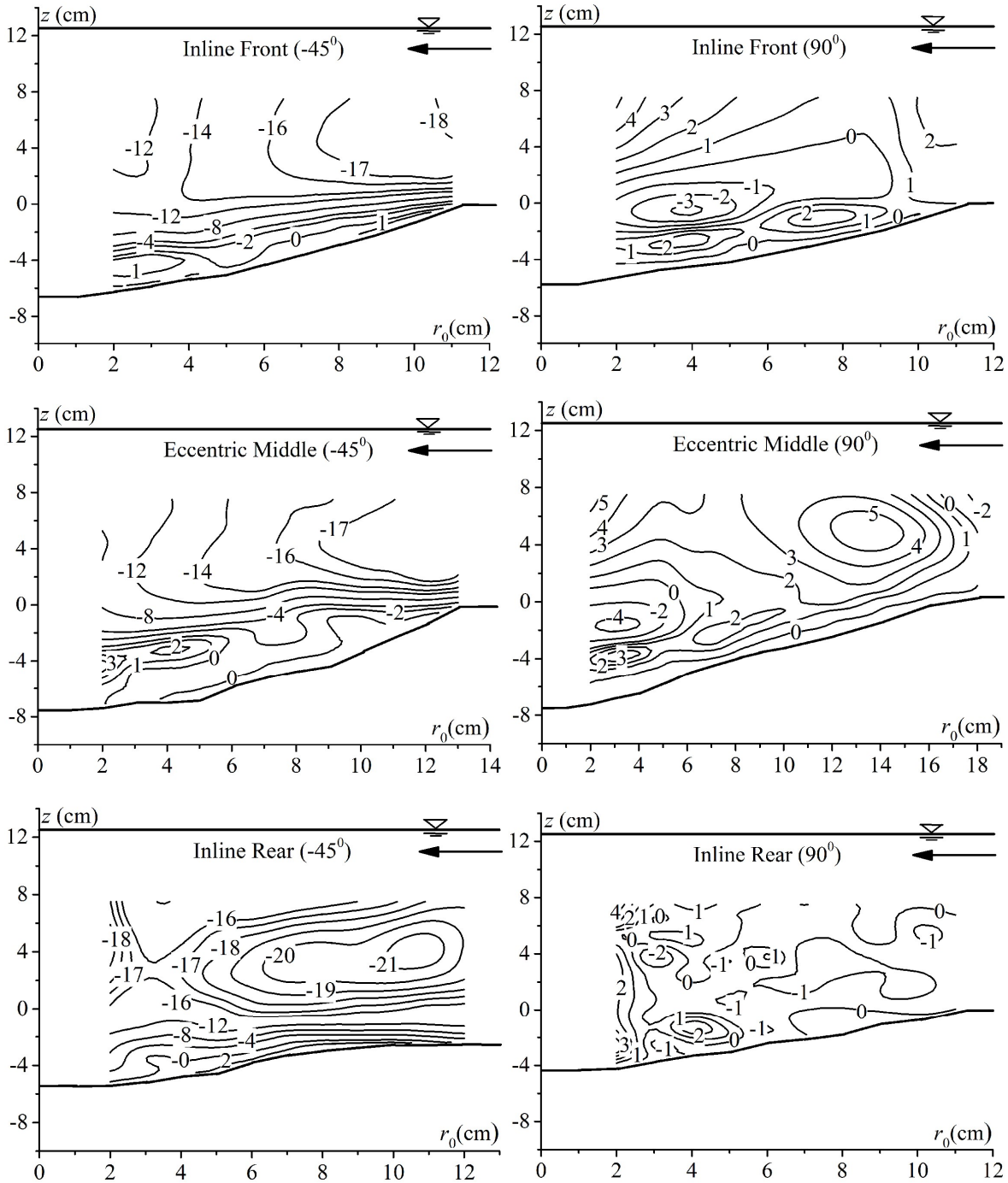


Fig. 3.14. Contours of radial velocity (v) in cm/s for inline-front, eccentric-middle and inline-rear circular piers at r - z planes for $\theta = -45^\circ$ and 90° .

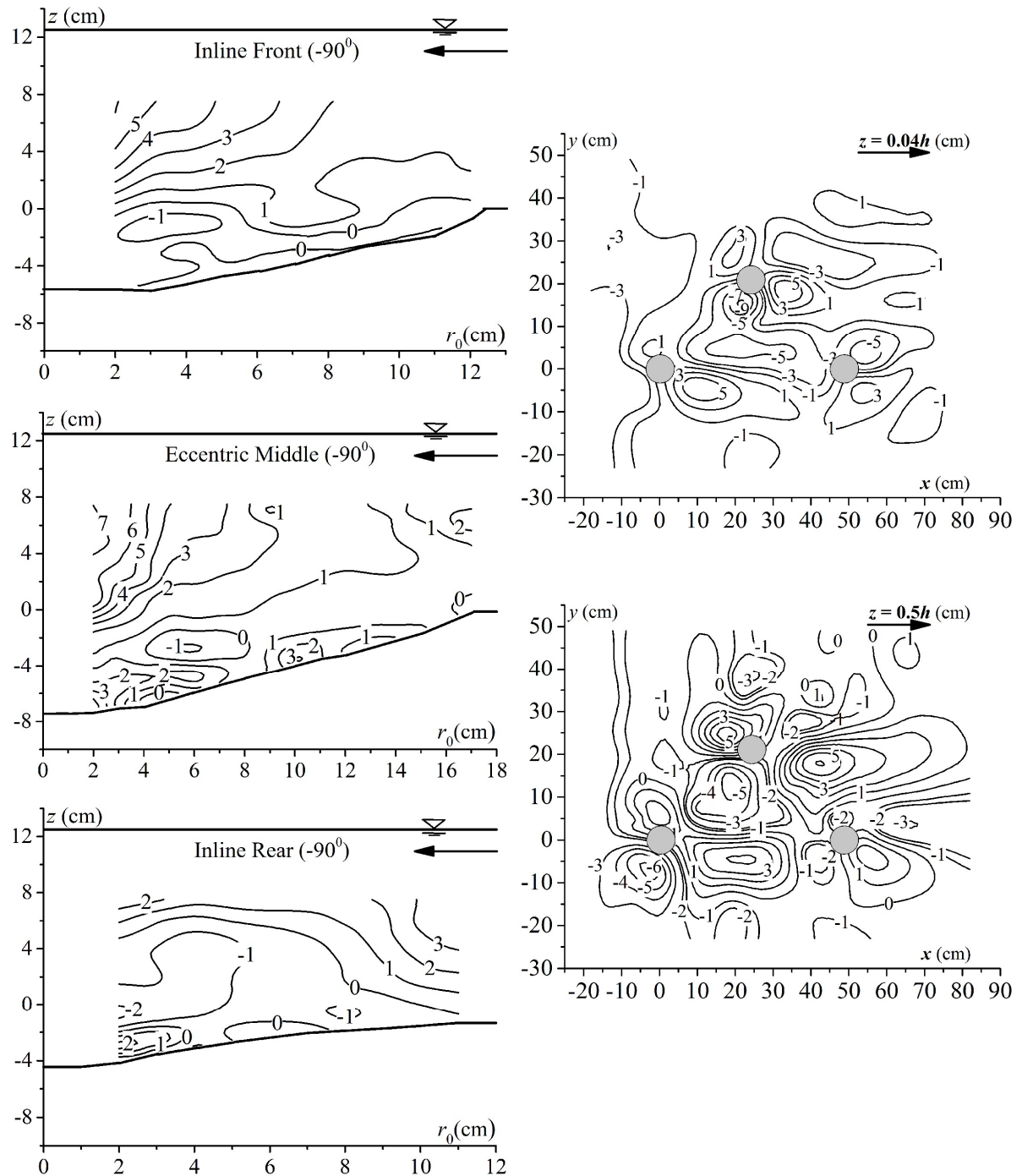


Fig. 3.15. Contours of radial velocity (v) in cm/s for inline-front, eccentric-middle and inline-rear circular piers at r - z planes for $\theta = -90^\circ$ and at x - y planes for $z=0.04h$ and $z=0.5h$.

The contours of time mean radial velocity v at two horizontal plane $z=0.04h$ and $z=0.5h$ above the bed level ($h=0$) are shown in Fig. 3.15. From these figures, it is observed that the approaching flow is separated near all the three circular piers. Transverse velocity v changes its direction on both side of zero contour line ($v=0$). The trend of the path of v is towards the right side of the wall. The part of radial velocity which flows towards the left side of the flume wall has positive values and the other part which flows towards right of flume wall has negative values. This phenomenon is prominent for the eccentric-middle circular pier, where the flow separates. At both x - y planes ($z=0.5$ cm and $z=6.25$ cm), maximum v is found at

upstream zone of eccentric-middle circular pier compared to other two inline circular piers. The radial velocity at the downstream zone of the three piers at $z=0.04h$ plane found very close to v at the downstream zone of the three piers for $z=0.5h$ plane but greater than that at $z=0.5h$ plane. At the upper middle depth, near upstream zone of each pier, v values are greater than those near the bed for existence of high momentum flow.

3.7.1.3 Vertical Velocity

Fig. 3.16, Fig.3.17 and Fig.3.18 represent the profiles of the time-averaged vertical velocity ' w ' at different azimuthal planes 0° , 45° , 90° , -45° and -90° and at two horizontal planes $z=0.04h$ and $z=0.5h$ from zero bed level for equilibrium clear-water scour state for the inline-front, eccentric-middle and inline-rear circular piers.

At 0° , around the middle-eccentric circular pier, from an investigation of the contours of vertical velocity, the separation of the approaching flow below the bed ($z < 0$) near the scour hole is evident (as it was observed in radial velocity contours) from the reversal nature of w near the scoured bed. The vertical velocity distribution in the majority of the flow region is downward (negative) for the three circular piers, while radial velocity v near the scoured bed is directed upward (positive) and rises in the downward direction from the free surface indicating that there is an existence of downward negative pressure gradient $[\partial(\rho v^2)/\partial z]$.

Cores of higher w magnitudes are observed near all the three piers at a depth of 0.22-0.37, 0.19-0.45 and 0.09-0.36 times the local scour depth of inline-front, eccentric-middle and inline-rear circular pier respectively, bellow the $z=0$ line (original bed level) and it decreases toward the base of the scour hole. The vortex core size is higher in the eccentric-middle circular pier. At 0° , for the inline-front, eccentric-middle and inline-rear circular pier the maximum w was detected as $0.59U$ at $z = 0.3$ times, $0.51U$ at $z = 0.39$ times and $0.35U$ at $z = 0.18$ times the corresponding local scour depth of the piers respectively. For the limitation of the vectrino+ (ADV) that the measurement by ADV is not possible at the edge of the pier ($r = 0$), the values were taken 2 cm away from the pier. Hence the maximum values of w are somewhat lesser than the values at the boundaries of the pier.

In the present study, the behaviour of the upstream flow around the three piers are similar, but behind the piers this similarity decreases due to presence of the downstream piers. Near the bed within the gap between the two inline piers (at 0° azimuthal plane for inline-rear circular pier), between the inline-front and eccentric-middle circular piers (at 90° azimuthal plane for eccentric-middle circular pier) and between the eccentric-middle and inline-rear piers (at 90° azimuthal plane for inline-rear circular pier), the reverse maximum w magnitudes are $0.26U$, $0.14U$ and $0.11U$ respectively. Here, due to sheltering effect, inline-front pier causes the flow velocity to decreases when the flow velocity comes towards the downstream of eccentric-middle pier and similarly, decreases when the flow velocity comes towards the downstream of inline-rear pier due to combined sheltering effect of inline-front and inline-rear circular piers. Vortex shading occurs partially in those scoured regions. The flow regimes formed within the transverse gap (between the three inline-eccentric-inline piers) is termed co-shedding regime or binary vortex street. In the reattachment regime (between the two inline tandem piers) everywhere the upflows are found. This phenomenon

can be referred for decreasing in downflow at frontal region of the inline-rear circular pier and due to combined effect of this downflow and an obstructed flow velocity increases the downflow, approaching the upstream region of the eccentric-middle circular pier. [Zdravkovich (1987)] Formation of turbulent flows of different velocities (different Reynolds number) along the flow depth due to the effect of bed roughness, along with pier spacing, can influence the flow regime type within the gap.

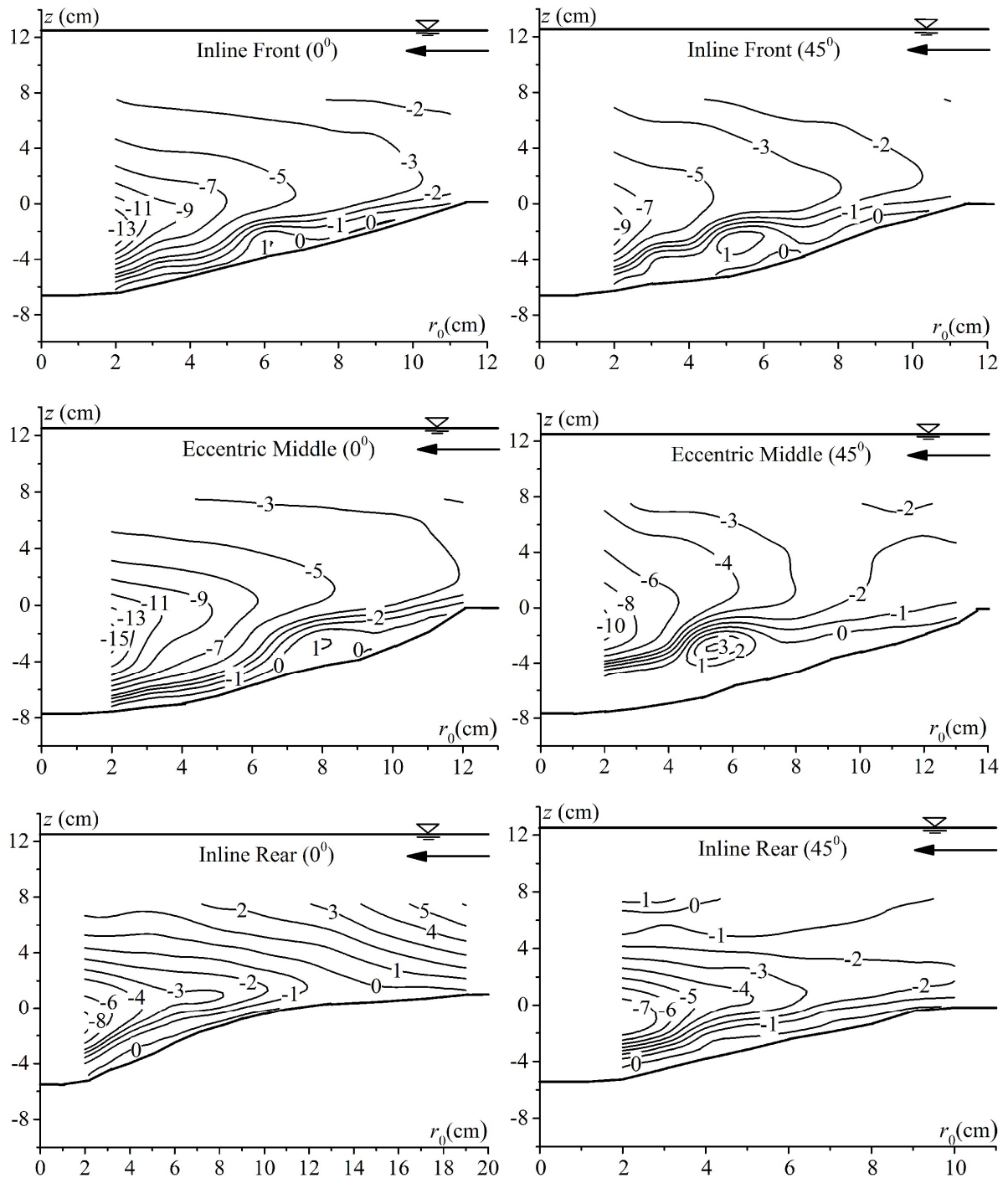


Fig. 3.16. Contours of vertical velocity (w) in cm/s for inline-front, eccentric-middle and inline-rear circular piers at r - z planes for $\theta = 0^\circ$ and 45° .

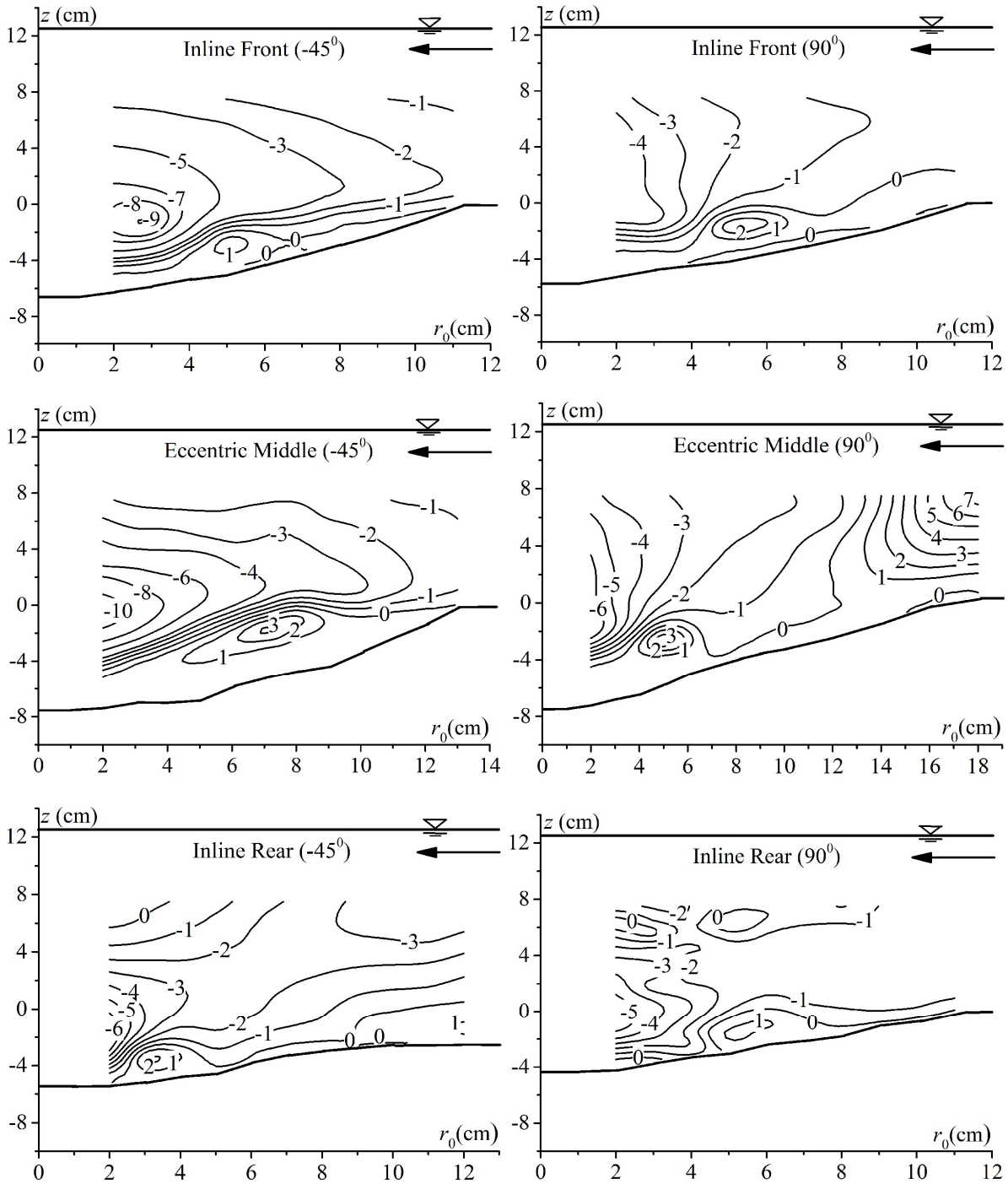


Fig. 3.17. Contours of vertical velocity (w) in cm/s for inline-front, eccentric-middle and inline-rear circular piers at r - z planes for $\theta = -45^\circ$ and 90° .

As θ increases to 0° to $\pm 90^\circ$, a gradual decrease in vertical velocity for all the three piers. Due to the downward negative stagnation pressure gradient of the non-uniform approaching flow close to the upstream region of all the three piers, a downflow develops and thus vortex thrusts the downflow [Dey *et al.* (1995)]. This observation, Dey *et al.* (1995) shows a good arrangement with the attenuation of radial velocity and when the horseshoe vortex reduction was observed experimentally when θ changes, with a equal 15° interval from 0° to 90° planes. Thus, it affirms the weakening of these horseshoe vortices along the downstream flow. At 45° , 90° , -45° and -90° plane for the inline-front circular pier the

maximum magnitude of downward w are 0.72, 0.35, 0.63 and 0.43 times than that at 0° , respectively. Similarly for eccentric-middle and inline-rear circular piers, it is 0.72, 0.45, 0.71, 0.49 and 0.92, 0.88, 0.66, 0.48 times than that at 0° for the corresponding piers, respectively. According to these outcomes, it explains, at eccentric-middle circular pier w is always higher than that at inline-front and inline-rear circular piers. For the inline-front circular pier, w is always almost higher than w at inline-rear circular pier.

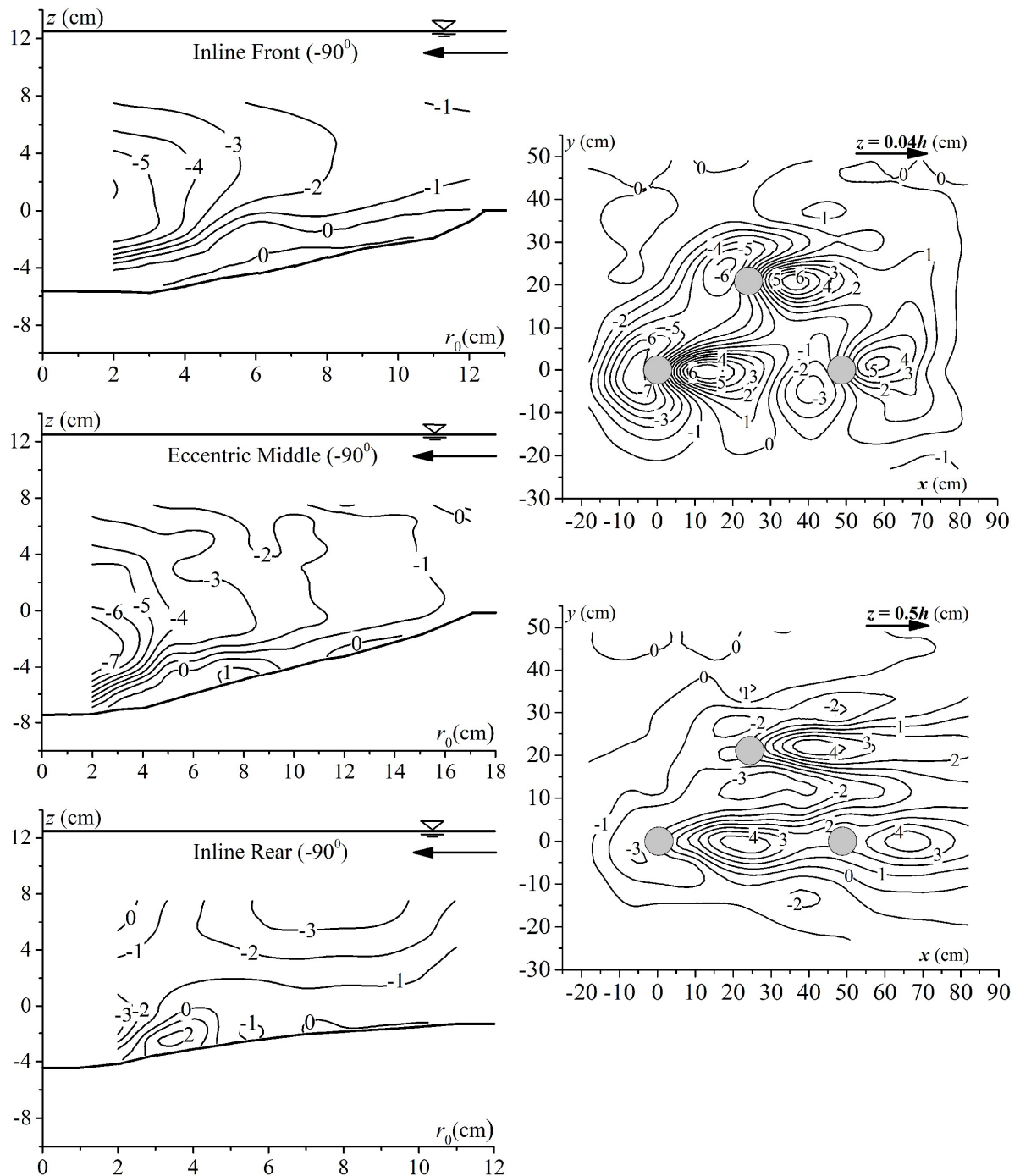


Fig. 3.18. Contours of vertical velocity (w) in cm/s for inline-front, eccentric-middle and inline-rear circular piers at r - z planes for $\theta = -90^\circ$ and at x - y planes for $z=0.04h$ and $z=0.5h$.

The contours of time-mean vertical velocity w are well addressed in Fig. 3.18 for $z=0.04h$ and $z=0.5h$ planes in the flow region, describing flow characteristics more accurately. As in figures, at the upstream zones of all the three circular piers, there is a downward negative velocity. Here, w is directed in upward direction. It is clear from those negative values that near the upstream zones of the three circular piers, there is a downward motion. Then flow is obstructed by all the three circular piers and upstream of stagnation point it begins to move downward.

Near upstream of the eccentric-middle circular pier, the maximum negative value of w is noticed. Hence, at the upstream zone of eccentric-middle circular pier it is clear maximum scour depth, as well as strongest circulation, is likely to be found. At the downstream region of the three circular piers, vertical flow velocity is found directed upward with positive magnitude. Hence, this specifies that the flow firstly passes downward at the upstream region of each circular pier forming horseshoe vortex, then passes from the side of the piers and finally it moves upward at the downstream region of each circular pier forming wake vortex. For $z=0.04h$ at the downstream zone of the three circular piers, this vertical velocity w is noticed maximum. The maximum w is found approximately 0.8 times that of v . Now, comparing the w contours as depicted in Fig. 3.18, it is clear that w magnitude at the upstream of the three circular piers for $z=0.04h$ plane is greater than w magnitude at the upstream of the three circular piers for $z=0.5h$ plane. For $z=0.04h$ horizontal plane, at the downstream of the three circular piers, value of w is more. Also, in the wake region, for $z=0.04h$ plane vertical velocity of higher value is observed as compared to vertical velocity in the wake region for $z=0.5h$ plane. This confirms that the flow moves upward producing a stronger wake vortex at the downstream of all the three circular piers and thus, at the downstream of three circular piers, there is little wake vortex effect.

3.7.1.4 Velocity Vector

Contour profiles of \vec{v} (velocity vectors) for equilibrium clear-water scour state at five azimuthal planes 0° , 45° , -45° , 90° and -90° for inline-front, eccentric-middle and inline-rear circular piers of magnitude $\sqrt{v^2 + w^2}$ and direction $\text{arc tan}(w/v)$ are shown in Figs. 3.19, 3.20 and 3.21. Also Fig. 3.21 shows velocity vectors at $z=0.04h$ and $z=0.5h$ horizontal planes around the piers, whose magnitude and direction are $\sqrt{u^2 + v^2}$ and $\text{arc tan}(v/u)$, respectively.

The vector plots at 0° , 45° and -45° shows the hydrodynamic characteristics of horseshoe vortices along with the downflow along the upstream of all three piers. The hydrodynamic characteristics of flows around the three circular piers are comparatively great secondary vortices flows and skewed velocity distributions. At the upstream edge of the three scour holes, the approaching flow separates to form vertical-flow in each scour hole, acts as a separation zone. The limiting stream lines along the pre experimental bed upstream merge due to the approaching-flow at the edge of the three scour holes forming diverged and/or separated stream lines, which produces a surface of separation. The pier induced separation in the upstream flow along the bed surface, the approaching flow curved downward into the holes and transversely rolls to form vortices which is called horseshoe vortex system which migrates downstream by the sides of the three circular piers.

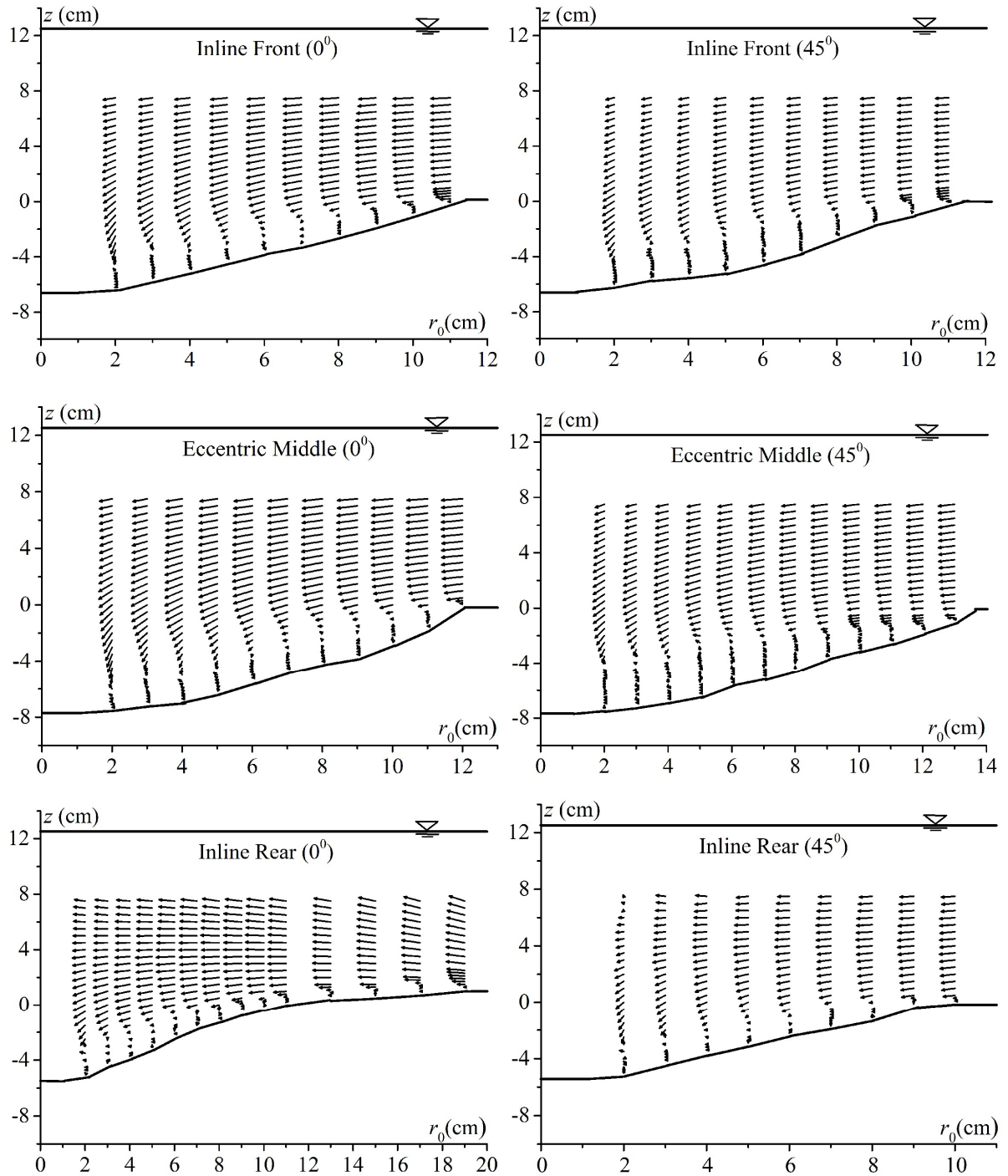


Fig. 3.19. Velocity vector plots for inline-front, eccentric-middle and inline-rear circular piers at r - z planes for $\theta = 0^\circ$ and 45° .

This Horseshoe vortex is considered as one of the major players in the development of the three scour holes, in agreement with the earlier researches [Dey and Raikar (2007), Das and Mazumdar (2015b)]. Here, for larger scour holes, the size of such horseshoe vortices, larger than that of the above-mentioned researches. These horseshoe vortices are part of systems of turbulence structures that combines with downflow, flow acceleration around side of the three circular piers and large-scale wake rollers, which are the erosive factors of the bed sediments in single pier experimentation. However, in the present experimentation,

besides these mechanisms, some alteration also occur in the flow velocity formation which are interference of vortex shedding, interference of horseshoe vortices and velocities increases between the inline-front and eccentric-middle and between the eccentric-middle and inline-rear circular piers.

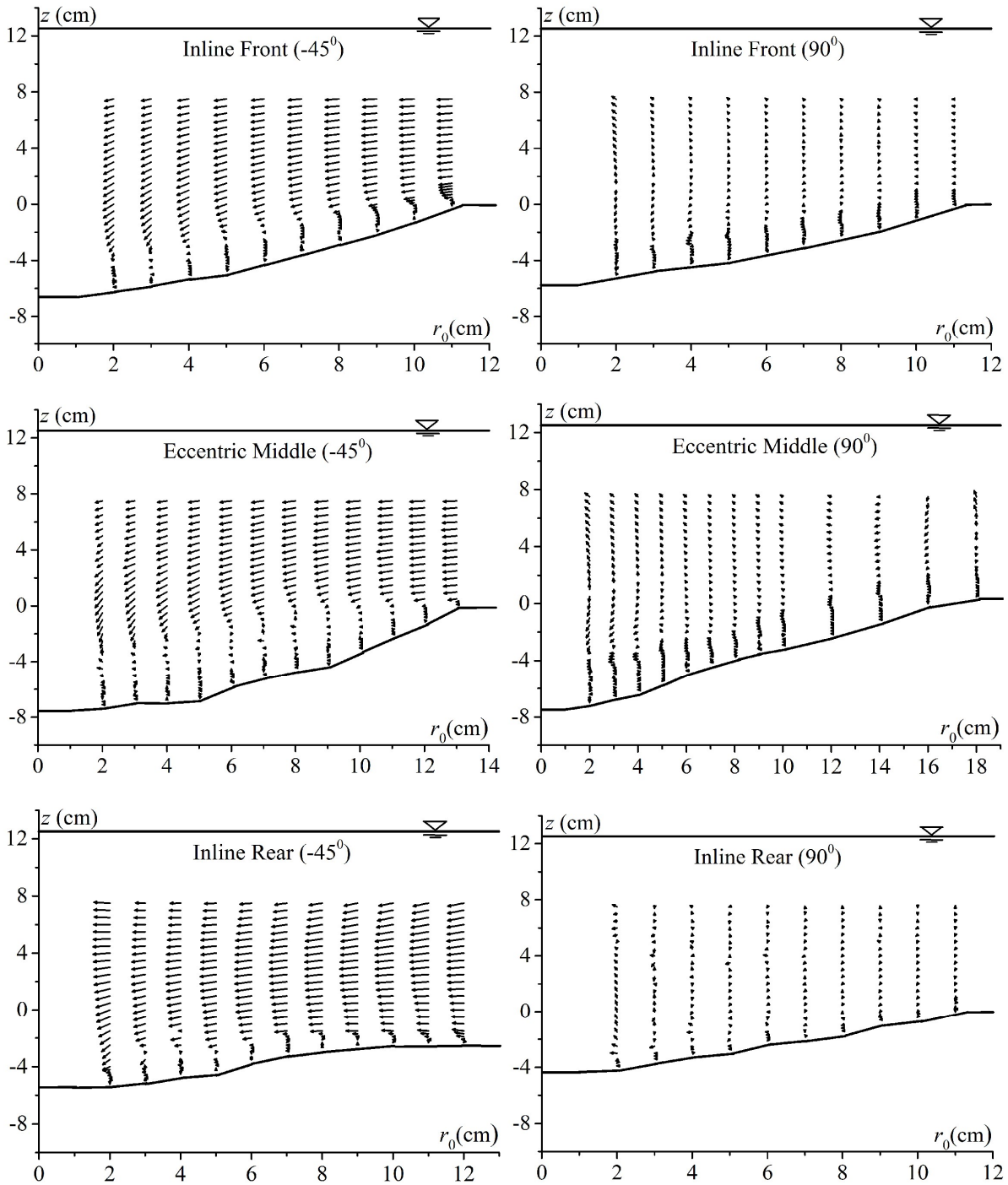


Fig. 3.20. Velocity vector plots for inline-front, eccentric-middle and inline-rear circular piers at r - z planes for $\theta = -45^\circ$ and 90° .

The cross sectional shape of each vortex is almost elliptical with the major axis being approximately the bisector of the angle made by scoured bed slope of the scour hole with

horizontal. The height i.e. length of the minor axis of the elliptical vortex at 0° is larger than at 45° and -45° . At 0° , the vertical flow is strongest and it decreases as θ increases. The strength and location of elliptical vortex system depend on the approaching flow velocity and it will be stronger near base of the piers for high flow velocity.

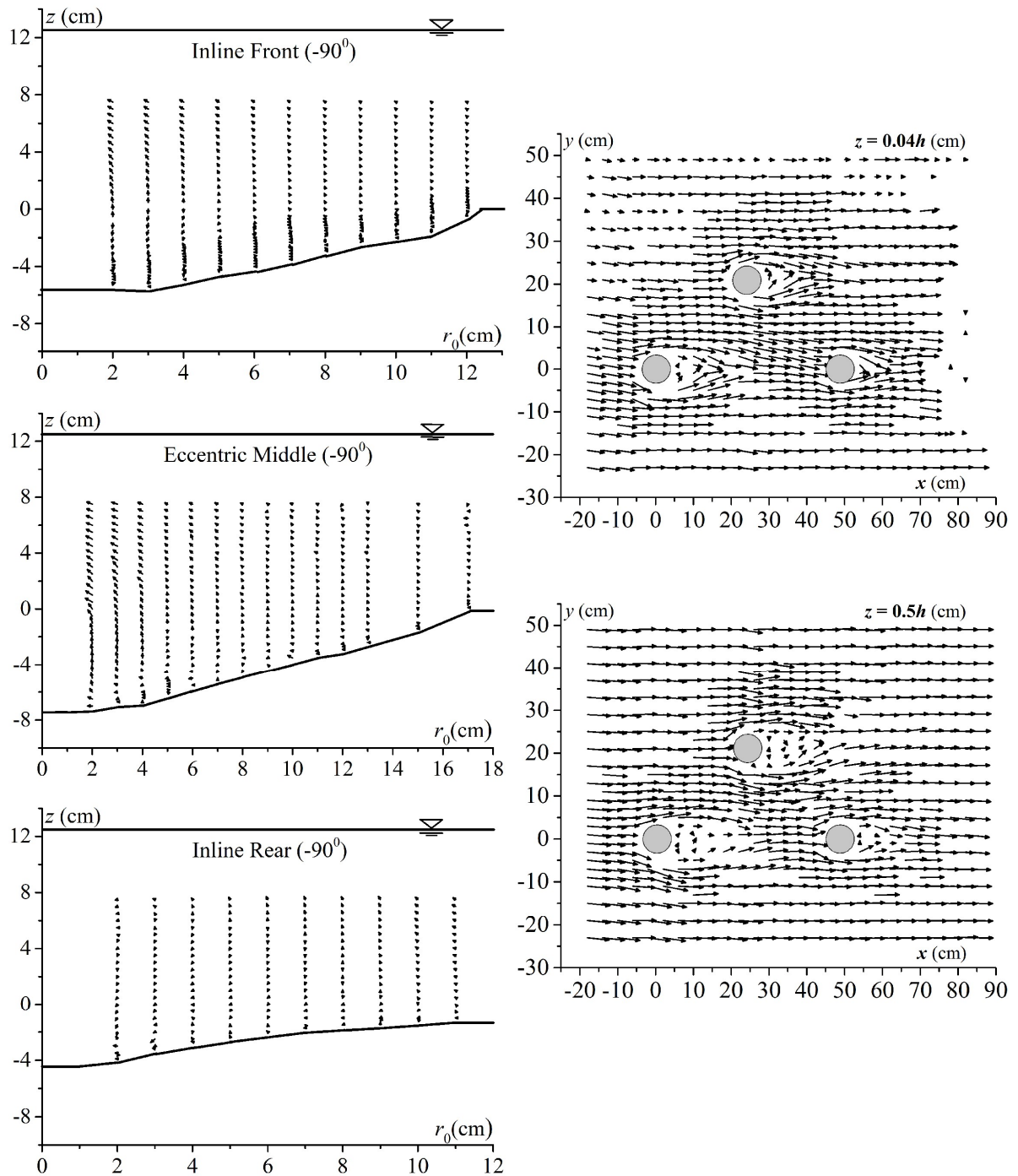


Fig. 3.21. Velocity vector plots for in-line-front, eccentric-middle and in-line-rear circular piers at r - z planes for $\theta = -90^\circ$ and at x - y planes for $z=0.04h$ and $z=0.5h$.

Here, the size of the vortex core for the eccentric-middle circular pier is observed larger than the in-line-front and in-line-rear circular piers. Above the scour hole i.e. for $z>0$, the flows are in horizontal directions and towards the piers, but near the piers the direction of flows are

downward. The vortical flows are not distinct at 90° and -90° , due to the separated flow. A close study of the vector fields at 90° and -90° for the three circular piers reveals that near the scour bed a weaker vertical flow exist.

The flow velocity characteristics are described more accurately in the flow zone for $z=0.04h$ and $z=0.5h$ horizontal planes. Fig. 3.21, plotted by OriginLab software, shows the velocity vectors at $z=0.04h$ and $z=0.5h$ planes. To avoid congested plotting of \vec{V} profile, some of the measured points are omitted from the plots. From the figure, plotting of \vec{V} , it is found that the velocity decreases in the downstream region of inline-front circular pier. It is also similar for eccentric-middle and inline-rear circular piers. Here, it is clearly observed, from the velocity vector profiles, that the wake zone length is larger for the inline-front circular pier than the other two eccentric-middle and inline-rear circular piers. The wake zone length is larger for eccentric-middle circular pier than inline-rear circular pier. Wake zone length is larger at $z=0.5h$ than $z=0.04h$ horizontal plane, observed from the figures. For the pier induced adverse pressure gradient near upstream zone of the three circular piers, boundary layer is separated and then shifts both sides of the circular piers towards downstream near the bed. This phenomenon results in larger wake at $z=0.5h$ plane in contrast with $z=0.04h$ plane for the effect of bed roughness on turbulence increase near the bed.

3.7.1.5 Absolute Velocity

The contours profiles of the time-averaged absolute velocity, $V = \sqrt{u^2 + v^2 + w^2}$ at five different azimuthal planes 0° , 45° , 90° , -45° and -90° and at two horizontal planes $z=0.04h$ and $z=0.5h$ from zero bed level for equilibrium clear-water scour state for the inline-front, eccentric-middle and inline-rear circular piers are shown in Fig. 3.22, Fig. 3.23 and Fig. 3.24 respectively. The contour lines of the absolute velocity V for the inline-front, eccentric-middle and inline-rear circular piers are almost similar. At 0° , as tangential velocity is negligible, these figures show the exclusive vertical flow at 0° . At 45° and -45° , the diminishing natures of absolute velocity in the horseshoe vortices with θ are displayed. On the other hand, at 90° and -90° , tangential velocity is a prime flow feature. Near the scoured bed, the contour lines of absolute velocity are concentrated, indicating regions of rapid change of the velocity magnitude. Near the scoured bed, V decreases, with the development of the three scour holes around three circular piers. At 90° and -90° , the radial and vertical velocities are negligible close to the three circular piers as the side of the piers are parallel with the flow direction. The flow separation takes place at $\theta = 45^\circ$ and -45° from the edge of the pier, resulting in the lower V magnitude near the pier.

Fig. 3.24 confirms that time-mean absolute velocity increases as V_0 increases. From the V contour profiles, it is found that in wake regions at the downstream zone near the three circular piers have lower values of absolute velocity V . At x - y horizontal planes for $x = 70$ – 90 cm, V decreases near the bed since the flow is obstructed by deposited sediment i.e. dune at pier downstream. At the downstream zone near the piers (wake zones) V has greater values at $z=0.5h$ plane than V at $z=0.04h$ plane.

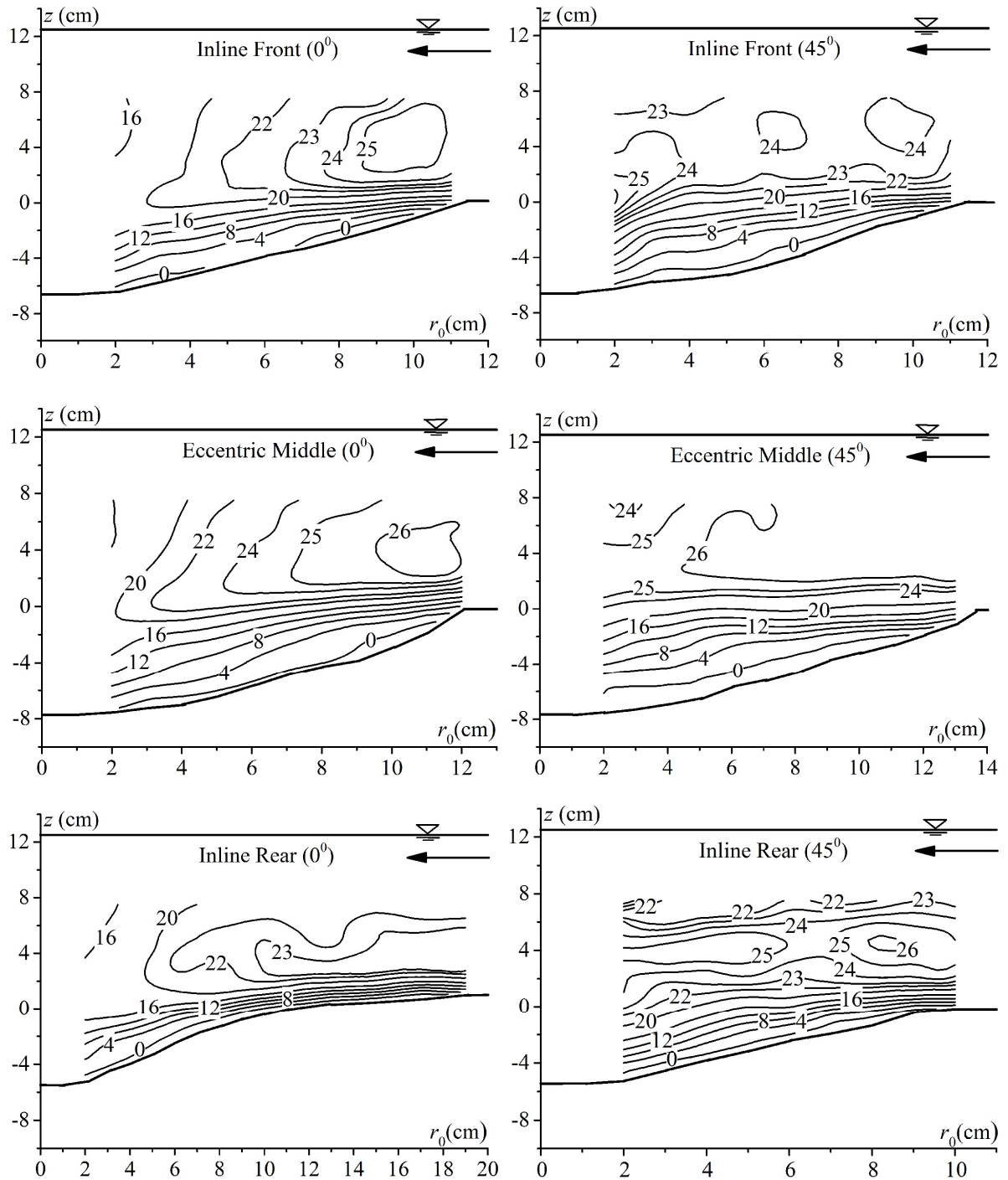


Fig. 3.22. Contours of absolute velocity (V) in cm/s for inline-front, eccentric-middle and inline-rear circular piers at r - z planes for $\theta = 0^\circ$ and 45° .

3.7.2 Vorticity and Circulation

Fig. 3.25, Fig. 3.26 and Fig. 3.27 shows the contours of vorticity $\zeta = (\partial v / \partial z - \partial w / \partial r)$ for equilibrium scour holes at 0° , 45° , -45° , 90° and -90° azimuthal angles at r - z planes around inline-front, eccentric-middle and inline-rear circular piers.

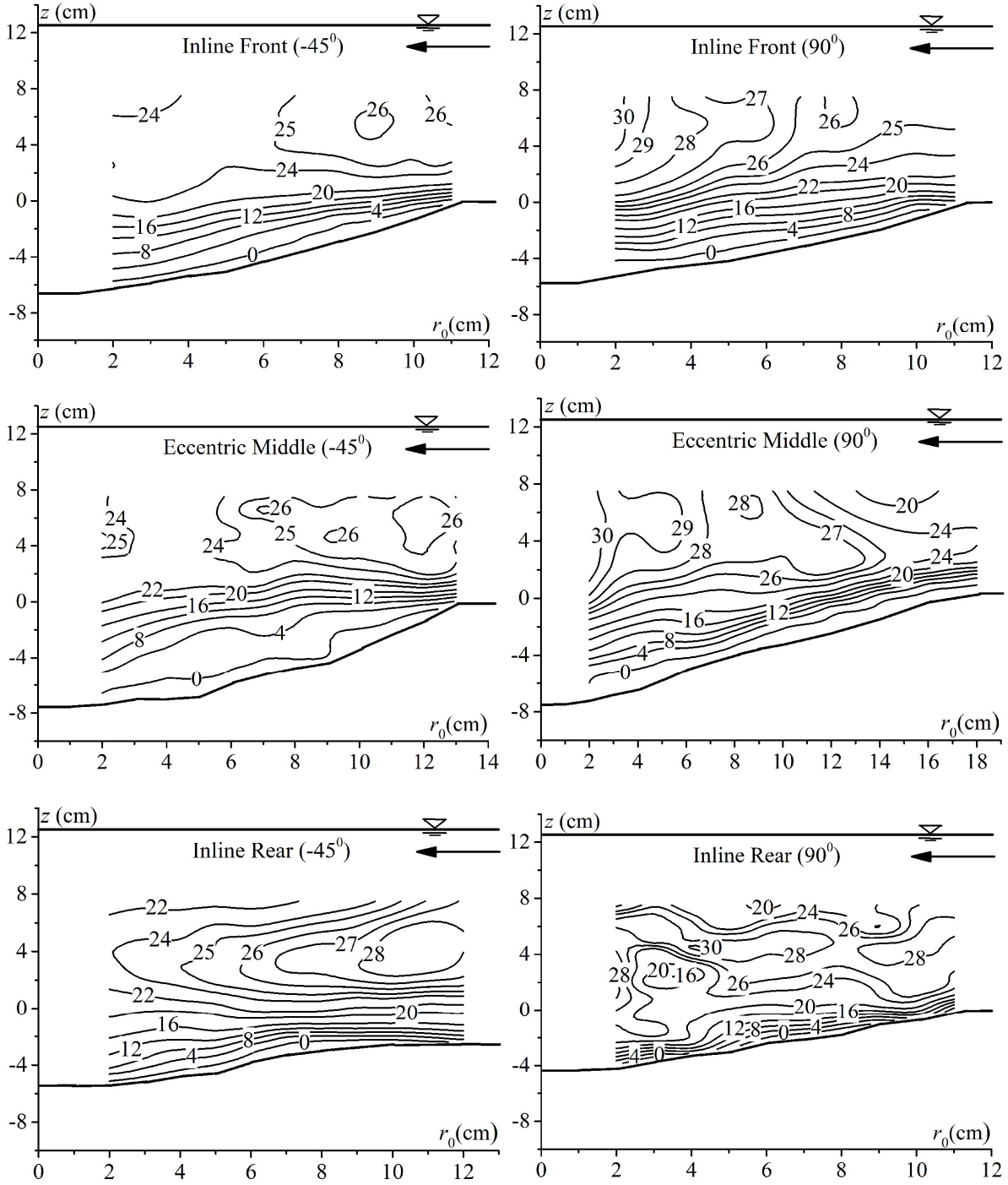


Fig. 3.23. Contours of absolute velocity (V) in cm/s for inline-front, eccentric-middle and inline-rear circular piers at r - z planes for $\theta = -45^\circ$ and 90° .

The coordinates for vorticity contours are computed by converting the partial differential equation into finite difference equation using a forward difference technique of computational hydrodynamics.

At a grid point (i,k) , vorticity equation (Eq. 1) is expressed as

$$\zeta = \frac{v_{i,k+1} - v_{i,k}}{\Delta z} - \frac{w_{i+1,k} - w_{i,k}}{\Delta r} + O(\Delta z, \Delta r) \quad (3.1)$$

where index i and index k run towards r and z -directions, respectively. Here, $O(\Delta z, \Delta r)$ is called 'terms of order Δz and Δr '. The scale model of above equation is given as in equation (Eqn. 2).

$$\zeta = \left(\frac{\partial v}{\partial z} - \frac{\partial w}{\partial r} \right) \approx \left(\frac{V}{Z} - \frac{W}{R} \right) \quad (3.2)$$

where, V , W , Z and R represent scaled variables of v , w , z and r respectively.

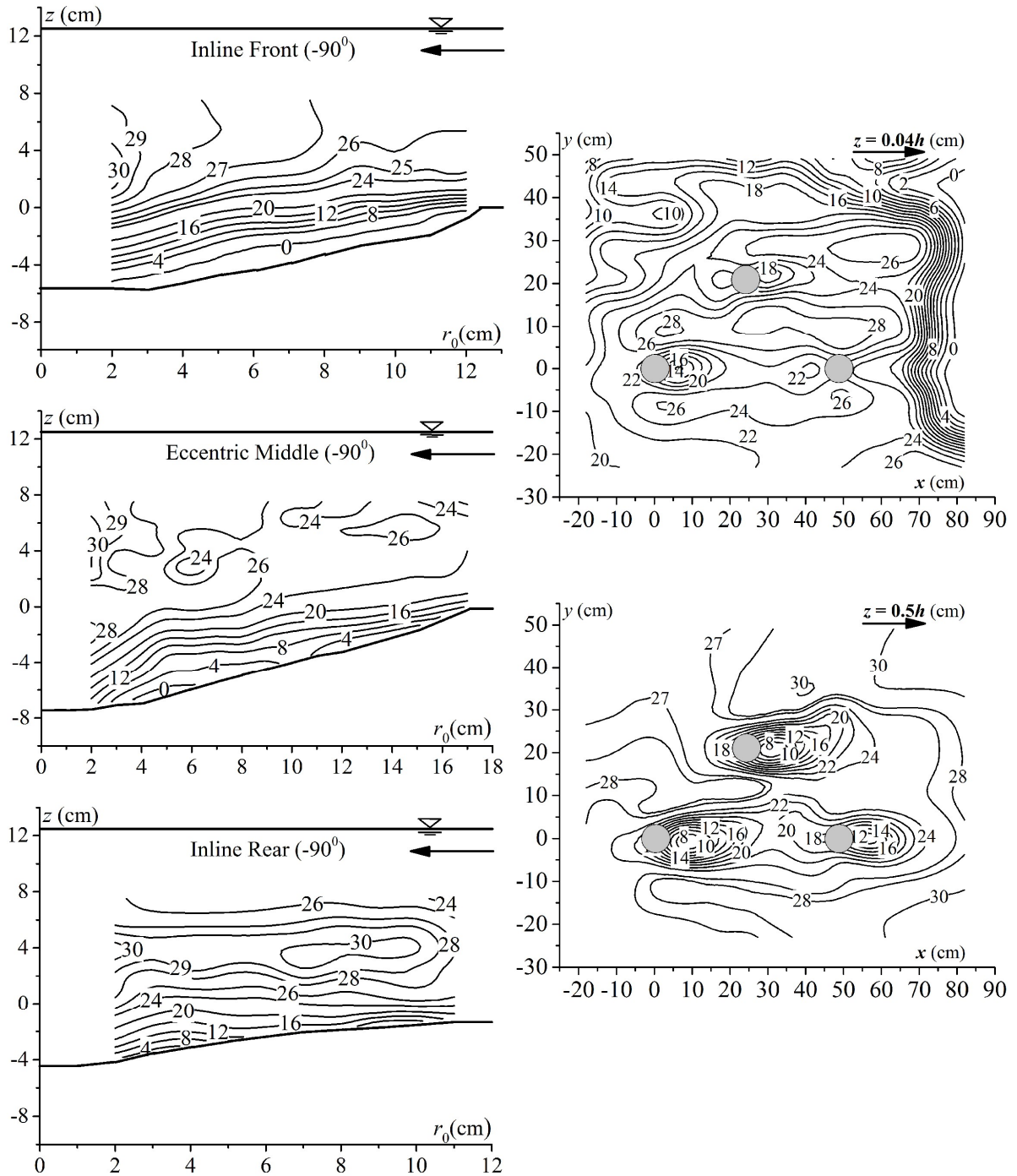


Fig. 3.24. Contours of absolute velocity (V) in cm/s for inline-front, eccentric-middle and inline-rear circular piers at r - z planes for $\theta = -90^\circ$ and at x - y planes for $z = 0.04h$ and $z = 0.5h$.

Only at pier boundaries where there is a presence of pressure gradient, formation of vorticity occurs. When the pressure increases and instantly becomes sufficiently strong, the 3D boundary layer undergoes flow separation and system rolls up frontal side of each pier, forming horseshoe vortex system at the base of the three circular piers. The vortical flow was measured primarily in the r - z plane, as rotational axis of the horseshoe vortex system is vertical to the r - z plane. The coordinates of vorticity contours are computed from the contours of radial and vertical velocity given in figures, respectively. The vorticity contours in Figs. 3.25, 3.26 and 3.27 confirm that the vorticities are concentrated within the scour holes. Further analysis of the vector plots and the vorticity contours confirms that the vortex flow is purely a forced vortex flow. Near such vortex centres high vorticity concentrations indicates the vortex cores. The vortices core size decreases as θ increases. At $\pm 90^\circ$ the vortices core size are relatively small and the vorticity is considerably weaker.

At the upstream zone of the three circular piers, the circulation Ω of each horseshoe vortex is calculated from vorticity contours, using normalized Stokes' theorem (Eq. 3).

$$\Omega = \oint_c \vec{v} \cdot d\vec{s} = \iint_A z \cdot d(rz) \quad (3.3)$$

where, \vec{v} = velocity vector, and $d\vec{s}$ = displacement vector. The circulations summed up for five azimuthal planes for the three piers are shown in the Table 3.3.

The circulation Ω decrease with further increase in azimuth angle θ (clockwise and anticlockwise) and also increases with further increase in scour depth. The circulation at 45° , 90° , -45° and -90° azimuthal plane for inline-front circular pier are 0.67, 0.12, 0.77 and 0.16 times of the respective circulation at 0° . Similarly the Ω at eccentric-middle circular pier at 45° , 90° , -45° and -90° azimuthal are 0.51, 0.17, 0.72 and 0.13 times and for the downstream most inline-rear circular pier Ω are 0.66, 0.12, 0.77 and 0.16 times of the respective Ω at 0° of the corresponding pier. Here, the calculated Ω are in obedience to Raikar and Dey (2007) and Das and Mazumdar (2015b) result and also confirms that the circulation decreases slowly from 0° to $\pm 45^\circ$ azimuth angle and then decreases rapidly $\pm 45^\circ$ to $\pm 90^\circ$ azimuth angle.

At -45° for the inline-front circular pier the separation streamline coincides with the separated streamline near 45° for eccentric-middle circular pier and also the separated streamline at 45° for eccentric-middle circular pier coincides with the separation streamline near -45° for inline-rear circular pier. For this reason, at eccentric-middle and inline-rear circular piers, Ω at -45° is slightly higher than that at 45° azimuth angle. For eccentric-middle circular pier, Ω at 90° is higher than at -90° and for inline rear circular pier the magnitude of Ω at -90° is slightly higher than Ω at 90° azimuth angle. It is due to the effect of co- shedding equilibrium regime, evolves in the wake part of the inline-front circular pier.

Table 3.3. Circulation Ω for five azimuth angles in r - z plane (units in $10^{-2} \times \text{m}^2/\text{s}$).

Pier position	Circulation, Ω (m^2/s)				
	$\theta = 0^\circ$	$\theta = 45^\circ$	$\theta = -45^\circ$	$\theta = 90^\circ$	$\theta = -90^\circ$
Inline front	1.597×10^{-2}	1.067×10^{-2}	1.226×10^{-2}	0.195×10^{-2}	0.267×10^{-2}
Eccentric middle	2.203×10^{-2}	1.128×10^{-2}	1.586×10^{-2}	0.371×10^{-2}	0.295×10^{-2}
Inline rear	1.447×10^{-2}	0.958×10^{-2}	1.111×10^{-2}	0.177×10^{-2}	0.242×10^{-2}

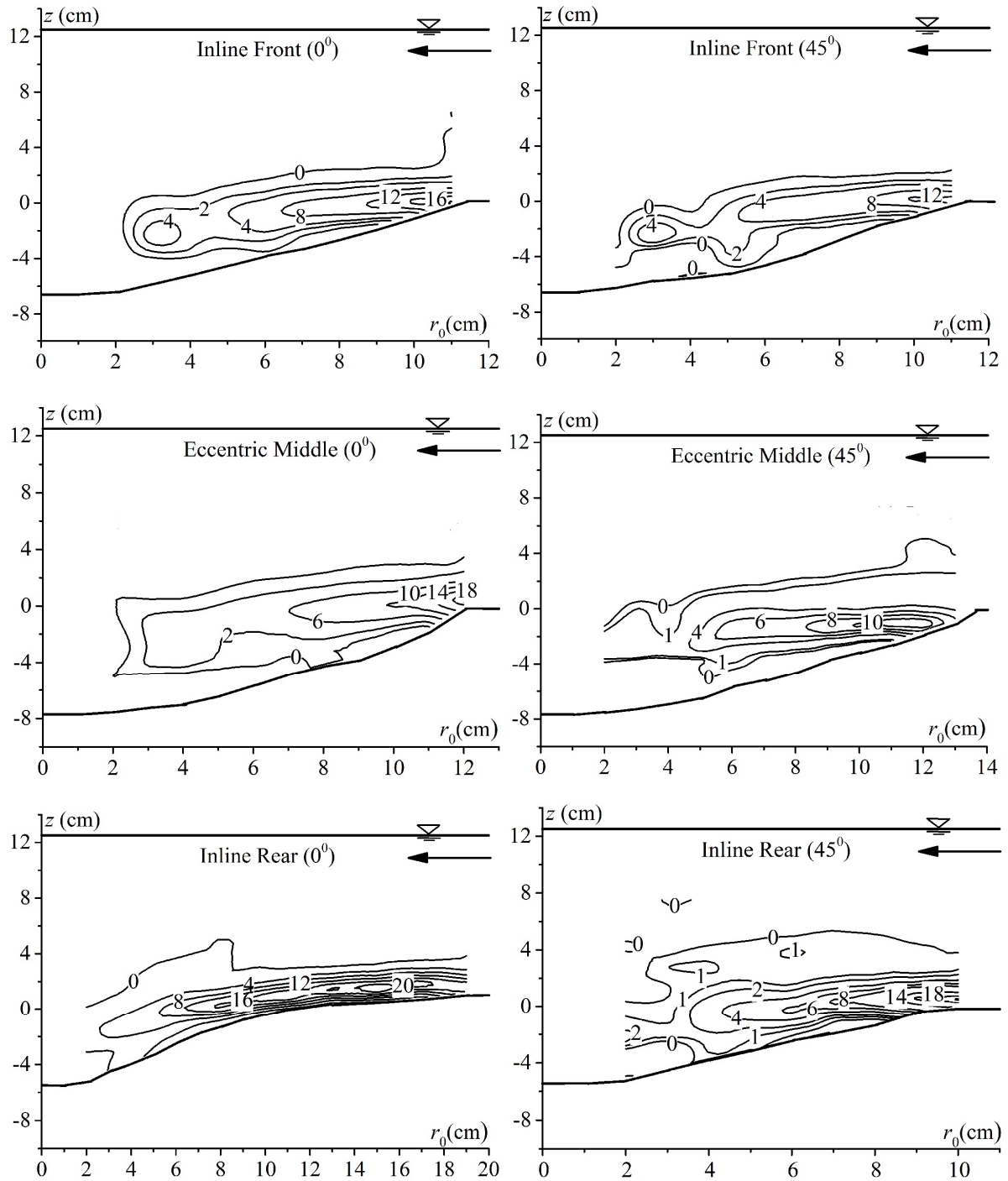


Fig. 3.25. Contours of vorticity ζ (in s^{-1}) for inline-front, eccentric-middle and inline-rear circular piers at r - z planes for $\theta = 0^\circ$ and 45° .

In the present study, circulation for the eccentric-middle circular pier is always greater than the circulation Ω for the inline-front and inline-rear circular pier at respective azimuthal planes. The circulation Ω for inline-front circular pier is greater than Ω for inline-rear circular pier at respective azimuth angle θ . For the eccentric-middle circular pier at 0° , 45° , 90° , -45° and -90° are 38%, 29%, 6%, 90%, 10% and 52%, 43%, 18%, 10%, 22% higher than the inline-front and inline-rear circular piers, respectively. This behaviour specifies the subsequent increase in sizes of vortices in r - z planes and increase in $\partial v/\partial z$ at corresponding

azimuth angle which are well observed in figures of radial velocity contours and velocity vectors plots.

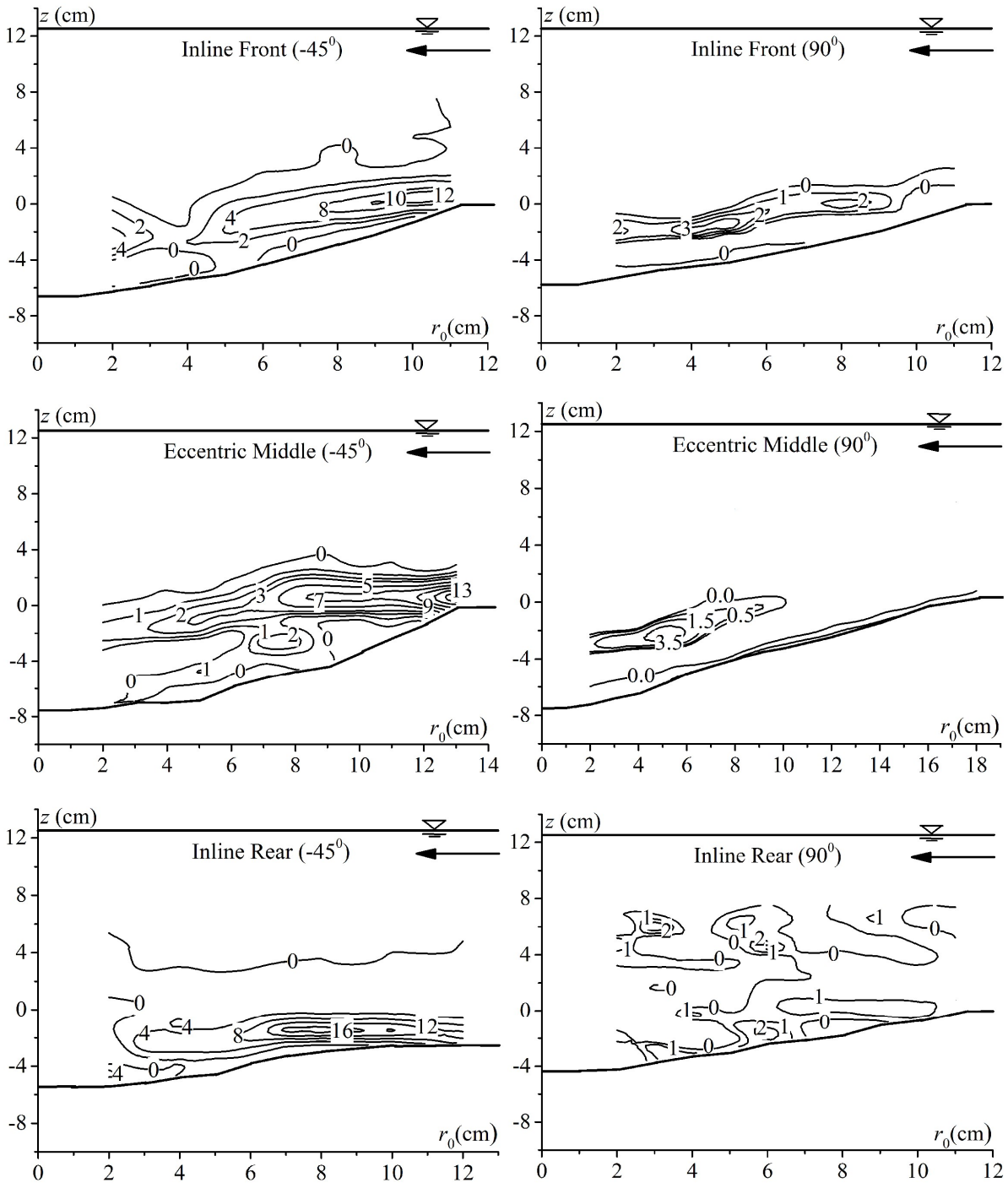


Fig. 3.26. Contours of vorticity ζ (in s^{-1}) for inline-front, eccentric-middle and inline-rear circular piers at r - z planes for $\theta = -45^\circ$ and 90° .

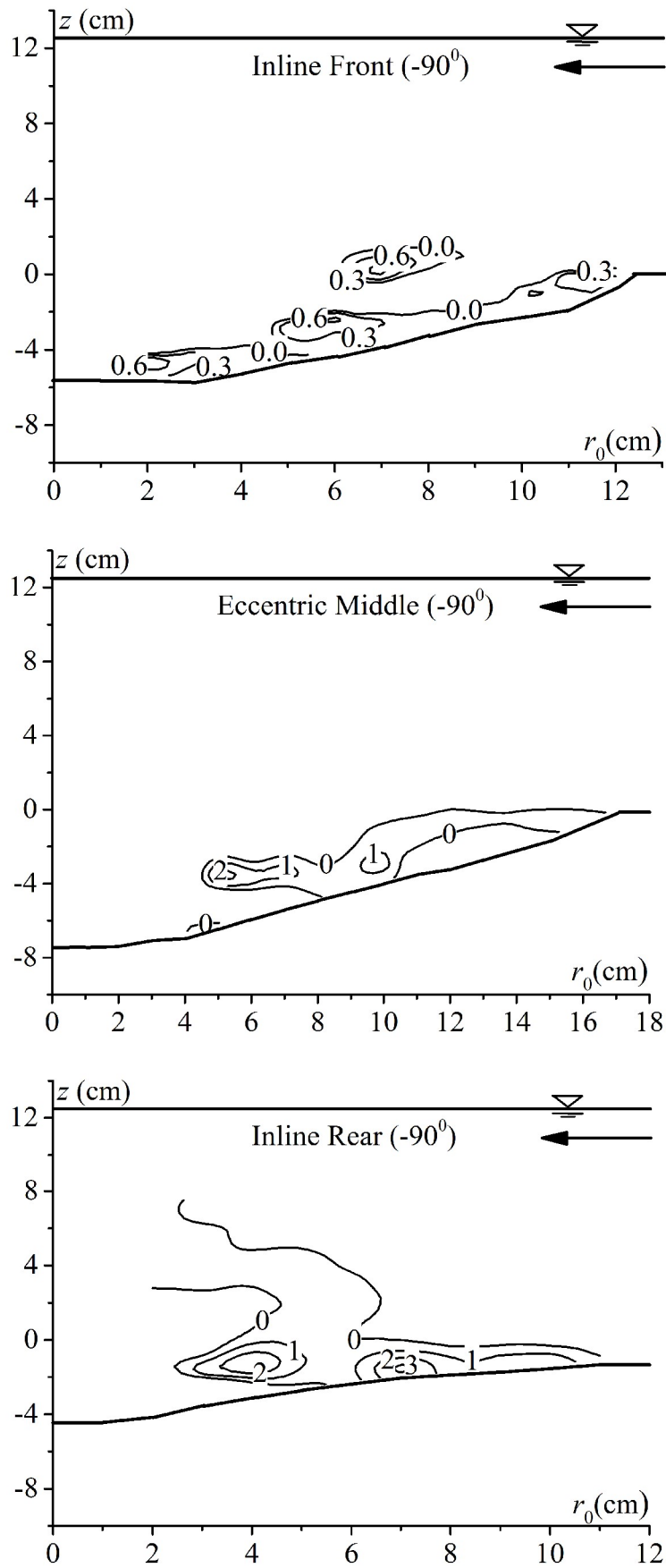


Fig. 3.27. Contours of vorticity ζ (in s^{-1}) for inline-front, eccentric-middle and inline-rear circular piers at r - z planes for $\theta = -90^\circ$.

3.7.3 Turbulence Fields

The tangential turbulent intensity $u^+ = \sqrt{u'u'}$, radial turbulent intensity $v^+ = \sqrt{v'v'}$ and vertical turbulent intensity $w^+ = \sqrt{w'w'}$ are the Root Mean Square (RMS) values of (u' , v' and w') velocity fluctuations of flow u , v and w , correspondingly. Fig. 3.28, Fig. 3.29 and Fig. 3.30 show the tangential turbulent intensity u^+ , radial turbulent intensity v^+ and vertical turbulent intensity w^+ , at an azimuthal plane 0° and at two horizontal planes $z=0.04h$ and $z=0.5h$ from zero bed level ($z=0$) for equilibrium clear-water scour state around the three circular piers. In the present study at the inline-front circular pier the maximum turbulent intensity values are found around $1.43b$ to $1.57b$ from the pier centre. Whereas in case of single pier experiment [Dey and Raikar (2007)] turbulence intensities have maximum values around $1.20b$ - $1.30b$ from the pier centre and in case of two inline-eccentric circular piers experiment [Das and Mazumdar (2015b)] at the upstream of the front pier, these have maximum values around $1.16b$ - $1.29b$ from the pier centre. From these figures, it is clear that the distribution nature of u^+ , v^+ and w^+ are almost identical, both at r - z plane and corresponding x - y plane.

Here, for the inline-front circular pier, the maximum u^+/U and v^+/U are 0.93 and 1.12 times higher than the maximum magnitude of w^+/U . Whereas, for the single pier experiment (Dey and Raikar, 2007) these maximum magnitudes of u^+/U and v^+/U were 1.67 and 1.73 times higher than w^+/U and for two pier case (Das and Mazumdar, 2015b) maximum magnitudes of u^+/U and v^+/U were 1.31 and 1.70 times of w^+/U . Turbulence intensities and turbulent kinetic energy profiles for the inline-front circular pier addressed in this present study match closely with past research findings.

For the eccentric-middle and inline-rear circular piers at 0° the maximum tangential and radial turbulent intensities are higher than maximum u^+/U and v^+/U of inline-front circular pier. As in Figs. 4.28 and 4.29, at 0° azimuth angle for the eccentric-middle and inline-rear circular pier the maximum u^+ , v^+ and w^+ are 1.05, 1.13, 1.04 and 1.82, 1.71, 1.06 times higher than the maximum u^+ , v^+ and w^+ of the inline-front circular pier at the corresponding azimuthal plane, respectively.

The higher magnitudes of u^+ and v^+ for the eccentric-middle and inline-rear circular piers are attributed here for the fact that shed vortices, observed from downstream region of the inline-front circular pier and from downstream region of the inline-front and eccentric-middle circular piers, respectively, are associated with the horseshoe vortices near upstream region of the eccentric-middle and near upstream region of the inline-rear circular piers. For the eccentric-middle circular pier the v^+ magnitude is 1.27 times higher than the u^+ magnitude because these shed-type vortices are associated with large tangential fluctuations.

Also for the inline-rear pier the v^+ magnitude is almost 1.11 times larger than u^+ magnitude because the shed-type vortices coming from the inline-front and eccentric-middle circular pier were directly obstructed by the inline-rear circular pier. Similar observation was observed for the tandem piers [Ashtiani and Kordkandi (2013)] where the v^+ magnitude was almost two times larger than the u^+ magnitude. However, at 0° azimuth angle, the maximum

w^+ magnitude for the eccentric-middle circular pier was little lower and w^+ magnitude for inline-rear circular pier was little higher as compared with w^+ magnitude for the inline-front circular pier. These phenomena can be attributed for the decreasing and increasing in downward flow near the upstream of the eccentric-middle and inline-rear circular piers, respectively, due to the presence of respective upward flow in the transverse gap between the three piers (reattachment regime).

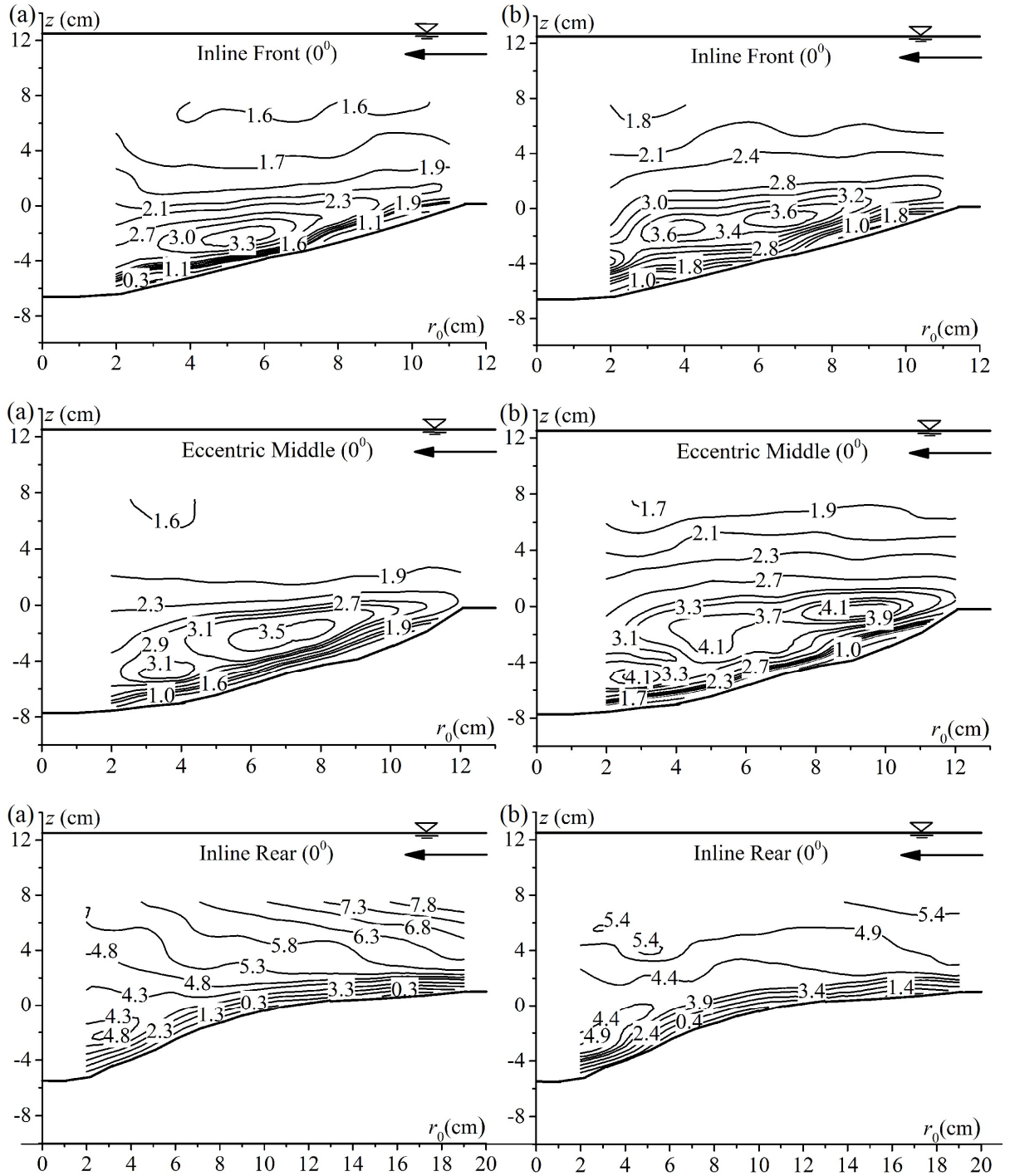


Fig. 3.28. Contours of (a) tangential (u^+) (b) radial (v^+) turbulent intensities in cm/s for inline-front, eccentric-middle and inline-rear circular piers at r - z plane for $\theta = 0^\circ$.

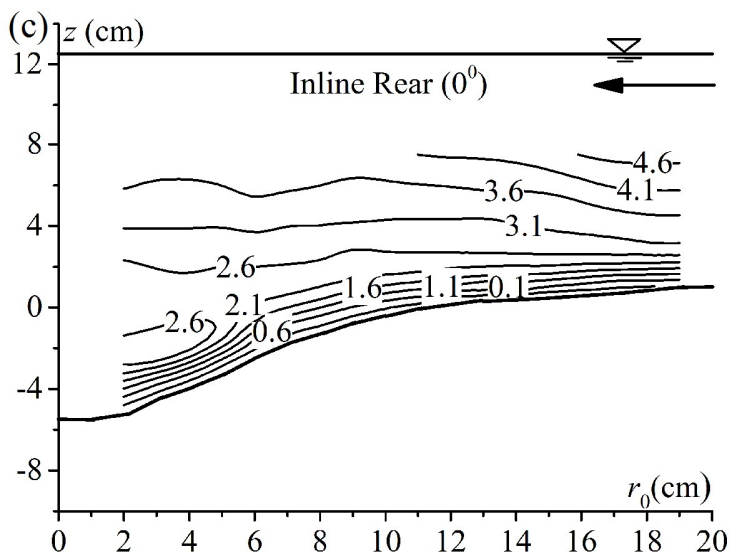
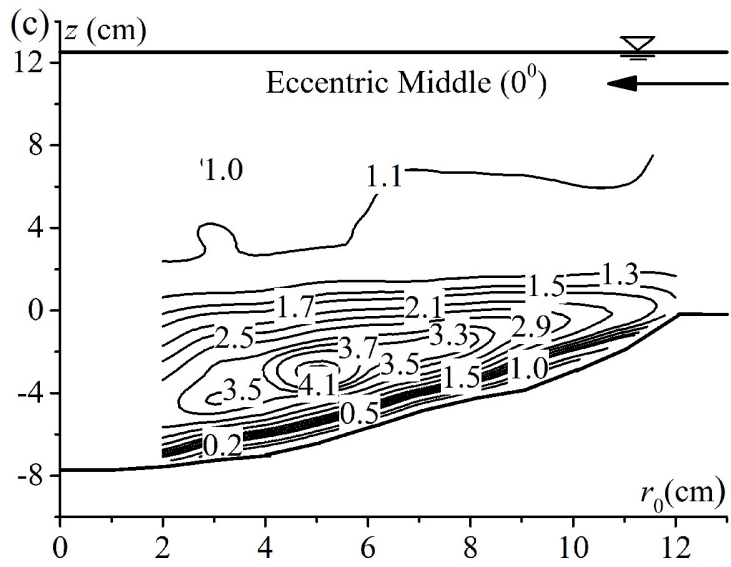
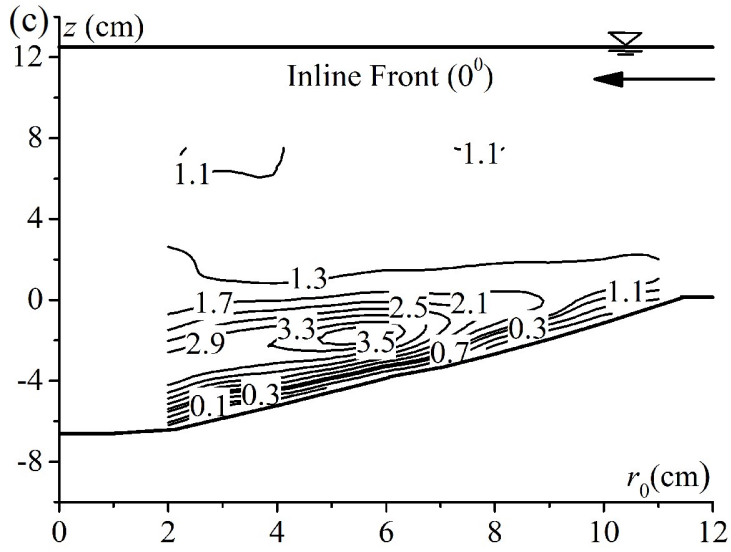


Fig. 3.29. Contours of vertical turbulent intensity (w^+) in cm/s for inline-front, eccentric-middle and inline-rear circular piers at r - z plane for $\theta = 0^\circ$.

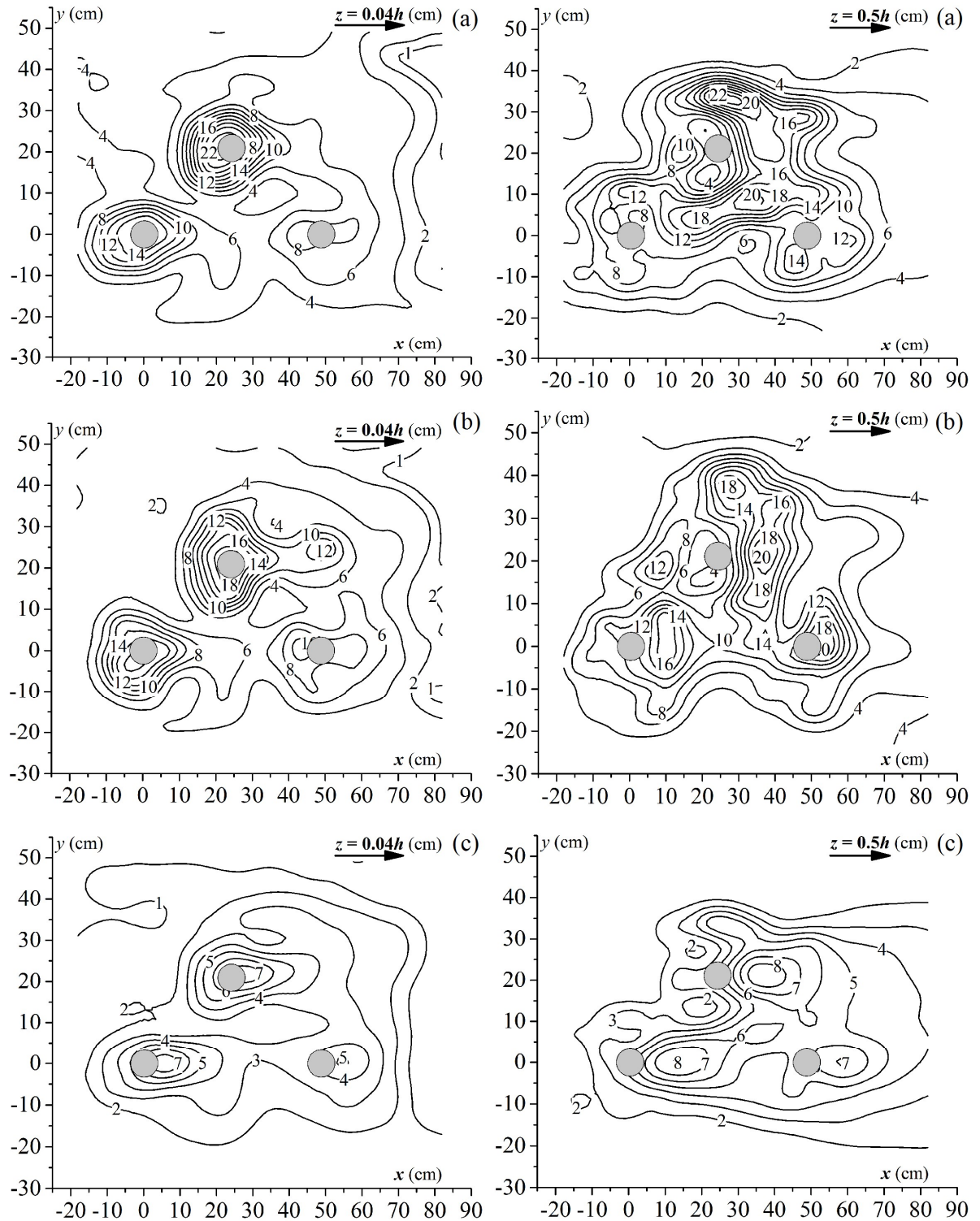


Fig. 3.30. Contours of (a) tangential (u^+), (b) radial (v^+), and (c) vertical (w^+) turbulent intensities in cm/s for inline-front-rear and eccentric-middle piers at x - y planes for $z=0.04h$ and $z=0.5h$.

From Fig. 3.30, maximum u^+ , v^+ and w^+ are observed just near upstream zone of inline-front, eccentric-middle and inline-rear circular piers having magnitudes of 22, 18, and 7 cm/s, respectively. At the two horizontal planes $z=0.04h$, and $z=0.5h$ for the three circular piers overall value of longitudinal turbulence intensity u^+ is noticed almost higher at all

corresponding locations around the circular piers, than the transverse turbulence intensity v^+ and vertical turbulence intensity w^+ .

The distribution of turbulent kinetic energy (k) at an azimuthal plane 0° and at two horizontal planes $z=0.04h$ and $z=0.5h$ from zero bed level ($z=0$) for equilibrium clear-water scour state around the three circular piers, are calculated and plotted in Fig. 3.31, using the equation (4).

$$k = \frac{1}{2}(u^{+2} + v^{+2} + w^{+2}) \quad (3.4)$$

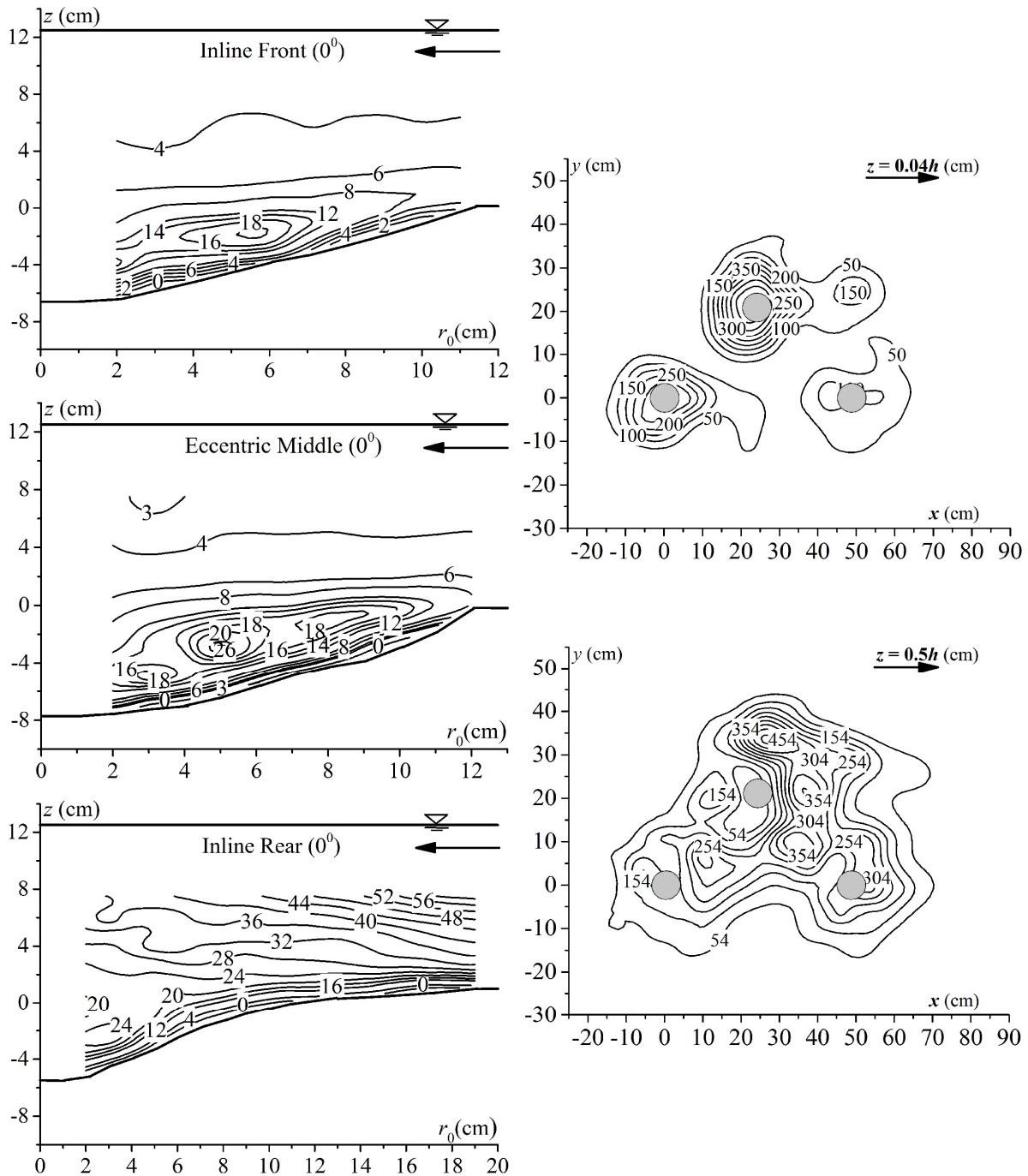


Fig. 3.31. Contours of turbulent kinetic energy (k) in cm^2/s^2 for inline-front, eccentric-middle and inline-rear circular piers at r - z plane for $\theta = 0^\circ$ and at x - y planes for $z = 0.04h$ and $z = 0.5h$.

The profiles of k are almost alike with the profiles of turbulence intensities.

At $\theta=0^\circ$, the maximum k for the eccentric-middle and inline-rear circular piers are 1.26 and 2.26 times higher than maximum k for the inline-front circular pier, respectively, as u^+ and v^+ for eccentric-middle and inline-rear circular piers are higher than u^+ and v^+ for the inline-front circular pier. The maximum turbulent kinetic energy for eccentric-middle and inline-rear circular piers are higher than maximum k for the inline-front circular pier at corresponding azimuthal planes (all are not shown).

From the Fig. 3.31, maximum turbulence kinetic energy k , at $z=0.04h$ just near the bed was found more around the eccentric-middle circular pier, then inline-front circular pier and inline-rear circular pier in the order of magnitude, respectively. Similarly, at $z=0.5h$, maximum k was found around the eccentric-middle circular pier, then inline-front circular pier and inline-rear circular pier in the order of magnitude, respectively. Hence, at eccentric-middle circular pier, it is clear that strongest vortices will form and circulation will occur. For the formation and shedding of shed vortices with very powerful rollers, higher magnitude core of k is found at wake zone of eccentric-middle circular pier, whereas upstream region of the pier values of k are lesser. At $z=0.5h$ plane, maximum k are always higher than those at $z=0.04h$. The distributed nature of turbulence kinetic energy is similar to the high-value cores of turbulent intensities, found within the region of the scour holes.

3.8 Conclusions

Here, the three circular piers of diameter 7cm were arranged in inline-eccentric-inline staggered manner. Two inline-front and inline-rear circular piers were placed at upstream frontal and downstream tandem locations. The third one eccentric-middle circular pier was placed eccentrically in between these two inline tandem piers.

The eccentricity was kept equal to $3b$ and the longitudinal gap between the inline-front circular pier and inline-rear circular pier and eccentric-middle circular pier were double and half of the lengths of the scour affected zone of the single circular pier experiment, respectively. At equilibrium clear-water condition nine experiments were conducted, for determining scouring geometry by varying such staggered arrangement. Further up, also the flow nature consequently the hydrodynamic effect of an inline-eccentric-inline arrangement of three circular piers was investigated from the flow fields of instantaneous velocities and turbulence fields measured by ADV only for the test no. 3. The contours of scour hole, time mean velocities, vector plots, turbulence intensities, turbulence kinetic energy are well explained. The major conclusions drawn are addressed below.

The interferences of horseshoe vortices and wake vortices between eccentric-middle and inline-rear circular piers along with the horseshoe vortices and wake vortices between inline-front and eccentric-middle circular piers play an imperative role in establishment of greater scour depth near middle pier. The scour depth around inline-rear circular pier is found minimum and the scour depth around eccentric-middle circular pier is found maximum among the three circular piers. Maximum equilibrium scour depth gauged at inline-front circular pier, eccentric-middle circular pier and inline-rear circular pier are about 40, 61 and 15 times larger than maximum equilibrium scour depth for single circular pier experiment. As

the intermediate longitudinal spacing in between the three circular piers increases, these vortices around the piers become independent and they are not influenced by the horseshoe and wake vortex of another pier, thus, scouring depth decrease around the piers and dunes are seen formed between piers. Dunes are formed in between inline-front and inline-rear circular piers when the longitudinal gap in-between inline-front and eccentric-middle circular pier (l) is increased after a certain limit. At all the three piers inline-front, eccentric-middle and inline-rear circular piers, the scour depth increases with subsequent increase in the longitudinal pier spacing in-between inline front and eccentric-middle circular pier (l) from $(2/8) l_{ss}$ to $(6/8) l_{ss}$. Around all the three circular (inline-eccentric-inline) piers, the scour depth is maximum when the longitudinal gap in-between inline front and eccentric-middle circular pier (l) is $(6/8) l_{ss}$. Also the scour depth, around all the three circular piers (inline-eccentric-inline), decreases with subsequent increase in intermediate longitudinal pier spacing (l) from $(6/8) l_{ss}$ to $(10/8) l_{ss}$. Dunes are formed in between inline-front and inline-rear piers when the longitudinal gap in-between inline front and eccentric-middle circular pier (l) is increased after a certain limit. On the eccentric-middle circular pier side formation of dune is more which is away from the line of symmetry. The angle of diversion representing the sediment shifting is seen more on eccentric-middle circular pier side.

The longitudinal velocity u increases in-between the three piers, inline-front, eccentric-middle and inline-rear circular piers. This longitudinal velocity increases in the downstream of the three circular piers near the bed. At 0° , for eccentric-middle circular pier and inline-rear circular pier, maximum values of longitudinal velocity are 1.33 and 2.44 times of the value of u at 0° for inline-front circular pier. As azimuthal angle θ increases, u increases and it turns finite.

At azimuth plane 0° , 45° , 90° , -45° and -90° the magnitude of radial velocity for the eccentric-middle circular pier is almost always higher than the magnitude of v for the inline-front and the inline-rear circular pier (away from the region near the base of the piers) at corresponding angles. Within the scour holes near pier bases, the radial velocity v changes its direction on both side of zero contour line ($v=0$).

At 0° azimuth plane, maximum vertical velocity at the upstream region of the eccentric-middle circular pier is 1.16 times the maximum w at the inline-front circular pier and similarly at the upstream region of eccentric-middle circular pier the maximum w is 1.42 times the maximum w at inline-rear circular pier. This confirms the clear existence of co-shedding regime formed within the three circular piers at downstream region of inline-front circular pier and eccentric-middle circular pier.

The velocity vector plots clear the presence of horseshoe vortex characteristics at upstream region of the three circular piers and wake vortex at downstream region of the three circular piers. Here, the size of the vortex core for the eccentric-middle circular pier is observed larger than the inline-front and inline-rear circular piers. The flow velocity characteristics are described more accurately in the flow zone for $z=0.5h$ and $z=0.04h$ horizontal planes. Here, it is clearly observed, from the velocity vector profiles, that the wake zone length is larger for the inline-front circular pier than the other two eccentric-middle and inline-rear circular piers. The wake zone length is larger for eccentric-middle circular pier than inline-rear circular pier. Wake zone length is larger at $z=0.5h$ than $z=0.04h$ horizontal plane, observed from the figures. These vortices take a bigger role in development of scour

holes around the three circular piers and large around eccentric-middle circular pier than other two circular piers.

The vortex circulation Ω decreases as θ increases (clock wise and anticlockwise) and also increases for a corresponding increase in scour depth. The calculated magnitude of Ω at 0° , 45° , 90° , -45° and -90° around eccentric-middle circular pier are all the time greater than Ω magnitude at corresponding azimuthal angles around inline-front circular pier and inline-rear circular pier. Strongest vortices and circulation are found at eccentric-middle circular pier. For inline-front circular pier and eccentric-middle circular pier and inline-rear circular pier, at -45° Ω is always found greater than Ω at 45° azimuth plane for corresponding pier locations, because of the existence of stronger pressure gradient. Whereas, Ω for eccentric-middle circular pier at -90° is less than Ω at 90° as the presence of co-shedding regime that develops near wake region of inline-front circular pier.

The radial, tangential and vertical turbulence intensities and turbulent kinetic energy are detected above and within the scour holes. The radial, tangential and vertical turbulence intensity and turbulent kinetic energy magnitudes above the scour holes were found greater than their maximum magnitudes within scour holes. For eccentric-middle and inline-rear circular piers, radial (v^+), tangential (u^+) and vertical (w^+) turbulence intensity magnitudes are larger than corresponding maximum magnitudes at the inline-front circular pier. Their maximum magnitudes at inline-rear circular pier are also greater than corresponding values at the inline-front and eccentric-middle circular piers. For the three piers, within the holes, core of larger k is observed. At eccentric-middle circular pier, k was found greater than k for inline-front and inline-rear circular piers.

Here all the flow patterns are well described which are uniquely related to three identical circular piers with inline-eccentric-inline arrangement that differs from previous single circular pier or two circular piers (eccentric/tandem/side-by-side) experimental researches. Hence, for better prediction of maximum scour depths at piers, the influence of flow characteristics on maximum scour depth can be converted into the semi empirical equations.

The experimental outcomes from this study may be applied as valuable records of data not only to help the further studies, related to turbulence structure around multi pier arrangement, but also to check and verify the composite turbulence fields computed from numerical models.

The inline-eccentric-inline (two inline and one eccentrically arranged middle pier) arranged three circular piers can cause sand particles to shift along flume wall and force to move downstream. The dune formation is identified maximum on eccentric-middle circular pier side. Hence, the sand shifting diversion angle is also more on eccentric-middle pier side. The sand particles are shifted from the region of the inline-eccentric-inline circular piers arrangement and deposited further downstream angling towards eccentric-middle circular pier side and further up towards the sidewall in the same direction. In between the three piers (inline-eccentric-inline arrangement), horseshoe vortices increases scour holes size of eccentric-middle circular pier while transporting sand particles far away from the symmetry line.

3.9 Nomenclature

a_s	planer surface area of equilibrium scour hole (cm ²)
b	pier width (cm)
d_{se}	maximum equilibrium scour depth for circular eccentric pier (cm)
d_{sf}	maximum equilibrium scour depth for circular front pier (cm)
d_{sr}	maximum equilibrium scour depth for circular rear pier (cm)
d_{16}	16% finer sand diameter (mm)
d_{50}	median diameter of sand (mm)
d_{84}	84% finer sand diameter (mm)
d_{90}	90% finer sand diameter (mm)
e	transversal gap between the centres of inline piers and eccentric pier (cm), $3b$
F	Froude number of flow, U/\sqrt{gh}
g	acceleration due to gravity
h	approaching flow depth (cm)
i, k	direction indices along the r and z axes, respectively
k	turbulent kinetic energy, $k = \frac{1}{2}(u'^2 + v'^2 + w'^2)$ (cm ² /s ²)
l	spacing along the flow between the centres of front and eccentric piers (cm)
$2l$	spacing along the flow between the centres of front and rear piers (cm)
l_s	maximum equilibrium scour length for three circular -pier combination (cm)
l_{ss}	maximum equilibrium scour length for single circular pier (cm)
L	maximum equilibrium length of sand transportation for three pier combination (cm)
r	radial distance (cm)
r_0	$r - 0.35b$ (cm)
R	hydraulic radius (cm)
Re	flow Reynolds number, UR/ν
R_p	pier Reynolds number
s	relative density of sand, ρ_s/ρ
u	time averaged tangential velocity in r or x -direction (cm/s)
u'	fluctuations of u (cm/s)
u^+	tangential turbulent intensity, $\sqrt{u'u'}$ (cm/s)
U	depth averaged approaching flow velocity (cm/s)
U_c	critical velocity (cm/s)
v	time averaged radial velocity in y or θ direction (cm/s)
v'	fluctuations of v (cm/s)
v^+	radial turbulent intensity, $\sqrt{v'v'}$ (cm/s)
v_s	volume of equilibrium scour hole (cm ³)
V	time averaged absolute velocity, $\sqrt{u^2 + v^2 + w^2}$ (cm/s)
\vec{V}	time averaged velocity vectors, $\sqrt{v^2 + w^2}$ (cm/s)
w	time averaged vertical velocity in z - direction (cm/s)

w' fluctuations of w (cm/s)
 w^+ vertical turbulent intensity, $w^+ = \sqrt{w'w'}$ (cm/s)
 x, y, z coordinate axes
 z vertical distance

Greek Symbol

ρ mass density of water (kg/m³)
 ρ_s mass density of sand (kg/m³)
 σ_g geometric standard deviation, $\sqrt{d_{84}/d_{16}}$
 ζ vorticity, $\partial v/\partial z - \partial w/\partial r$ (s⁻¹)
 Ω circulation (m²/s)
 θ azimuth angle

Subscript

16, 50, 84, 90 16 %, 50 %, 84 % and 90 % finer respectively
 sf, se, sr inline front, eccentric and inline rear pier respectively

3.10 References

- Ahmed, F.; Rajaratnam, N.: Flow around bridge piers. *J. Hydraul. Eng.* 124(3), 288-300 (1998)
- Akilli, H.; Akar, A.; Karakus, C.: Flow characteristics of circular cylinders arranged side-by-side in shallow water. *Flow Meas. Instrum.* 15(4), 187-189 (2004)
- Ashtiani, A.B.; Beheshti, A.A.: Experimental investigation of clear-water local scour at pile groups. *J. Hydraul. Eng.* 132(10), 1100-1104 (2006)
- Ashtiani, A. B.; Baratian-Ghorghi, Z.; Beheshti, A.A.: Experimental Investigation of Clear-Water Local Scour of Compound Piers. *J. Hydraul. Eng.* 136(6), 343–351 (2010)
- Ashtiani, A.B.; Kordkandi, A.A.: Flow field around side-by-side piers with and without a scour hole. *Eur. J. Mech. B/Fluid.* 36, 152-166 (2012)
- Ashtiani, A. B.; Kordkandi, A. A.: Flow field around single and tandem piers. *Flow Turbul. Combust.* 90(3), 471-490 (2013)
- Blanckaert, K.; Lemmin, U.: Means of noise reduction in acoustic turbulence measurements, *J. Hydraul Res.* 44(1), 3–17 (2006)
- Breusers, H.N.C.; Raudkivi, A.J.: Scouring, IAHR Hydraulic Structures Design Manual, Vol. 2, A. A. Balkema Publ., Rotterdam, The Netherlands. (1991)
- Breusers, H.N.C.; Nicollet, G.; Shen, H.W.: Local Scour Around Cylindrical Piers. *J. Hydraul. Res.* 15(3), 211-252 (1977)
- Coleman, S. E.: Clear water local scour at complex piers. *J. Hydraul. Eng.* 131(4), 330-334 (2005)

- Dargahi, B.: The turbulent flow field around a circular cylinder. *Exp. in Fluids*. 8(1–2), 1–12 (1989)
- Dargahi, B.: Controlling Mechanism of Local Scouring, *J. Hydraul. Eng.* 116(10), 1197–1214 (1990)
- Das, R.; Khwairakpam, P.; Das, S.; Mazumdar, A.: Clear-water local scour around eccentric multiple piers to shift the line of sediment deposition. *Asian J. Water Environ. Pollut.* 11(3), 47-54 (2014)
- Das, S.; Das, R.; Mazumdar, A.: Velocity profile measurement technique for scour using ADV. In: Proceedings of the 2015 International Conference on Testing and Measurement: Techniques and Applications, TMTA 2015. Taylor & Francis Group, London, pp. 249-252 (2015)
- Das, S.; Das, R.; Mazumdar, A.: Comparison of local scour characteristics around two eccentric piers of different shapes. *Arab. J. Sci. Eng.* 41(4), 1193-1213 (2016)
- Das, S.; Mazumdar, A.: Comparison of kinematics of horseshoe vortex at a flat plate and different shaped piers. *Int. J. Fluid Mech. Res.* 42(5), 418-448 (2015a)
- Das, S.; Mazumdar, A.: Turbulence flow field around two eccentric circular piers in scour hole. *Int. J. River Basin Manag.* 13(3), 343-361 (2015b)
- Das, S., Mazumdar, A.: Evaluation of Hydrodynamic Consequences for Horseshoe Vortex System developing around two eccentrically arranged Identical Piers of Diverse Shapes. *KSCE J. Civil Eng.* 22(7), 2300-2314 (2018)
- Das, S.; Das, R.; Mazumdar, A.: Circulation characteristics of horseshoe vortex in the scour region around circular piers. *Water Sci. and Eng.* 6(1), 59-77 (2013a)
- Das, S.; Das, R.; Mazumdar, A.: Comparison of Characteristics of Horseshoe Vortex at Circular and Square Piers. *Res. J. Appl. Sci. Eng. Tech.* 5(17), 4373-4387 (2013b)
- Das, S.; Midya, R.; Das R.; Mazumdar, A.: A Study of Wake Vortex in the Scour Region around a Circular Pier. *Int. J. Fluid Mech. Res.* 40(1), 42-59 (2013c)
- Das, S.; Das, R.; Mazumdar, A.: Variations of clear water scour geometry at piers of different effective widths. *Turkish J. Eng. Environ. Sci.* 38(1), 97-111 (2014a)
- Das, S.; Ghosh, S.; Mazumdar, A.: Kinematics of horseshoe vortex in a scour hole around two eccentric triangular piers. *Int. J. Fluid Mech. Res.* 41(4), 296-317 (2014b)
- Das, S.; Ghosh, R.; Das, R.; Mazumdar, A.: Clear Water Scour Geometry around Circular Piers. *Ecol. Environ. Conserv.* 20(2), 479-492 (2014c).
- Dey, S.: Local Scour at Piers, Part 1: A Review of Development of Research, *Int. J. Sediment Res.* 12(2), 23–44 (1997).
- Dey, S.; Bose, S.K.; Sastry, G.L.N.: Clear water scour at circular piers: a model. *J. Hydraul. Eng.* 121(12), 869-876 (1995)
- Dey, S.; Raikar, R.V.: Characteristics of horseshoe vortex in developing scour holes at piers. *J. Hydraul. Eng.* 133(4), 399-413(2007)
- Ettema, R.; Kirkil, G.; Muste, M.: Similitude of large scale turbulence in experiments on local scour at cylinders. *J. Hydraul. Eng.* 132(1), 33–40 (2006)

- Elliott, K.R.; Baker, C.J.: Effect of pier spacing on scour around bridge piers. *J. Hydraul. Res.* 111(7), 1105-1109 (1985)
- Graf, W.H.: *Fluvial Hydraulics, Flow and transport processes in channels of simple geometry.* John Wiley and Sons, Great Britain. (2003)
- Graf, W.H.; Istiarto, I.: Flow pattern in the scour hole around a cylinder. *J. Hydraul. Res.* 40 (1), 13-20 (2002)
- Graf, W.H.; Yulistiyanto, B.: Experiments on flow around a cylinder: the velocity and vorticity fields. *J. Hydraul. Res.* 36(4), 637-653 (1998)
- Hoffmans, G.J.C.M.; Verheij, H.C.: *Scour Manual.* Balkema, Rotterdam, The Netherlands. (1997)
- Istiarto, I.; Graf, W.H.: Experiments on flow around a cylinder in a scoured channel bed. *Int. J. Sediment Res.* 16(4), 431-444 (2001)
- Khwaitrakpam, P.; Ray, S.S.; Das, S.; Das, R.; Mazumdar, A.: Scour hole characteristics around a vertical pier under clear water scour conditions. *ARPN J. Eng. Appl. Sci.* 7(6), 649-654 (2012)
- Kirkil, G.; Constantinescu, S.G.; and Ettema, R.: Detached eddy simulation investigation of turbulence at a circular pier with scour hole. *J. Hydraul. Eng.* 135(11), 888–901 (2009)
- Kirkil, G.; Constantineous, S.G.; Ettema, R.: Detached eddy simulation investigation of turbulence at a circular pier with scour hole. *J. Hydraul. Eng.* 135(11), 888-901 (2009)
- Mahjoub, S.N.; Mhiri, H.; Bournot, P.H.; LePalec, G.: Experimental and numerical modeling of the three-dimensional incompressible flow behavior in the near wake of circular cylinders. *J. Wind Eng. Ind. Aerodyn.* 96(5), 471-502 (2008)
- Melville, B.W.: Local scour at bridge sites. *Ph.D. Thesis.* School of Eng., Univ. Auckland, New Zealand. (1975)
- Melville, B.W.: Local Scour at Bridge Abutments, *J. Hydraul. Eng.* 118(4), 615–631. (1992)
- Melville, B.W.; Chiew, Y.M.: Time scale for local scour at bridge piers, *J. Hydraul. Eng.* 125(1), 59-65 (1999)
- Melville, B.W.; Coleman, S.E.: Bridge scour, *Water Res. Pub.* Fort Collins, Colorado, USA. (2000)
- Melville, B.W.; Raudkivi, A.J.: Flow characteristics in local scour at bridge piers. *J. Hydraul. Res.* 15(4), 373-380 (1977)
- Muzzammil, M.; Gangadhariah, T.: The mean characteristics of horseshoe vortex at a cylindrical pier. *J. Hydraul. Res.* 41(3), 285–297 (2003)
- Michael, S.A.; Mohamed, G.M.; Mohamed, S.B.A.M.: Wake vortex scour at bridge piers. *J. Hydraul. Eng.* 117(7), 891–904 (1991).
- Raudkivi, A.J.: *Loose Boundary Hydraulics.* A. A. Balkama, Rotterdam (1998)
- Richardson, E.V.; Davis, S.R.: Evaluating scour at bridges. *HEC18 FHWA NHI-001.* Federal Highway Administration, US department of transportation, Washington, USA (2001)

- Roulund, A.; Sumer, B.M.; Fredsøe, J.; Michelsen, J.: Numerical and experimental investigation of flow and scour around a circular pile. *J. Fluid Mech.* 534, 351–401 (2005)
- Sheppard, D.M.; Zhao, G.; Copps, T.H.: Local scour near multiple pile piers in steady currents. In: Proceedings of ASCE, International Conference on Water Resources Engineering, San Antonio, USA (1995)
- Song, T.; Chiew, Y.M.: Turbulence measurement in nonuniform open-channel flow using Acoustic Doppler Velocimeter (ADV). *J. Eng. Mech.* 127(3), 219-232 (2001)
- Sumner, D.; Wong, S.S.T.; Price, S.J.; Paidoussis, M.P.: Fluid behavior of side-by-side circular cylinders in steady cross-flow. *J. Fluid. Struct.* 13(3), 309-338 (1999)
- Yilmaz, M.; Yanmaz, A.M.; Koken, M.: Clear-water scour evolution at dual bridge piers. *Canadian J. Civil Eng.* 44(4), 298-307 (2017)
- Zdravkovich, M.M.: The effects of interference between circular cylinders in cross flow. *J. Fluid. Struct.* 1(2), 239-261 (1987)

4. FLOW AROUND THREE INLINE ECCENTRIC SQUARE PIERS

4.1 Introduction

The hydrodynamic flow patterns after attaining equilibrium scour around three identical shaped square piers having base width of 7 cm were analysed experimentally. The two piers - front and rear ones were positioned along the flow and the third one was set eccentrically in mid region of two inline piers. The experimental research was carried out at clear water condition upto equilibrium scour state. Throughout the experiment, depth mean approach flow velocity and approaching flow depth were fixed at 24.7 cm/sec and 12.5 cm, respectively on a uniform sand bed having median diameter of 0.825 mm. The formation of scour and thereby the hydrodynamic outcomes are explained in this chapter. Five different clear water equilibrium scour experiments were carried out by varying the longitudinal spacing between the inline piers. These experiments were carried out to find out the location and nature of scour evolved due mutual interference of one pier on another. Another main aim was to study the flow physics between the piers after the formation of equilibrium scour hole by varying the longitudinal spacing between the two inline piers.

The eccentricity was kept constant and set equal to $3b$ where b is the base width of each pier. The considered spacing along the flow between the square front and square eccentric and between the square eccentric and square rear piers were $(2/8)l_{ss}$, $(3/8)l_{ss}$, $(4/8)l_{ss}$, $(5/8)l_{ss}$ and $(6/8)l_{ss}$ where l_{ss} is the maximum equilibrium length of sediment transport (sum of maximum equilibrium scour length and dune length) for a single pier experiment. For each experiment, maximum equilibrium scour depth, length, width, surface area and volume were observed and determined.

In order to have a comparative study, this chapter also provides the experimental results of the hydrodynamic turbulent flow pattern around the three identical square piers arranged inline-eccentrically with constant longitudinal spacing equal to half of the l_{ss} and constant eccentricity $3b$. The detailed three dimensional velocities were captured instantaneously by using an ADV Vectrino+ (made by Nortek AS in USA) at five different vertical azimuthal planes (-90° , -45° , 0° , 45° and 90°) positioning around the three square piers and also at two horizontal planes having 4% and 50% of approaching flow-depth above bed level ($h=0$). The non-dimensional contour profiles and distribution of non-dimensional velocity components, turbulence kinetic energy and intensities have been computed and analyzed at the vertical r - z planes and horizontal r - y planes around three square piers. The velocity vectors plotting and dimensionless time mean absolute velocity acquired from velocity profile show detailed hydrodynamic flow characteristics. Vorticity and circulation generated at the upstream zone near the three square piers are elaborately presented.

Three square piers combined arrangement and interferences between each other, play an essential role in formation and enhancement of larger scour depth near square eccentric pier and the sand particles transport is more towards the experimental flume wall. During the experimentation, pressure drag becomes much higher than skin friction drag, because of the presence of bluff body. Vortices strength was found maximum for square eccentric pier while minimum for square rear pier.

4.2 Brief Review of Relevant Works

The hydrodynamic flow characteristics around a group of piers are a big problem. For hydraulic engineers it is an important matter to find the extent of scour near multiple piers combination as well as to understand the flow hydraulics. Nowadays pier group arrangements are more accepted in bridge designing for its geotechnical and economic benefits. The mechanism of scour and flow characteristics for multiple piers arrangement is too complex and it is also very complicated to predict or find out scour depth from the single pier experiment.

Over the years, a large number of investigation on single pier (of various shapes) arrangement have been studied by many researchers using laboratory flume based experiments and incorporating the use of non-dimensional equations inferencing in some semi-empirical equations for simulating scour depth. A long-standing concern is the tendency of some of these equations to over predict the maximum scour depth for field or even for laboratory conditions. A lack of understanding of the flow structure around the bridge piers and their interaction with the bed sediment seems to be at least partly responsible for this problem. Therefore, many laboratory flume based experiments were investigated by numerous researchers for accumulating more information on flow behaviour and scour mechanism and to compute scour depth with more precision. Many of the researchers stressed on velocity and subsequent pattern of the turbulent flow field at differently shaped piers but there are a few researches conducted experiments taking square piers [Dey and Raikar (2007), Raikar and Dey (2008) and Das and Mazumdar (2015a)].

Dey and Raikar (2007) stated the outcomes of an experimental research on turbulent horseshoe vortex flow within the developing intermediate stages (having depths of 0.25, 0.5 and 0.75 times the equilibrium scour depth) and equilibrium scour holes at cylindrical and square piers captured by an ADV. The vector plots and contours of time averaged velocities, turbulence intensities and Reynolds stresses at azimuth angle 0° , 45° and 90° were presented. The change of the characteristics of horseshoe vortex flow associated with a downflow from intermediate stages to equilibrium condition of scour hole was revealed through the vector plots of the flow field at different azimuthal planes. The flow characteristics of horseshoe vortex were discussed from the point of view of the similarity with the velocity and turbulence characteristics scale. The flow and turbulence intensities in the horseshoe vortex flow in a developing scour hole were found almost similar.

Raikar and Dey (2008) made an experimental investigation on the characteristics of the development of turbulent horseshoe vortex flow in an evolving intermediate stages (having depths of 0.25, 0.5 and 0.75 times the equilibrium scour depth) and equilibrium scour hole around square cylinder gauged by ADV. At azimuthal angles 0° , 45° and 90° , the vector plots and contours of time averaged velocities, turbulence intensities and Reynolds stresses were presented. The flow characteristics of the horseshoe vortex were studied from the point of view of similarity with the velocity and turbulence characteristic scales. The flow and the turbulence intensities in horseshoe vortex flow in a developing scour hole were observed reasonably similar.

For better understanding of the hydrodynamic flow fields at clear water equilibrium condition, Das and Mazumdar (2015a) conducted experiments on single flat plate, circular pier, square pier, and equilateral triangular pier (side facing flow) for determining more accurate scour depth. The vector plots and contours of time averaged velocities, turbulence intensities and turbulence kinetic energy at azimuthal angles 0° , 45° and 90° were presented. Using forward difference technique of computational hydrodynamics and Stokes theorem the vorticity and circulation of the horseshoe vortex were determined. The horseshoe vortex flow and turbulence characteristics were discussed from the point of similarity with velocity and turbulence intensity characteristic scales.

In view of geotechnical and economic reasons, design of a new bridge sometimes encourage to a multi pier arrangement, in which the direct use of the outcomes are taken only from single pier arrangement that may be problematical. A few researches were conducted on multi pier arrangement to estimate the scour depth and effect of pier spacing on scour depth. For a pier in a multi pier arrangement, combined effects are notable with those parameters which influence scour around single pier arrangement. Most of the multi pier experiments were restricted to two circular pier arrangements, positioning either eccentric, inline or side by side that focused on the prediction of flow field, turbulent field and the scour geometry [Zdravkovich (1987), Sheppard *et al.* (1995), Sumner *et al.* (1999), Akilli *et al.* (2004), Coleman (2005), Ashtiani and Beheshti (2006), Mahjoub (2008), Ashtiani and Kordkandi (2012, 2013), Das *et al.* (2014) and Das and Mazumdar (2015b)] and the consequences of longitudinal pier spacing on flow characteristics and on scour-depth [Raudkivi (1998), Graf (2003), Das *et al.* (2014, 2016) and Yilmaz *et al.* (2017)].

There are very few previous researchers which describe some detailed analysis of turbulent flow fields around two square pier arrangements at clear water equilibrium scour condition.

Three dimensional flow fields, turbulence fields for horseshoe vortex around two equilateral triangular piers [Das *et al.* (2014)], two circular piers [Das and Mazumdar (2015b)] and two square piers [Das and Mazumdar (2018)] of equal width b positioning front one inline and rear one eccentrically with constant eccentricity $3b$ under similar experimental conditions were investigated. Longitudinal gap was taken as half the maximum length transported by sediment particles at equilibrium condition for single pier experiment. Here, the three dimensional flow fields and turbulence field interactions were observed and measured by ADV. The contours and distributions of the time averaged velocity components, turbulence intensities and turbulence kinetic energy at different vertical planes were presented. The researchers addressed how the horseshoe vortex flow and corresponding turbulence characteristics change between the two piers and how the two piers influence the flow structures and its intensity. Velocity vectors were obtained from the time averaged velocity fields to illustrate further flow features. The two square piers influence the structure of flow and its flow intensity. The plots of time averaged absolute velocity components presented a good perceptive of vortex characteristics at pier upstream. Vorticity determination and circulation estimation were conducted using the technique of computational fluid dynamics and Stokes theorem. For eccentric rear pier, magnitude of circulation was found always more than the magnitude of circulation for inline front pier. It was detected that the streamlines at the frontal side of eccentric rear pier diverged with a

higher tangential velocity than that of the inline pier. A partial sheltering effect occurred in between the piers. For the eccentric rear pier, the magnitude of radial velocity was almost always higher than inline front pier. The co-shedding regime was developed at the downstream of inline pier. The horseshoe vortex core size for eccentric rear pier was found always bigger than the inline front pier. Also for eccentric rear pier, magnitude of circulation was always found higher compared to inline front pier at different azimuthal angles in vertical planes. The end results of all experiments were compared with the result of a single pier experiments for corresponding pier shape at same experimental conditions.

Further laboratory flume experiments were executed by Das *et al.* (2016) for investigating the pattern of scour formation around two circular, square and triangular tandem piers at constant eccentricity. It was observed that the pattern of scour varies by changing longitudinal spacing (0.25, 0.375, 0.5, 0.625 and 0.75 times the scour affected lengths for a single pier experiment) between the piers. The inline eccentric pier arrangement and the interference between the horseshoe vortex of the rear pier and wake vortex of the front pier may also play an important role in the creation and formation of the greater scour depth at the eccentric rear piers. The scour angle of diversion and deposition of the sand was observed more on the eccentric pier side towards the wall. Biggest scour hole was found for square pier experiment compared to the equilateral triangular pier and the circular pier experiment experiments.

In previous chapter, the hydrodynamic flow characteristics were studied around identical three circular piers group arranged inline and eccentrically in a staggered manner at clear water equilibrium scour condition. The three dimensional velocities were recorded around the piers at five vertical azimuthal planes and two horizontal planes. The three circular piers combined arrangement and the interferences between them result in the improvement of larger scour depth just near the circular eccentric pier and more transportation of sand along the left (eccentric pier) side wall due to formations of such flow and characteristics of such horseshoe vortices. For inline rear and eccentric middle piers, strengths of vortices are found lowest and greatest, respectively as compared with inline front pier.

4.3 Scope of the Present Work

On basis of the former studies on scouring, the current study has been inspired on the topic of dealing with three identical square shaped piers and how the scouring differs with it. No experimental investigation was conducted by previous researchers to find out the vortex flow pattern and characteristics around three square piers placing two of them inline along the flow and the third one eccentrically in mid of them. Here the experiments were conducted at similar experimental conditions as mentioned in previous chapter only. Only circular piers were replaced by the square piers. In the present study an attempt has been made to carry out experiments with inline eccentric arrangement of pier groups varying the longitudinal spacing and to delineate the scour geometry. Here, the vital objective is to study the hydrodynamic interplay between three-dimensional turbulent velocity flow fields around the square piers. This study also addresses the change of flow patterns due to horseshoe vortices and related

variations in turbulence characteristics in the zone around the three piers. This study represents the contours and the distributions of non-dimensional time averaged non-dimensional velocity components, non-dimensional turbulence intensities, and non-dimensional turbulence kinetic energy at vertical planes and at two horizontal planes (4% and 50% of the approaching flow depth) around the three square piers. The velocity vectors and non-dimensional absolute velocity addresses more hydrodynamic flow characteristics. Beside this, the vorticity and the circulation of the horseshoe vortex around the square piers are also furnished.

4.4 General Experimental Setup and Technique

In this present study, analysis of instantaneous tangential (u), radial (v) and vertical (w) velocities were achieved with the help of ADV. Figures 4.1, 4.2 and 4.3 show detailed laboratory experimental setup. Table. 4.1 list the experimental conditions.

All the laboratory flume experiments were conducted in the Fluvial Hydraulics Laboratory of the School of Water Resources Engineering in Jadavpur University, Kolkata, West Bengal, India.

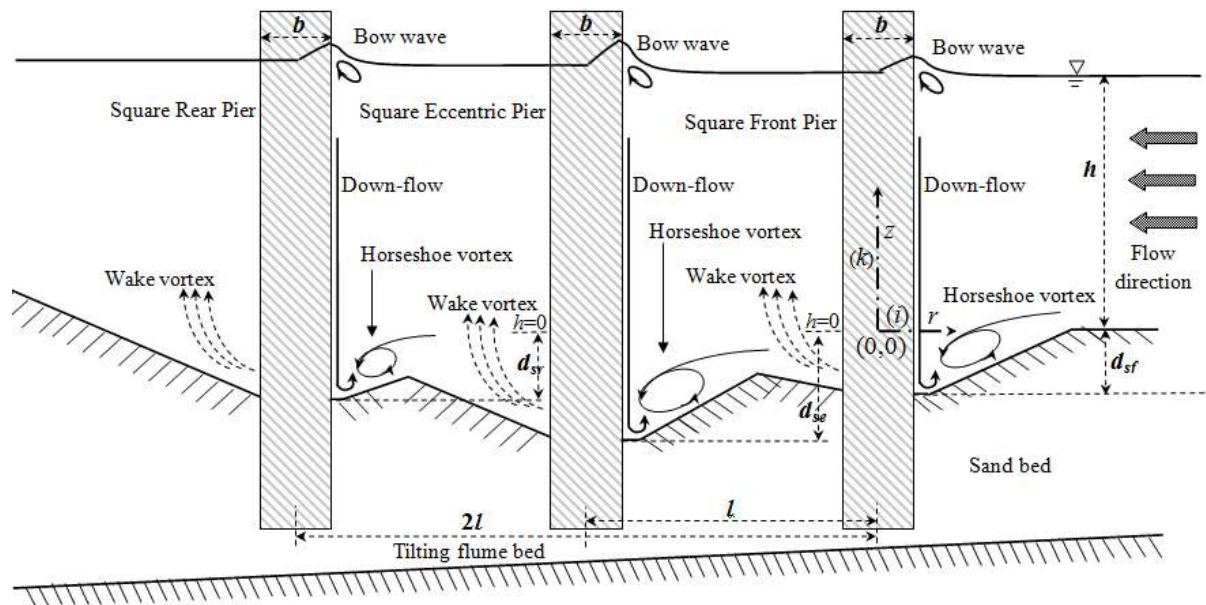


Fig. 4.1. Schematic diagram of flow pattern at three inline eccentrically arranged square piers.

The experiments were carried out in a perspex sided re-circulating rectangular flume. The flume is 11 m long, 0.81 m wide (internal) and 0.60 m deep. The effective working section of flume was located 2.90 m downstream from inlet of the flume, piled up with sand particles of fixed thickness 0.20 m and length of 3 m. Sand particle sizes (d_{16} , d_{50} , d_{84} and d_{90}) were calculated from sieve analysis using a vibrating shaker and geometric standard deviation $\sigma_g = \sqrt{d_{84}/d_{16}} = 1.8$, were used in all experiments. According to Raudkivi (1998), as $\sigma_g < 2$, therefore the sediment is uniform.

Here, three identical hollow square piers (perspex made) of 7 cm width (b) were placed centrally on the effective working section of flume as displayed in Fig. 4.1. Based on the

concept stated by Das and Mazumdar (2018), piers of 7 cm side was considered, for comparing the outcomes between present study and previous study [Das and Mazumdar (2018)]. The sidewall of flume has no impact on scouring, because width of the flume and pier ratio is higher than 6.5 [Ashtiani and Kordkandi (2012)] and size of sand particle has no impact on scoured-depth, because $b/d_{50} > 50$ [Melville and Raudkivi (1977)].

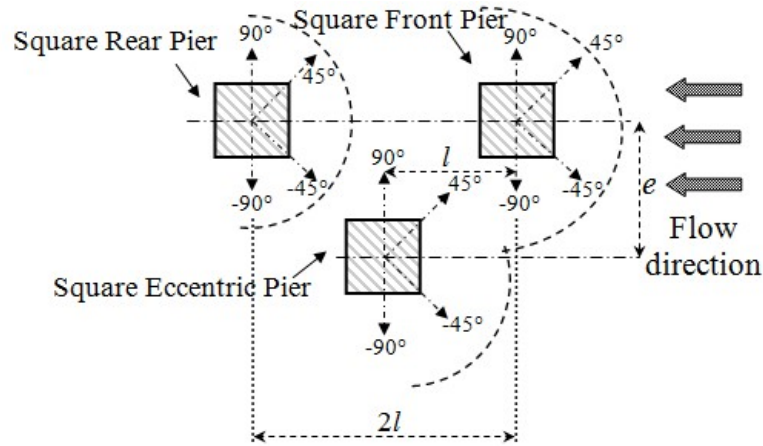


Fig. 4.2. Top view for three inline eccentrically arranged square piers.

Table 4.1. Experimental conditions for all conducted tests.

Parameter description	Magnitude
Pier width (b)	= 7 cm
Water discharge (Q)	= 25 L/s
Bed slope, S ($=\tan \lambda$)	= 1:2400
Eccentricity between front and eccentric pier, e ($=3b$)	= 21 cm
16% finer sand diameter (d_{16})	= 0.500 mm
Median diameter of sand (d_{50})	= 0.825 mm
84% finer sand diameter (d_{84})	= 1.620 mm
90% finer sand diameter (d_{90})	= 1.780 mm
Geometric standard deviation of sediment size, σ_g ($=\sqrt{d_{84}/d_{16}}$)	= 1.8
Relative density of sand material (s)	= 2.582
Approaching flow depth (h)	= 12.5 cm
Depth averaged approaching flow velocity (U)	= 24.7 cm/s
Froude number of flow F ($=U/\sqrt{gh}$)	= 0.223
Critical velocity (u_c)	= 36.2 cm/s
Angle of repose (ϕ_r)	= 36°
Average bed shear stress (τ_o)	= 0.39 Pa
Critical bed shear stress (τ_{oc})	= 0.40 Pa
Flow Reynolds number (R_e)	= 24165
Pier Reynolds number (R_p)	= 17709

Here, the transverse gap between the line joining the inline piers and square eccentric pier was kept equal to $e = 3b$ ($3 \times 7 = 21$ cm) because $b = 7$ cm is maximum allowable limit for

avoiding sidewall influences of flume having width of 81 cm. Longitudinal spacing or gap between square front pier and square eccentric pier (l) along the direction of flow was $(2/8)$, $(3/8)$, $(4/8)$, $(5/8)$ and $(6/8)^{\text{th}}$ of the maximum lengths of sediment transportation for single square pier under equilibrium scour [equal to the sum of maximum scour and maximum dune lengths at equilibrium scour = $l_{ss} = 66$ cm as investigated by Das *et al.* (2016) and Das and Mazumdar (2018)]. In the figures, longitudinal gap between square front pier and square rear pier was twice ($2l$) of the longitudinal gap between square front pier and square eccentric pier. Ashtiani and Beheshti (2006) observed that the maximum scour depth ($d_{s \text{ max}}$) rises by 20% in case of two tandem piers with the eccentricity (e) of $3b$. Eccentricity (e) and pier width (b) ratio will be seven as a limit for obtaining independent piers, as suggested by Elliott and Baker (1985). After placing the piers properly, lastly, effective working section of sand bed was piled and levelled carefully. The flow of the re-circulating system was maintained through a variable speed 7 hp centrifugal pump with maximum discharge of 25.5 L/s, rpm of 1450 and power of 7.5 kW. Water enters into the flume with a discharge of 25 L/s, which was measured with an analogue type flow meter coupled to flume inlet by adjusting both the outlet and bypass valves. A point-gauge of Vernier-type, fixed within a movable trolley to slide on the flume having ± 0.1 mm accuracy was used to measure water depth, initial bed depth and scour hole near the piers.

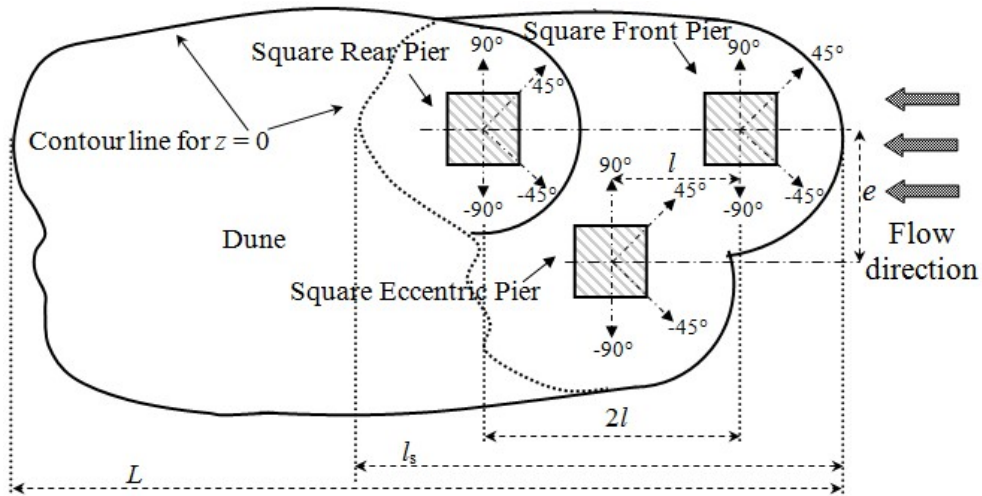


Fig. 4.3. Plan view for gauge and Vectrino measurements for three inline eccentrically arranged square piers.

Approach flow depth (h) in the flume was retained as 12.5 cm by operating flume tailgate. Bed slope (S) of sand particle was retained at 1:2400. The ratio of mean depth (h) to pier width (b) i.e. h/b is 1.786. It is greater than 0.6 which confirms uninterrupted approach depth of flow throughout all the experiments and possibly is considered to be 2-D as $h/b > 1.7$. Pier Reynolds number (R_p) is 17709. Flow Reynolds number (R_e) is 24165 and subcritical (F) Froude number is 0.223. To fulfil clear water scour condition, depth mean approach velocity of flow (U) was kept as 24.7 cm/s, that is 68.18% of threshold velocity U_c as expressed by a threshold velocity ratio (U/U_c) equal to 0.6818 [Das and Mazumdar (2015a, 2018)] was measured from 2.1 m upstream of square front pier, thus, presence of piers does not change U .

As shown in Table 4.2, total duration of experimental run was kept 72 h to 155 h. For attaining the equilibrium scour, the rate of increase in scour depth was observed after every 2 h after 68 h. The experiment was stopped when the increase in scour depth increases is less than 1 mm after 2 h [Dey and Raikar (2007) and Das and Mazumdar (2018)]. After stopping experiment, water was drained out from the flume. Thereafter, equilibrium maximum scour depths around each square pier were carefully measured with a Vernier type point gauge of ± 0.1 mm accuracy. From the gauged data, contour profiles of scoured zone around three square piers are plotted. A thorough study of the contours of equilibrium scour hole, it is clear that the dune forms more along the sidewall of square eccentric pier. It shows that the sand particles are transported from surrounding area of piers and it is deflected and settled toward square eccentric pier.

Table 4.2. Run duration for all conducted tests.

Test No.	Longitudinal spacing between inline and eccentric piers (l) (cm)	Run duration (hours)
1	$(2/8) l_{ss}$	72
2	$(3/8) l_{ss}$	75
3	$(4/8) l_{ss}$	80
4	$(5/8) l_{ss}$	95
5	$(6/8) l_{ss}$	155

Only for the test no. 3, the sand bed was allowed to dry after carefully releasing water from the flume. Then glue mixed with water, in 1:3 ratio by volume, was sprayed over the sand bed to stabilize it and also to freeze it. The scoured bed was then saturated and soaked with glue so that it becomes hard rock when left over for a time-period of 72 h. Then, same experiment was repeated again at equilibrium scour condition under same experimental condition i.e. at flow discharge 25 L/s, approach depth 12.5 cm, and mean approach velocity of flow (U) 24.7 cm/s, for facilitating 3-D velocity measurements at different azimuthal planes and horizontal planes.

4.5 Analysis of Scour Geometry

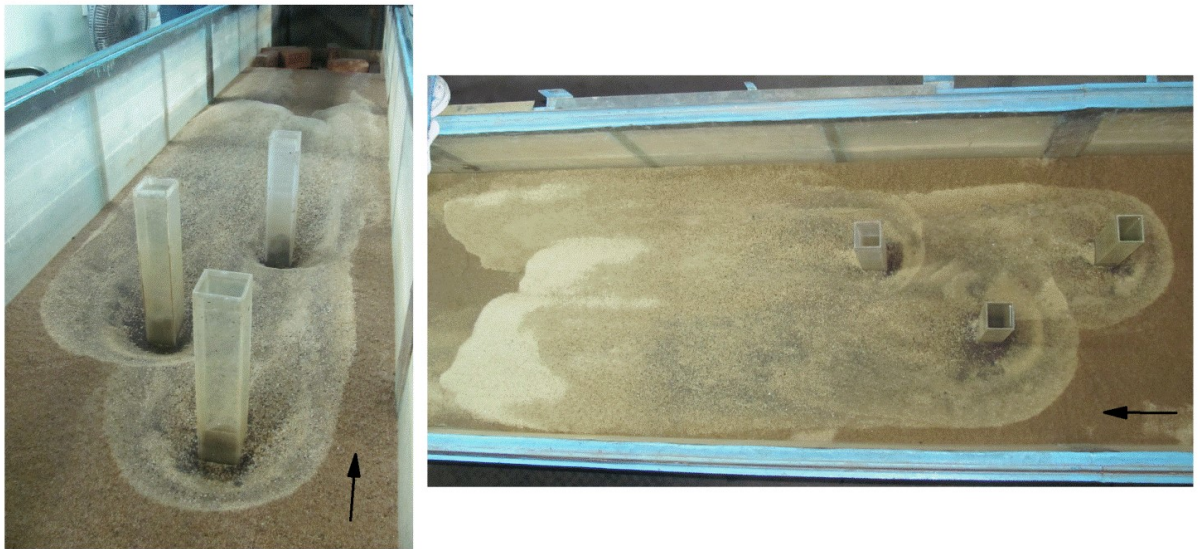
The three pier arrangement exhibit a mutual interference on scouring and on hydraulic behaviour. In the present study the scour affected zones around the piers at equilibrium state are displayed in Figs. 4.4 and 4.5. As shown in Fig. 4.6 and 4.7, from the gauged data, contour lines of the equilibrium scour holes around the square piers have been plotted with Golden software Surfer v8.06.39. For all tests, the outcomes obtained for the equilibrium scour parameters are summarized in the Table. 4.3.



Test No. 1



Test No. 2

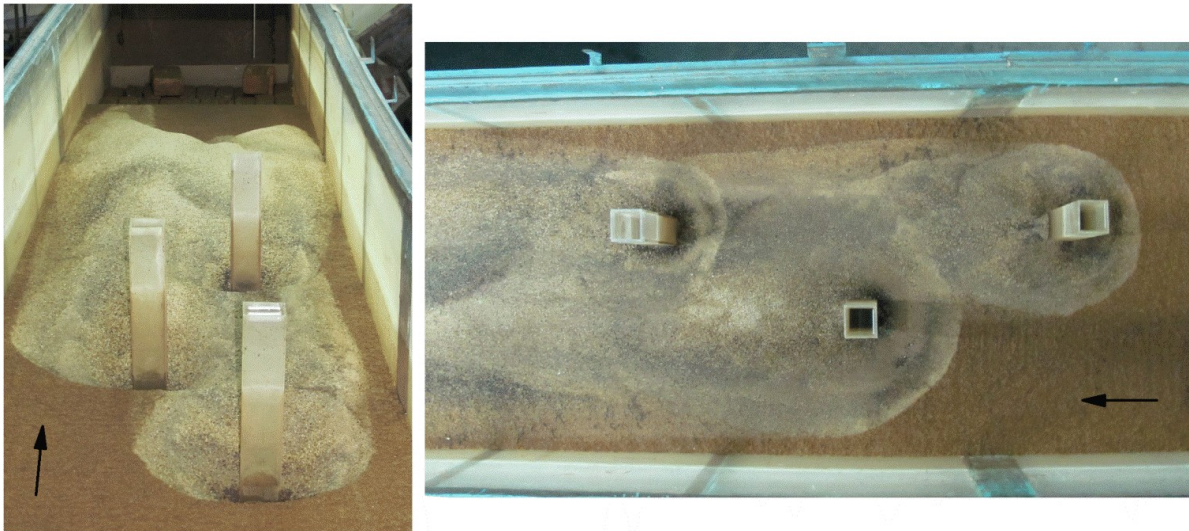


Test No. 3

Fig. 4.4. Scoured zones around three square piers for test nos. 1, 2 and 3.



Test No. 4

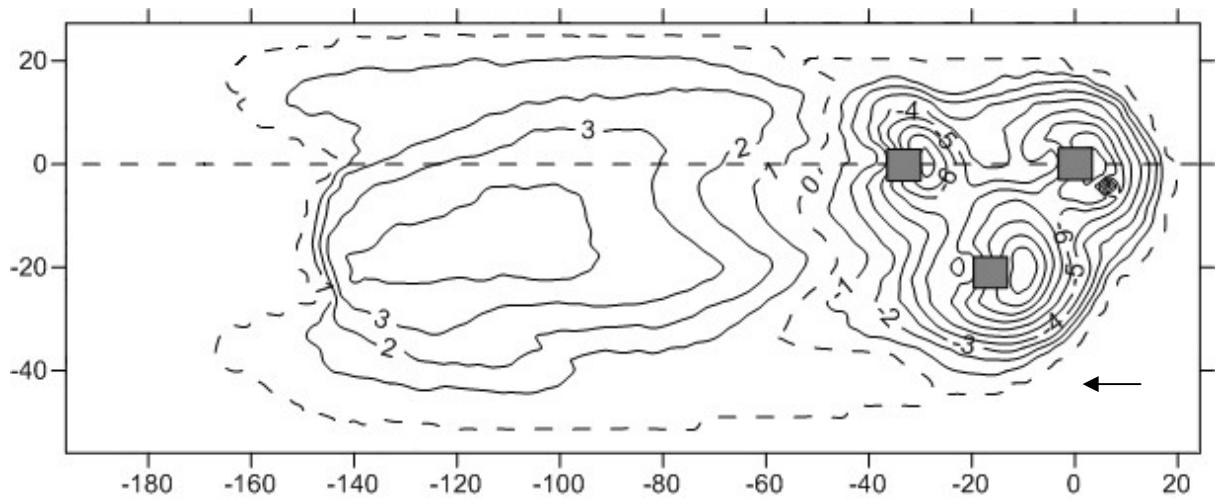


Test No. 5

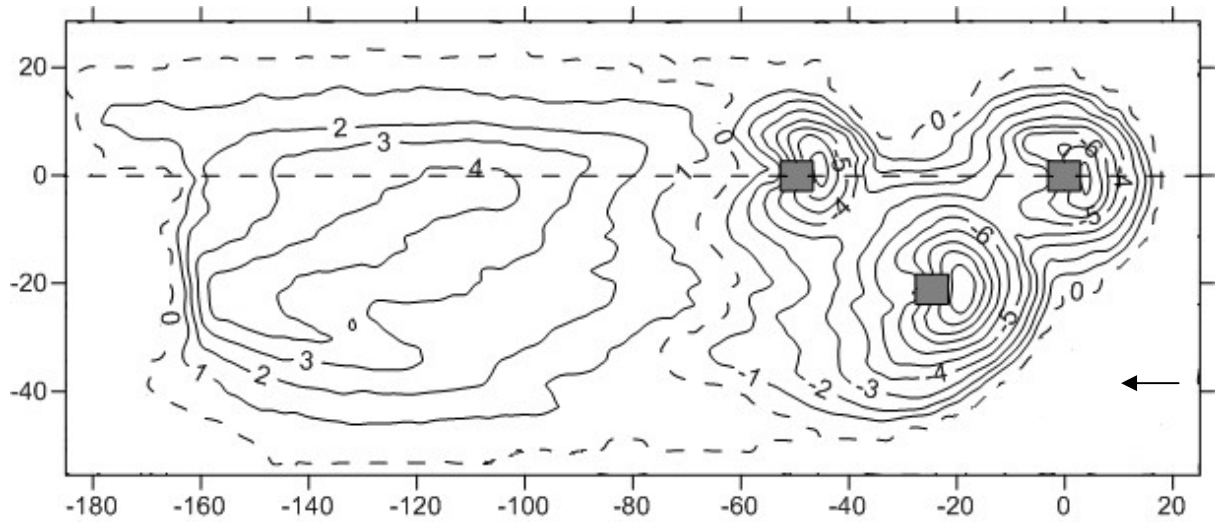
Fig. 4.5. Scoured zones around three identical square piers for test nos. 4 and 5.

Table 4.3. Magnitudes of geometric parameters at equilibrium scour for five tests conducted.

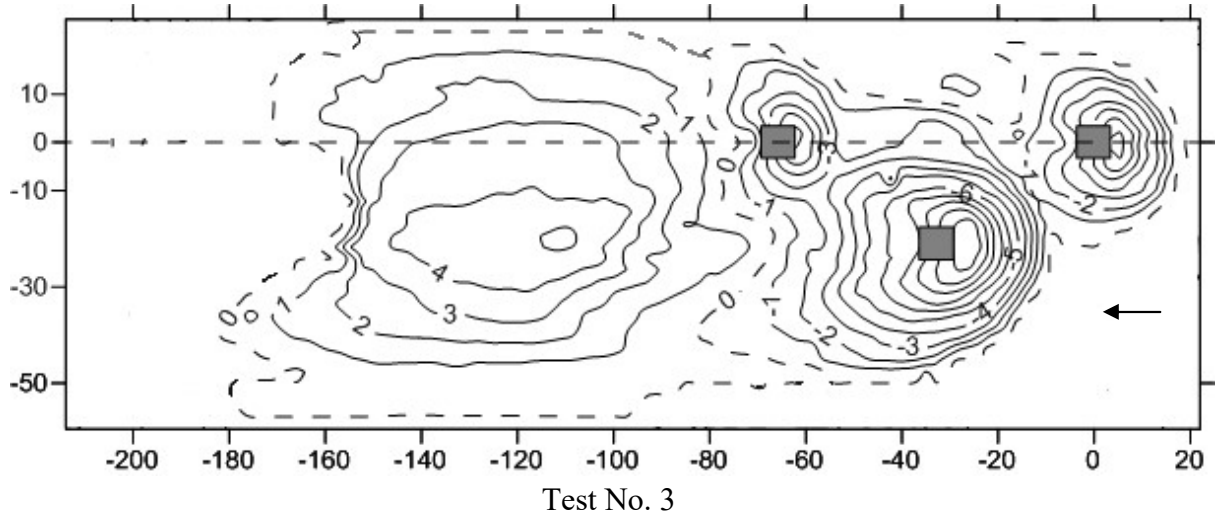
Test No.	b (cm)	(l) (cm)	d_{sf} (cm)	d_{se} (cm)	d_{sr} (cm)	l_s (cm)	w_s (cm)	L (cm)	a_s (cm ²)	∇_s (cm ³)
1	7	(2/8) l_{ss}	6.4	13.5	6.0	77.51	65.47	186.97	6789	13555
2	7	(3/8) l_{ss}	7.0	14.1	6.6	95.08	70.15	204.79	7176	14257
3	7	(4/8) l_{ss}	7.5	15.5	7.0	102.44	71.80	210.16	8332	15123
4	7	(5/8) l_{ss}	8.0	15.8	7.5	96.19	75.30	263.21	9369	17611
5	7	(6/8) l_{ss}	8.1	15.9	7.7	116.19	74.05	280.70	11455	19494



Test No. 1



Test No. 2



Test No. 3

Fig. 4.6. Contours of equilibrium scour hole around three square piers for test nos. 1, 2 and 3. (all units are in cm)

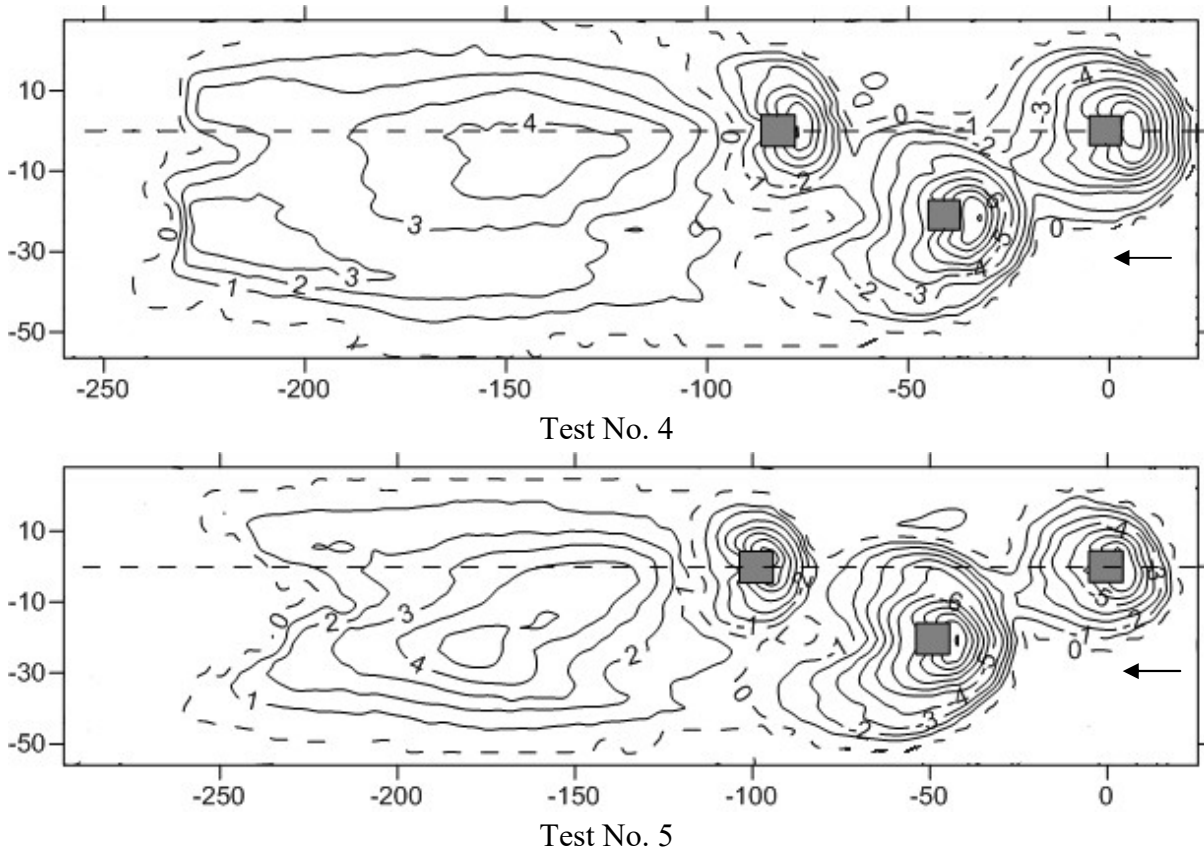


Fig. 4.7. Contours of equilibrium scour hole around three square piers for test nos. 4 and 5. (all units are in cm)

4.6 Velocity Measurement

The three components of velocity were recorded instantaneously using a down facing acoustic Doppler type Nortek made VectrinoPlus probe [Das *et al.* (2015)]. An adjustable cylindrical type sampling volume, 6 mm diameter having sampling height (Δz) of 2-5 mm was selected for sampling. Sampling height 5 and 2 mm were used for the measurement of discharge above and within the interfacial sub-layer when the velocity component decreases rapidly. Instant velocity-components are sampled at 100 Hz sampling rate. Minimum horizontal or radial resolution (Δr) during the Vectrino sampling was 1 cm. Sampling by ADV down-facing probe was impossible in the region 4.5 mm above sand bed. Because of the interference due to echoes from the bed, the received signal is disturbed, which results in inaccurate velocity measurement [Song and Chew (2010)]. Vectrino output readings were converted by VectrinoPlus software, version 1.18. Throughout filtering of converted ADV data, the minimum signal to noise ratio and minimum correlation coefficient were maintained at 17 or above and 70% and above, respectively [Das *et al.* (2013)]. A sampling time of 2–3 minutes was considered for verifying a statically time independent averaged velocity. Comparatively long sampling time of 3 min near scoured bed was taken as taken by previous researches [Das *et al.* (2014), Das and Mazumdar (2015b, 2018)]. To minimize standard errors, such time span may be amid 1 to 1.5 min as determined by Be'langer and Roy (2005). Measured ADV data near bed sometimes found with more spikes due to the interference

between incident and reflected beams. Spikes were removed by filtering the measured data using an algorithm as done by Blanckaert and Lemmin (2006). The minimum limit for despiking was selected in a way that the power spectra of velocity fit with $-5/3$ scaling law of Kolmogorov in inertial sub range [Das and Mazumdar (2015b)]. The error analysis of Vectrino gauged data was done by calculating standard deviation and average of maximum errors E_{\max} for u , v and w . The magnitudes of standard deviation and E_{\max} for u , v and w are found 0.0261, 0.0167, 0.0203 and 0.451%, 0.163%, 0.279%, respectively.

4.7 Analysis of Flow and Turbulence Fields

A cylindrical polar axis system, given in Figs. 4.1, 4.2 and 4.3, is utilized to represent non-dimensional velocity and subsequent dimensionless turbulence flow fields at five vertical azimuthal planes 0° , 45° , -45° , 90° and -90° around the piers. The time mean velocities in (r, θ, z) are symbolized by (u, v, w) , whose resulting fluctuations are (u', v', w') . Positive direction of tangential velocity (u), radial velocity (v) and vertical velocity (w) are counter clockwise, outward and upward, respectively. The flow fields projected in r - z planes for five azimuthal planes around the three piers.

To ignore solid section of piers in the plotted diagram, abscissa scale is taken by r_0/h [$=(r-b/2)/h$], i.e. $r_0/h = 0$ shows the square pier boundary. The scales in abscissa are considered larger than scales of ordinate for showing a clear presentation of velocity flow fields inward scour holes of smaller dimension and enlarges the figures along horizontal for a better illustration of velocity turbulence contour profiles. Velocity gauging was possible close to 2 cm from the piers boundary since the external radius of vectrino+ probe is around 2 cm.

A Cartesian coordinate axis system is also used to address velocity and resulting turbulent flow fields at two horizontal r - y planes $z = 0.5$ cm and $z = 6.25$ cm from the zero bed level (or $z = 0.04h$ and $z = 0.5h$ of the flow) around the piers. Similarly, components of time mean velocity are symbolized by $(u, v$ and $w)$, whose resulting fluctuations are $(u', v'$ and $w')$. According the right hand thumb rule, positive direction of u is along the flow, v is towards the left side from the symmetry line and w is upward. The flow fields are projected in r - y plane for $z/h = 0.04$ and $z/h = 0.5$.

4.7.1 Flow Fields

4.7.1.1 Tangential Velocity

At clear water condition for equilibrium scour, contours of dimensionless time mean tangential velocity (u/U) have been plotted using OriginLab software at five azimuthal planes 0° , 45° , 90° , -45° and -90° and at two horizontal planes $z=0.04h$ and $z=0.5h$ from zero bed level around the three square piers as shown in Figs. 4.8, 4.9 and 4.10. The figures displaying contour profiles show the flow velocity behaviour near and around the three square piers.

At 0° azimuthal plane, u is nearly zero and is inconsiderable as was recorded by the ADV. As azimuthal angle θ increases, value of u increases and turns finite. At square front

pier close to scour hole value of u is a bit lower than square eccentric pier and square rear pier. From the past [Das and Mazumdar (2018)] and current investigation maximum value of u is $0.061U$ and $0.043U$, respectively, at any location upstream of square front pier and decreases as it moves downward and increases toward bed. Maximum values of u just near upstream of scour region around square front pier, square eccentric pier and square rear pier are obtained approximately $0.054U$, $0.15U$ and $0.21U$, correspondingly.

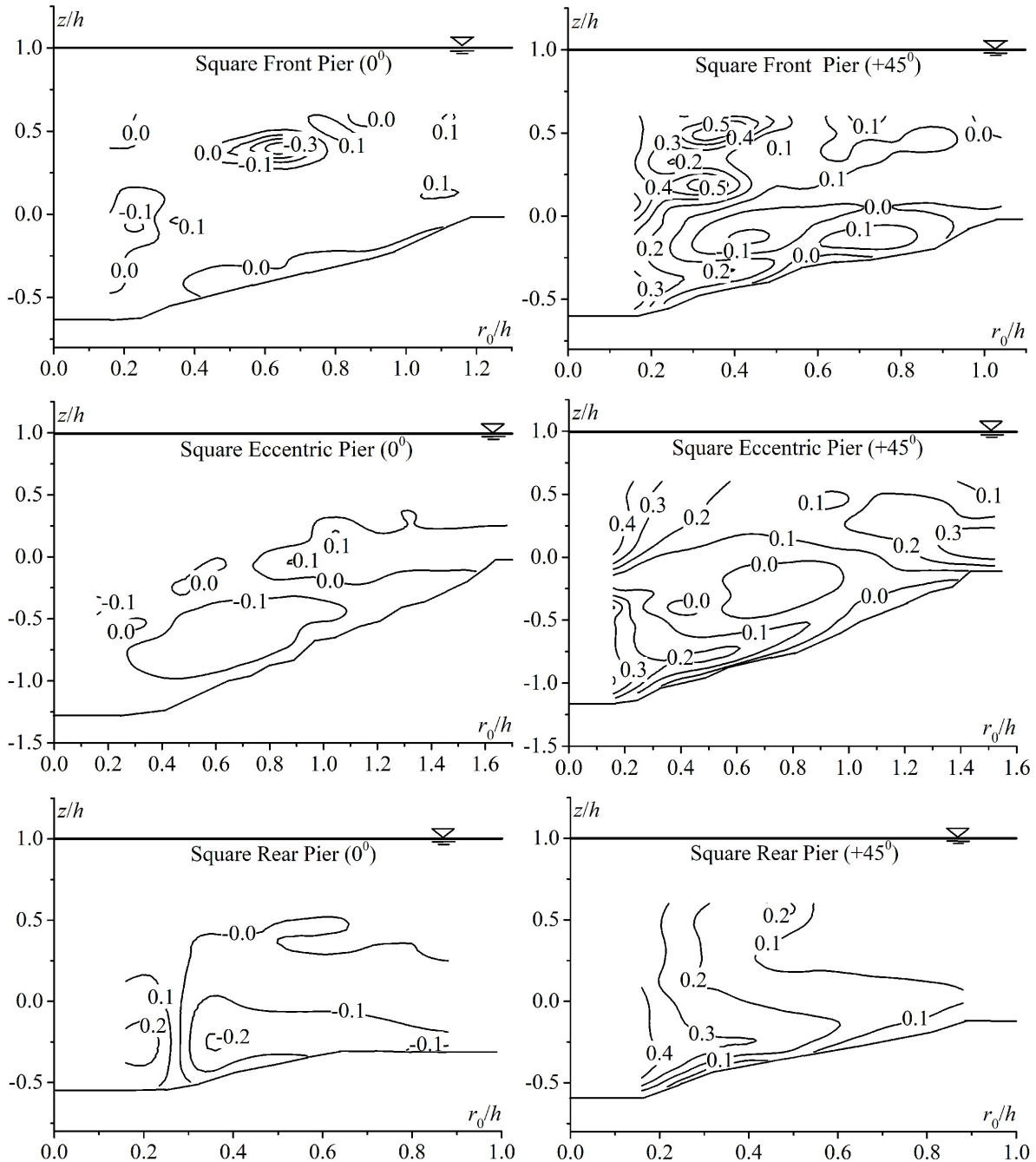


Fig. 4.8. Contours of non-dimensional tangential velocity (u/U) for square front, square eccentric and square rear piers at r - z planes for $\theta = 0^\circ$ and 45° .

In those zones, u varies with higher magnitudes for square front pier and square eccentric pier corresponding to the square rear pier. Horseshoe vortices, with downward and

subsequent reverse flow, are formed at pier bases just upstream near bed at a small region of all three piers. In similar way, upward and subsequent reverse flows are found downstream region of the three piers extending by flowing away from scoured bed. These horseshoe vortex flow move downstream of three piers and combine with the corresponding wake region of the piers.

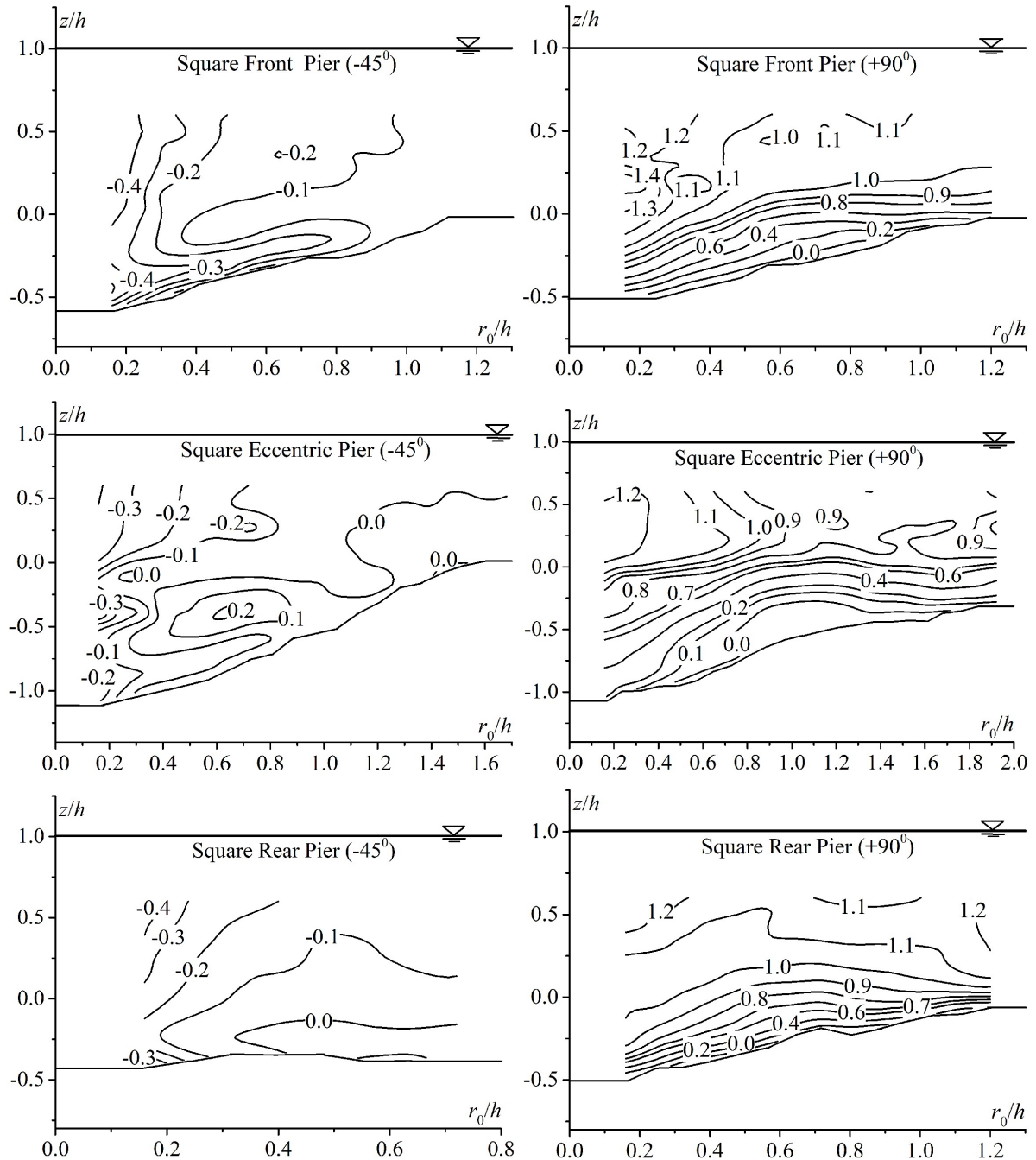


Fig. 4.9. Contours of non-dimensional tangential velocity (u/U) for square front, square eccentric and square rear piers at r - z planes for $\theta = -45^\circ$ and 90° .

The downward and corresponding reverse flows are noticed. These are magnitude wise greater for square eccentric pier among three piers and also found that they are higher for

square front pier than for square rear pier. It shows that at 0° , just upstream near the bed, values of u for square eccentric pier are lesser than the other two square piers. The value of u amplifies with increase in elevation z and $\partial u/\partial z$ (i.e. vertical gradients of u) inside scour holes (i.e. $z \leq 0$), and are found more than $\partial u/\partial z$ above scour holes (i.e. $z > 0$).

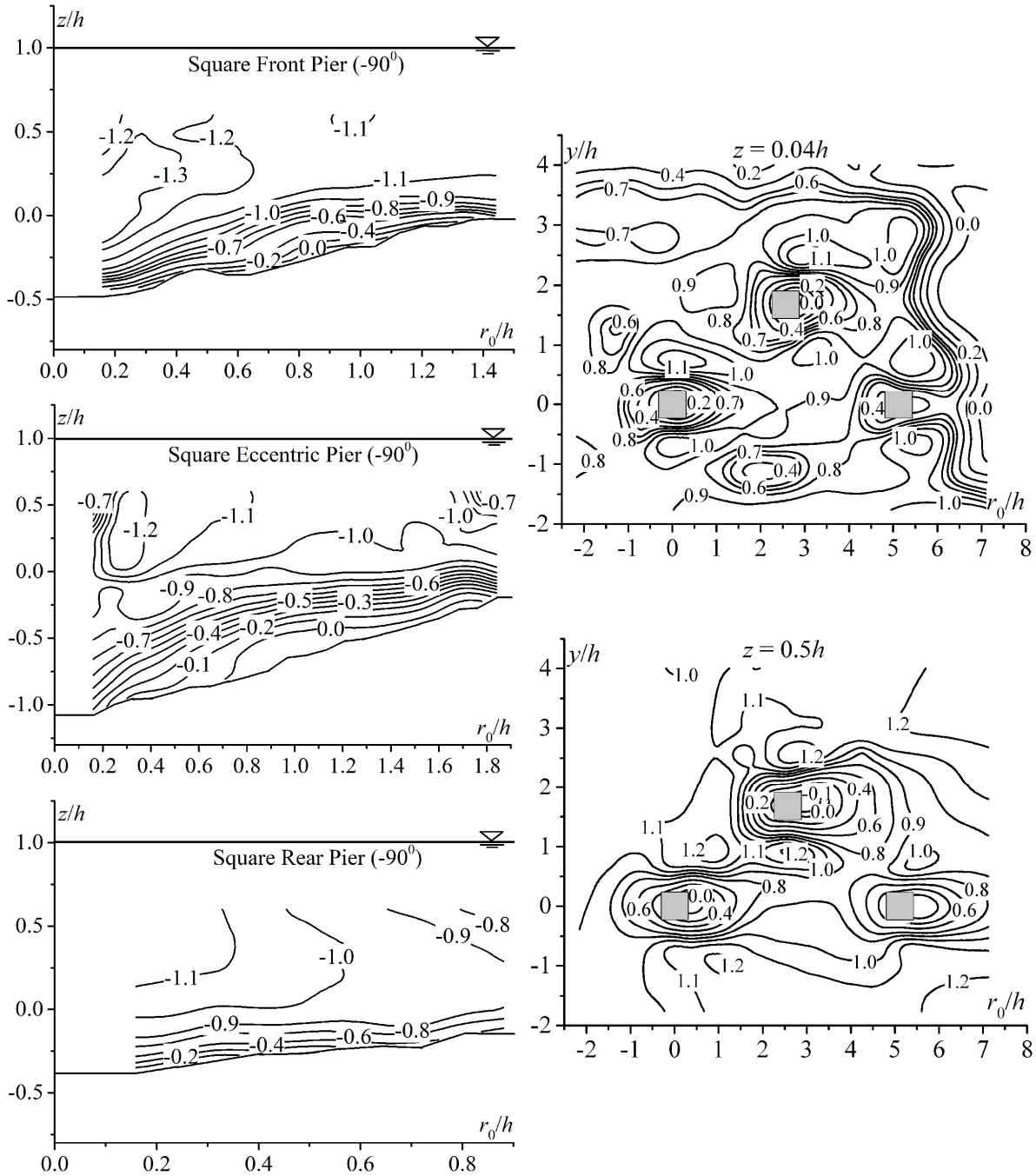


Fig. 4.10. Contours of non-dimensional tangential velocity (u/U) for square front, square eccentric and square rear piers at r - z plane for $\theta = -90^\circ$ and at r - y planes for $z=0.04h$ and $z=0.5h$.

In present study, at $\pm 45^\circ$ azimuthal planes of the three square piers value of u are found greater than value at 0° azimuthal plane of corresponding points for corresponding piers. For the three piers in the arrangement maximum value of u at 45° azimuthal plane are 1.04, 1.12 and 1.01 times of maximum value of u at -45° , respectively. It proves that small sheltering

effect takes place between 45° azimuthal plane for square eccentric pier and -45° plane for square front pier and between -45° plane for square eccentric pier and 45° azimuthal plane for square rear pier.

Because of these sheltering effects of square front pier and square eccentric pier, it is clear that maximum value of u at 90° azimuthal plane for square front pier, square eccentric pier, and square rear pier is 0.99, 0.98 and 1.009 times than the maximum value of u at -90° azimuthal plane for corresponding piers. The flow behaviour of u for square front pier, square eccentric pier and square rear pier at azimuthal planes $\pm 90^\circ$ are similar. The tangential velocity u at $\pm 90^\circ$ planes for the three square pier are always higher than u at $\pm 45^\circ$ planes for corresponding piers, as the dimension of scoured holes are small, but it decreases progressively. Also u at 45° , 90° , -45° and -90° is comparatively strong as the dimensions of scour holes are small, but decreases progressively due to increase in flow area as the scour depth increases. Due to the way of the downflow flux along the sides of the three square piers, a significant increase in u near the piers is found and then reduces as radial distance r_0 increases from each pier and all over the flatbed u remains almost constant.

For the two horizontal planes $z=0.04h$ and $z=0.5h$ above the bed level ($h=0$) as in Fig. 4.10, shows from the dimensionless contours of time mean longitudinal velocity u/U is more in the downstream of square rear pier, compared to square front pier and square eccentric pier due to united effect of the inline square front and square eccentric pier, u is found more around the square rear pier. In between the region surrounded by the piers has higher order longitudinal velocity than depth mean approaching velocity of flow. This increase becomes visible in the combined form of expansion in the high velocity region and magnitude of u . Since the formation of wake occurs in a recirculating zone that does not contribute to net transportation of sediment towards downstream, flow in that region next to the wake leads to accelerate and results in transport of the extra quantity of sediment. Formation of vortex behind the square front pier has an effect over the square eccentric pier and therefore combined action of square front pier and square eccentric pier over square rear pier. The velocity U in downstream of the three piers at $z = 0.04h$ is almost similar to the corresponding values of u at $z = 0.5h$ but a bit higher in magnitude.

Stagnation pressure becomes zero, as u moves near the pier. The velocity U decreases from upper level of water toward the bed and it confirms, stagnation pressure decreases while depth decreases, the reason of formation of weak pressure gradient in the upstream of piers and increase in downflow magnitude.

At the upstream region of square front pier, flow starts decelerating and subsequently layers separate and move further towards square eccentric pier and both reaches on surface of square eccentric pier. Similarly, the layers from square front and square eccentric pier are separated and move downstream and both reaches on frontal surface of square rear pier i.e. the boundary layer moves at low velocity than velocity at free stream. Hence, negative velocities exist at inner area of boundary layer. In the downstream of square front and square eccentric and square rear piers, u -contours, zero velocity lines divide the regions of positive velocity and negative velocity and show the existent of flow separation. With the development of negative velocity, pressure within the region is small, compared to those in free stream; hence, the outward fluid is dragged down inward to the low pressured zone. The

eddies generate from the square front pier are then flowed downstream and comes to the 0° to -90° plane of square eccentric pier and 0° to -90° of square rear pier and simultaneously the eddies generated from square eccentric pier comes to the 0° to -90° plane of square rear pier.

4.7.1.2 Radial Velocity

The contours of dimensionless time-mean radial velocity (v/U) at five azimuthal planes 0° , 45° , 90° , -45° and -90° and at two horizontal planes $z = 0.04h$ and $z = 0.5h$ from the zero bed level around the three square-piers for equilibrium scour at clear water condition are plotted using OriginLab software, displayed in Figs. 4.11, 4.12 and 4.13.

At 0° azimuthal plane as v approaches near upstream region of the three square piers, stagnation pressure decreases with the establishment of depth itself and produces a weaker pressure gradient $[\partial(\rho v^2)/\partial z]$ along front zone of the three square piers and therefore generates downward velocities of decreasing nature. This downstream flow velocity deflects laterally as strong pressure gradients exist around the three square-piers. As stated in previous research [Graf and Yulistiyanto (1998)], component of vertical flow is liable for scouring. As increasing stagnation pressure becomes adequately strong, resulting 3-D boundary layer to goes through a flow separation. Formation of horseshoe vortices systems itself near the three pier base and reducing its strength stretched into downstream way. Those horseshoe vortices systems are very strong in local scour activity. For the three square piers, in downstream zones, trailing wake vortices systems are found over complete flow depth. Their turbulence intensities are increased, and concurrently, erosion and transfer of sediments are enhanced. It is seen that the scour rate is much more around square eccentric pier than the inline square front pier and inline square rear pier.

For the three piers at 0° azimuthal plane, flow separation is visible below the boundary of all scour holes, developing reversal flow within scour hole ($z \leq 0$). The velocity v changes its direction on both side of zero contour line ($v=0$) within the scour hole, at altered depths for square front pier, square eccentric pier and square rear pier are around 0.60, 0.65 and 0.71 times of corresponding maximum scour depth below the non-scoured bed level ($z=0$) for the corresponding pier, respectively. As published in a previous research, [Das and Mazumdar (2018)] for two square piers experiment under same experimental condition, it is 0.65 and 0.67 times maximum scour depth below the non-scoured bed level for corresponding front square pier and eccentric square pier and for square single pier experiment under same experimental condition, it is 0.65 and 0.62 times of maximum scour depth for $z \leq 0$, respectively [Dey and Raikar (2007), Das and Mazumdar (2015a)]. These confirm the existence of powerful horseshoe vortices within scour holes near upstream zone of all three square piers.

The region $z \leq 0$ and $z > 0$ along vertical-axis, v varies differently. In $z \leq 0$, within the scour hole from $z=0$ towards the bed, v decreases quickly to become zero. Values of v become positive just near the bed outwards from the piers after flow come back from the base of each three pier resulting in backflow through the scour hole sloping bed.

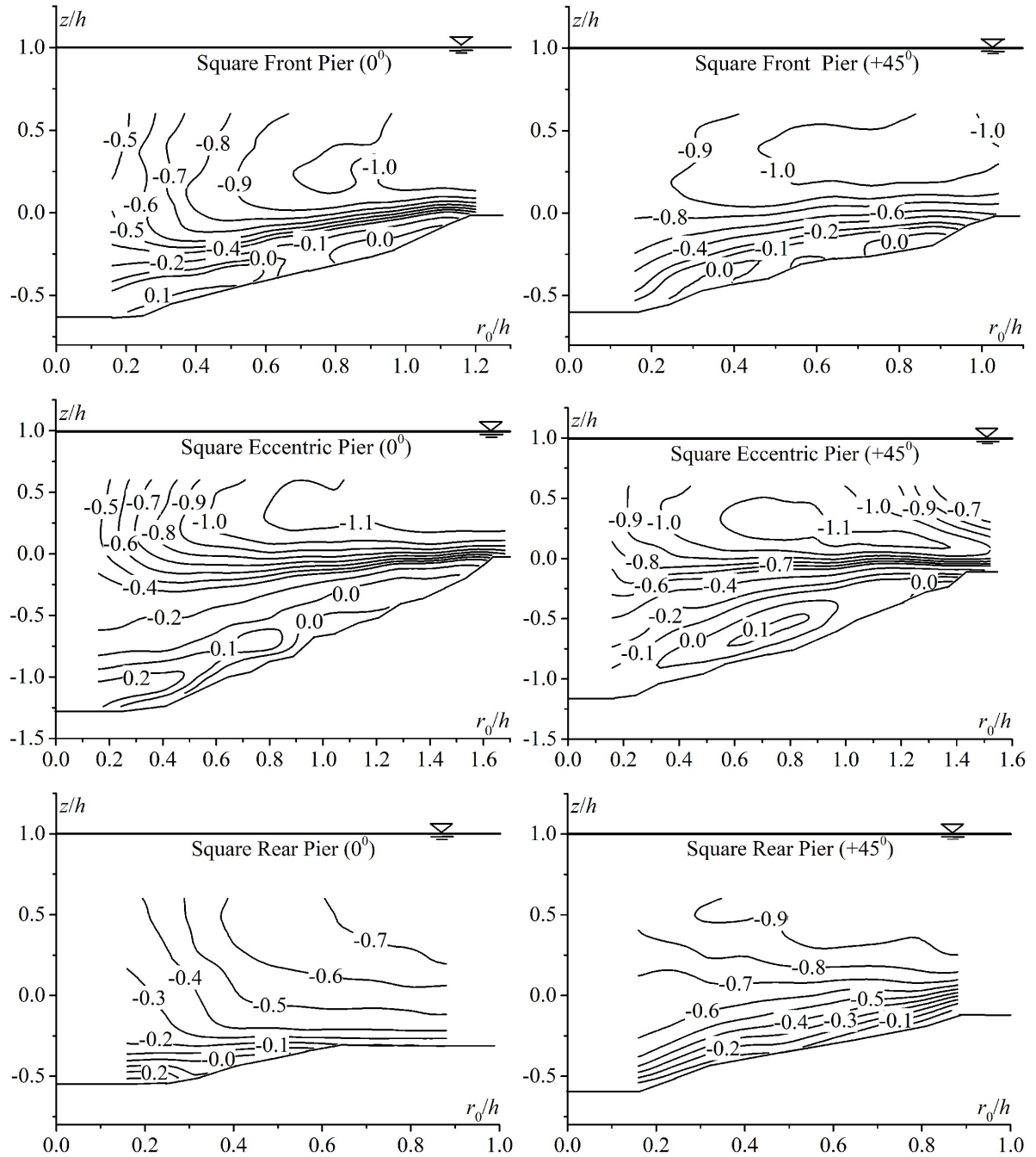


Fig. 4.11. Contours of non-dimensional radial velocity (v/U) for square front, square eccentric and square rear piers at r - z planes for $\theta = 0^\circ$ and 45° .

The maximum reversed v are seen upstream near the beds of square front pier, square eccentric pier and square rear pier are about $0.24U$, $0.35U$ and $0.23U$, respectively whereas for two square pier experiments [Das and Mazumdar (2018)] maximum value of v observed near bases of inline front square pier and eccentric square pier are around $0.21U$ and $0.31U$, respectively and for single pier experiment maximum value of v near bases of pier are $0.20U$ and $0.32U$ as observed by Dey and Raikar (2007), and Das and Mazumdar (2015a), respectively. The velocity v is positive due to the obstruction of piers and for backflow and unidirectional flow just above scour bed.

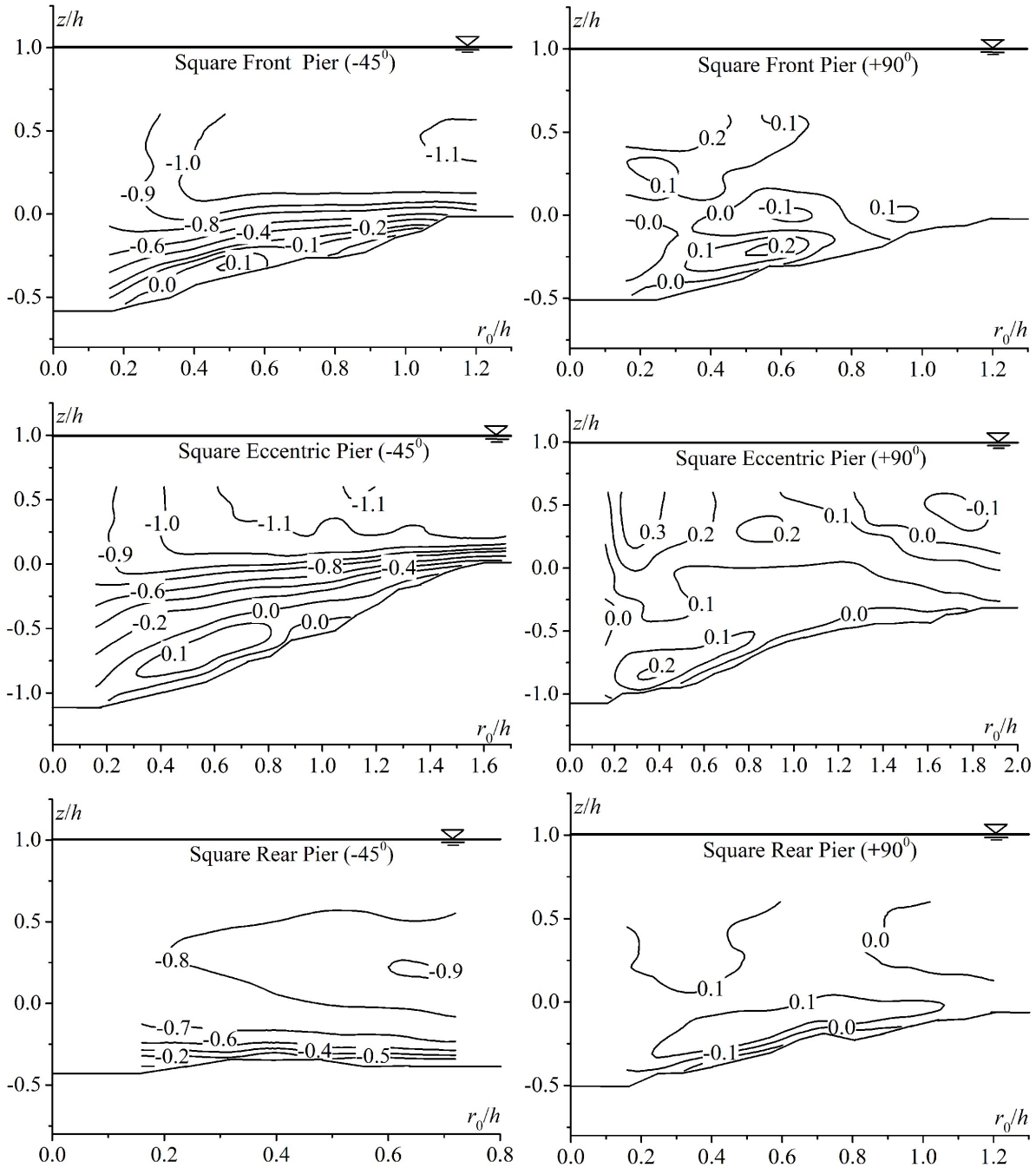


Fig. 4.12. Contours of non-dimensional radial velocity (v/U) for square front, square eccentric and square rear piers at r - z planes for $\theta = -45^\circ$ and 90° .

Above the scour hole ($z > 0$) v varies comparatively less and is nearly logarithmic because of the impact of non-uniform impending flow which begins from contour line $v = 0$ and turns maximum, negative in sign near free stream. In the turbulent logarithmic layer, v varies exponentially along vertical axis. In r - z plane along radial axis, radial velocity distribution shows a parabolic variant that begins with zero contour line ($v = 0$) near all the three pier boundaries and turns positive velocity near the bed when $z > 0$ and negative-velocity on other sides of locus of $v = 0$ at $z < 0$. As stated in previous literatures, on upstream of flatbed v remains basically logarithmic and decreases upon entering into the exposure of the larger flow region of scour hole [Dey and Raikar (2007), Das *et al.* (2014), Das and Mazumdar

(2015a,b, 2018)] and reduces slowly as it approaches towards the piers because of the presence of vertical square piers.

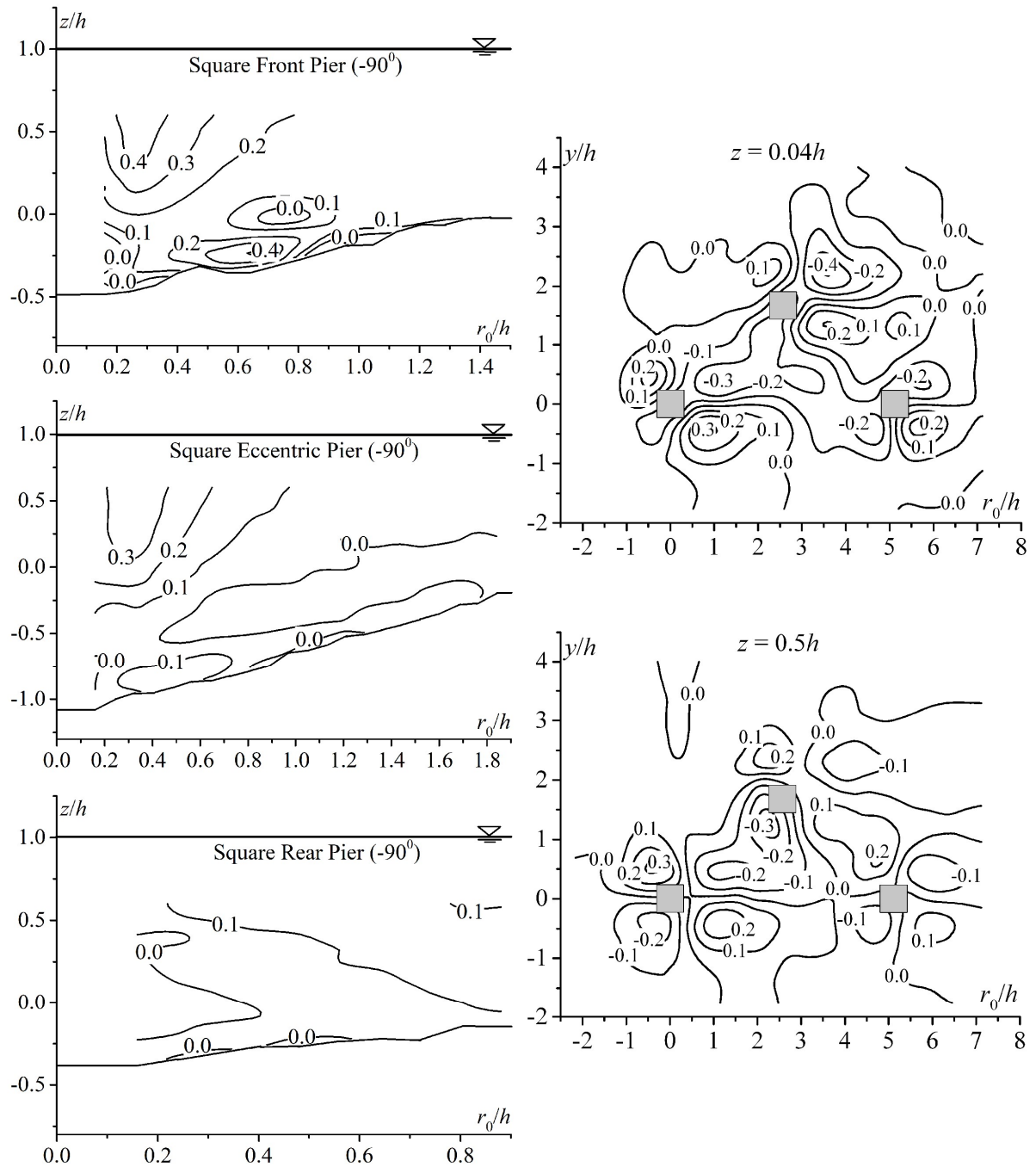


Fig. 4.13. Contours of non-dimensional radial velocity (v/U) for square front, square eccentric and square rear piers at r - z planes for $\theta = -90^\circ$ and at r - y planes for $z=0.04h$ and $z=0.5h$.

It results in separation of flow velocity and increase in depth of scour around the piers.

The distribution of v at $\pm 45^\circ$ azimuthal planes of the three piers is nearly similar to distribution of v at 0° azimuthal plane of corresponding piers. Presently distribution of v at 0° is greater than that at $\pm 45^\circ$ at respective locations. At the upstream near the scour hole edges of all three square piers, there is an existence of flow velocity separation. At $\partial v / \partial z = 0$ i.e. at the separation point, flow velocity is separated due to velocity reduction within boundary

layer, in addition with positive $\partial(\rho v^2)/\partial z$ opposing the flow. For the three square piers at $\pm 45^\circ$ the flow velocity separation line is shallower than at 0° .

As the flow velocity separates at $\pm 45^\circ$ from sharp edges of three square piers, horseshoe vortices detaches at azimuthal planes $\pm 45^\circ$. Therefore, flow velocity at $\pm 90^\circ$ is lesser than those at 0° and $\pm 45^\circ$. At $\pm 90^\circ$ azimuthal planes for the three square piers within the scour holes ($z \leq 0$), v acts towards each pier and a thin region of reversed flow velocity exists just near the bed. Above the scour holes ($z > 0$), flow velocity deflects outwards apart from scour holes alongside the three square piers. At all five azimuthal planes around the three square piers, maximum v for square eccentric pier is measured higher than maximum v for other two front and rear piers.

Up-flows are observed everywhere within longitudinal gap above scour hole between two square tandem piers in reattachment regime [Ashtiani and Kordkandi (2013)]. In between square front pier and square eccentric piers, up-flows are seen. It indicates the primary wake of square front pier (as illustrated in Fig. 4.19 for three piers at -90° azimuthal plane). The interaction in between these up-flows and succeeding down flows [as changes in $\partial(\rho v^2)/\partial z$], result in decrease of down flow (as illustrated in Fig. 4.14 for square eccentric pier at 0° azimuthal plane). Between square front pier and square rear pier up-flows indicate the existence of wake of square front pier and square eccentric pier. Similarly, interaction between these up-flows and subsequent down flows occur [as $\partial(\rho v^2)/\partial z$ varies] the resultant down flow decreases (as in Fig.4.14 for rear pier at 0° azimuthal plane). Thus dynamic pressure ($\rho v^2/2$) increases and v increases at the upstream region near square front pier and square eccentric pier and also v becomes maximum for square front pier at same locations.

The contours of dimensionless time mean radial velocity at two horizontal plane $z=0.04h$ and $z=0.5h$ above the bed level ($h=0$) are shown in Fig. 4.13. From the figure, it is observed that the approaching flow is separated near all three square piers. Radial velocity v changes its direction on either side of zero contour line ($v=0$). The direction of v is towards the right side of the wall. A part of v which flows towards the left of the flume wall has positive value and the other part which flows towards right of flume wall has negative value. This occurrence is prominent for all three piers, where the approaching flow separates. At both horizontal planes, maximum v is spotted at upstream of eccentric pier compared to other two piers. And v in the downstream of the piers at $z = 0.04h$ plane found very similar to that at $z = 0.5h$ plane and also greater than that at $z= 0.5h$ plane. At $z = 0.5h$ plane and near upstream zone of each pier, values of v are greater than those at $z = 0.04h$ plane due to existence of high momentum flow.

4.7.1.3 Vertical Velocity

Figs. 4.14, 4.15 and 4.16 depict the contours of dimensionless time mean vertical velocity (w/U) at five azimuthal planes 0° , 45° , -45° , 90° and -90° and at two horizontal planes, $z = 0.5$ cm and $z = 6.25$ cm from zero bed level around the equilibrium scour holes at three square piers at clear water condition. At 0° azimuthal plane around square eccentric

pier, from a study of w -contours, separation of resembling flow is clearly visible beneath bed level ($z=0$) within scour-hole ($z<0$) (as noticed in contours of v) from reversal character of vertical velocity near scoured bed. The distribution of w in majority within the flow area is downward (negative) for all three square piers, while radial velocity just near scour bed, is directed upward (positive) and increases in a downward way from the open surface specifying the existence of a downward negative $\partial(\rho v^2)/\partial z$.

The maximum value of w is observed near square front pier, square eccentric pier and square rear pier at depths of 0.20-0.67, 0.06-0.65 and 0.50-0.71 times of corresponding maximum scour depths under the non-scoured bed level ($z=0$), respectively, and decreases towards the scour hole bed. Size and core of maximum w are higher for square eccentric pier. For the three square piers, square front pier, square eccentric pier and square rear pier at 0° azimuthal planes maximum value of w is measured as $0.67U$ at $z = 0.40d_{sf}$, $0.71U$ at $z = 0.19d_{se}$ and $0.37U$ at $z = 0.64d_{sr}$ at $z=0$, respectively. Previous study showed, for Vectrino limitations, at pier faces velocity measurements are not possible. At least 2 cm gap is required from pier face to ADV. Therefore, maximum values of w are somewhat lesser than those values at pier boundaries. These maximum values of w are observed at r equal to 2-3 cm as compared with the previous study [Das and Mazumdar (2018)].

In present study, the behaviour of w at the upstream near the three square piers are similar, but these resemblances reduce behind the piers due to their existence at downstream. Near bed, gap between square front pier and square rear pier (for square rear pier at 0° azimuthal plane), between square front pier and square eccentric pier (at 90° azimuthal plane for square eccentric pier) and square eccentric pier and square rear piers (at 90° azimuthal plane for square rear pier), the maximum value of reverse w are $0.05U$, $0.17U$ and $0.19U$, respectively. Due to square front pier sheltering effect, flow velocity decreases while comes towards square eccentric pier downstream. Similarly, flow velocity decreases while coming towards square rear pier downstream due to combined sheltering action of square front pier and square eccentric pier. Hence, vortex shading occurs partly in those zones. The flow regimes developed between the three square piers within transverse gap are entitled co-shedding regime [Chapter 3]. Between two tandem piers, in reattachment regime, up-flows are found everywhere.

This phenomenon can be cited for decreasing in down flow near upstream region of square rear pier and combined interaction of this down flow and an obstructed flow velocity, increases the down flow which approaches upstream of square eccentric pier. Generation of turbulent flows of different velocities (or of different Reynolds numbers) along the flow depth caused by the impact of pier spacing and bed roughness, can affect the nature of flow regimes within the transverse gap [Zdravkovich (1987)].

Around three piers as θ increases from 0° to $\pm 45^\circ$ to $\pm 90^\circ$ azimuthal planes, it is noticed that w decreases gradually. A down flow develops near upstream of all three square piers because of downward negative stagnation pressure gradient of the varied approach flow, and thus vortex pushes the down flow [Dey *et al.* (1995)]. The moderate reducing character of v and w with an increase in θ are found, when decreasing character of horseshow vortex is also found. It confirms the reduction of strength of horseshoe vortex towards downstream flow.

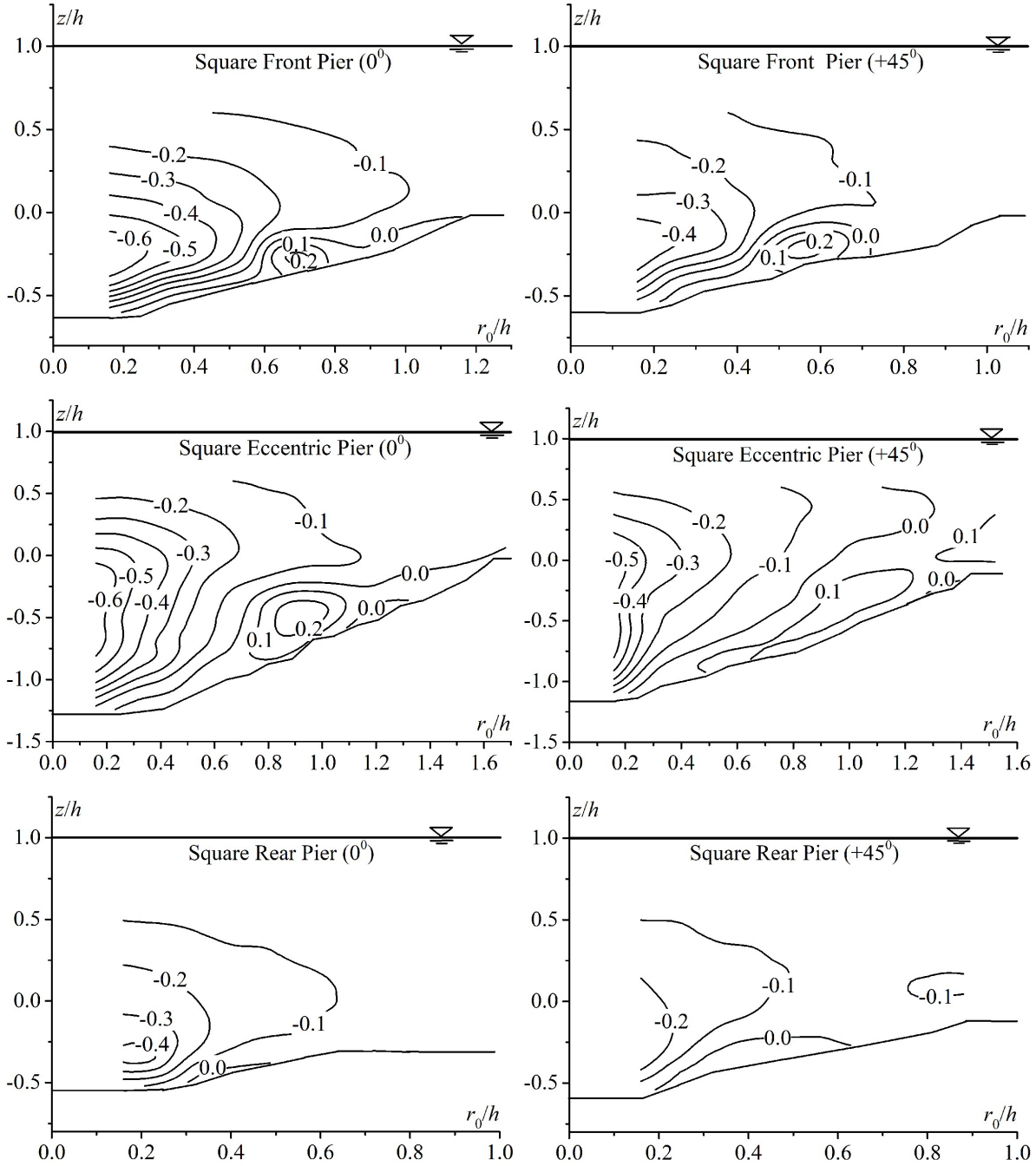


Fig. 4.14. Contours of non-dimensional vertical velocity (w/U) for square front, square eccentric and square rear piers at r - z planes for $\theta = 0^\circ$ and 45° .

At 45° , -45° , 90° and -90° azimuthal planes around square front pier, square eccentric pier and square rear pier, maximum values of downward w are 0.72, 0.79, 0.52, 0.55; 0.84, 0.79, 0.66, 0.80; and 0.71, 0.65, 0.62, 0.46 times of maximum values of downward w at 0° for corresponding pier locations, respectively. As studied by previous researchers for two piers experiment, it was 0.96, 0.89, 0.76 and 0.67 times for square front pier and 0.95, 0.66, 0.83 and 0.72 times for square eccentric pier [Das And Mazumdar (2018)] and also for square single pier experiment at 45° and 90° , maximum values of w were observed 0.80 and 0.73 times of results [Dey and Raikar (2007)] and 0.81 and 0.63 times of the results [Das and

Mazumdar (2015a)]. From these observations, down-flows around square eccentric pier are always greater than w around other two square-piers and around square front pier w always higher than around square rear pier.

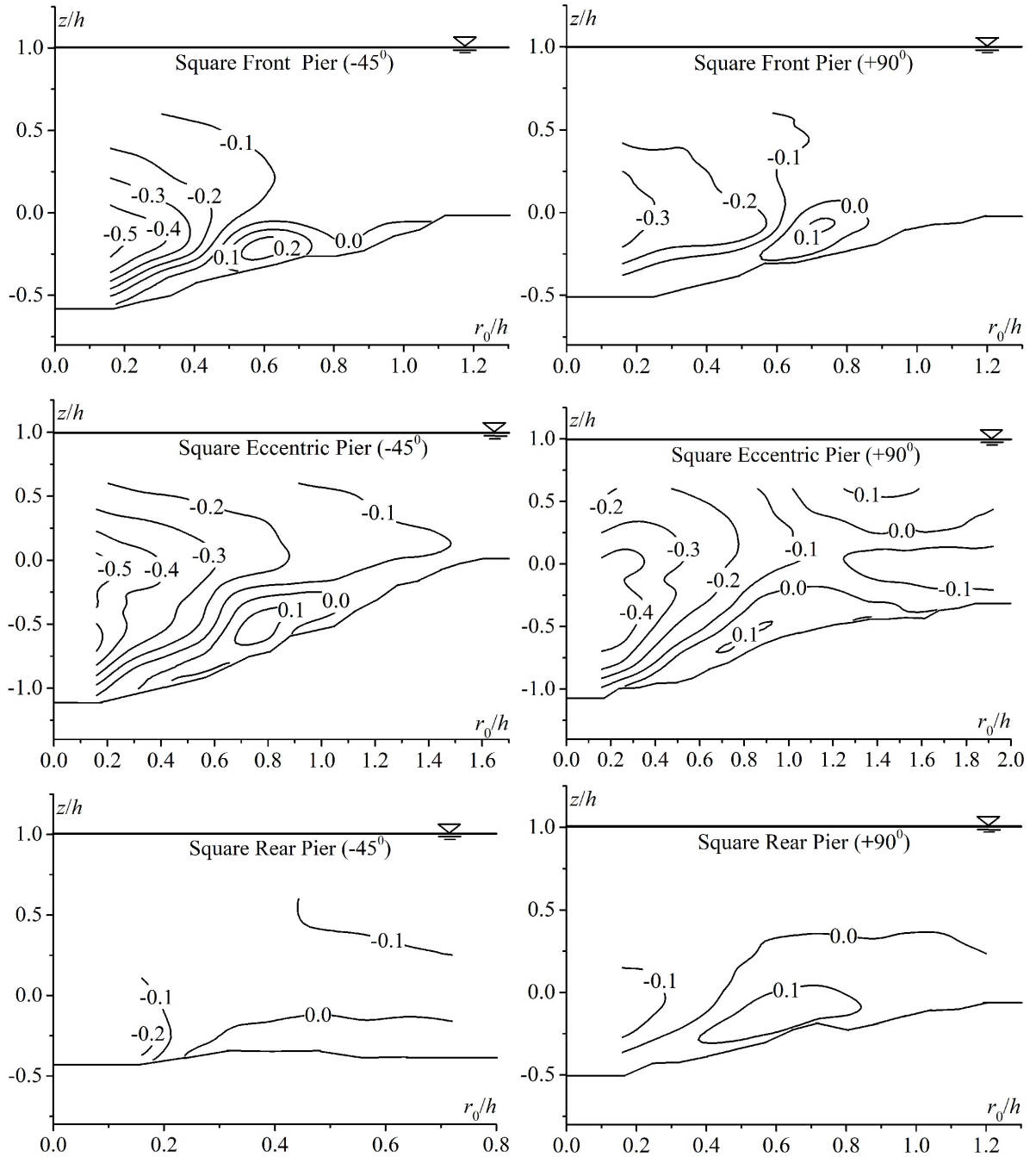


Fig. 4.15. Contours of non-dimensional vertical velocity (w/U) for square front, square eccentric and square rear piers at r - z planes for $\theta = -45^\circ$ and 90° .

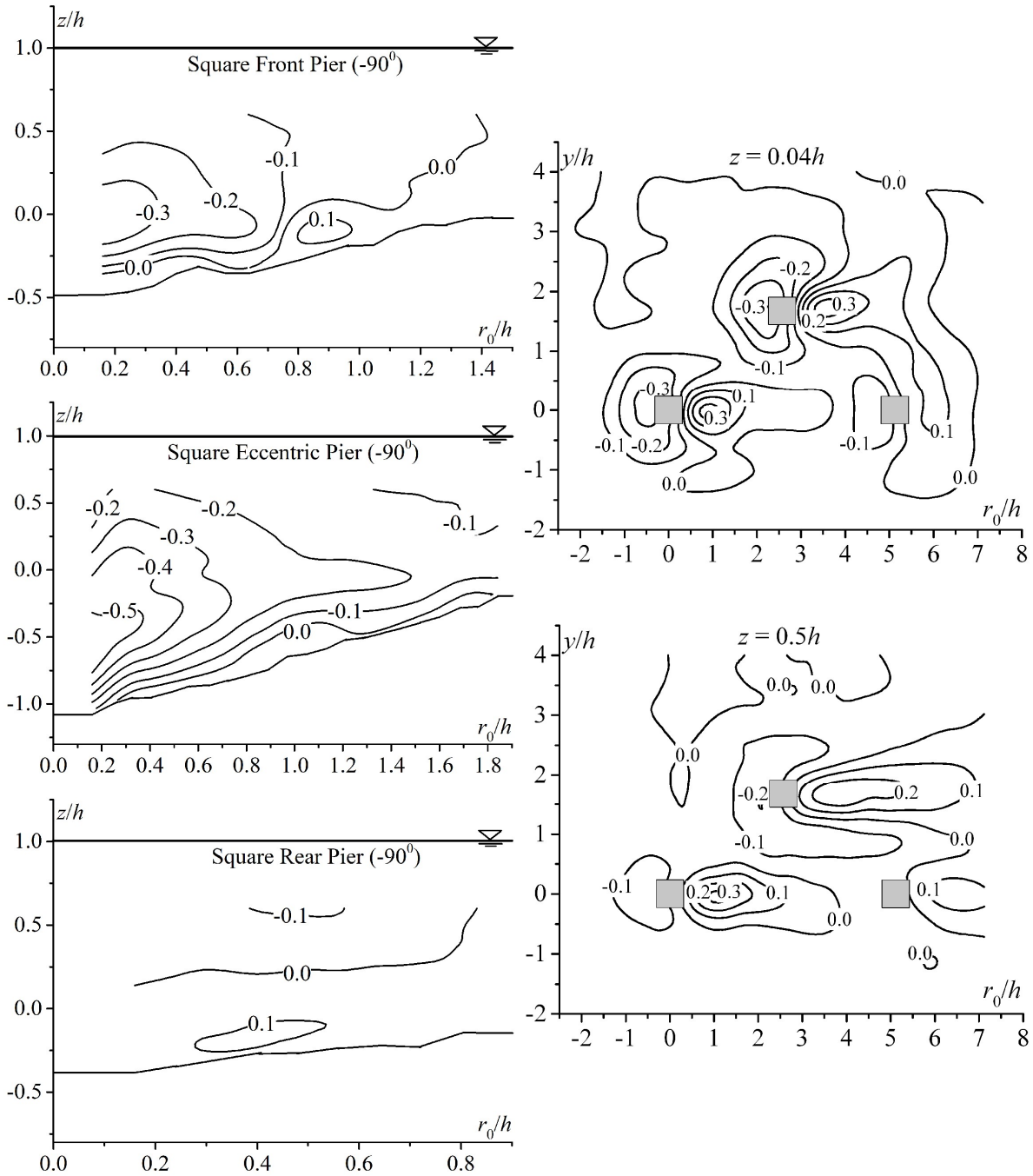


Fig. 4.16. Contours of non-dimensional vertical velocity (w/U) for square front, square eccentric and square rear piers at r - z planes for $\theta = -90^\circ$ and at r - y planes for $z=0.04h$ and $z=0.5h$.

In the flow zone for $z=0.04h$ and $z=0.5h$ plane, the contours of dimensionless time mean vertical velocity w/U are addressed well in Fig. 4.16 to describe flow characteristics more accurately. In this study, w is directed in upward direction. Whereas, upstream of all three square piers, there is a downward negative velocity. Then flow is obstructed by all three square piers and upstream of stagnation point it begins to move downward.

Maximum value of negative w is noticed at the upstream of square eccentric pier. Hence, at upstream of square eccentric pier it is clear maximum scour depth, as well as strongest circulation, is likely to be found. Vertical velocity at the downstream of the three square piers is noticed with positive magnitude. Here the flow is directed upward. It specifies

that the flow firstly passes downward at the upstream region of each pier forming horseshoe vortex, then passes from the side of piers and finally it moves upward at the downstream region of the three square piers forming wake vortices. For $z=0.04h$ at the piers downstream, value of time mean vertical velocity w is observed maximum. The maximum value of w is found about 0.6-0.7 times of v . Now, by comparing the last two (horizontal) contours as depicted in Fig. 4.16, it is clear that at the upstream of piers, w has more magnitude at $z=0.04h$ plane than that at $z=0.5h$ plane. At the downstream of piers, value of w is more at $z=0.04h$ plane. At $z=0.04h$ plane in wake region, velocity of higher value is observed as compared to $z=0.5h$ plane. It confirms that the flow moves upward producing a stronger wake vortex at the downstream of piers. Thus, the wake vortex effect is little at downstream of three square piers.

4.7.1.4 Velocity Vector

Profiles of \vec{v} (velocity vectors) for equilibrium scour holes at clear water scour condition at azimuthal planes 0° , 45° , -45° , 90° and -90° for square front pier, square eccentric pier and square rear pier of magnitude $\sqrt{v^2 + w^2}$ and direction $\text{arc tan}(w/v)$ are shown in Figs. 4.17, 4.18 and 4.19. Also Fig. 4.19 shows velocity vectors at $z=0.04h$ and $z=0.5h$ horizontal planes around the piers, whose magnitude and direction are $\sqrt{u^2 + v^2}$ and $\text{arc tan}(v/u)$, respectively.

Plotting of \vec{v} at 0° and $\pm 45^\circ$ shows the hydraulic flow behaviour of horseshoe vortices along with down flow moving towards upstream direction of three square piers. The hydraulic flow patterns of flow around the three piers are mainly large vortices flow and skewed distribution of flow velocities along the sides of three square piers. The separation of approaching flow occurs beneath the effect of transverse gradient generated by the piers. The slower flow near the pier walls and smaller momentum at bed surface, form faster moving fluid apart from piers and bed surface. Therefore the value and the direction of approaching velocity vector vary with distance from wall of three piers and the bed surface creating the distribution of skewed velocity.

Horseshoe vortices, are almost similar to the ground rollers at downstream of dune crest, found within the three scour holes. The pier induced upstream flow separation along edge of the scour holes (i.e. separation line), the approaching flow curves down within the holes and transversely rolls to form vortex which is called horseshoe vortex system and which migrates downstream by sides of piers. On account of stagnation pressure gradient of unsteady approach flow velocity near upstream of piers, down flows develop. The down flow is found maximum at free surface and zero at scoured bed surface for the three square piers. The downward flow is accelerated further downward by the horseshoe vortices. In this way, approaching flow deflects downward and rolls into scour holes forming helicoidal flow as the horseshoe vortices. These vortices take a bigger role in development of scour hole around three piers, in conformity with older researches [Dey and Raikar (2007) and Das and Mazumdar (2018)]. Here, for large scour holes, size of those vortices is large as compared with the mentioned researches. In single pier case, these vortices combine with down flow.

The flow accelerations around side of pier and large scale wake rollers are the erosive issues of bed sediments.

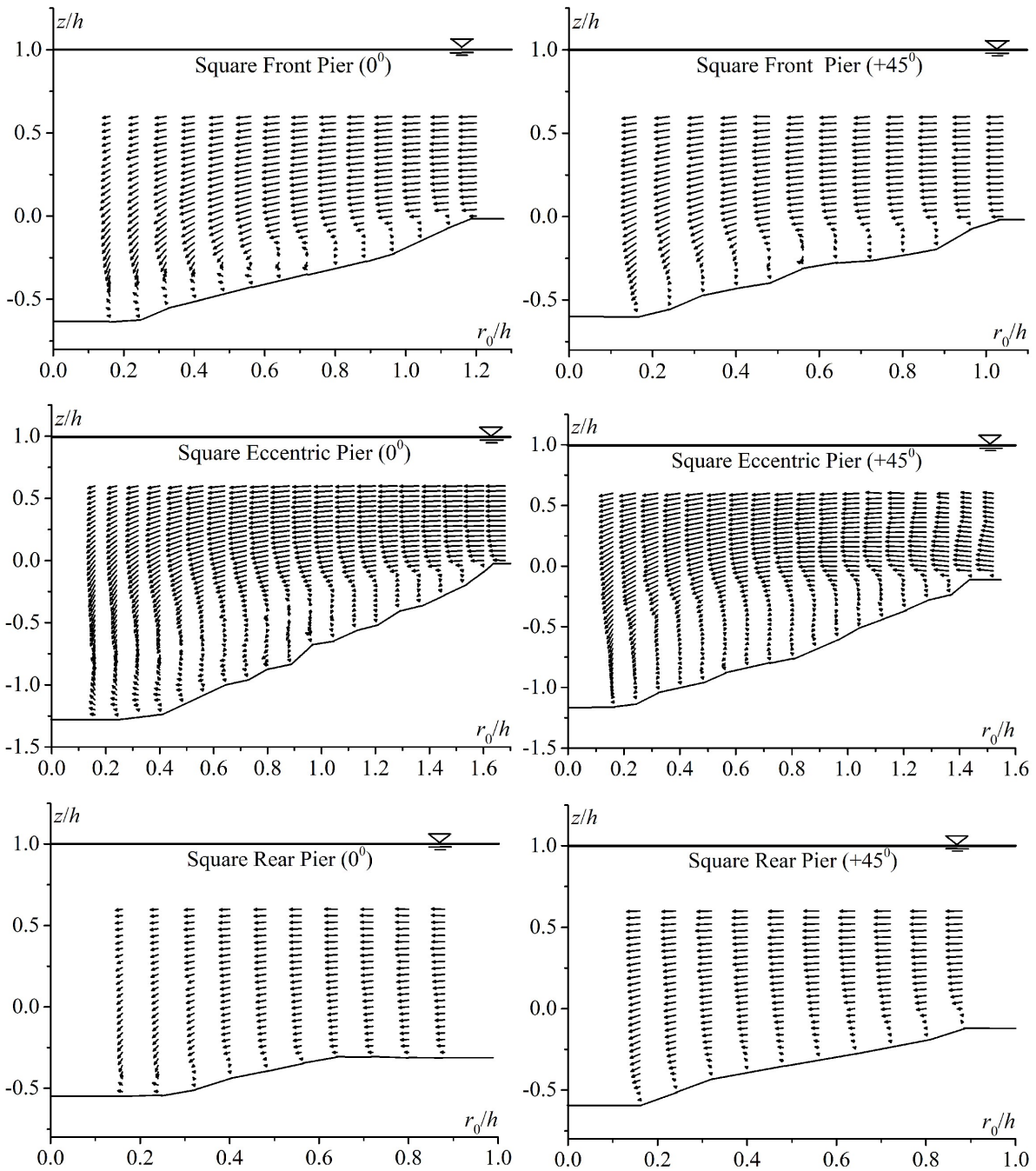


Fig. 4.17. Velocity vector plots for square front, square eccentric and square rear piers at r - z planes for $\theta = 0^\circ$ and 45° .

Here, in this experiment in addition to these scouring mechanisms, some alterations also appears in flow formations which are interferences of vortices shedding and interferences of vortices and velocities increase between square front square eccentric piers and square eccentric square rear piers.

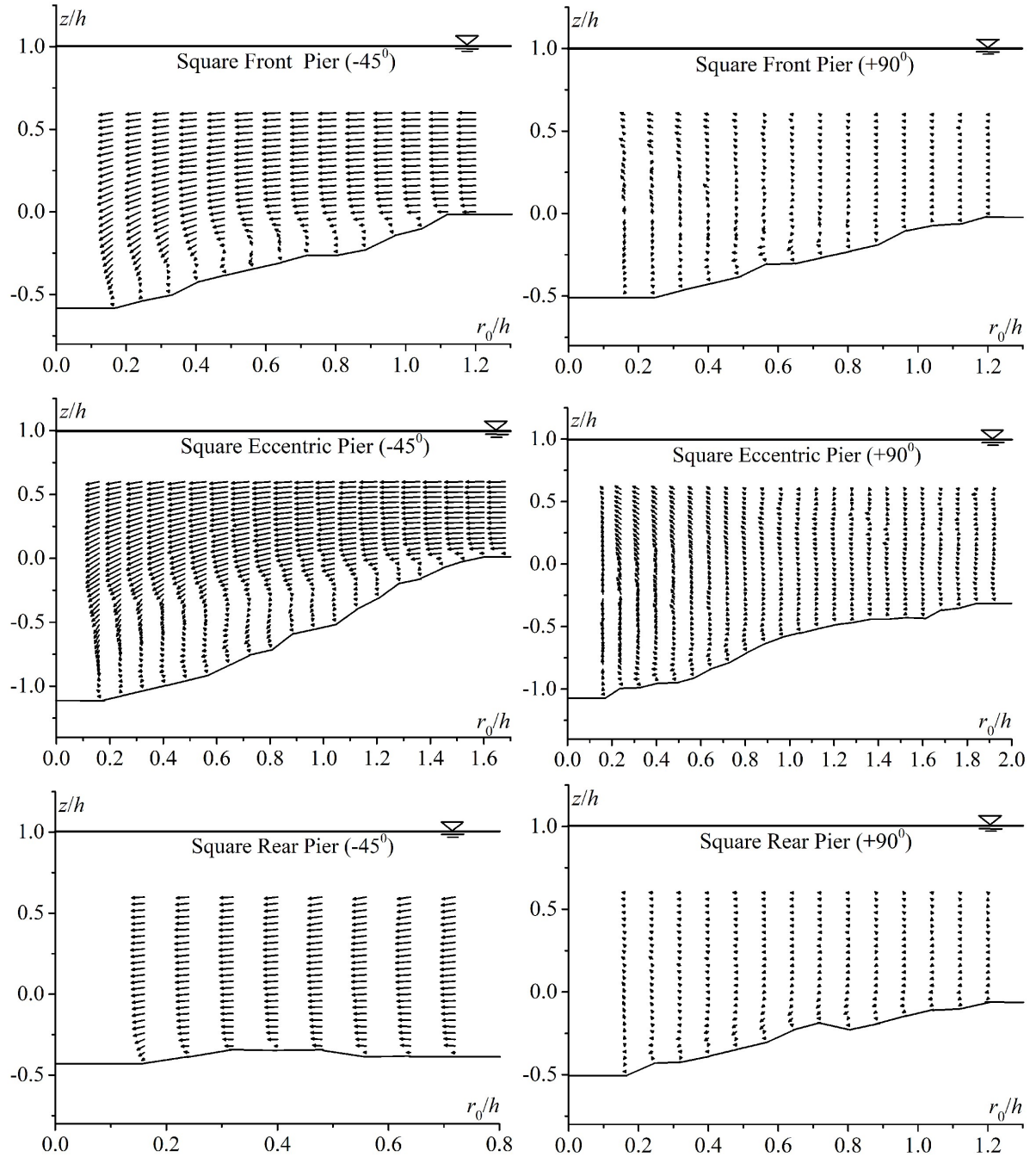


Fig. 4.18. Velocity vector plots for square front, square eccentric and square rear piers at r - z planes for $\theta = -45^\circ$ and 90° .

Each vortex cross section is nearly elliptical in shape, whose major axis is approximately the bisector of angle formed by the slope of scour hole with horizontal. For all three piers, height i.e. minor axis lengths of elliptical vortices at 0° , are larger than that at $\pm 45^\circ$. At 0° for all three square piers, vertical flow is strongest and decreases as θ increases. These elliptical vortices strengths and locations depend on approaching flow velocity. Near pier bases, at high approaching flow velocity, these vortices are stronger.

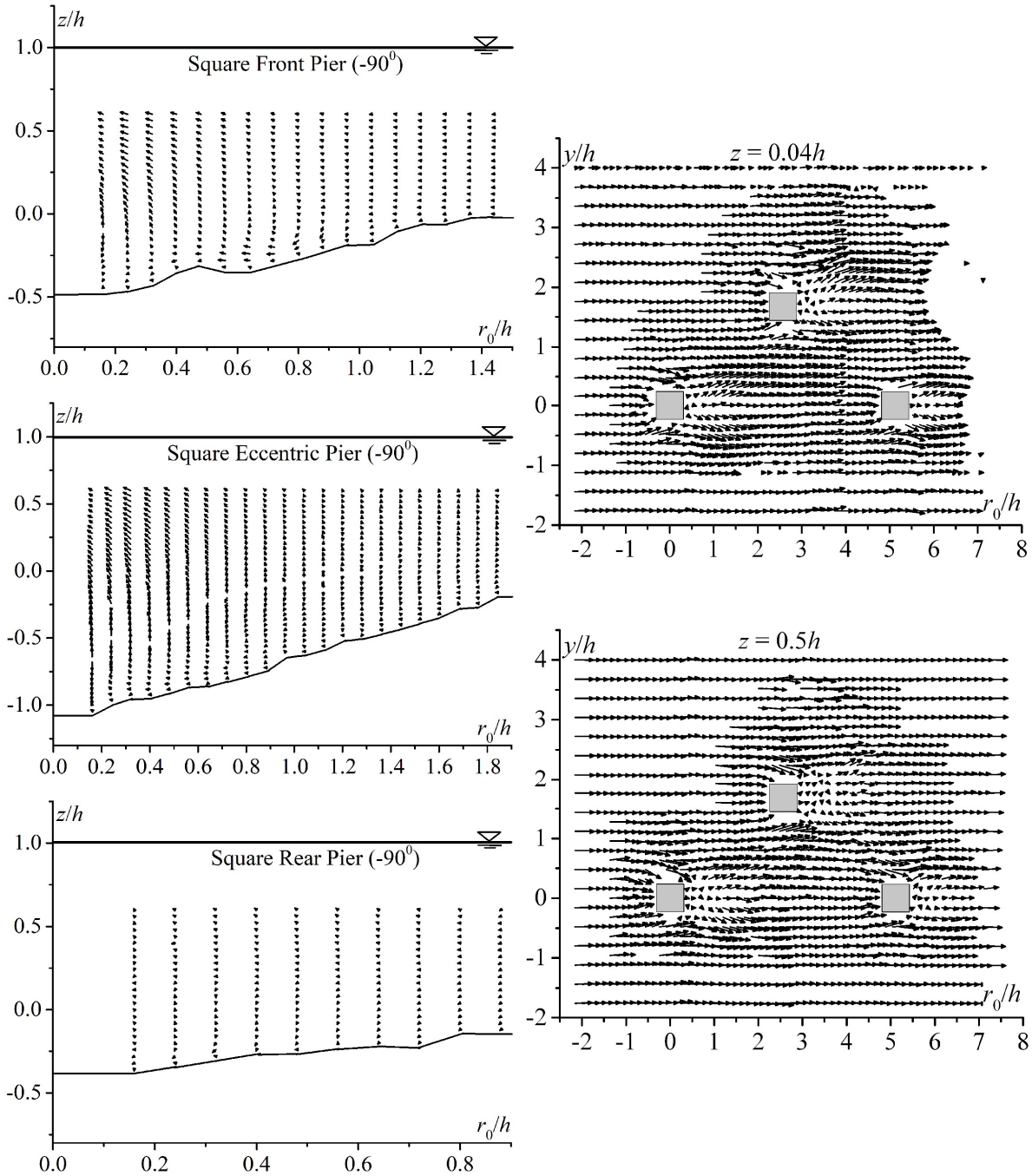


Fig. 4.19. Velocity vector plots for square front, square eccentric and square rear piers at r - z planes for $\theta = -90^\circ$ and at r - y planes for $z=0.5h$ and $z=0.04h$.

Here, vortex core size near square eccentric pier is bigger than vortex core sizes near the square front pier and square rear pier. At $z > 0$ that is above scour hole, directions of flow are horizontal and approaches towards the piers, but the directions are downward near all three piers. At $\pm 90^\circ$ for separated flow, the vertical flows are indistinct. At $\pm 90^\circ$, also a close study of the six vector fields near scoured bed for all piers shows the existence of weaker vortical flow.

The characteristics of flow velocity are well described in the flow zone for $z=0.04h$ and $z=0.5h$ horizontal planes. To evade congested plotting of \vec{v} profile, a few of the measured points are deleted from the plots. From the plotting of \vec{v} , it is clear that in downstream zone

of square front pier, velocity decreases. It is also similar to square eccentric pier and square rear pier. Here, from the profile, wake zone length is larger for square front pier, compared with other two square piers. And the length is larger for square eccentric pier than square rear pier. Wake zone length is larger at $z=0.5h$ than $z=0.04h$ horizontal plane. Due to pier induced adverse pressure gradient near upstream of piers, boundary layer is separated and then shifts both sides of the piers towards downstream near the bed. This phenomenon results in larger wake at $z=0.5h$ horizontal planes in contrast with $z=0.04h$ horizontal plane. This condition is caused by the effect of bed roughness on turbulence increase near the bed.

4.7.1.5 Absolute Velocity

The contour of non-dimensional time mean absolute velocity, $V/U = \sqrt{u^2 + v^2 + w^2} / U$ for equilibrium scour under clear water state at five azimuth-planes 0° , 45° , -45° , 90° and -90° and at two horizontal planes $z=0.04h$ and $z=0.5h$ around the three piers are highlighted in Figs. 4.20, 4.21 and 4.22.

The contour profiles of dimensionless V/U for the square front pier, square eccentric pier, and square rear pier are almost similar. It shows absence of u at 0° and dominating nature of u at $\pm 90^\circ$. At azimuthal angle 0° for all three square piers u is negligible; hence it is evident that there is an exclusive vertical flow at azimuth angle 0° for all the square piers. For the three-piers at $\pm 45^\circ$ azimuthal planes starting from sharp pier edge, flow separation is observed which leads to decrease V near the piers. Also, at $\pm 90^\circ$ azimuthal planes, u is the main flow feature. For all three square piers near scour bed, contour lines of V are concentrated, focusing rapid changes of velocity regions. At $\pm 90^\circ$ u and w are negligible near all the square piers because pier side faces and direction of flow are parallel with each other.

Fig. 4.22 confirms that V increases as R_0 increases. From the dimensionless contour profiles, it is clear that in wake regions at downstream near the piers has lower values of time mean absolute velocity V . At r - y horizontal planes for $r=6.5$ to 7.5 , V decreases near the bed since the flow is obstructed by deposited sediment i.e. dune at pier downstream. At the downstream near the piers (wake zones) V has greater values at $z=0.5h$ plane than that at $z=0.04h$ plane.

4.7.2 Vorticity and Circulation

Figures 4.23, 4.24 and 4.25 exhibit contours of vorticity $\zeta = (\partial v / \partial z - \partial w / \partial r)$ for equilibrium scour holes at 0° , 45° , -45° , 90° and -90° azimuthal angles at r - z planes around square front, square eccentric and square rear piers.

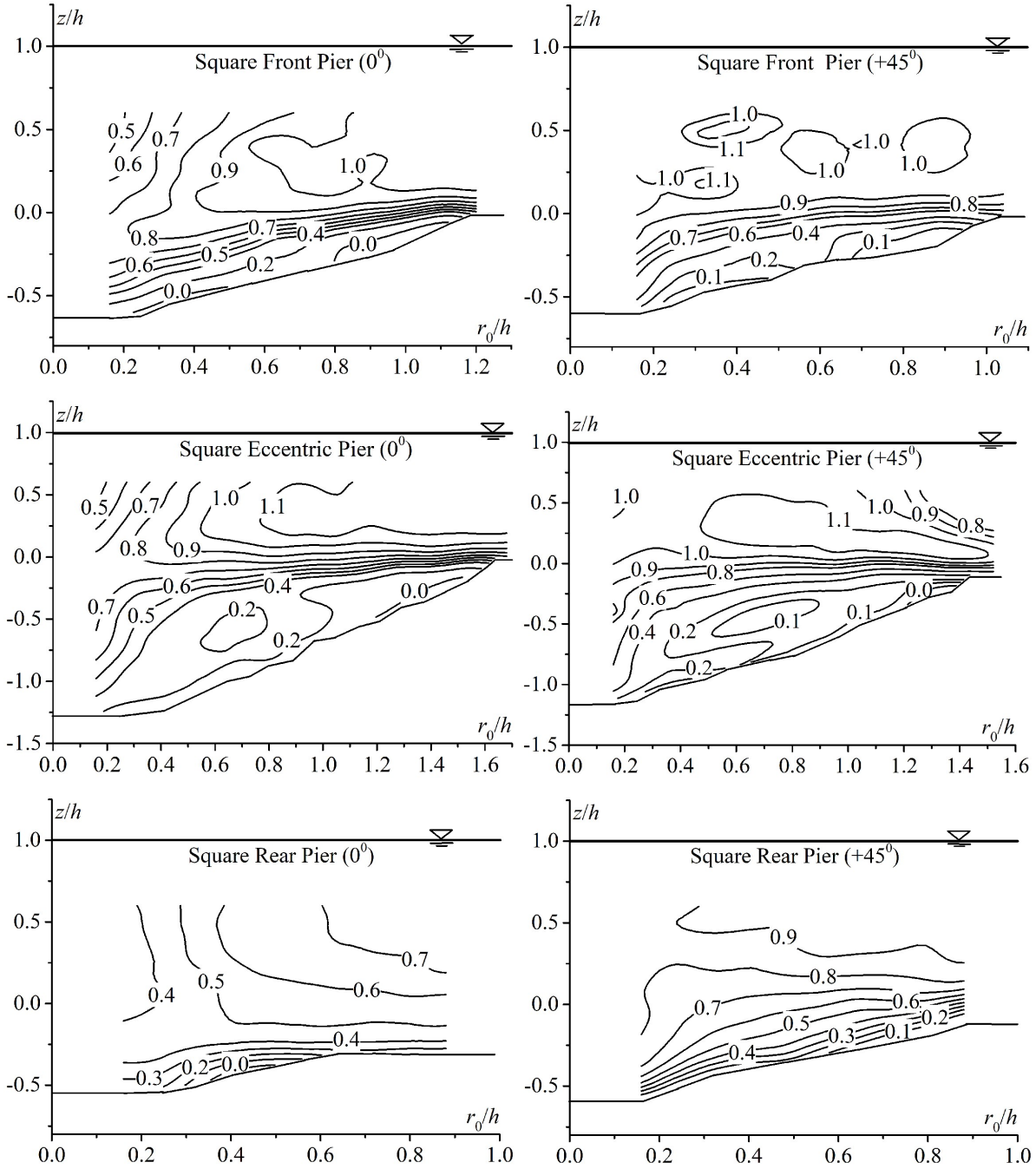


Fig. 4.20. Contours of non-dimensional absolute velocity (V/U) for square front, square eccentric and square rear piers at r - z planes for $\theta = 0^\circ$ and 45° .

For computing vorticity contours using a technique of forward difference of computational hydrodynamics, differential equation is converted into an equation of finite difference.

At a grid point, (i,k) vorticity equation (1) is expressed as

$$\zeta = \frac{v_{i,k+1} - v_{i,k}}{\Delta z} - \frac{w_{i+1,k} - w_{i,k}}{\Delta r} + O(\Delta z, \Delta r) \quad (4.1)$$

where index i and index k run towards r and z -directions, respectively. Here, $O(\Delta z, \Delta r)$ is called ‘terms of order Δz and Δr ’. The scale model of above equation is given as in equation (4.2).

$$\zeta = \left(\frac{\partial v}{\partial z} - \frac{\partial w}{\partial r} \right) \approx \left(\frac{V}{Z} - \frac{W}{R} \right) \quad (4.2)$$

where, V , W , Z and R are scaled variables of v , w , z and r respectively.

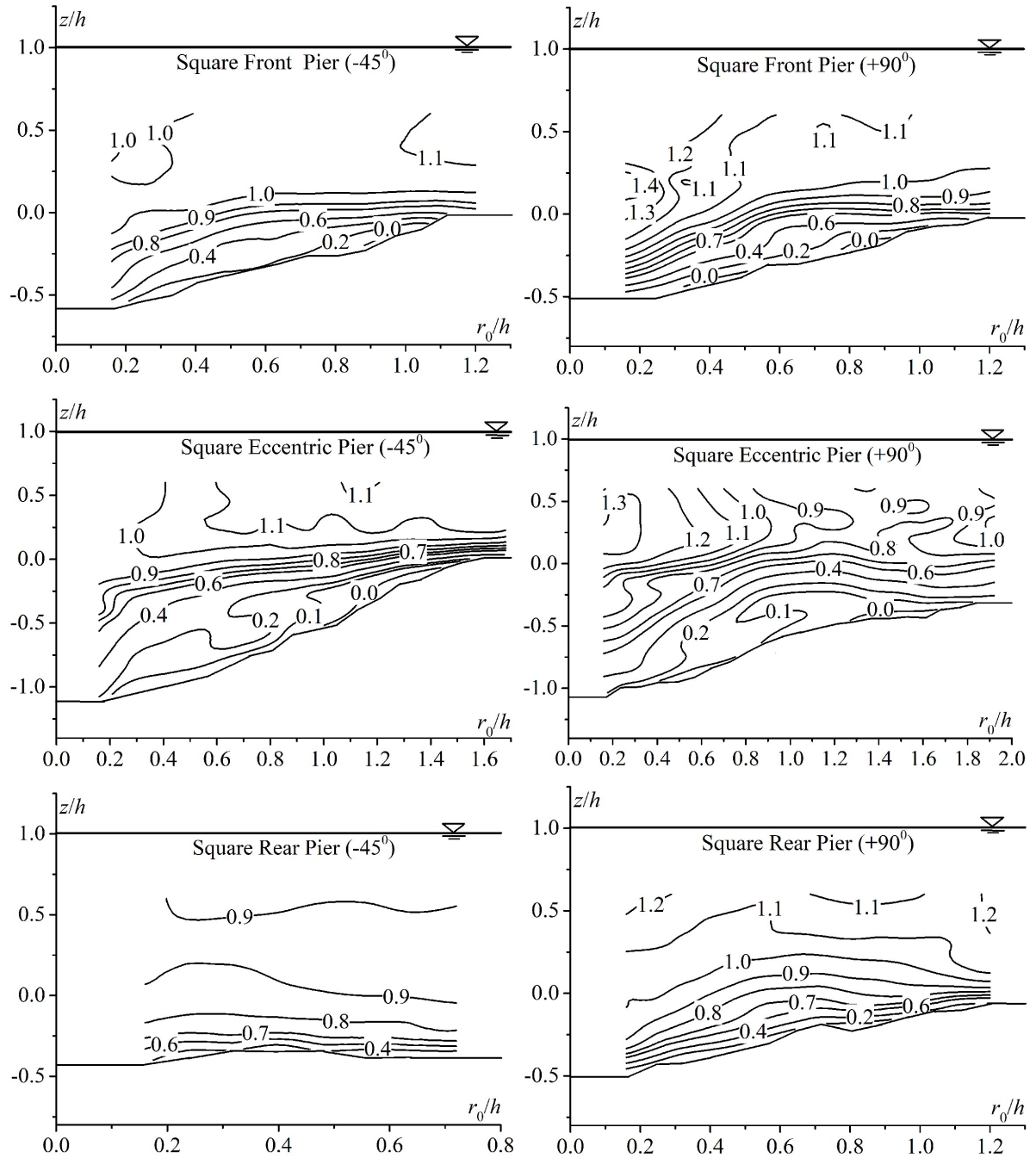


Fig. 4.21. Contours of non-dimensional absolute velocity (V/U) for square front, square eccentric and square rear piers at r - z planes for $\theta = -45^\circ$ and 90° .

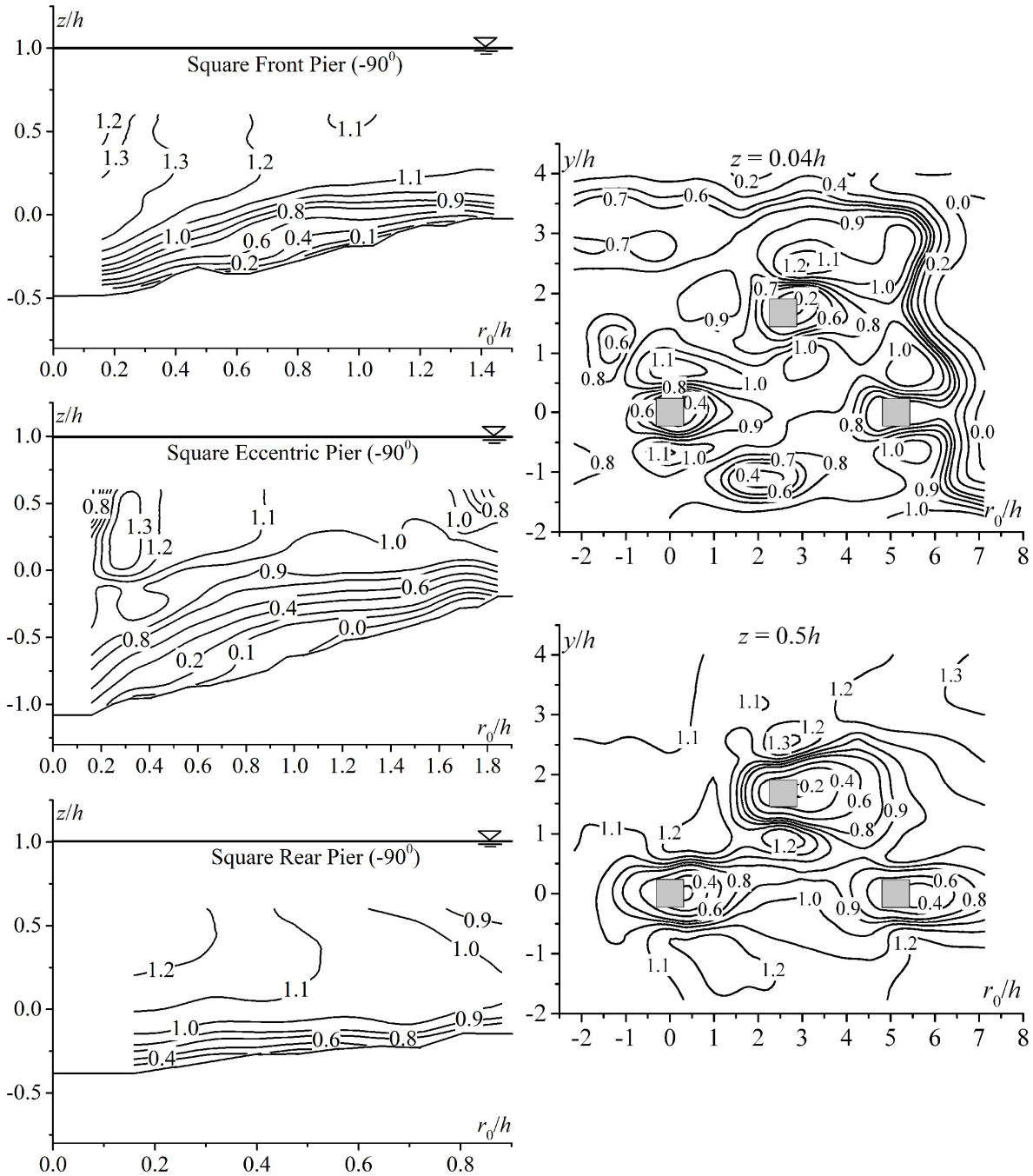


Fig. 4.22. Contours of non-dimensional absolute velocity (V/U) for square front, square eccentric and square rear piers at r - z planes for $\theta = -90^\circ$ and at r - y planes for $z=0.04h$ and $z=0.5h$.

Only at pier boundaries where there is a presence of pressure gradient, formation of vorticity occurs. When the pressure increases sufficiently to become strong, subsequently 3D boundary layer goes through flow separation and system rolls up, front side near each pier, forming horseshoe vortex system at all the bases of piers. This type of vertical flow is measured particularly in the r - z plane, as its axis of rotation is erect to the r - z plane. Vorticity contours are calculated from the contours of v and w . Figs. 4.23, 4.24 and 4.25, contours of vorticity, confirms that the vorticities are concentrated inside the scour holes. Further study of velocity vector plots and vorticity contours confirm that the flow is a forced type vortex flow. Near centre of the horseshoe vortex, a high vorticity concentration shows the vortex core.

Vortex core size decreases as θ increases, becoming relatively smaller at $\pm 90^\circ$ and vorticity is significantly weaker.

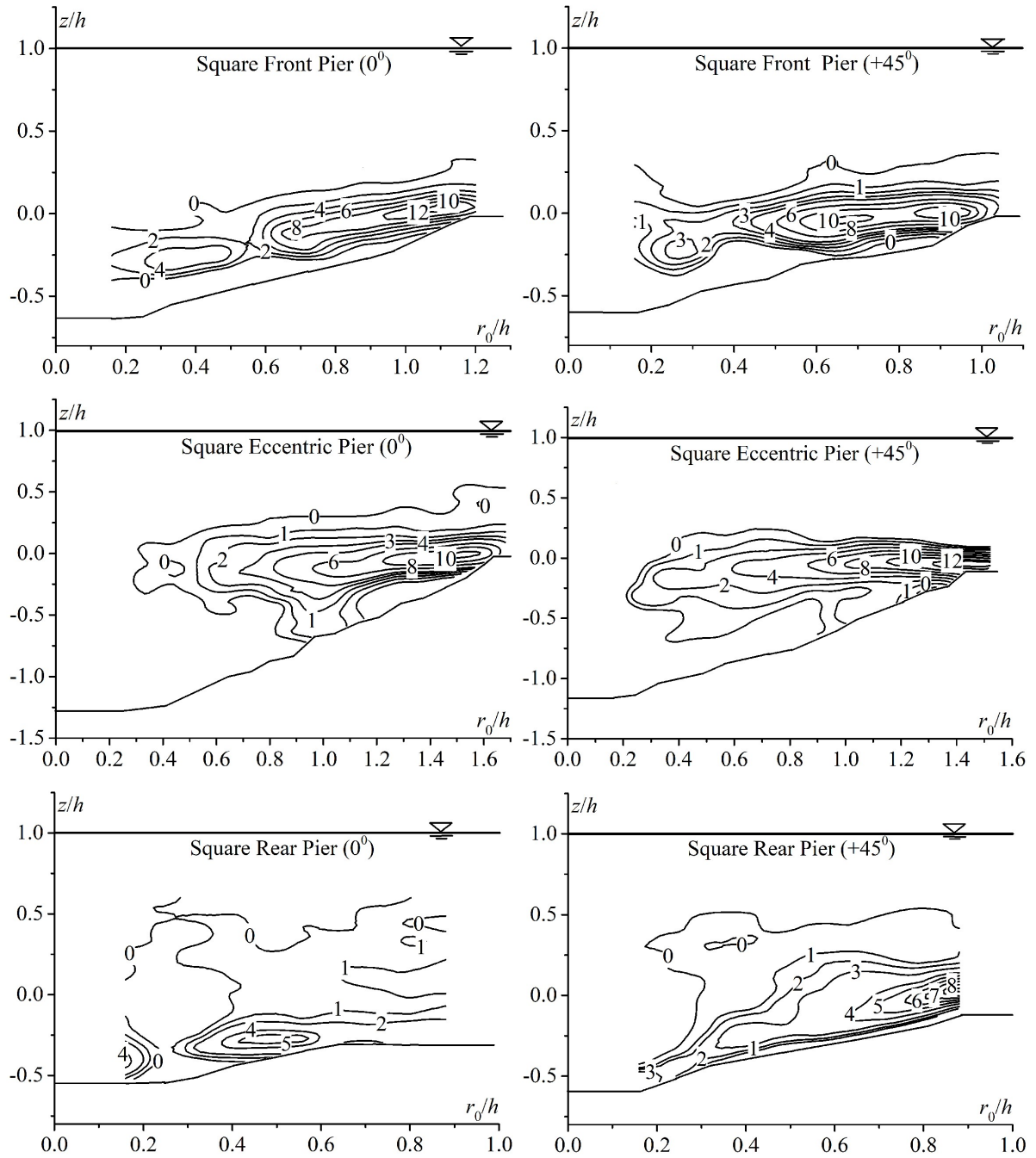


Fig. 4.23. Contours of vorticity ζ (in s^{-1}) for square front, square eccentric and square rear piers at r - z planes for $\theta = 0^\circ$ and 45° .

At upstream of each pier, circulation of each horseshoe vortex is calculated from vorticity contours, using normalized Stokes' theorem [equation (4.3)].

$$\Omega = \oint_c \vec{v} \cdot d\vec{s} = \iint_A z \cdot d(rz) \quad (4.3)$$

where, \vec{v} = velocity vector, and $d\vec{s}$ = displacement vector. The circulations summed up for five azimuthal planes around the three piers are given in Table 4.4.

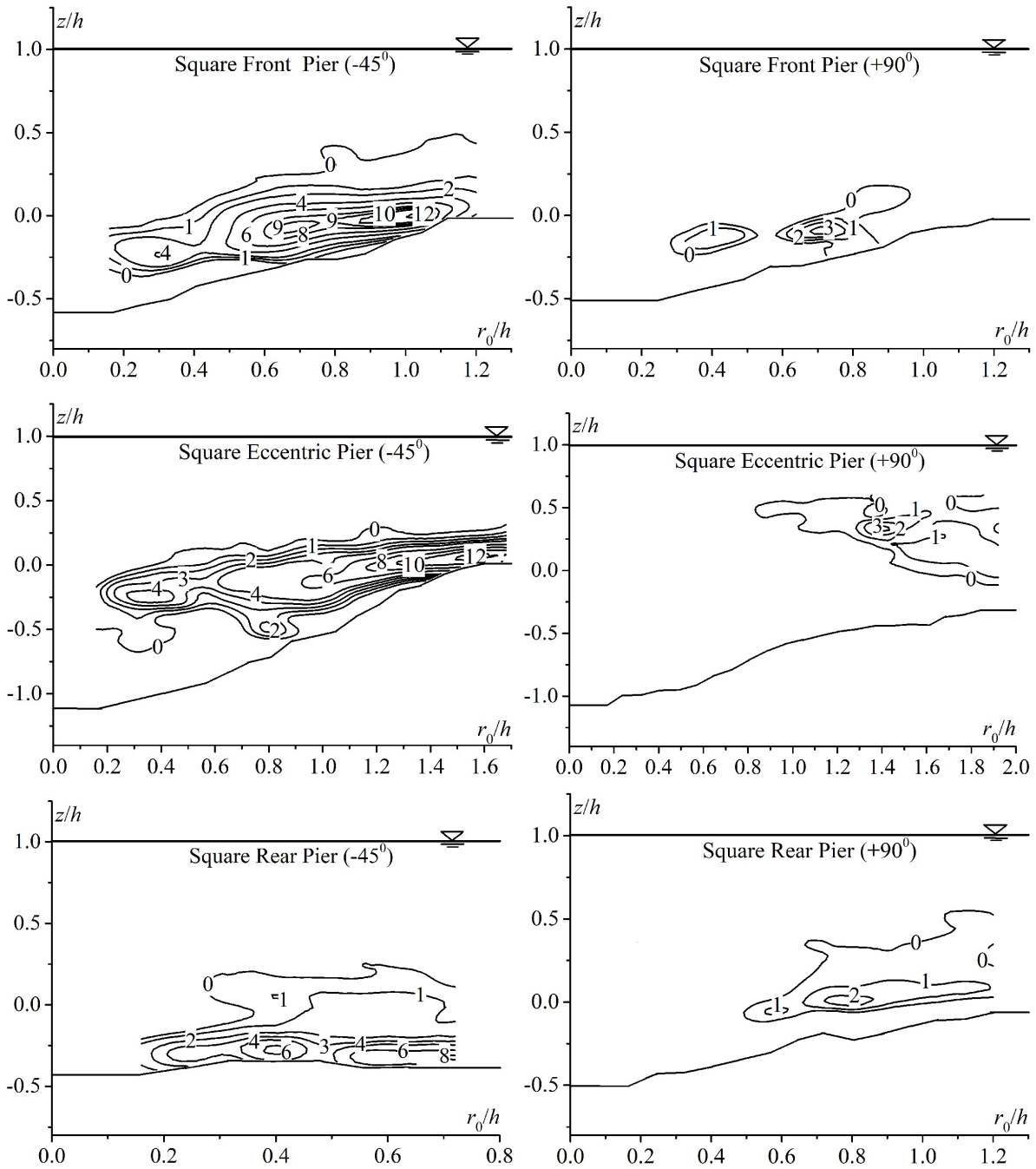


Fig. 4.24. Contours of vorticity ζ (in s^{-1}) for square front, square eccentric and square rear piers at r - z planes for $\theta = -45^\circ$ and 90° .

As azimuthal angle (negative/positive) increases circulation decreases. The circulation increases as scour depth increases. At azimuthal angles 0° , 45° , -45° , 90° and -90° near upstream zone of the front square pier circulations are found 0.71, 0.83, 0.31 and 0.35 times of respective circulation at 0° . Likewise for square eccentric pier and square rear pier at azimuthal angles 0° , 45° , -45° , 90° and -90° , values of Ω are calculated as 0.73, 0.65, 0.37, 0.32 and 0.83, 0.95, 0.34, 0.40 times of circulation at 0° for corresponding pier. The calculated values of Ω are in obedience with the past researchers [Dey and Raikar (2007) and Das and Mazumdar (2018)] and also affirms that Ω decreases steadily from azimuthal

angle 0° to $\pm 45^\circ$ and then decreases rapidly from $\pm 45^\circ$ to $\pm 90^\circ$. Therefore horseshoe vortex core size becomes somewhat small when shifts from 0° to $\pm 45^\circ$ and further becomes smaller when shifts from for $\pm 45^\circ$ to ± 90 .

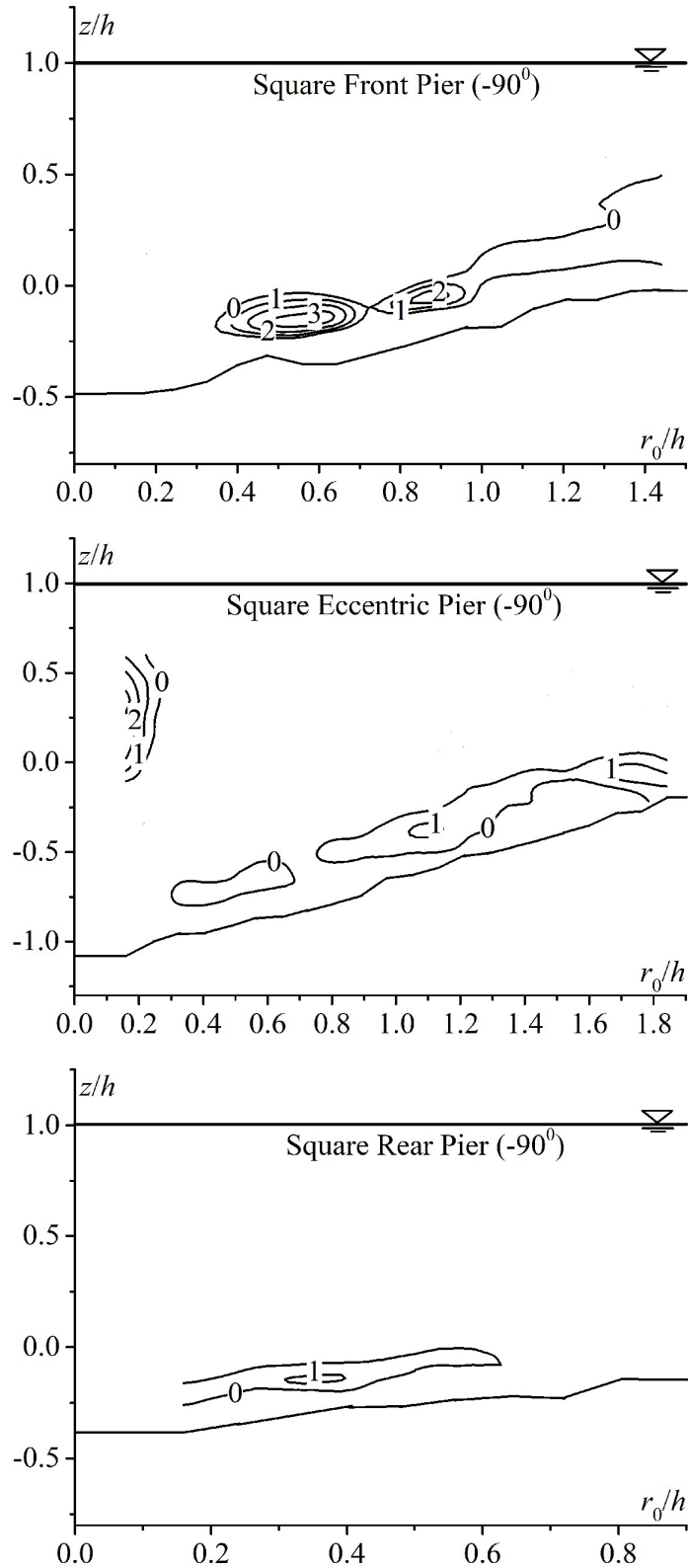


Fig. 4.25. Contours of vorticity ζ (in s^{-1}) for square front, square eccentric and square rear piers at r - z planes for $\theta = -90^\circ$.

Due to existence of square eccentric pier, the separated streamline from square front pier at -45° concurs with streamline separated at 45° . In $r-\theta$ plane, direction of resultant velocity $[\tan^{-1}(u/v)]$ for square front pier at 45° is apart from square eccentric pier but at -45° it is along square eccentric pier. As a result for square front pier, a strong pressure gradient is observed at azimuthal angle -45° than that at 45° . At -45° azimuthal angle of square front pier, separated streamline joins with another separated streamline near azimuthal angle 45° of square eccentric pier and also for square eccentric pier separated streamline at azimuthal angle 45° coincides with separated streamline near azimuthal angle -45° of square rear pier. Hence, Ω at square eccentric pier at 45° is greater than Ω at -45° azimuthal angle and at square rear pier, Ω at -45° azimuthal angle is greater than at 45° azimuthal angle. As a result, effect of co-shedding regime develops in wake region of square front pier, for square eccentric pier at 90° azimuthal angle is slightly higher than Ω at -90° and for square rear pier at -90° is slightly higher than that at 90° .

Table 4.4. Circulation Ω for five azimuth angles in $r-z$ plane (units in $10^{-2} \times \text{m}^2/\text{s}$).

Pier position	Circulation, Ω				
	$\theta = 0^\circ$	$\theta = 45^\circ$	$\theta = -45^\circ$	$\theta = 90^\circ$	$\theta = -90^\circ$
Square front	1.875×10^{-2}	1.328×10^{-2}	1.562×10^{-2}	0.579×10^{-2}	0.656×10^{-2}
Square eccentric	2.862×10^{-2}	2.101×10^{-2}	1.865×10^{-2}	1.048×10^{-2}	0.944×10^{-2}
Square rear	1.526×10^{-2}	1.273×10^{-2}	1.444×10^{-2}	0.525×10^{-2}	0.613×10^{-2}

In present study, it is evident, that Ω at five azimuthal angles around square eccentric pier is constantly greater than Ω at corresponding five azimuthal angles around square front pier and square rear pier. Around square front pier, circulation is calculated greater than that at corresponding azimuthal angle around square rear pier. At the five azimuthal angle 0° , 45° , 90° , -45° and -90° around square eccentric pier, magnitudes of circulation are 53%, 58%, 19%, 81%, 43% and 87%, 65%, 29%, 99%, 53% greater than the magnitudes of circulation at corresponding θ around square front pier and square rear pier, respectively. This nature specifies the subsequent rise in sizes of vortices in $r-z$ planes and rise in $\partial v/\partial z$ at corresponding locations which are well depicted in figures of non-dimensional tangential velocity contours and velocity vectors plots.

4.7.3 Turbulence Fields

The tangential turbulent intensity $u^+ = \sqrt{u'u'}$, radial turbulent intensity $v^+ = \sqrt{v'v'}$ and vertical turbulent intensity $w^+ = \sqrt{w'w'}$ are the Root Mean Square (RMS) values of velocity fluctuations of flow u , v and w , correspondingly. The dimensionless tangential turbulent intensity $\sqrt{u'u'}/U$, dimensionless radial turbulent intensity $\sqrt{v'v'}/U$ and dimensionless vertical turbulent intensity $\sqrt{w'w'}/U$ at an azimuth plane 0° and at two

($z=0.04h$ and $z=0.5h$) horizontal planes around the three square piers are presented in Figs. 4.26, 4.27 and 4.28, respectively. From these figures, it is apparent that the distribution nature of u^+ , v^+ and w^+ are almost identical both at r - z plane and corresponding r - y plane.

Here, at square front pier at azimuthal plane 0° , the maximum turbulent intensities are found around $1.33b$ to $1.70b$ from pier centre. Whereas, in an experiment with two piers at square front pier at 0° those are found about $1.35b$ to $1.50b$ from pier-centre [Das and Mazumdar (2018)] and for single pier experiment, those are found around $0.85b$ and $1.50b$ from pier centre [Dey and Raikar (2007) and Das and Mazumdar (2015a)].

Generally, from the Figs. 4.26 and 4.27, within scour holes a high turbulence intensity core is found thus, separation of flow and turbulence intensities decreases as r_0 and z increases. With the greater scour hole around the square eccentric pier, high turbulence intensity cores are found. With the change in θ , there is a minor modification in the distribution nature of u^+ , v^+ and w^+ (not shown in present study).

Here, for square front pier maximum value of $\sqrt{u'u'}/U$ and maximum value of $\sqrt{v'v'}/U$ are found 1.75 and 1.95 times the maximum value of $\sqrt{w'w'}/U$, whereas for square single pier experiment maximum values of $\sqrt{u'u'}/U$ and $\sqrt{v'v'}/U$ are 2.04 and 2.29 times of the maximum value of $\sqrt{w'w'}/U$ [Das and Mazumdar (2015a)] and for two square pier experiment for square front pier, maximum values of $\sqrt{u'u'}/U$ and $\sqrt{v'v'}/U$ are 2.11 and 2.55 times of the maximum value of $\sqrt{w'w'}/U$ [Das and Mazumdar (2018)].

In present study for square eccentric pier and square rear pier at 0° , maximum values of $\sqrt{u'u'}/U$ and $\sqrt{v'v'}/U$ are found higher than the maximum values of $\sqrt{u'u'}/U$ and $\sqrt{v'v'}/U$ of square front pier at 0° . Also at 0° for square eccentric pier and square rear pier maximum values of $\sqrt{u'u'}/U$, $\sqrt{v'v'}/U$ and $\sqrt{w'w'}/U$ are 1.16, 1.46, 1.32 and 1.11, 1.10, 1.34 times of the maximum values of $\sqrt{u'u'}/U$, $\sqrt{v'v'}/U$ and $\sqrt{w'w'}/U$ for square front pier at 0° , respectively.

As a result of shed vortices, observed from downstream zone of square front pier and from downstream zone of square front pier and square eccentric piers, associated with horseshoe vortices close to upstream region of square eccentric and upstream region of square rear piers, higher values of u^+ , v^+ and w^+ for square eccentric and square rear piers are found. As these shed vortices are mixed with large tangential fluctuations, maximum v^+ is 1.14 times greater than maximum u^+ at 0° for square eccentric pier. Also approaching shed vortices from square front pier and square eccentric pier were directly clogged by square rear pier; hence maximum v^+ is 1.15 times greater than maximum u^+ at 0° for square rear pier. Similar investigation was noticed for piers in tandem where v^+ was nearly twice of u^+ [Ashtiani and Kordkandi (2013)]. The magnitude of w^+/U at 0° for square eccentric pier was slightly lesser and for square rear pier was slightly greater than w^+/U at 0° for square front pier.

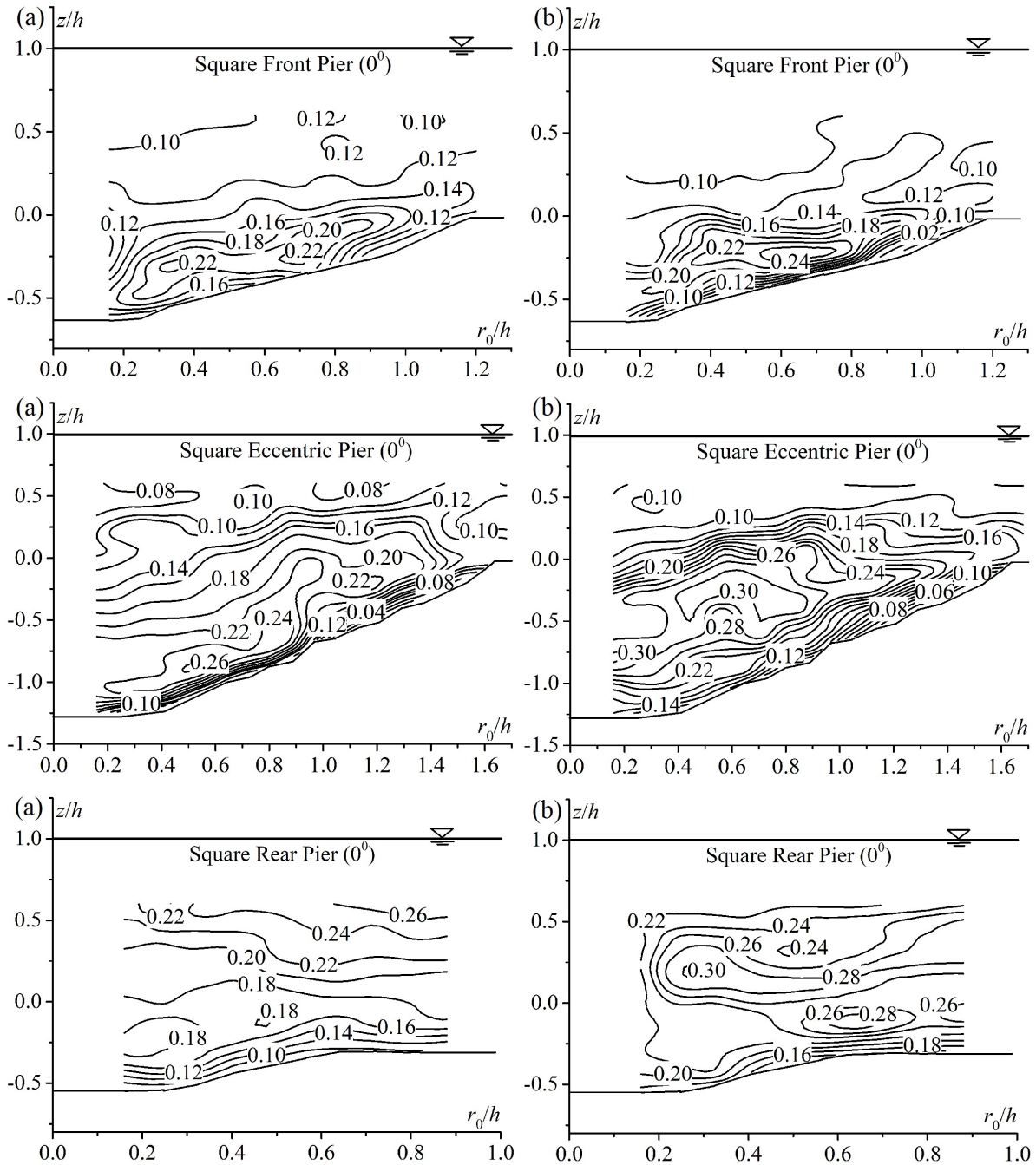


Fig. 4.26. Contours of non-dimensional (a) tangential (u^+/U) (b) radial (v^+/U) turbulent intensities for square front, square eccentric and square rear piers at r - z plane for $\theta = 0^\circ$.

This occurrence is responsible for reducing and increasing nature of down flow near the upstream region of square eccentric pier and square rear pier, respectively, for the existence of up-flow in reattachment regime (gap between three piers).

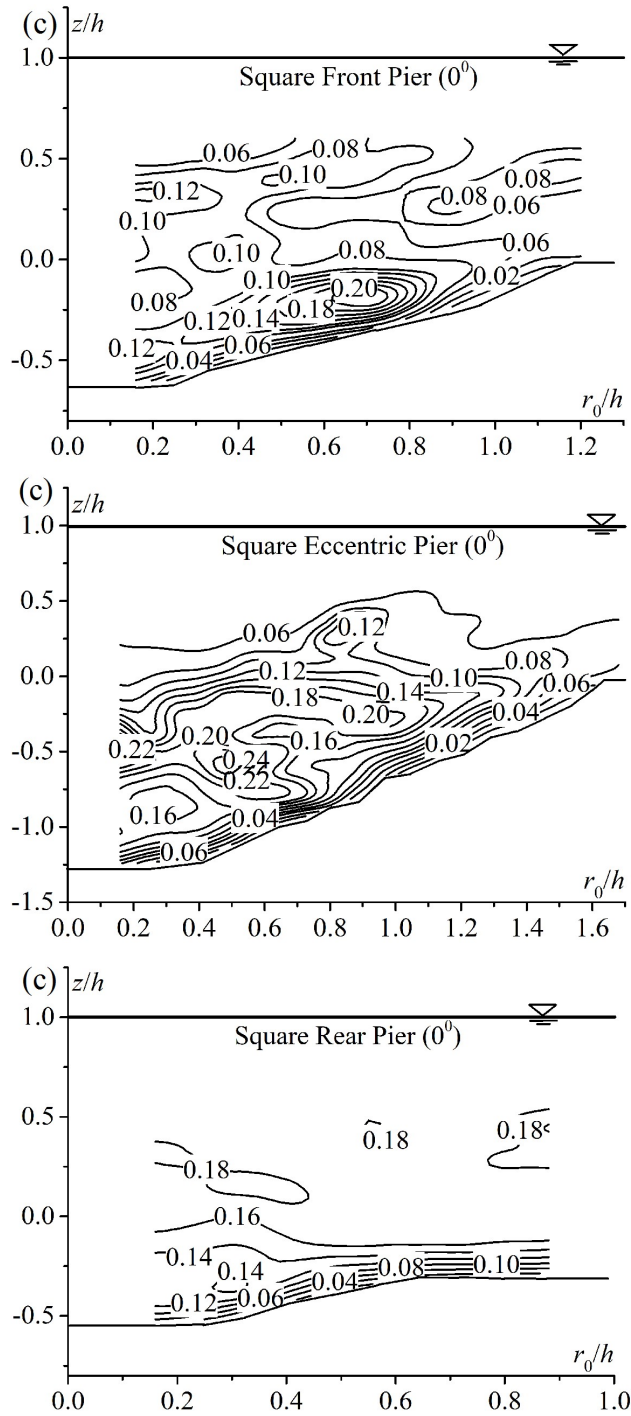


Fig. 4.27. Contours of non-dimensional vertical turbulent intensity (w^+/U) for square front, square eccentric and square rear piers at r - z plane for $\theta = 0^\circ$.

From Figs. 4.28, maximum values of $\sqrt{u'u'}/U$, $\sqrt{v'v'}/U$ and $\sqrt{w'w'}/U$ are observed just near upstream of square front pier, square eccentric pier and square rear pier having magnitudes of 0.90, 0.80 and 0.35, respectively. Overall value of longitudinal turbulence intensity u^+ is noticed almost higher at all corresponding locations around the piers (at two different horizontal planes, $z=0.04h$, and $z=0.5h$) than transverse turbulence intensity v^+ and vertical turbulence intensity w^+ .

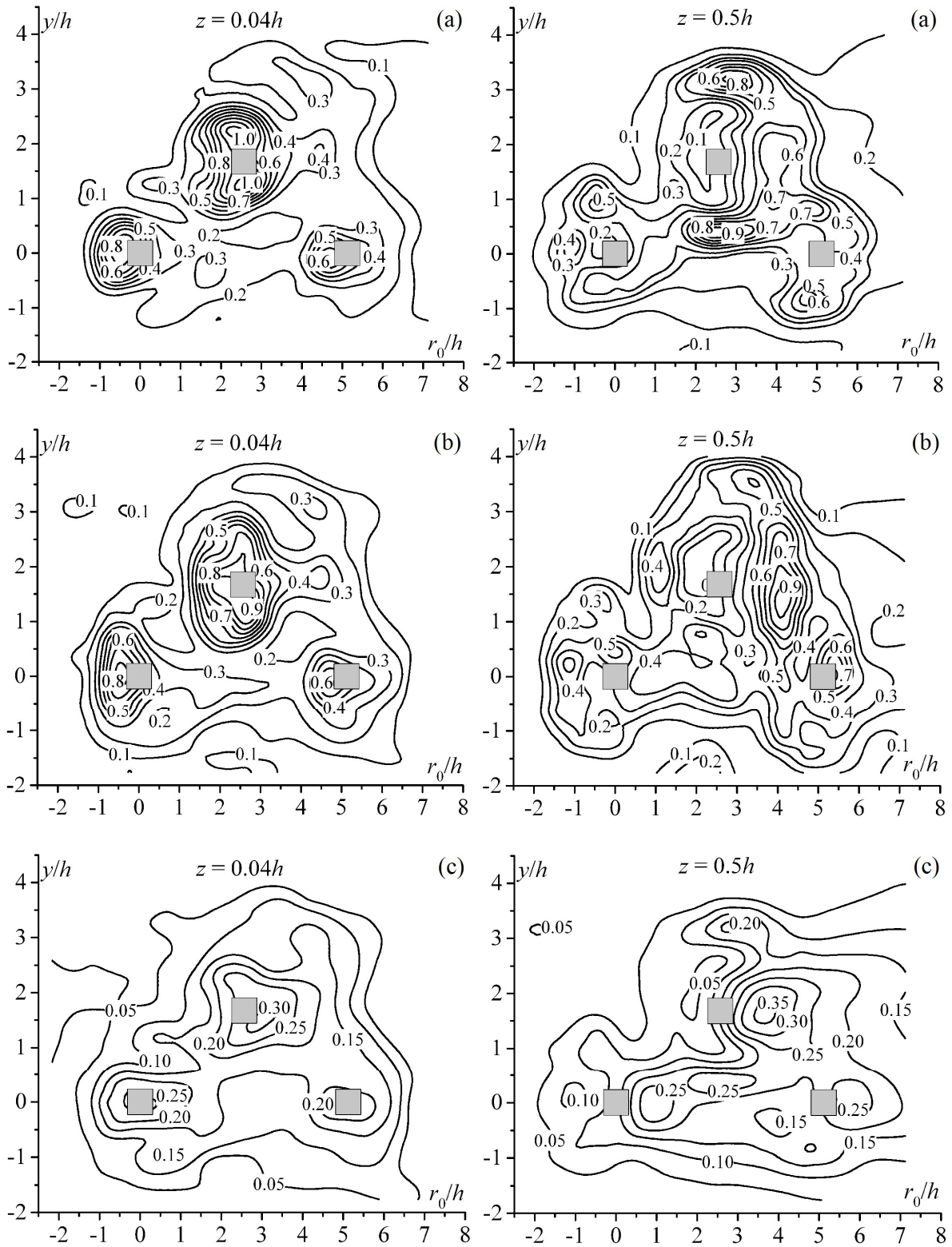


Fig. 4.28. Contours of non-dimensional (a) tangential (u^+/U), (b) radial (v^+/U), and (c) vertical (w^+/U) turbulent intensities for square front, square eccentric and square rear piers at r - y plane for $z=0.04h$ and $z=0.5h$.

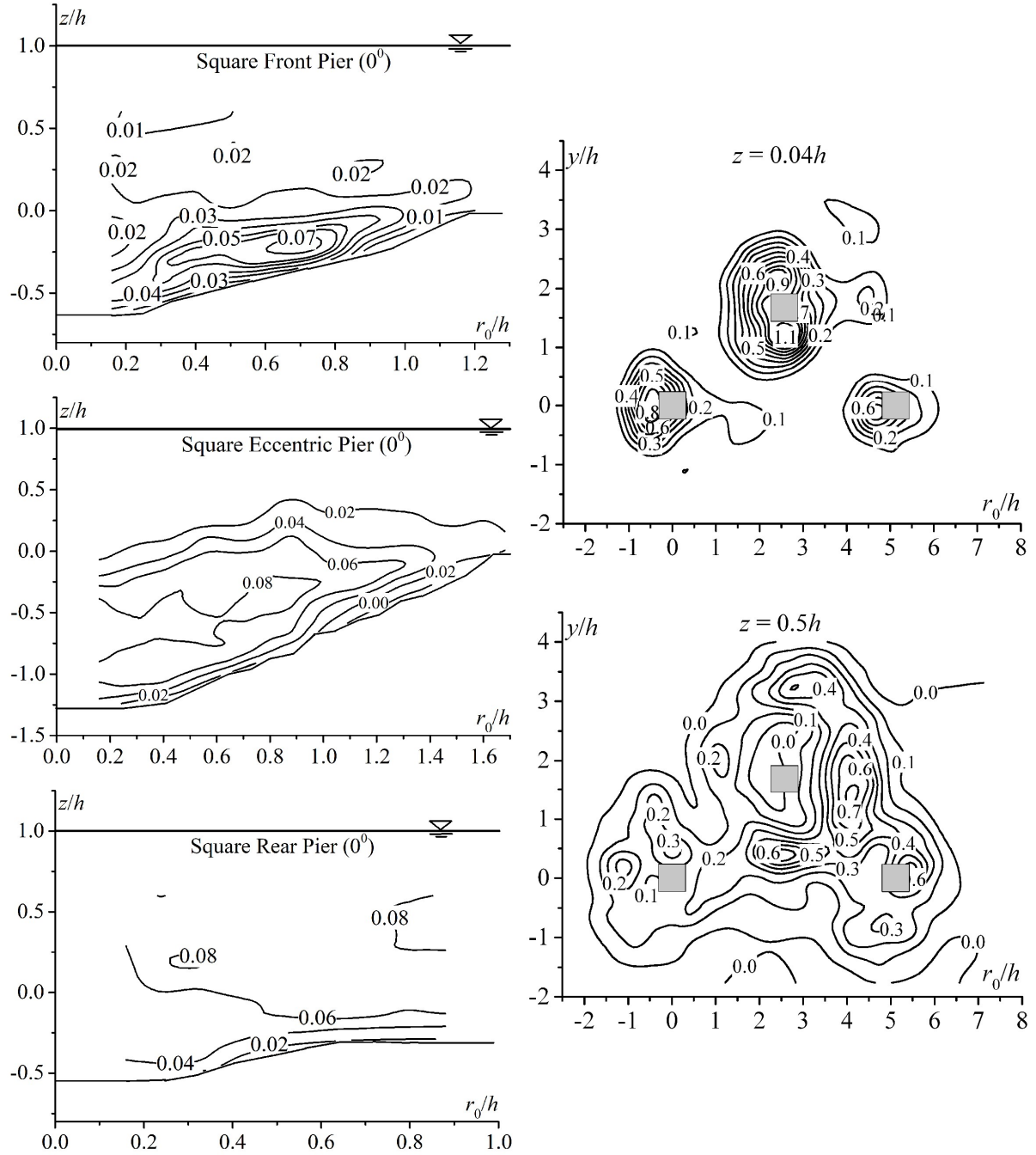


Fig. 4.29. Contours of non-dimensional turbulent kinetic energy (k/U^2) for square front, square eccentric and square rear piers at r - z plane for $\theta = 0^\circ$ and at r - y plane for $z = 0.04h$ and $z = 0.5h$.

Non-dimensional turbulent kinetic energy (k/U^2) at an azimuthal plane 0° and at two ($z = 0.5h$ and $z = 0.04h$) horizontal planes around three square piers are calculated and plotted in Fig. 4.29, using the equation (4.4).

$$k/U^2 = \frac{1}{2}(u'^2 + v'^2 + w'^2)/U^2 \quad (4.4)$$

The profiles of k/U^2 are almost alike with the profiles of non-dimensional turbulence intensities. For square eccentric pier and square rear pier at 0° , maximum values of k are 1.40 and 1.33 times of the maximum values of k for square front pier, respectively. According to two square pier experiment [Das and Mazumdar (2018)], at 0° for square eccentric pier it was

found 1.27 times of maximum value of k for square front pier. At 0° for square eccentric pier and square rear pier, maximum values of $\sqrt{u'u'}/U$, $\sqrt{v'v'}/U$ are greater than maximum values of $\sqrt{u'u'}/U$, $\sqrt{v'v'}/U$ for square front pier at 0° , respectively. Also at 0° for square eccentric pier and square rear pier, maximum value of k are higher than maximum values of k for square front pier at 0° azimuthal plane as shown in Fig. 4. 29 (All are not shown here).

From the Fig. 4.29, maximum value of non-dimensional turbulence kinetic energy i.e. k/U^2 just near the bed ($z=0.04h$) was found more in the order of magnitude around the square eccentric pier, then square front pier and square rear pier, respectively. Whereas at $z=0.5h$, maximum value of k was found around square eccentric pier, then square rear pier and square front pier in order of magnitude, respectively. Hence, it is clear that strongest vortices will form and circulation will occur at square eccentric pier. As a result of formation and shedding of shed vortices with very powerful rollers, higher magnitude core of k is found at wake zone of square eccentric pier, whereas values of k are lesser in the upstream region of the pier. At $z=0.5h$, maximum value of k are always higher than those at $z=0.04h$. The distributed nature of turbulence kinetic energy is similar to the high-value cores of turbulent intensities, found within the scour hole region.

4.8 Conclusions

Here, flow nature consequently the hydrodynamics of scour hole development were executed experimentally at clear water and equilibrium condition around three identical square piers with front, rear, and eccentric arrangement. The eccentricity was kept equal to $3b$ and the longitudinal spacings between the square front pier to square rear pier and square eccentric pier were 1.0 times and 0.5 times of the lengths of the scour affected zone of the single square pier experiment, respectively. Around the piers, distribution of flow fields and turbulence fields are studied using a velocimeter by measuring velocities instantaneously. Due to existence of scour holes, both flow development and flow intensities vary within these piers. The contours of non-dimensional time mean velocities, vector plots, non-dimensional turbulence intensities, non-dimensional turbulence kinetic energy are well explained. The major conclusions drawn are addressed below.

Maximum equilibrium scour depth gauged at square front pier, square eccentric pier and square rear pier are about 1.5, 3.1 and 1.4 times larger than single pier maximum equilibrium scour depth. Also, these maximum scour depths at three piers are more than two pier experiment with inline eccentric arrangement. The dune formation is more on the square eccentric pier side which is away from the line of symmetry. The diversion angle representing the sediment shifting is seen more on square eccentric pier side.

The longitudinal velocity u increases in between inline square front, square rear pier and square eccentric pier. This velocity component increases in the downstream of the piers near the bed. At 0° , for square eccentric pier and square rear pier, maximum values of u are found 1.17 and 2.44 times of the value of u at 0° for square front pier. As azimuthal angle θ increases, u increases and turns finite.

The radial velocity v changes its direction on both side of zero contour line ($v=0$) within the scour holes near pier bases. Along azimuthal angles 0° , 45° , 90° , -45° and -90° , around square eccentric pier (away from pier bases) v is higher than v for two inline square front pier and square rear pier at corresponding angles.

At 0° , upstream region of square eccentric pier maximum values of w are 1.05 and 1.89 times of maximum value of w at corresponding locations of square front pier and square rear pier, respectively. This validates the clear existence of co-shedding regime formed within the three square piers at downstream of square front pier and square eccentric pier.

The plotting of velocity vectors depict the horseshoe vortex characteristics at upstream region of each pier and wake vortex at downstream region of each pier. Size of horseshoe vortex core for square eccentric pier is ever larger than other two square front pier and square rear pier. Here, in order of magnitude, the wake zone length is largest for square front pier, then square eccentric pier and then square rear pier. Larger wake at $z=0.5h$ horizontal planes is found in comparison with $z=0.04h$ horizontal plane. These vortices take a bigger role in development of scour holes around three piers and large around square eccentric pier than other two piers.

Turbulence flow mixing acts as a conclusive role in developing turbulent logarithmic and turbulent outer layers as friction drag is lower than pressure drag. Due to presence of bluff body effect and separated streamline, at square eccentric pier horseshoe-vortex distributions are not similar with square front and square rear pier. The vortex circulation Ω increases as θ decreases and also increases for a corresponding increase in scour depth. The magnitude of Ω at 0° , 45° , 90° , -45° and -90° around square eccentric pier are all the time greater than Ω at corresponding azimuthal angles around square front pier and square rear pier. Strongest vortices and circulation are found at square eccentric pier. For square front pier and square rear pier, at -45° Ω is always found greater than Ω at 45° because of the existence of stronger pressure gradient. Whereas, Ω for square eccentric pier at -90° is less than that at 90° as the presence of co-shedding regime that develops near wake region of square front pier.

The three turbulence intensities and turbulent kinetic energy are detected above and within the scour holes. Their maximum magnitudes around square eccentric pier is found greater than their maximum magnitudes around square front and square rear piers. Tangential and radial turbulence intensities and turbulence kinetic energy for square eccentric pier are consistently seen greater than that of the square rear pier and square front pier. Whereas vertical turbulence intensity for square eccentric pier at 0° is slightly lesser and for square rear pier is slightly greater than w^+ at 0° for square front pier due to reducing and increasing nature of down flow near the upstream zone for square eccentric pier and square rear pier, respectively, for the existence of up-flow in reattachment regime. Also, the three turbulence velocity intensity and k at 0° square rear pier are greater than for square rear pier.

Here all the flow patterns are well described which are uniquely related to square three-pier arrangement that differs from previous square single-pier or square two-pier researches. Hence, for better prediction of maximum scour depths at piers, the influence of flow characteristics on maximum scour depth can be converted into the semi empirical equations. The experimental consequences from this research may be applied as valuable

records of data for related further researches but also for confirming complex turbulence velocity fields achieved by numeral simulations.

As a result of the two inline square front and square rear piers and one square eccentrically arranged pier can cause sand to shift along the flume wall carrying downstream. The dune development is found maximum on square eccentric pier side and the diversion angle for sand shifting is also maximum. From the region between the piers the sand is shifted and deposited further downstream towards square eccentric pier side and thereafter the sidewall in the same direction. Within the three piers, formed vortices increases scour holes size of square eccentric pier while transporting sands far from the symmetry line.

4.9 Nomenclature

a_s	planer surface area of equilibrium scour hole (cm ²)
b	pier width (cm)
d_{se}	maximum Equilibrium scour depth for square eccentric pier (cm)
d_{sf}	maximum equilibrium scour depth for square front pier (cm)
d_{sr}	maximum equilibrium scour depth for square rear pier (cm)
d_{16}	16% finer sand diameter (mm)
d_{50}	median diameter of sand (mm)
d_{84}	84% finer sand diameter (mm)
d_{90}	90% finer sand diameter (mm)
e	transversal gap between the centres of inline piers and eccentric pier (cm), $3b$
F	Froude number of flow, U/\sqrt{gh}
g	acceleration due to gravity
h	approaching flow depth (cm)
i, k	direction indices along the r and z axes, respectively
k	turbulent kinetic energy, $k = \frac{1}{2}(u'^2 + v'^2 + w'^2)$ (cm ² /s ²)
l	spacing along the flow between the centres of front and eccentric piers (cm)
$2l$	spacing along the flow between the centres of front and rear piers (cm)
l_s	maximum equilibrium scour length for three square-pier combination (cm)
l_{ss}	maximum equilibrium scour length for single square pier (cm)
L	maximum equilibrium length of sand transportation for three pier combination (cm)
r	radial distance (cm)
r_0	$r-0.35b$ (cm)
R	hydraulic radius (cm)
Re	flow Reynolds number, UR/ν
Re_p	pier Reynolds number, Ub/ν
s	relative density of sand, ρ_s/ρ
u	time averaged tangential velocity in r or x -direction (cm/s)
u'	fluctuations of u (cm/s)
u^+	tangential turbulent intensity, $\sqrt{u'u'}$ (cm/s)
U	depth averaged approaching flow velocity (cm/s)

U_c	critical velocity (cm/s)
v	time averaged radial velocity in y or θ direction (cm/s)
v'	fluctuations of v (cm/s)
v^+	radial turbulent intensity, $\sqrt{v'v'}$ (cm/s)
v_s	volume of equilibrium scour hole (cm ³)
V	time averaged absolute velocity, $\sqrt{u^2 + v^2 + w^2}$ (cm/s)
\bar{v}	time averaged velocity vectors, $\sqrt{v^2 + w^2}$ (cm/s)
w	time averaged vertical velocity in z - direction (cm/s)
w'	fluctuations of w (cm/s)
w^+	vertical turbulent intensity, $w^+ = \sqrt{w'w'}$ (cm/s)
x, y, z	coordinate axes
z	vertical distance

Greek Symbol

ρ	mass density of water (kg/m ³)
ρ_s	mass density of sand (kg/m ³)
σ_g	geometric standard deviation, $\sqrt{d_{84}/d_{16}}$
ζ	vorticity, $\partial v/\partial z - \partial w/\partial r$ (s ⁻¹)
Ω	circulation (m ² /s)
θ	azimuth angle

Subscript

16, 50, 84, 90	16 %, 50 %, 84 % and 90 % finer respectively
<i>sf, se, sr</i>	inline front, eccentric and inline rear pier respectively

4.10 References

- Akilli, H.; Akar, A.; Karakus, C.: Flow characteristics of circular cylinders arranged side-by-side in shallow water. *Flow Meas. Instrum.* 15(4), 187-189 (2004)
- Ashtiani, A.B.; Beheshti, A.A.: Experimental investigation of clear-water local scour at pile groups. *J. Hydraul. Eng.* 132(10), 1100-1104 (2006)
- Ashtiani, A.B.; Kordkandi, A.A.: Flow field around side-by-side piers with and without a scour hole. *Eur. J. Mech. B/Fluid.* 36, 152-166 (2012)
- Ashtiani, A. B.; Kordkandi, A. A.: Flow field around single and tandem piers. *Flow Turbul. Combust.* 90(3), 471-490 (2013)
- Blanckaert, K.; Lemmin, U.: Means of noise reduction in acoustic turbulence measurements. *J. Hydraul Res.* 44(1), 3-17 (2006)
- Coleman, S. E.: Clear water local scour at complex piers. *J. Hydraul. Eng.* 131(4), 330-334 (2005)
- Das, S.; Das, R.; Mazumdar, A.: Velocity profile measurement technique for scour using ADV. In: *Proceedings of the 2015 International Conference on Testing and*

- Measurement: Techniques and Applications*, TMTA 2015. Taylor & Francis Group, London, pp. 249-252 (2015)
- Das, S.; Das, R.; Mazumdar, A.: Comparison of local scour characteristics around two eccentric piers of different shapes. *Arab. J. Sci. Eng.* 41(4), 1193-1213 (2016)
- Das, S.; Mazumdar, A.: Comparison of kinematics of horseshoe vortex at a flat plate and different shaped piers. *Int. J. Fluid Mech. Res.* 42(5), 418-448 (2015a)
- Das, S.; Mazumdar, A.: Turbulence flow field around two eccentric circular piers in scour hole. *Int. J. River Basin Manag.* 13(3), 343-361 (2015b)
- Das, S., Mazumdar, A.: Evaluation of Hydrodynamic Consequences for Horseshoe Vortex System developing around two eccentrically arranged Identical Piers of Diverse Shapes. *KSCE J. Civil Eng.* 22(7), 2300-2314 (2018)
- Das, S.; Midya, R.; Das R.; Mazumdar, A.: A Study of Wake Vortex in the Scour Region around a Circular Pier. *Int. J. Fluid Mech. Res.* 40(1), 42-59 (2013)
- Das, S.; Ghosh, S.; Mazumdar, A.: Kinematics of horseshoe vortex in a scour hole around two eccentric triangular piers. *Int. J. Fluid Mech. Res.* 41(4), 296-317 (2014)
- Das, R.; Khwairakpam, P.; Das, S.; Mazumdar, A.: Clear-water local scour around eccentric multiple piers to shift the line of sediment deposition. *Asian J. Water Environ. Pollut.* 11(3), 47-54 (2014)
- Dey, S.; Bose, S.K.; Sastry, G.L.N.: Clear water scour at circular piers: a model. *J. Hydraul. Eng.* 121(12), 869-876 (1995)
- Dey, S.; Raikar, R.V.: Characteristics of horseshoe vortex in developing scour holes at piers. *J. Hydraul. Eng.* 133(4), 399-413(2007)
- Elliott, K.R.; Baker, C.J.: Effect of pier spacing on scour around bridge piers. *J. Hydraul. Res.* 111(7), 1105-1109 (1985)
- Graf, W.H.; Yulistiyanto, B.: Experiments on flow around a cylinder: the velocity and vorticity fields. *J. Hydraul. Res.* 36(4), 637-653 (1998)
- Mahjoub, S. N.; Mhiri, H.; Bournot, P. H.; LePelec, G.: Experimental and numerical modeling of the three-dimensional incompressible flow behavior in the near wake of circular cylinders. *J. Wind Eng. Ind. Aerodyn.* 96(5), 471-502 (2008)
- Melville, B.W.; Raudkivi, A.J.: Flow characteristics in local scour at bridge piers. *J. Hydraul. Res.* 15(4), 373-380 (1977)
- Raikar, R.V.; Dey, S.: Kinematics of horseshoe vortex development in an evolving scour hole at a square cylinder. *J. Hydraul. Res.* 46(2), 247-264 (2008)
- Raudkivi, A.J.: *Loose Boundary Hydraulics*. A. A. Balkama, Rotterdam (1998)
- Sheppard, D. M.; Zhao, G.; Copps, T. H.: Local scour near multiple pile piers in steady currents. In: *Proceedings of ASCE, International Conference on Water Resources Engineering*, San Antonio, USA (1995)
- Song, T.; Chiew, Y. M.: Turbulence measurement in nonuniform open-channel flow using Acoustic Doppler Velocimeter (ADV). *J. Eng. Mech.* 127(3), 219-232 (2001)
- Sumner, D.; Wong, S.S.T.; Price, S.J.; Paidoussis, M.P.: Fluid behavior of side-by-side circular cylinders in steady cross-flow. *J. Fluid. Struct.* 13(3), 309-338 (1999)
- Yilmaz, M.; Yanmaz, A. M.; Koken, M.: Clear-water scour evolution at dual bridge piers. *Canadian J. of Civil Eng.* 44(4), 298-307 (2017)
- Zdravkovich, M.M.: The effects of interference between circular cylinders in cross flow. *J. Fluid Struct.* 1(2), 239-261 (1987)

5. COMPARISON OF SCOUR GEOMETRY AND HORSESHOE VORTEX CHARACTERISTICS

After conducting all the nine circular and five square pier tests in same experimental conditions, the outcomes obtained for the clear water equilibrium scour holes, geometrical parameters like scour depth, length, width, hole surface area and volume and flow fields and turbulence fields were analysed. It is essential to compare the present findings of scour geometry and horseshoe vortex characteristics at square pier with the circular shaped piers. In previous chapters 3-4, the laboratory flume experiments were found on cylindrical piers and square piers under similar investigational setup and conditions. The comparisons of the new findings between circular and square pier investigations are furnished below:

- Three (inline-front, eccentric-middle and inline-rear) circular and square piers combined arrangement and interferences between on another, play an essential role in formation and enhancement of larger scour-depth near the eccentric pier and the sand particles transport was more toward the flume-wall side. The flow removes less sand particles from the vicinity of the inline-rear pier compared to the inline-front pier. The same phenomenon was found in case of all other parameters such as scour area, scour volume etc. The parameters of equilibrium scour geometry are found increasing for inline-front, eccentric-middle and inline-rear circular and square piers, respectively. These parameters are found approximately $\bullet < \blacksquare$. Here the representation \blacksquare and \bullet represent the magnitudes for several factors at same azimuth angles and horizontal planes for square and circular piers, in that order.
- At 0° , max- u magnitudes for the eccentric-middle circular and square piers are 1.54, 1.46 times and 1.77, 1.20 times of max- u for the inline-front and inline-rear piers respectively. Thus, at the upstream of eccentric-middle piers, streamlines are separated with a higher u magnitude compared with the inline-front and inline-rear piers. Max- u values just near upstream of scour region around inline-front, eccentric-middle and inline-rear square and circular piers are obtained approximately $0.054U$, $0.15U$, $0.21U$ and $0.08U$, $0.12U$, $0.22U$, correspondingly.
- At $\pm 45^\circ$, tangential velocity u at subsequent positions are found in increasing order for inline-front, eccentric-middle and inline-rear square and circular piers, respectively i.e. $\blacksquare < \bullet$.
- At $\pm 90^\circ$ at subsequent positions, magnitudes of u are found increasing for inline-front, eccentric-middle and inline-rear circular and square piers, respectively. Therefore at $\pm 90^\circ$ angle, magnitude of tangential velocity u is found approximately $\bullet < \blacksquare$.
- For $\pm 45^\circ$ at subsequent positions, the u magnitude for square piers is lesser than cylindrical piers i.e. $\bullet < \blacksquare$.

- For the three circular and square piers downstream region, u at $z = 0.04h$ is almost similar to the corresponding values of u at $z = 0.5h$ but a bit higher in magnitude as compared to the velocities at $z = 0.5h$. The tangential velocities are observed approximately $\bullet < \blacksquare$.
- At 0° at subsequent positions, radial velocity v are found in an increasing order for inline-front, eccentric-middle and inline-rear circular and square piers, respectively i.e. $\bullet < \blacksquare$.
- At $\pm 45^\circ$ at subsequent positions, v magnitudes are observed in an increasing trend for inline-front, eccentric-middle and inline-rear cylindrical and square shaped piers, respectively i.e. $\bullet < \blacksquare$.
- At $\pm 90^\circ$ at subsequent positions, magnitudes of v are also found in an increasing trend for inline-front, eccentric-middle and inline-rear cylindrical and square shaped piers, respectively i.e. $\bullet < \blacksquare$.
- Radial velocity v at $\pm 45^\circ$ and $\pm 90^\circ$ are found more than those v at 0° at subsequent positions.
- Radial velocity v for eccentric-middle pier v is observed more than those v for inline-front and inline-rears piers at subsequent positions.
- At $\pm 45^\circ$ the v magnitude for cylindrical pier is found lesser than those for the square pier.
- Also for circular and square piers at $\pm 90^\circ$ the magnitude orders for tangential and radial velocity are reverse in nature. Tangential velocity is found maximum for cylindrical shape because, at 90° flow detachment is very slow compared to the square shaped piers.
- At both horizontal planes ($z=6.25$ cm and $z=0.5$ cm) for the three circular and square piers, maximum radial velocity v is found at the upstream zone of eccentric-middle pier compared to two inline piers. The radial velocity at the downstream zone of the three piers at $z=0.04h$ plane is found very close to v at the downstream zone of the three piers for $z=0.5h$ plane but greater than that at $z=0.5h$ plane. At the upper middle depth, near upstream zone of each pier, v values are greater than those near the bed for existence of high momentum flow. This radial velocity magnitude is observed approximately $\bullet < \blacksquare$.
- At 0° at subsequent positions vertical velocity w magnitudes are in increasing trend for inline-front, eccentric-middle and inline-rear circular and square piers, respectively, i.e. $\bullet < \blacksquare$.

- At $\pm 45^\circ$, at subsequent positions magnitudes of w are in increasing trend for inline-front, eccentric-middle and inline-rear cylindrical and square shaped piers, respectively, respectively i.e. $\bullet < \blacksquare$.
- Around inline-front, eccentric-middle and inline-rear circular and square piers as θ increases from 0° to $\pm 45^\circ$ to $\pm 90^\circ$ azimuthal planes, it is noticed that w decreases gradually. At $\pm 90^\circ$, at subsequent positions eccentric-middle circular and square pier w is always higher than that at inline-front and inline-rear circular and square piers. For the inline-front circular and square pier, w is always almost higher than w at inline-rear circular and square pier i.e. $\bullet < \blacksquare$.
- At 0° angle, max- w for inline-front, eccentric-middle and inline-rear circular are measured as $0.59U$ at $z = 0.3d_{sf}$, $0.51U$ at $z = 0.39d_{se}$ and $0.35U$ at $z = 0.18d_{sr}$ respectively. Whereas, at 0° , max- w for inline-front, eccentric-middle and inline-rear square piers are measured as $0.67U$ at $z = 0.40d_{sf}$, $0.71U$ at $z = 0.19d_{se}$ and $0.37U$ at $z = 0.64d_{sr}$, respectively.
- For both circular and square shaped piers maximum value of negative w is noticed at the upstream of eccentric pier, whereas w at the downstream of the three piers are noticed with positive magnitude. Wake vortices at the downstream for the three circular and square piers are in increasing trend i.e. $\bullet < \blacksquare$. For both circular and square piers in the wake region, for $z=0.04h$ plane vertical velocity of higher value is observed as compared to vertical velocity in the wake region for $z=0.5h$ plane. The maximum values of w for circular and square piers are found about 0.8 and 0.6-0.7 times of v respectively. This vertical velocity magnitude is observed approximately $\bullet < \blacksquare$.
- At 0° , $\pm 45^\circ$ and $\pm 90^\circ$, magnitudes of absolute velocity for circular and square shaped piers are relatively similar at corresponding inline-front, eccentric-middle and inline-rear positions at vertical and horizontal planes.
- The vortices core size decreases as azimuthal angle θ increases. At $\pm 90^\circ$ the vortices core size are relatively small and the vorticity is considerably weaker. The vorticity around cylindrical piers are about 35-65% weaker than those at inline-front square pier respectively i.e. $\bullet < \blacksquare$.
- The horseshoe vortex circulation Ω decreases with increase in azimuth angle θ (clock wise and anticlockwise) and also increases with increase in scour depth. At azimuthal angles $\pm 45^\circ$ and $\pm 90^\circ$ near upstream zone of the inline-front, eccentric-middle and inline-rear circular circulations are found 0.67, 0.12, 0.77, 0.16 times, 0.51, 0.17, 0.72, 0.13 times and 0.66, 0.12, 0.77, 0.16 times of the respective circulations at 0° of the corresponding pier, whereas for square pier circulations are found 0.83, 0.31, 0.35

times, 0.73, 0.65, 0.37, 0.32 times and 0.83, 0.95, 0.34, 0.40 times of circulation at 0° for corresponding pier. For the eccentric-middle circular pier at 0° , 45° , 90° , -45° and -90° circulations are 38%, 29%, 6%, 90%, 10% and 52%, 43%, 18%, 10%, 22% higher than the inline-front and inline-rear circular piers, respectively, whereas for square eccentric pier, are 53%, 58%, 19%, 81%, 43% and 87%, 65%, 29%, 99%, 53% greater than the magnitudes of circulation at corresponding azimuth angles around square front pier and square rear pier, respectively.

- The circulation at subsequent positions are found increasing for various cases for inline-front, eccentric-middle and inline-rear cylindrical and square shaped piers, respectively i.e. ● < ■.
- The distributions of tangential, radial and vertical intensities (u^+ , v^+ , w^+) and turbulent kinetic energy k due to turbulence are relatively similar. The magnitudes of u^+ , v^+ , w^+ and k at subsequent positions for inline-front, eccentric-middle and inline-rear cylindrical and square shaped piers are found in increasing order, respectively i.e. ● < ■.
- At the two horizontal planes $z=0.5h$, and $z=0.04h$ for the three circular and square piers overall value of u^+ is noticed almost higher, than the transverse turbulence intensity v^+ and vertical turbulence intensity w^+ at all corresponding locations around the circular and square piers. At $z=0.5h$ plane, maximum k are always found higher than those at $z=0.04h$ for both ● and ■.

6. CONCLUDING REMARKS

6.1 Synthesis of the Present Research

Now-a-days parallel or side-by-side bridges are constructed beside old bridges for similar or different types of transport facilities. Therefore it is obvious that there will be an impact of upstream bridge pier on downstream bridge pier and vice versa. The longitudinal spacing (gap) and transversal spacing (eccentricity) between the bridge piers may play important role on bridge stability. Thereafter it is very much needed to know the scour pattern and flow kinematics around such eccentric or inline bridge pier combinations for safe bridge pier design. By identifying the scour patterns and flow characteristics governed by the vortices in scour holes around such interfering piers may help to improve the pier positioning thereby to enhance the bridge stability. But till now almost no such study was carried out to find out the characteristics of vortices on this aspect. Hence an initiative has been taken out in this study to find out the clear water scour kinematics around such type of model inline-eccentric bridge pier arrangements.

In the first part (third chapter) of this research, the equilibrium scour geometry and turbulent horseshoe vortex flow field around inline-eccentric-inline arranged three longitudinally equidistant circular piers of width 7cm were analysed by conducting nine clear-water scour tests. The two piers - front and rear ones were positioned along the flow and the third one was set eccentrically in mid region of two inline piers. Here, the eccentricity was kept constant equal to $3b$ (where b =base of a pier) and the spacing along the flow between the inline front and eccentric-middle pier considered were (2/8), (3/8), (4/8), (5/8), (6/8), (7/8), (8/8), (9/8) and (10/8)times the maximum equilibrium length of sediment transport (sum of maximum equilibrium scour length and dune length) of a single circular pier. The vital conclusions drawn from those test results are summarised below.

1. The variations and relations between the maximum equilibrium scour depths, scour lengths and scour widths are observed with respect to the longitudinal spacings. Also the rate of change of planer surface areas and the volumes of the scour holes are also observed relative to the change of longitudinal spacings.
2. For all the tests conducted, the maximum scour depths around the eccentric middle circular pier is found always higher than the maximum scour depths around the inline front and inline-rear circular piers at different longitudinal spacings. And also the maximum scour depths around the inline front circular pier are always found higher than the maximum scour depths around the inline rear circular pier.
3. For all the experimental tests, it is found that maximum equilibrium scour depths, scour lengths, scour widths, planer surface areas and volumes gradually increases with increasing pier distances until the inline-front and eccentric-middle pier spacing is (6/8)times the maximum equilibrium length of sediment transport of a single circular pier, but further increase in pier distance shows that it decreases. This phenomenon is similar for all the three piers inline-front, inline-rear and eccentric-middle circular piers.

4. The vector plots of the time mean absolute velocity components present a good understanding of the characteristics of the horseshoe vortex at the very upstream of the pier. It is clear from the velocity vector profiles, that the wake zone length is larger for the inline front circular pier than the other two eccentric middle and inline rear circular piers. The wake zone length is larger for eccentric middle circular pier than inline rear circular pier.
5. The longitudinal velocity u increases in-between the three piers, inline-front, eccentric-middle and inline-rear circular piers. As azimuthal angle θ increases, u increases and turns finite.
6. The magnitude of time mean radial velocity v for the eccentric middle pier is always higher than the magnitude of v for inline front and inline rear circular piers.
7. At $\theta = 0^\circ$ azimuth plane, for the inline-front, eccentric-middle and inline-rear circular pier the maximum vertical velocity w was detected as $0.59U$ at $z = -2.01$ cm, $0.51U$ at $z = -3.00$ cm and $0.35U$ at $z = -0.99$ cm, respectively. Maximum w at upstream region of eccentric middle pier is 1.17 times and 1.42 times of maximum w for inline-front pier and for inline-rear pier, respectively. It clears presence of co-shedding regime formed at downstream of inline front and eccentric middle circular piers.
8. As azimuthal angle, θ increases from 0° plane to 90° plane and 0° plane to -90° plane, a gradual decrease in w is observed for three circular piers.
9. Three circular-piers combined inline-eccentric-inline arrangement and interferences between on another, plays an essential role in formation and enhancement of larger scour-depth near circular eccentric pier and the sand-particles transport was more toward flume-wall. During the experimentation, in the turbulent outer layer and turbulent logarithmic layer, the turbulence mixing plays a significant role as pressure drag becomes much higher than skin friction drag, because of the presence of separated streamlines and bluff body. The vortex strengths at three piers are not similar.
10. The vortex strength of the eccentric middle circular pier is found higher than the inline front and inline rear circular piers at corresponding azimuthal planes. Also vortex strength of inline rear circular pier is found higher than the inline front circular pier at corresponding azimuthal planes.
11. The magnitude of circulation of the horseshoe vortex decreases with the increase of azimuthal angle θ .
12. At negative azimuth planes around the three circular piers, the circulation magnitude is found higher than the circulation magnitude at positive azimuth planes of same magnitude around the respective piers. This may be for the presence of strong mixing of turbulent flow in between the three circular piers.
13. The radial, tangential and vertical turbulence intensity and turbulent kinetic energy magnitudes above the scour holes were found greater than their maximum magnitudes within scour holes below the bed level.
14. For eccentric middle and inline rear circular piers - radial, tangential and vertical turbulence intensity magnitudes are larger than subsequent maximum intensity magnitudes at the inline front circular pier. Their maximum magnitudes at inline rear

- circular pier are also greater than corresponding values at the inline-front and eccentric-middle circular piers.
15. For the three circular piers, within the holes, core of larger turbulent kinetic energy is observed. At eccentric middle circular pier, it was found greater than for inline-front and inline-rear circular piers.

In the second part (fourth chapter) of this experimental research, the equilibrium scour geometry and turbulent horseshoe vortex flow field around inline-eccentric-inline arranged three identical square piers of width 7cm were analysed by conducting five clear-water scour tests. Two of them were placed in line along the flow and the third one eccentrically in mid of them with a constant eccentricity $3b$. Here the experiments were conducted at similar experimental conditions as mentioned in previous chapter but only three circular piers were replaced by three square piers. The spacing along the flow between the inline front and eccentric middle square piers considered were (2/8), (3/8), (4/8), (5/8) and (6/8) times the maximum equilibrium length of sediment transport of a single square pier. The major conclusions drawn from those experiments are summarised below.

1. The variations of maximum equilibrium scour depths, scour lengths, scour widths, planer surface areas and the volumes are observed with respect to the longitudinal spacings. Among the scour parameters some functional relations are also observed relative to the change of longitudinal spacings.
2. For all the tests conducted, the maximum scour depths around the eccentric middle square pier is found always higher than the maximum scour depths around the inline front and inline rear square piers at different longitudinal spacing. And also the maximum scour depths around the inline front square pier is always found higher than the maximum scour depths around the inline rear square pier.
3. For all the experimental tests, it is found that maximum equilibrium scour depths, scour lengths, scour widths, planer surface areas and volumes gradually increases with increasing pier distances. This phenomenon is similar for all the three inline front, inline rear and eccentric middle square piers.
4. The longitudinal velocity u increases in between inline square front, inline square rear pier and square eccentric pier. This velocity component increases in the downstream of the piers near the bed. As azimuthal angle θ increases, u increases and turns finite.
5. The magnitude of time mean radial velocity v for the square eccentric pier is always higher than the magnitude of v for inline square front and inline square rear piers. The velocity v changes its direction on both sides of zero contour line within the scour holes near pier bases.
6. At 0° azimuthal planes, for square front pier, square eccentric pier and square rear pier maximum value of vertical velocity w is measured as $0.67U$ at $z = 3$ cm, $0.71U$ at $z = 2.95$ and $0.37U$ at $z = 4.48$ respectively. At upstream region of square eccentric pier maximum values of w are 1.05 and 1.89 times of maximum value of w at corresponding locations of square front pier and square rear pier, respectively. This validates the clear existence of co-shedding regime formed within the three square piers at downstream of square front pier and square eccentric pier.

7. Around three piers as θ increases from 0° to $\pm 45^\circ$ to $\pm 90^\circ$ azimuthal planes, it is noticed that w decreases gradually.
8. Down-flows around square eccentric pier are always greater than w around other inline two square-piers and around square front pier w always higher than around square rear pier.
9. The plotting of velocity vectors of the time mean absolute velocity components depict the horseshoe vortex characteristics at upstream region of each pier and wake vortex at downstream region of each pier. Size of horseshoe vortex core for square eccentric pier is ever larger than other two square front pier and square rear pier. Here, in order of magnitude, the wake zone length is largest for square front pier, then square eccentric pier and then square rear pier.
10. For the presence of bluff body effect and separated streamline, at square eccentric pier horseshoe-vortex distributions are not similar with square front and square rear pier. The vortex circulation increases as θ decreases and also increases for a corresponding increase in scour depth.
11. Here, in order of magnitude, circulation is greatest around square eccentric pier, then square front and then square rear pier.
12. Tangential and radial turbulence intensities for square eccentric pier are consistently seen greater than that of the square rear pier and square front pier. Whereas vertical turbulence intensity for square eccentric pier at 0° is slightly lesser and for square rear pier is slightly greater than w^+ at 0° for square front pier.
13. Also for square eccentric pier and square rear pier, maximum value of turbulence kinetic energy, TKE, are higher than maximum values of k for square front pier at 0° azimuthal plane. The TKE k just near the bed ($z= 0.04h$) was found more in the order of magnitude around the square eccentric pier, then square front pier and square rear pier, respectively. Whereas at $z=0.5h$, maximum value of k was found around square eccentric pier, then square rear pier and square front pier in order of magnitude, respectively.

In the last part (fifth chapter) in this research, a comparison has been made between the present findings of scour geometry and horseshoe vortex characteristics around circular shaped pier with the square shaped pier experiments. Comparing the outcomes for two different shapes like square, and circular, the major conclusions drawn are summarised below.

1. The parameters of equilibrium scour geometry are found maximum for square piers.
2. The diversion angle of the scour and also the deposition is more on the side of the eccentric square pier than on the side of the eccentric middle circular pier. It indicates that the sand, removed from the surroundings of the pier in the flume or open-channel bed, is deposited on one side of the channel. This finding is significant as it proves that the transported sand load in an open channel can be shifted more towards the sidewall of the flume by self-scouring around piers with the help of suitable three pier combinations, eccentricity and longitudinal spacing.

3. For all the five azimuthal angles, the tangential, radial and vertical velocities are observed approximately greater for square piers than for circular piers.
4. The characteristics of horseshoe vortex that is considered to be the prime cause of greater scour at three inline-eccentric-inline arranged square piers experiment than at three inline-eccentric-inline arranged circular pier experiment.
5. The size of the horseshoe vortex core was observed larger for the square piers than the circulars. Similar trend was observed in case of magnitude of vorticity, circulation and turbulent kinetic energy.
6. The magnitudes of tangential, radial, vertical turbulent intensities and turbulent kinetic energy at subsequent positions for inline-front, eccentric-middle and inline-rear circular and square shaped piers are found in increasing order.

In this research, flow characteristics for inline-eccentric-inline positioning of piers and their comparison with previous literatures are extremely interrelated with the outcomes from single pier test and three piers tests. In this research, experimental test were carried out with special emphasis on clear water scour mechanism and turbulence effect around three piers inline-eccentric-inline arrangement. The increased rate of sediment transport and strengths of vortices were found maximum for the square pier. Therefore, the square pier causes to develop more scour than the circular pier and thereby shifts more sand towards the side walls of the flume. It is also important that if the longitudinal spacing increases beyond a certain limit then the rate of sediment transport will gradually decrease. It indicates that if the piers are extremely separated then the reference pier will not be influenced by the middle and downstream piers. The circulation of the horseshoe vortex at the positive and negative azimuthal planes of the same magnitude are not always similar due to the strong mixing of turbulence, separation of the streamline and bluff body effect.

6.2 Future Scope of Similar Research

From the experience gained during the present work, the following suggestions are proposed in conducting additional experimental research works on flow around piers:

- Flow visualization and pressure measurement may be carried out by concluding the same laboratory experiments.
- Despiking of ADV data may be done using Kolmogorov's hypotheses.
- Numerical simulation may be carried out introducing the boundary treatments like the solid boundaries and water surface computation (for example, pressure correction technique of computational hydrodynamics)
- The enhancement of sediment transport mechanism and its flow dynamics may be observed using three or more number of piers of different shapes as well as different eccentricity and longitudinal spacing. The same may be observed at different the flow and bed conditions.
- Reynolds stresses and bed shear stresses may also be determined at different azimuthal planes from the present study.

- In case of three piers inline-eccentric-inline arrangement, the flow and turbulence characteristics of the horseshoe vortex may be deduced from the point of view of the similarity with the velocity and turbulence intensity characteristics scale.
- Similar kind of experimental works (at same flow and bed conditions) may be carried using three triangular or any other pies and the results may be compared with present study.
- Similar kind of experimental works may be carried at different eccentricity and the results may be compared with present study.
- Similar kind of experimental work may be carried at different flow and bed conditions and the results may be compared with present study.
- Time evolution of scour geometry and sediment transport of similar kind of works may be carried out and the results may be compared with present study.

Curriculum Vitae



Identity

<i>Name</i>	HASANUR JAMAN
<i>Father's Name</i>	Hasan Imam Nurala
<i>Mother's Name</i>	Tahasina Begum
<i>Date of Birth</i>	9 th April 1983
<i>Place of Birth</i>	Rampurhat, Birbhum, West Bengal, India
<i>Marital Status</i>	Married

Education

2011	M.E. – Water Resources and Hydraulics Engineering, School of Water Resources Engineering, Jadavpur University, Kolkata, India
2008	B.Tech. – Mechanical Engineering, West Bengal University of Technology, Birbhum Institute of Engineering and Technology, Suri, Birbhum, West Bengal, India
2005	D.M.E. - Mechanical Engineering, West Bengal State Council of Technical Education, Shree Ramkrishna Silpa Vidyapith, Suri, Birbhum, West Bengal, India
2001	12 th Standard (Science), West Bengal council of higher secondary Education, Rampurhat High School, Rampurhat, Birbhum, West Bengal, India
1999	10 th Standard, West Bengal Board of Secondary Education, Rampurhat High School, Rampurhat, Birbhum, West Bengal, India

Field of Research Interest

Applied Hydraulics, Fluvial Hydraulics, Open Channel Hydraulics, Turbulence

Professional Award

Recipient of U.G.C Maulana Azad National Fellowship.

Language

<i>Bengali</i>	Mother Tongue
<i>English</i>	Good theoretical and practical knowledge

Hydrodynamic Flow Patterns Around Three Inline Eccentrically Arranged Circular Piers

Hasanur Jaman¹ · Subhasish Das¹  · Asim Kuila¹ · Asis Mazumdar¹

Received: 6 January 2017 / Accepted: 10 April 2017 / Published online: 22 April 2017
© King Fahd University of Petroleum & Minerals 2017

Abstract An experiment was conducted under clear-water equilibrium scour state to measure flow formations and characteristics using a velocimeter, in local-scour holes around three identical circular-type piers arranged inline and eccentrically in staggered manner. Two inline piers were positioned towards flow, and eccentric one was placed in middle region of two inline piers. The flume experiment was done for an approach flow depth 0.125 m on uniform bed of sand particles having 0.825 mm median diameter. The hydrodynamic consequences of three-pier arrangement on scour were investigated here. The contour profiles and subsequent distributions of time-independent velocities, turbulence kinetic energy and intensities are well addressed for different vertical azimuthal planes 0° , $\pm 45^\circ$ and $\pm 90^\circ$ around the piers. Velocity vectors derived from velocity profiles are also utilized to explain further flow attributes. Vorticity and all circulation values for horseshoe vortices, developed at upstream zone of each pier, are determined. The three-pier combination and their interferences caused by them play a key function in the enhancement of greater scour depth near the eccentric-middle pier and more shifting of sand towards the side wall. Flow formations and characteristics of such horseshoe vortices, responsible for above-noted phenomena, are explained here in detail. Vortices strengths for eccentric-middle and inline-rear piers are found greatest and lowest, respectively, compared with strength of inline-front pier.

Keywords Open channel · Turbulent flow · Clear-water scour · Longitudinal gap · Inline-eccentric piers · Vortex · Circulation

✉ Subhasish Das
subhasishju@gmail.com

¹ School of Water Resources Engineering, Jadavpur University, Kolkata 700032, India

1 Introduction

Flow behaviour around multiple piers is a classical problem. Prediction of magnitude of scour near multiple piers is an important issue to the hydraulic engineers. Nowadays, pier groups are becoming very popular to design bridges for geo-technical and economical benefits. An estimation of maximum plausible scour $[(d_s)_{\max}]$ around today's bridge piers' is highly needed for its secure design. The scour mechanism for pier groups is highly complex and also much more complicated to predict local-scour depth, where direct use of outcomes obtained from particular pier experimentation (d_s) may be difficult.

There are numerous investigations over the years using laboratory-based flume experiments for predicting scour depth (d_s) around pier bases [1–11]. But these are confined to single pier. These investigations were conducted by laboratory flume, including use of non-dimensional equations ultimately producing in some semiempirical equations to compute $(d_s)_{\max}$. Minimum knowledge on flow patterns around multiple piers and subsequently their interactions with bed sediment are responsible for over-predicting $(d_s)_{\max}$ for fields and laboratory conditions using these equations. Therefore, many flume experiments were done for gathering detailed information on flow structures to present more insights into scouring processes and determining scour depths with more accuracy. Many researchers highlighted information on velocity and subsequent turbulent fields around piers or cylinders [12–20]. Many experiments were restrained to one pier experiment for providing detailed conclusive information around them. Few experiments were performed for determination of more accurate scour depths based on vortex velocity fields at single piers [21–23].

Due to geo-technical and economical benefits, design of bridges very often leads to multiple piers where direct uti-



Hydrodynamics of Flow Obstructed by Inline and Eccentrically-Arranged Circular Piers on a Horizontal Bed Surface

Hasanur Jaman¹ · Subhasish Das¹ · Rajib Das¹ · Asis Mazumdar¹

Received: 6 December 2016 / Accepted: 20 April 2017 / Published online: 27 April 2017
© The Institution of Engineers (India) 2017

Abstract An attempt has been made to study and analyse the hydrodynamic effects of turbulent flow including its pattern and characteristics around three identical circular shaped piers. Experimentation was conducted under clear-water scour condition. Three pier groups were placed with inline and eccentric arrangement in tandem manner on a flume. Two piers were positioned inline along the flow direction and third pier was placed eccentrically in the middle of two inline piers having a transverse distance equal to three times of pier width. Three dimensional velocities were gauged at a horizontal plane located at 4% depth above the zero bed level. The readings were captured in the Cartesian coordinate-system to compute the time-mean longitudinal, transversal and vertical velocities. The hydrodynamic consequences of three piers arrangement near the horizontal bed were investigated. The contour profile and variations of time aggregated mean velocity components, kinetic energy and turbulence intensities are measured or determined and analysed. Velocity vectors and absolute velocity at horizontal plane obtained from velocity measuring areas are utilised to explain further hydrodynamic flow features. The measured depth for scour at equilibrium state for the eccentric middle pier is observed

higher than the inline front and inline rear circular piers. The three pier group positioning and the interfering between the circular piers act an important function in flow characteristics and for creating and forming the larger scoured depth around the eccentric middle pier.

Keywords Open channel hydraulics · Scour · Turbulence · Inline and eccentric arrangement

Introduction

Prediction of magnitude of scour at piers is a topic of importance to the field engineers. Nowadays pier groups are becoming popular in bridge design. An estimation of possible maximum scour around many bridge pier groups is crucial for its protected design. The scour system for pier groups is very complex and it is much more complex to predict local scour depth.

There have been numerous investigations over the years using laboratory oriented flume experiments to forecast scour-depth around the base area of the piers [1–8]. Most of these experimentations have been confined to single pier. Many researchers focused on flow fields and turbulent flows at clear water for equilibrium scour condition around single piers and cylinders [9–20].

Due to economical and geotechnical reasons, design of many bridges often direct to pier groups wherein case the straight application of these results derived from single piers may be problematic. Most of these pier group investigations have been confined to double pier arrangements, either inline or side by side or eccentric arrangement that highlights the forecast of flow field, turbulent field and the scour geometry [21–27]. Some of the investigations around piers were confined to near-wake region

✉ Subhasish Das
subhasishju@gmail.com

Hasanur Jaman
hasanurju@gmail.com

Rajib Das
rajibdas79@gmail.com

Asis Mazumdar
asismazumdar@yahoo.com

¹ School of Water Resources Engineering, Jadavpur University, Kolkata 700032, India

HYDRODYNAMIC BEHAVIOR OF FLOW PAST THREE TYPICALLY ARRANGED CIRCULAR PIERS ON DIFFERENT HORIZONTAL PLANES

Subhasish Das,* Hasanur Jaman, Anik Chatterjee, Rajib Das, & Asis Mazumdar

School of Water Resources Engineering, Jadavpur University, Kolkata 700032, India

*Address all correspondence to: Subhasish Das, Assistant Professor, School of Water Resources Engineering, Jadavpur University, Kolkata 700032, India, E-mail: subhasishju@gmail.com

Original Manuscript Submitted: 12/6/2016; Final Draft Received: 4/14/2017

In this paper an attempt has been made to study the hydrodynamic behavior of flow in terms of three-dimensional turbulent flow patterns and characteristics around three identical circular shaped piers of 7 cm diameter at two horizontal planes. Three pier groups were placed with inline and eccentric arrangement in a staggered manner on a flume. The experiment was conducted under clear water scour conditions. In this experiment two inline piers were placed along the flow, and a third pier was placed eccentrically in the middle of the two inline piers with a transverse spacing. The hydrodynamic effects of the three-pier arrangement were investigated near the bed and near the middle of the flow depth, in order to show the flow behavior at the area close and far away from the sediment bed, respectively. All over the scoured zone at two horizontal planes, the contour profiles and distributions of the time-averaged longitudinal, transverse, and vertical velocity components, turbulence kinetic energy, and turbulence intensities are determined and analyzed. Velocity vectors and absolute velocity obtained from velocity fields are used to show further hydrodynamic flow features. The scour depth of the eccentric circular pier was observed to be higher than the inline front and inline rear circular piers. The three-pier arrangement and the interference between the circular piers play an important role in the flow characteristics and in the creation and formation of the greatest scour depth at the eccentric middle pier.

KEY WORDS: open channel hydraulics, inline and eccentric arrangement, scour, turbulence

1. INTRODUCTION

Prediction of magnitude of scour at piers is a topic of importance to field engineers. Due to geotechnical and economical reasons, bridge designs often lead to pier groups, in which case the direct application of the results derived from single piers may be problematic. Nowadays pier groups are becoming popular in bridge plan and design. An estimation of the maximum possible scour around a bridge pier group is necessary for its safe design. The scour mechanism for pier groups is very complex and it is much more difficult to predict local scour depth.

Michael et al. (1991) explained how eccentrically arranged piers can cause sediment to move toward the riverbank flowing downstream. The suitability and efficiency of this kind of natural phenomenon with a particular reference to enhancement of scour may also be explored to use it as an alternative to dredging.

There have been several investigations over the years by means of laboratory flume experiments to predict the scour depth around the base of piers by Breusers et al. (1977), Raudkivi and Ettema (1983), Dey (1997), and Das et al. (2014a–c). Most of these studies have been confined to a single pier. Many researchers, such as Melville (1975), Dey et al. (1995), Graf and Yulistiyanto (1998), Dey and Raikar (2007), and Das et al. (2012a–b, 2013a–c, 2014a–c, 2015a), have focused on the flow fields and turbulent flow fields at clear water equilibrium scour conditions around single piers.

Most of the pier group investigations have been confined to double-pier arrangements, either inline, side by side, or eccentric arrangements that focused on the prediction of flow fields, turbulent fields, and the scour geome-



Impact of Upstream Bridge Pier on the Scouring Around Adjacent Downstream Bridge Pier

Rajib Das¹ · Subhasish Das¹ · Hasanur Jaman¹ · Asis Mazumdar¹

Received: 19 October 2017 / Accepted: 26 June 2018
 © King Fahd University of Petroleum & Minerals 2018

Abstract

The study aspires to investigate a relative scour condition around three-pier group. It identifies the upstream downstream scour geometries when two tandem piers are placed inline and third pier is placed eccentrically in middle of tandem piers. Laboratory scale experiments were physically performed by gradually varying the intermediate longitudinal spacing in between tandem piers. After each experimental run, the scour formation around the pier group and the dune formation downstream of the pier group are investigated. The main aim here is to experimentally identify and highlight the nature and location of scour formed around and also to identify the location of the dune formed downstream of this pier group due to combined interference of flow. The spacing between the inline piers were varied to identify which relative spacing produces the maximum scour. A detailed investigation shows significant effect of inline pier spacing on scour parameters. It was observed that for such three pier combinations, the scour so formed near staggered piers was found maximum and around tandem downstream pier was found minimum. It confirms the shifting of sediment load away from this pier group and is deposited downstream, drifting more towards the staggered pier that is towards channel sidewall. Equations are proposed with respect to the pier spacing between tandem piers to evaluate the scour depth around individual pier of the pier group combination.

Keywords Pier · Inline pier · Eccentric pier · Scouring depth · Scouring volume

List of Symbols

a_s	Scouring hole surface area for three pier's group at equilibrium (m^2)	d_{sr}	Maximum depth for equilibrium scouring for tandem rear pier (m)
a_{ss}	Scouring hole surface area for one pier at equilibrium (m^2)	d_{ss}	Maximum depth for equilibrium scouring for one pier (m)
A	Y intercept	d_{xx}	xx indicates three different piers: tandem front, eccentric middle and tandem rear piers
b	Pier diameter or width (m)	d_{16}	16% thinner sand grain diameter (mm)
b_{cf}, b_{cr}	Characteristic widths of upstream tandem and downstream tandem piers, respectively (m)	d_{50}	Median sand grain diameter (mm)
B	Slope of the regression line	d_{90}, d_{84}	90 and 84% thinner sand grain diameter, respectively (mm)
d_{se}	Maximum depth for equilibrium scouring for middle eccentric pier (m)	e	Centre-to-centre distance in between upstream tandem and middle eccentric piers (m), $3b$
d_{sf}	Maximum depth for equilibrium scouring for tandem front pier (m)	g	Gravity acceleration (m/s^2)
		g'	Relative gravity [$g' = g(\rho_s - \rho)/\rho$]
		h	Approach depth (m)
		K_{sf}, K_{sr}	Shape co-efficient of upstream tandem and downstream tandem piers
		b_e	Effective widths of pier (m)

✉ Subhasish Das
 subhasish.das@jadavpuruniversity.in;
 subhasishju@gmail.com

¹ School of Water Resources Engineering, Jadavpur University, Kolkata, West Bengal 700032, India